DEVELOPMENT OF MATHEMATICAL MODELS FOR CLEAN UP OF Cr (VI) CONTAMINATED AQUIFERS USING BIOREMEDIATION

Final Report Submitted to

Indian National Committee on Ground Water

Ministry of Water Resources

GOVERNMENT OF INDIA

By

Dr. Ligy Philip
and
Dr. B. S. Murty

Environmental and Water Resource Engineering Division
Department of Civil Engineering
Indian Institute of Technology Madras
Chennai -600036

July-2010

TABLE OF CONTENTS

ACKNOWLEDGEMENTS

We wish to acknowledge the Ministry of Water Resources, Government of India for funding the work reported here through the grant No. 23/57/2006-R&D/2479-91 dated October 17, 2006. We sincerely thank Dr. Ramakar Jha (earlier Member secretary of Indian National Committee on Hydrology), Dr. Rakesh Kumar (present member secretary of Indian National Committee on Hydrology) and Dr. Uma Kapoor, Member Secretary of Indian National Committee on Ground Water for their excellent cooperation. We also thank very much Mr. S. Masood Husain, earlier Director (R&D) and Mr. R. S. Ram, present Director (R&D) in Central Water Commission for their constant encouragement. We also thank Dr. N. Varadaraj, Regional Director and the scientists from CGWB-SECR, Chennai, Mr. B.P. Shukla and Dr. Ranganathan from the regional office of Central Pollution Control Board in Bangalore and Dr. Gurunatha Rao, Scientist, National Geophysical Research Institute (NGRI), Hyderabad for the many fruitful discussions. We deeply appreciate the help rendered by the officials of Tamilnadu Pollution Control Board (TNPCB), Chennai during our field visits.

We deeply acknowledge and appreciate the help we received from our past and present students: Mr. J. Jeya Singh, Dr. T. Shashidhar, Mr. V. Somasundaram, Mr. P. Balasubramanian, Ms. Nisha Nandanan, and Mr. G. Sivaprakash. This project could not have been completed successfully without their contributions in conducting experiments and development of computer codes. We place on record our appreciation to Mr. D. Kumaran, Project Associate in the EWRE Division of Department of Civil Engineering, IIT Madras for being there for us whenever we needed him.

We are also grateful to Indian Institute of Technology Madras for providing all necessary infrastructures to carry out this project work.

LIST OF TABLES

LIST OF FIGURES

EXECUTIVE SUMMARY

There is an urgent need to find cost-effective and environmentally friendly techniques for remediation of chromium contaminated aquifers. In-situ bioremediation is an attractive alternative for this purpose. To achive this objective**,** bacterial strains were isolated and enriched from the contaminated site of Tamil Nadu Chromates and Chemicals Limited (TCCL) premises, Ranipet, Tamilnadu, India. The strain which was isolated from the highly contaminated location had shown high Cr(VI) reduction potential. Cr(VI) reduction was evaluated both in aerobic and anaerobic conditions. Though the aerobic system performed better than the anaerobic one, further study were carried out in the anaerobic condition due to its economic viability. At higher initial concentration, Cr(VI) reduction was not complete even after 108 hrs, however, specific Cr(VI) reduction, unit weight of Cr reduced/unit weight of biomass was greater at higher concentration. It was found that a bacterial concentration of 15$\pm$1.0 mg/g of soil (wet weight) 50 mg of molasses /g of soil as carbon source were required for the maximum Cr(VI) reduction. Cr(VI) reduction studies were also carried out with Chromium Reducing Bacteria (CRB), Sulphate Reducing Bacteria (SRB) and Iron Reducing Bacteria (IRB), individually and in combination. Biokinetic parameters such as maximum specific growth rate (μ_{max}), half saturation constant (K_s), yield coefficient (Y_T) and inhibition coefficient (K_i) for individual cultures were evaluated.

Bench scale soil column exp eriments were conducted to study the effectiveness of Cr(VI) containment in aquifers using in-situ bio-transformation. Batch adsorption studies were carried out to estimate the adsorption capacities of two different soils for Cr(VI) and Cr(III). Transport studies indicated that it would not be possible to contain Cr(VI) by adsorption alone. Transport and bio-transformation studies indicated that the pore velocity and the initial bio-mass concentration significantly affect the containment process. In-situ bio-remediation is effective in the case of silty aquifers. Cr(VI) concentration of 25 mg/L was effectively contained within 60 cm of a confined silty aquifer. Cr(VI) containment could be achieved in sandy aquifers when the pore velocity was very low and the initial augmented bio-mass was high. A bio-barrier of

approximately one meter width would be able to contain Cr(VI) if the initial Cr(VI) concentration is as much as 25 mg/L.

In-situ remediation of aquifers contaminated with hexavalent chromium is evaluated using pilot scale reactors (3.0 x 1.0 x 0.5 m) employing Cr(VI) reducing microbes isolated from a chromium contaminated site. In one of the reactors, a 10 cm wide portion of the reactor, at 75 cm from the inlet end, was filled with sand containing Cr(VI) reducing biomass to act as the bio-barrier. A constant Darcy velocity was maintained for flow of water through the reactor. Water samples were collected from inlet and outlet chambers, and from the monitoring wells periodically and were analyzed for Cr(VI), total chromium, and COD concentrations. Experiments were also conducted with reactive zones created by injection of bacteria and substrate through injection wells of 4 cm diameter. Results showed that Cr(VI) concentration was zero in wells located downstream of the biobarrier and in the influence zone of the well even after 75 days indicating that both technologies are effective in containing the plume.

A basic mathematical model for Cr(VI) reduction, COD utilization and biomass growth, by individual cultures as well as by a combination of two or three different cultures, for different initial Cr(VI), SO_4^{2-} and Fe(III) concentrations. The biokinetic parameters evaluated from one set of experiments for individual cultures were utilized in all the validation studies. The performance of the mathematical model in terms of the dimensionless modified coefficient of efficiency (E) indicated that the proposed model simulates the system behavior very well. This basic model was integrated with a transport and biotransformation model for Cr(VI) fate and migration in aquifers.

A one-dimensional mathematical model was initially developed based on one-dimensional advection-dispersion reaction equations for Cr(VI) and molasses in saturated, homogeneous porous medium. The transport of Cr(VI) and molasses was coupled with adsorption and Monod"s inhibition kinetics for immobile bacteria. It was found that this model was able to simulate the experimental results satisfactorily. Clay content and gasses released due to high microbial activity altered the hydro-geological

conditions in the system. In such cases, there was disparity between the numerically simulated and experimental breakthrough curves for Cr(VI) and molasses.

The one-dimensional mathematical model was extended to formulate a two-dimensional model for simulating transport and biotransformation of Cr^{6+} in aquifers. Mathematical model for the transport accounts for the two-dimensional advective-dispersive-reactive transport, along with adsorption and source/sink terms of Cr^{6+}, molasses and mobile bacteria, reactive equation for immobile bacteria, and ground water flow equations. Freundlich non-linear isotherm was adopted for adsorption term in the transport equations. Monod‟s inhibition kinetics was used to model the microbial growth. The governing equations for groundwater flow are discretized by Crank-Nicolson Scheme and are solved using the Newton-Raphson method. In the partial differential equations for transport, the advection part is discretized using Essentially Non-Varying Scheme with minmod limiter and the dispersion part is approximated by the second order central difference. The transport equations for chromium, substrate and bacteria are also discretized by Crank-Nicolson scheme and are solved using sequential iterative technique. This model is validated using the bench scale and pilot scale experimental results. Mathematical model satisfactorily simulated the complete Cr(VI) reduction in both biobarrier and reaction zones so far as the Cr(VI) concentration did not exceed 60 mg/L. Model also simulated the decrease in Cr(VI) reduction by the microbes when the Cr(VI) concentration exceeded 250 mg/L due to ininhibition effect. The applicability of the model, for studying effectiveness of reactive-zone method for chromium containment, is demonstrated through an illustrative example.

Optimal design of trench type bio-barriers for the containment of Cr(VI) in aquifers was also attempted. The management problem for the optimal design of bio-barriers was formulated. A simulation optimization code using Genetic Algorithms was developed for this purpose. The one-dimensional simulation model is linked with the Genetic algorithm to obtain the optimal solution. Based on the optimal solutions obtained, the design charts were prepared. The results presented here indicate only a general trend in the optimal design parameters.

Chapter 1

INTRODUCTION

Use of thousands of inorganic and organic chemicals increased since the advent of industrial revolution. Uncontrolled release of domestic and industrial effluents has contaminated the surrounding environment, including the groundwater resources all over the world (James, 1996; Langard, 1980). Contaminants which enter aquifers travel long distances along with the water and make the water unusable. Environmental aspects of groundwater resources have become a prime concern in the last few decades, and many aquifers have been designated as super fund sites for remediation (Riley et al., 1992). Also, more stringent regulations are being implemented by the regulating agencies for the storage and disposal of industrial wastes, fuels and chemicals in order to safe guard the groundwater (U.S. EPA, 1997).

There are many reports on the aquifers contaminated by hydrocarbons, heavy metals, nutrients, micro-organisms etc. (Fetter, 1993; Chen et al., 1992; Riley et al., 1992). Several sites / aquifers have been contaminated by highly toxic and mobile hexavalent chromium (Cr (VI)). Sukhinda valley in Orissa (India) is an example of a site where Cr (VI) contamination is of natural origin. Cr (VI) compounds are widely used in industries such as leather tanning, electroplating, stainless-steel and automobile manufacturing, pigment production and other industries (Patterson, 1985). Uncontrolled discharge of solid and liquid wastes from these industries has contaminated many aquifers. Hanford area of the Columbia River Basin in U.S.A., Vaniyambadi in Tamilnadu (India), and Jajmau in Kanpur (India) are examples of sites contaminated with Cr (VI) due to anthropogenic activities (Barnhart, 1997; CPCB, 1996).

Cr (VI) compounds are highly water-soluble and highly toxic thus necessitating the treatment of wastewater, soil, and sediment containing this pollutant. Trivalent chromium (Cr (III)), compounds are less soluble and less toxic than Cr (VI) compounds (Rai et al., 1989). Reduction of Cr (VI) to Cr (III) represents a means by which toxicity is reduced and removal of chromium is thus facilitated. The conventional treatment methodology for

soils and groundwater systems contaminated with hexavalent chromium includes excavation or pumping of the contaminated material, addition of a chemical reductant, precipitation, and sedimentation. These physical-chemical methods suffer from high costs associated with energy use, chemical addition, pumping, and excavation.

Bioremediation has been proven to be an effective, environmentally friendly and less expensive treatment option for remediation of aquifers contaminated with hydrocarbons (Shen and Wang, 1994; Jardine and Taylor, 1995; Ganguli and Tirupathi, 2002). Biotransformation is the process by which a highly toxic compound is converted to less toxic/no toxic compound using biological process. This process can be aerobic/ anaerobic/ anoxic or combination of these three, based on the microorganisms. It has been reported that several microorganisms, under various environmental conditions, can reduce Cr (VI) to Cr (III) very effectively. This process depends on carbon source, pH, temperature, dissolved oxygen, ORP, and presence of other oxyanions and metal cations (Chen and Hao, 1998).

Aquifer remediation by biotransformation can be achieved by either in-situ or ex-situ methods. Ex-situ methods involve pumping the contaminated water and treating at the ground level, using appropriate biological process. In-situ techniques involve biotransformation of Cr (VI) to less toxic and less mobile Cr (III), leading to the containment of the contaminant in the aquifer itself. In-situ method involves either the enhancement of native chromium reducing bacteria (bio-stimulation) or bio-augmenting the groundwater with enriched Cr (VI) reducing bacteria. Mobility of a contaminant plays a major role in in-situ bioremediation technique (Chapelle, 1995). If the contaminant mobilization is very slow then the opportunity time is high for biotransformation process, which makes aquifer remediation more effective. High mobilization of contaminants on the other hand, makes the in-situ bioremediation ineffective. Thus a good understanding of the subsurface transport (advection and dispersion) processes along with chemical (adsorption, ion exchange, precipitation etc.) and biochemical reactions is essential for designing the optimal bioremediation strategy. Mathematical models can be used as effective tools for this purpose. They can also be used for management and design of remediation processes for contaminated aquifers (Minsker and Shoemaker, 1998).

Many earlier works on the transport of Cr (VI) concentrated on understanding only the advection, dispersion, adsorption and geo-chemical processes in different soils through batch and continuous column studies (Tokunaga et al., 2001; Weng et al., 2002; Jardine et al, 1999). There were also several batch studies on biotransformation of Cr (VI) to Cr (III) under various environmental conditions (Chen and Hao, 1996; Komori et al., 1989; Philip et al., 1998; Ohtake et al., 1990). Only recently, combined transport and biotransformation studies have been reported (Guha, 2004). In these studies, the focus has been the transport of Cr (VI) through saturated sand column under the influence of adsorption and biotransformation. So far, no study has truly considered the effectiveness of Cr (VI) containment in aquifers under different hydro-geologic conditions. Though many mathematical models are available for transport and biotransformation of pollutants like hydrocarbons, nitrates etc. (Chen et al., 1992; Haran et al., 1997; Mayer et al., 2002), only a few models focused on the transport and transformation of Cr (VI) in aquifers (Guha, 2004, Hossain et al., 2005b).

Several of the recent research studies have focused on the engineered passive bio-reactive barrier technology as it is becoming popular at commercial scale to manage contaminated soil and groundwater risks (Kalin 2004). Borden et al. (1997) reported a field study for control of BTEX migration using a biologically enhanced permeable barrier. Warith et al. (1999) conducted laboratory experiments for the development of an in situ microbial filter for the remediation of groundwater contaminated with naphthalene. Puls et al. (1999) conducted a small-scale field test to evaluate the in situ remediation of groundwater contaminated with chromate using permeable reactive barrier of a mixture of Fe^0, sand, and aquifer sediment. Kao et al. (2001) conducted laboratory experiments for development of a bio-barrier for the remediation of PCE-contaminated aquifer. The proposed bio-barrier system included a peat layer to enhance the anaerobic reductive dechlorination of PCE in situ. Vogan et al. (1999), Delvin et al. (2004), and Birke et al. (2003) conducted experiments and obtained optimal parameters for the design and the performance evaluation of permeable reactive barriers for different VOCs, under various conditions. Wilkin et al. (2005) studied geochemical and microbiological factors that control long-term performance of subsurface reactive barriers.

Construction and operation of the bio-barriers is costly, involving large volume of earth work, mixing of the soil with appropriate microbes, backfilling of the trench and continuous feeding of aquifer with the substrate required for the microbial growth. In any bio-augmentation problem, the design variables that need to be determined are length of the bio-barrier (L), initial microbial concentration (M_0) and the substrate to be provided for the microbial growth (S_0). A good understanding of the subsurface transport (advection and dispersion) processes along with chemical (adsorption, ion exchange, precipitation, etc.) and bio-chemical reactions is essential for optimal design of the bio-barriers.

Optimal design of groundwater remediation systems has become an active area of research in the last several years (Yoon 1999; Zheng and Wang, 1999; Shieh and Peralta 2005). A variety of optimization methods have been used for this purpose. Computational performances of eight such optimization algorithms were compared by Yoon (1999). Results showed that no one algorithm is consistently the most accurate on all the problems. Maskey et al. (2002) have developed a ground water remediation strategy using Global Optimization Algorithms, for pump and treat systems. Hu et al. (2006) have developed a dynamic predictive control system for in situ bioremediation process. This control system includes an optimization tool that consists of a simulation model and an optimization function. Shieh and Peralta (2005) developed a model combining genetic algorithms and simulated annealing with BIOPLUME II for the optimal design of bioremediation systems. Liu and Minsker (2004) developed full multi-scale approach to exploit interaction between partial differential equation (PDE) discretization and optimization, and achieved significant computational saving.

Literature review revealed that although many generic simulation-optimization packages are available for optimal design of aquifer remediation strategies, most of them have been applied to the case of pump and treat method. Very few attempts are made on the optimal design of trench type bio-barrier, especially for the containment of Cr (VI) in contaminated confined aquifers

The present work focused on understanding the transport and biotransformation of Cr(VI) in contaminated aquifers through batch experiments, bench- scale column studies, pilot

scale studies including bio-barriers and reactive zones. The data from batch experiments was used to propose a mathematical model for simulating the processes of Cr(VI) reduction, substrate consumption and bacterial growth during the bio-transformation of Cr(VI) to Cr(III) in presence of molasses and bacteria. This model was developed not only for bio-transformation by chromium reducing bacteria (CRB) alone but also for bio-transformation of Cr(VI) to Cr(III) by CRB, iron reducing bacteria (IRB), and sulphate reducing bacteria (SRB) in presence of molasses, Fe and suphates. The reaction model was then used to develop a one-dimensional transport and transformation model based on the numerical solution of advection-dispersion-reaction equation. This one-dimensional model was validated using the bench-scale column experiments conducted as part of this study. The proposed model was then extended to the case of two-dimensional transport and transformation that would occur when contaminated aquifers are remediated using either the bio-barrier technology or the reaction zone technology. The two-dimensional mathematical models are applicable for both confined and unconfined aquifers. These mathematical models were validated using the pilot scale experimental studies carried out as part of this project. It was demonstrated how the proposed mathematical models can be linked to optimization models in a simulation-optimization framework in order to arrive at an optimal design of bio-barriers. The mathematical models were also applied to study the viability of reaction zone technology for remediating contaminated aquifers. These results are being used at present to design and operate a field level pilot study for remediating chromium contaminated aquifer in Ranipet: a project which is being funded by Central Pollution Control Board (CPCB).

Chapter 2

LITERATURE REVIEW

2.1 CHROMIUM: PHYSICAL AND CHEMICAL PROPERTIES

Chromium is one of the most abundant elements on earth and it ranks 21 in terms of availability (Barnhart, 1997). Chromium concentration in earth‟s crust ranges from 100 to 300 µg/g. In fresh waters, chromium concentration varies from 0.1 to 0.5 mg/L. Chromium has the following characteristics: atomic weight, 52; atomic number, 24; density, 7.2; melting point, 1857 ± 20°C; boiling point, 2.672°C; crystalline form, steel-gray, cubic, very hard; oxidations states mainly +2, +3, +6. The quite unstable divalent (chromous) ion is rapidly oxidized to the trivalent (Cr (III), chromic) form. Hexavalent chromium (Cr (VI), chromates) compounds are oxidizing agents. Chromic acid is also a hexavalent compound. Natural chromates are rare and they enter into the various environmental compartments due to anthropogenic activities. Rai et al. (1986; 1987) and Reddy and Chinthamreddy (1999) observed that Cr^{3+}, $Cr(OH)_3^0$ and $Cr(OH)^-_4$ are the main aqueous chromium species in low Eh environments. These Cr^{3+} species are dominant only at pH lower than 3.6, and it is rare to find polymeric species such as $Cr_2(OH)^{4+}_2$, $Cr_3(OH)^{5+}_4$ and $Cr_4(OH)^{6+}$ in natural systems. Under oxidizing conditions, aqueous chromium exists as anion, specifically $HCrO_4^-$, $Cr_2O_7^{2-}$ and CrO_4^{2-}, depending on the pH. Reduction of Cr (VI) to Cr (III) is of significance as far as toxicity is concerned. Chromium in biological materials is most likely to be found in trivalent form, except shortly after exposure to Cr (VI) compounds. Thus, it is unsafe for humans to directly get exposed to Cr (VI) compounds, but they can consume plants and animals that have been exposed to Cr (VI), as Cr (VI) would have been reduced to Cr (III) in these organisms (Horitsu et al., 1987; Bopp and Erhlich, 1988).

Cr (III) predominates as ionic species (i.e., Cr^{+3}) at pH values less than 3.0. At pH values above 3.5, hydrolysis of Cr (III) in a Cr (III) water system yields trivalent chromium

hydroxy species [$CrOH^{2+}$, $Cr(OH)_2^+$, $Cr(OH)_3^o$, and $Cr(OH)_4^-$]. $Cr(OH)_3$ is the only solid species, existing as an amorphous precipitate (Palmer and Wittbrodt, 1991). In wastewater and/or biological reactors, when Cr (III) is in excess or in comparable concentration to that of the organic compounds, no significant modification of its solubility behavior is expected (Remoundaki et al., 2007). The solubility of Cr (III) is significantly enhanced when the concentration of organic compounds in wastewater is 10 fold or higher than that of Cr (III) (Yang and Fan, 1990). Under these circumstances, treatment schemes based on Cr (III) precipitation have a limited effect on Cr (III) removal (Remoundaki et al., 2007).

2.1.1 Redox Behaviour of Chromium

Biotic and abiotic oxidation – reduction reactions regulates the distribution between Cr (VI) and Cr (III) in aqueous systems. Figure 2.1 shows the Eh-pH diagram for chromium solutions in equilibrium with $Cr(OH)_3(s)$. The redox transformation of Cr (III) to Cr (VI) or vice versa can only take place in the presence of another redox couple, like H_2O/O_2 (aq), Mn(II)/Mn(IV), NO_2/NO_3, Fe (II)/Fe(III), S^{2-}/SO^{2-}_4 or CH_4/CO_2 which either accepts or donates the necessary electrons in the transformation of Cr (VI) to Cr (III) or vice versa (Richard and Bourg, 1991).

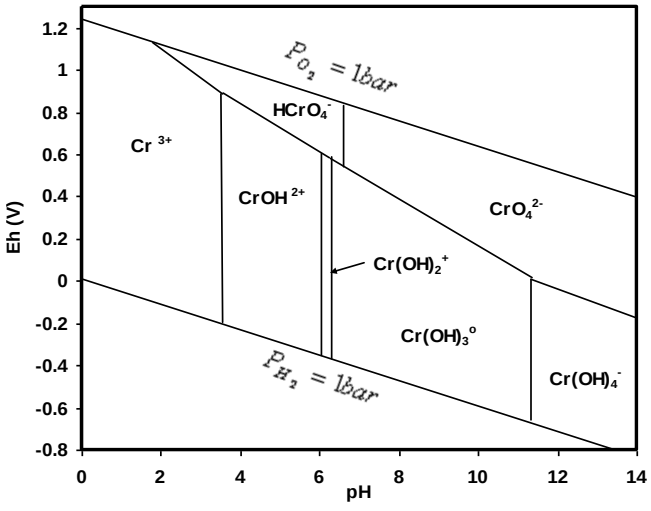

Fig 2.1: Eh-pH diagram for chromium (Palmer and Wittbrodt, 1991)

Reduction of Cr (VI) is also possible in presence of sulfides and Fe (II). Sulphate and organic matter, most commonly found in industrial wastes, can enhance the Cr (VI) reduction. Sulphates reduced to sulphides in presence of organic matter, which can reduce most of the Cr (VI) rapidly within 5min, and the reaction gets completed within a day. Cr $(OH)_3$ gets precipitated under neutral to alkaline conditions within 2 min. In acidic conditions, Cr (VI) can directly reduce in presence of organic matter such as simple amino-acids, humic acid, and fulvic acid. In these reactions, intermediate Cr (V) species are produced, which ultimately get converted to Cr (III) in a few days. Cr (III) can be oxidized to Cr (VI) in presence of dissolved oxygen, but the rate of oxidation at room temperature is insignificant (Rai et al., 1987). Studies on interaction of dissolved oxygen with Cr (III) revealed that there is no oxidation of Cr (III) to Cr (VI) even after 24 days at a pH of 12.5. Naturally occurring manganese oxides are responsible for Cr (III) oxidation in aquatic environments (Barlett and James, 1979; Johnson and Xyla, 1991; Manceau and Charlet, 1992).

2.2 SOURCES AND USES OF CHROMIUM

2.2.1 Natural Sources

Chromium is found in nature primarily as chromite ore with chromium in the trivalent form. Chromite and other minerals are formed when magma cooled inside the earth‟s crust. These minerals might have undergone changes to form rocks. These rocks get weathered and mixed with water under specific environmental conditions and get transported in both surface and subsurface waters. Chromium enters the atmosphere along with other gasses during volcanic eruptions.

2.2.2 Anthropogenic Sources

Chromite ore is used for the manufacturing of monochromates, dichromates, chromic acid, chromium pigments, and chromium metal. Chromium and its salts have a wide range of applications in the chemical industry, graphics industry, artistic paints, anticorrosion paints, electroplating, steel alloys, stainless steel (SS) welding, and a multitude of other operations (Budavari, 1996). Anthropogenic sources of chromium are

the wastes from these industries. The tanning industry is an important consumer of chromium for many years for the stabilization of hides. Large volumes of effluents containing chromium together with organic matter are generated in tanneries. There are millions of SS welders worldwide and SS welding may, at present, be the most common source of human exposure to chromium in the workplace (Wang and Li, 2006). Table 2.1 gives the important uses of chromium in various industries and the characteristics of wastewater generated from such industries.

Table 2.1 Important uses of chromium in various industries and the effluent characteristics.

S.No	Name of the industry	Important uses of chromium	Effluent Characteristics
1	Wood preservative	Oxidising agent	Cr (VI), C(III), COD, phenolic compounds
2	Metal finishing\ Electroplating with chromium	Catalysis	High concentrations of Cr (VI), CN, Low pH values
3	Leather tanning and finishing	Ceramic coatings	Cr (VI), C(III), High COD and BOD, suspended solids
4	Textile mordants	Safety matches	Cr (VI), C(III), COD, Colour
5	Magnetic tape	Glues and adhesives	Cr, Cu, Hg, Pb, Ni, Zn and COD
6	Colored glass	Enchant for plastics	Cr (VI), C(III), COD, Si.
7	Paints and pigments	Abrasives and refractories	Cr (VI), C(III), COD, organic maters

8	Pulp and paper	-	Cr, Cu, Hg, Pb, Ni, Zn and COD

Source: Mohan and Pittman, (2006); Manivasakam, (1987).

Many industrial wastewaters, such as those coming from tanneries, textile, paints and pigments, pulp and paper and wood processing industries, contain high organic matter along with Cr (VI) (Khan and Mahmood, 2007). Presence of high organic matter along with Cr (VI) can also occur when wastewaters from more than one industry are mixed.

2.3 CHROMIUM TOXICITY

2.3.1 Chromium toxicity on humans

Hexavalent chromium is highly toxic and carcinogenic. It causes mutagenic effects in both humans and animals. Compared to Cr (VI), trivalent chromium is less toxic. Hexavalent chromium is classified as an EPA Group A pollutant (human carcinogen) for inhalation and a Group D pollutant (not classifiable as to human carcinogenicity) for the oral route of entry. Toxicity levels were developed through human and rat studies (Grevatt, 1998). Exposure to Cr (VI) was found to increase the risk of lung cancer. Asthma, bronchitis, and nasal irritation are potential health hazards due to the inhalation of hexavalent chromium compounds. It is reported that there is an excess mortality from lung cancer where workers are exposed to hexavalent chromium, including stainless steel welders, although welders are also exposed to other carcinogens apart from Cr (VI). Dermal contact may also occur during occupational exposure. Dermal contact results in dermatitis and skin ulcerations (De Camp, 2006). Nishioka (1975) performed mutagenic assays in presence of a reducing agent like sodium sulphite and observed that this caused the dichromate to lose its mutagenic activity. He suggested that the oxidised state of Cr (VI) was required for its toxicity. Nakamuro et al (1978) also investigated the comparative cytogenic and mutagenic effects between Cr (VI) and Cr (III). Further studies undertaken by Lofroth and Ames (1978) showed that Cr (III) was required at

concentrations 1000 times greater than Cr (VI), to obtain similar mutation frequency. They also observed that the mutagenic activity of Cr (VI) was lost after treating the samples with rat liver microsomes. The metabolic deactivation, after the addition of the reducing chemicals can be attributed to the reduction of toxic Cr (VI) to Cr (III) form which is neither toxic nor mutagenic (Venitt and Levy, 1974). It is generally considered that Cr (VI) is 10-100 times more toxic than Cr (III) when both are administrated orally. High dosage of Cr (VI) compounds also causes nephro toxicity. A dose greater than 1750 mg/L of potassium dichromate is generally required to sensitize persons to Cr (VI) (Myers, 1998).

2.3.2 Chromium toxicity in microorganisms

Microorganisms are sensitive to the effects of heavy metal pollution like other components of the ecology. Soil micro-flora may play a key role in the modification of heavy metals added to the soil through antropogenic activities. Toxic effects of chromium on bacteria and algae have been reviewed by Wong and Trevors (1988). The growth of Chlorella vulgaris was unaffected by 45-100 mg/L of Cr (III) or Cr (VI), whereas no growth of Scenedesmus acutus was detected at concentrations of chromium higher than 15 mg/L. However, Brady et al. (1994) reported the growth of Scenedesmus and Selenastrum with 100 mg/L of Cr (III) but not with 100 mg/L of Cr (VI). The mechanism responsible for different sensitivities to chromium in algae is not yet elucidated. A lengthening in the lag phase induced by Cr (VI) and a decreased growth rate caused by Cr (III) have been observed in Euglena gracilis. Inhibition of growth in Euglena correlates with the arrest of cells in the G-2 phase of the cell cycle and inhibition of respiration and photosynthesis were also reported. Cr (VI) also induced alterations in the cytoskeleton, which may be involved in the loss of motility. Inhibition of photosynthesis by chromium has also been reported for Chlorella and Scenedesmus. Light-grown Euglena cells were more sensitive to Cr (VI) than dark-grown cells. Lower concentrations of chromium were well tolerated in both culture conditions. In estuarine algae, Cr (VI) toxicity is inversely proportional to salinity. In Scenedesmus, Cr and Cu showed a synergistic effect with Cd for growth inhibition. In S. cerevisiae, chromate toxicity was stronger in cells grown in non-fermentable carbon sources than in those grown in fermentable substrates; other effects included inhibition of oxygen uptake and induction of petite mutations. These

results suggest that chromate targets specifically the mitochondria of S. cerevisiae. Additional effects of chromium in S. cerevisiae include gene conversion and mutation (Dayan and Paine, 2001). Cr (VI) accumulated by organisms is reduced to Cr (III) with the concomitant production of intermediate Cr(V) and Cr(IV) products, oxygen and carbon based radicals (Cervantes et al., 2001; O' Brien et al., 2001; Ackerley et al., 2004). These species are known to be associated with a spectrum of DNA lesions occurring during Cr (VI) exposure (Aiyar et al., 1991; Luo et al., 1996; O' Brien et al., 2002; Reynolds et al., 2004), many of which are oxidative in nature.

2.3.3 Chromium toxicity in plants

Cr (VI) produces serious damage to living cells. However, Cr (III) is less toxic because of its extremely low solubility, which prevents its leaching into groundwater or its uptake by plants. However, studies in plants have shown that Cr (III) also produces serious problems in living tissues, although at higher concentrations than Cr (VI). Barley seedlings grown with 100 µM of Cr (III) showed 40% of growth inhibition whereas, inhibition caused by the same concentration of Cr (VI) reached up to 75% in shoots and 90% in roots (Skeffington et al., 1976).

2.4 FATE OF CHROMIUM IN AQUATIC ENVIRONMENTS

2.4.1 Mobility of Chromium

Mobility of contaminant depends on the solubility. Solubility of chromium varies with its oxidation state, redox chemistry and nature of solids (adsorbent) present in the aquifer. The hydro-geochemical cycles of chromium are mainly controlled by the local environmental conditions.

Cr (III) is mostly immobile in natural systems and readily precipitate in neutral to alkaline pH range. As a result, dissolved Cr (III) concentrations are relatively low in natural aquatic environments. In neutral to slightly acidic waters, Cr (III) is highly adsorbed to soil and can be contained easily. Under acidic conditions (pH<5), the dissolved Cr (III) concentration can be higher and it can easily migrate. Cr (III) can form complexes with organic matter present in nature, and can enhance migration by inhibiting

precipitation and adsorption (Gerritsee et al., 1982). Very rarely Cr (III) can be solubilized following surface oxidation in the presence of solid MnO_2.

Hexavalent chromium exists as anion, which is highly mobile in water. Under acidic and oxidizing conditions, presence of Fe (II) and dissolved organic matter reduces Cr (VI) to Cr (III), which is rapidly precipitated or sorbed to soil. In presence of competing background anions under alkaline environment, the effect of adsorption process reduces significantly, which keeps Cr (VI) in highly mobile condition (Eary and Rai, 1987).

2.4.2 Adsorption of Chromium on Natural Solids

Chromate ions can be adsorbed by the oxides of Mn, Al and Fe, clay minerals, natural soils and colloids (Rai et al., 1986; Zachara et al., 1987). Adsorption of Cr (VI) is a surface complexation reaction between aqueous chromates and hydroxyl-specific surface sites. Each Cr (VI) surface complex covers 3-4 hydroxyl surface sites, which are pH dependent. Irrespective of adsorbent, Cr (VI) adsorption increases with decrease in pH.

Increase in chromate concentration decreases the fractional adsorption, but increases the adsorption density. A larger ionic strength decreases the adsorption of chromate, which may be due to lowering in CrO^{2-}_4 activity, reduction in columbic attraction for chromate species on solid surfaces and/or the presence of competing anions. Cations such as K^+, Ca^{2+}, Mg^{2+} can compete with hexavalent chromium and slightly influence the Cr (VI) adsorption. Cation sorption enhances the positive surface charge and favours electrostatic adsorption of anions. Competition between chromates and other heavy metals such as Cd^{2+}, Co^{2+}, Zn^{2+} for surface sites is insignificant and has no effect on adsorption. In systems where metal binding is enhanced, a secondary surface phase like iron chromate may form (Rai et al., 1986; Reddy and Chinthamreddy, 1999).

Presence of other anions can significantly change the Cr (VI) adsorption. The competing effect depends on (i) dissolved concentrations of the competing anion and CrO^{2-}_4, (ii) relative affinities of anions and CrO^{2-}_4 for the solid surface and (iii) surface site concentration. Richard and Bourg (1991) found that adsorption characteristics varied with pH of the solution. At lower pH value, anions such as Cl^-, NO^{3-}, SO^{2-}_4, HCO^{3-}, $H_2SiO^{2-}_4$, phosphate mixture (HPO^{2-}_4 /$H_2PO^-_4$, 1:1) and MoO^{2-}_4 reduced the adsorption of Cr (VI).

Adsorption of chromates on soils follows a two step reaction rate (Amacher et al., 1988). It is observed that faster reversible reactions reach equilibrium within 24 h. However, the overall chromium retention reaction does not reach complete equilibrium even after 2 weeks. This may be due to irreversible or slow reversible reactions such as co-precipitation or internal diffusion (Amacher et al., 1986). Adsorption of Cr (VI) can be influenced by electrostatic condition imposed by several common anions that are bound to soil surface, which may be the cause for minimal Cr (VI) adsorption in ground water.

2.5 TREATMENT OF CHROMIUM CONTAMINATED GROUNDWATER

Groundwater can become contaminated with metals directly by infiltration of leachate from land disposal of solid wastes, sewage or sewage sludge; leachate from mining wastes; seepage from industrial lagoons; and spills and leaks from industrial metal processing or wood preserving facilities. Numerous waste and site conditions control and influence the leachability of the metals and wastes and their transport into groundwater.

At many industrial and waste disposal locations, chromium has been released to the environment via leakage and poor storage during manufacturing or improper disposal practices (Palmer and Wittbrodt, 1991). Industrial applications most commonly use chromium in the hexavalent chromium [Cr (VI)] form, which is acutely toxic and very mobile in groundwater. Groundwater extraction and treatment has traditionally been used to remediate chromium-contaminant plumes. This method, while providing interception and hydraulic containment of the plume, may require long-term application to meet Cr (VI) remediation goals and may not be effective at remediating source-zone Cr (VI). The poor performance of pump-and-treat systems in the mid-1980s provides the driving force for research of subsurface processes in order to develop more efficient groundwater remediation strategies and techniques.

New information and treatment approaches have been developed for chromium-contaminated soil and groundwater treatment. A number of available in situ technologies or treatment approaches use chemical reduction and fixation for chromium remediation. These include geochemical fixation, permeable reactive barriers (PRBs) and reactive zones. Other types of in situ treatment that are under development include enhanced

extraction, electro kinetics, reactive zones, natural attenuation, phytoremediation and bio-transformation.

2.5.1 Geochemical fixation

The goal of this technology is to reduce Cr (VI) in groundwater and contaminated soil to the more thermodynamically stable Cr (III). In this treatment, Cr (VI) is reduced to Cr (III) by using reductants such as SO_2, $NaHSO_3$, and $Na_2S_2O_3$ (Palmer and Wittbrodt, 1991). Cr (III) is then immobilised onto aquifer solids by providing sufficient iron and manganese oxide adsorption sites with in the treatment zone. The technology is based upon the concept of extracting contaminated groundwater and treating it above ground, followed by reinjection of the treated groundwater into the aquifer. The reinjected groundwater is dosed with reductant to reduce any residual Cr (VI) contamination remaining in the interstitial water.

Extraction and injection wells are required to remove contaminated groundwater for above ground treatment and to reinject the treated and amended water into the treatment zone. Extraction wells from an existing pump-and-treat system can often be utilized. The aboveground system consists of the selected treatment apparatus for initial chromium removal, tanks for storing treatment chemicals and extracted and treated groundwater, and a reductant dosing system for the treated water. A sheltered area or building is needed to perform the on-site chemical tests, handle and prepare the chemical reductant, and to store spare parts such as backup pumps and valves. A significant advantage to using in situ geochemical fixation is that it has the potential to substantially reduce (up to 75 percent) the time required to remediate chromium-contaminated sites to meet cleanup goals, and thus reduce treatment (operating) costs.

2.5.2 Permeable reactive barriers

In this method, reactive barriers of permeable nature are installed as permanent, semi-permanent, or replaceable units across the flow path of a contaminant plume, which act as treatment walls. When the contaminated water passes through the reactive zone of the barrier, the contaminants are either immobilized or chemically transformed to non-toxic or less toxic compounds. These barriers can be designed either as funnel and-gate or as a continuous trench system (U.S.EPA, 1997a). In case of funnel and-gate system, flow of

contaminated waste is directed to a gate or gates, which connect the permeable reactive media by impermeable funnel, made of either interlocking sheet pilings or slurry walls. To capture the complete plume, the length of a funnel-and-gate system should be more than 1.2 to 2.5 times the plume width, depending on the funnel-to-gate ratio and the number of gates. In such barriers, it is easy to replace the reactive material. However, they are more susceptible to hydraulic uncertainties, which cause bypass of flow around the system (O" Hannesin, 1999). The continuous trench is simply a trench that has been excavated and simultaneously backfilled with reactive media. They allow the water to pass through the barrier under its natural gradient. Zero-valent reactive iron (Fe°) in combination with dithionite and zeolites are commonly used as reactive media in case of groundwater contaminated with hexavalent chromium (Cercona, 1995). The Schematic of a simple treatment wall system is shown in Fig. 2.2. The conceptual configuration of a permeable reactive barrier is shown in Fig. 2.3.

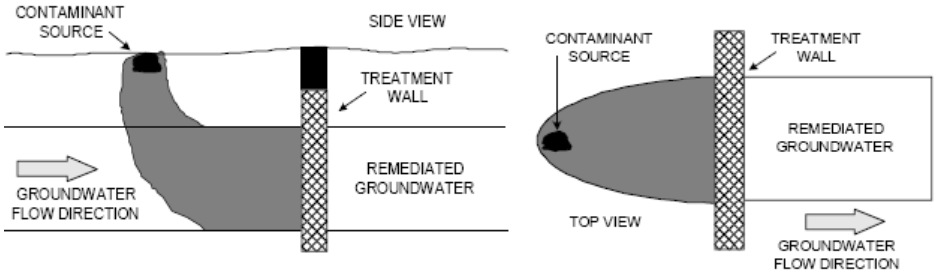

Fig. 2.2: Schematic of a simple Treatment Wall System

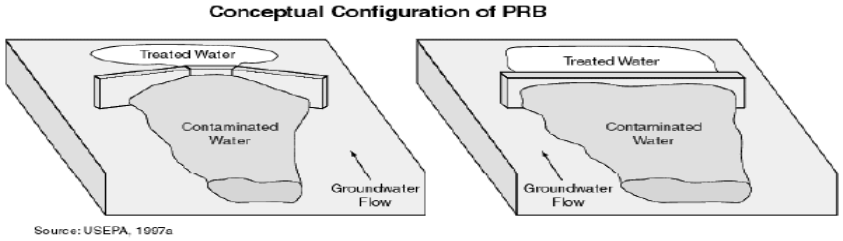

Plume capture by a funnel-and-gate system.

Plume capture by a continuous trench system

Fig. 2.3: Conceptual configuration of PRB

2.5.3 Reactive zones

The plan view of the in situ reactive zone is shown in Fig. 2.4.

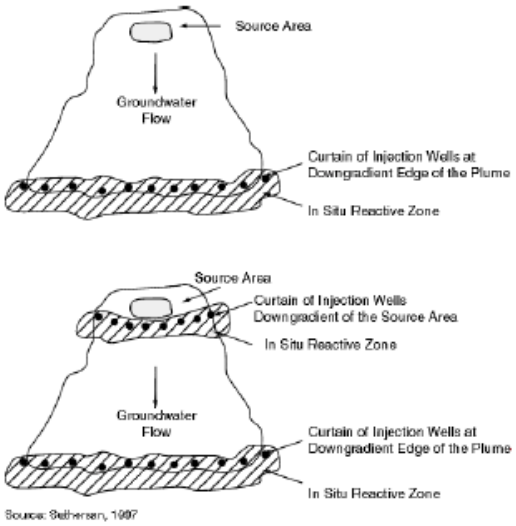

Fig. 2.4: In Situ reactive zones (plan view)

Reactive zones are subsurface zones where migrating contaminants are intercepted and permanently immobilized or degraded into harmless end products. These zones are established in-situ by injecting reagents and solutions in predetermined locations within the contaminated groundwater plume, and allowing them to "react" with the contaminants (US EPA 2000). These reactions can happen in different pathways, either abiotic or biotic or both. Abiotic pathways include oxidation, reduction, sorption and precipitation, where as biotically mediated processes include reduction, oxidation, precipitation, biosorption, bioaccumulation, bio-transformation, organo-metal complexation, and phyto-remediation (Suthersan, 1997).

2.5.4 Soil Flushing/Chromium Extraction

The schematic of in situ flushing system is shown in Fig. 2.5.

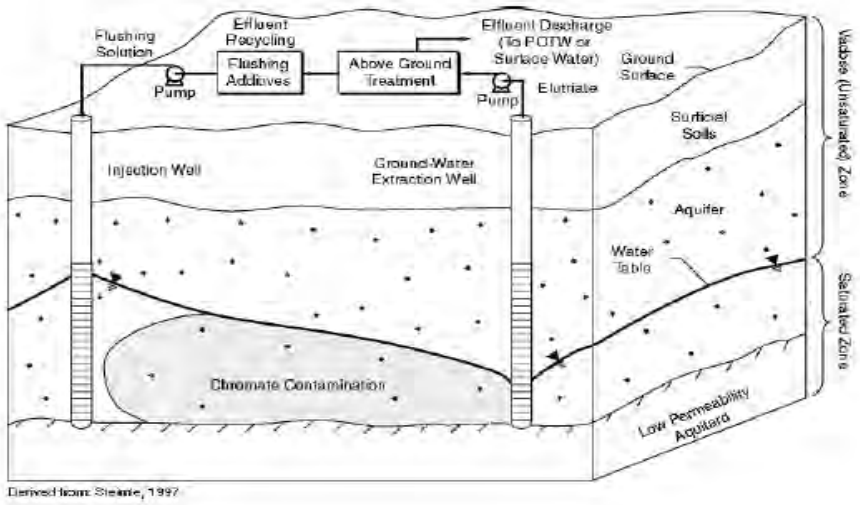

Fig. 2.5: Schematic of in situ flushing system

In this method, metals are leached out from the soils by flushing with water or aqueous solution by different methods like surface flooding, sprinklers, leach fields, vertical or horizontal injection wells, basin infiltration systems, or trench infiltration systems. In situ soil flushing is used to mobilize metals by leaching contaminants from soils so that they can be extracted without excavating the contaminated materials. The flushing solution is collected for disposal or treatment and reuse (US EPA 1997).

2.5.5 Natural Attenuation

Natural attenuation includes a variety of physical, chemical, or biological processes that, under favourable conditions, act without human intervention to reduce the mass, toxicity, mobility, volume or concentration of contaminants in groundwater. Biodegradation, dispersion, sorption, dilution, volatilisation, and chemical or biological stabilization, transformation, or destruction of contaminants is the common in situ processes. Natural attenuation is effective in sites where sorption and redox reactions are dominant mechanisms (USEPA1997, 2000).

2.5.6 Phyto-remediation

Remediation of contaminated soil and ground water by plants, which can take up, accumulate, and/or degrade inorganic and organic constituents, is called phyto-remediation. This is a proven technology for remediation of cadmium and mercury. It can be applied to the sites with low to moderate soil contamination over large areas, and to sites with large volumes of groundwater with low levels of contamination. This remediation is more effective if soil contamination is limited to within 1 m of the surface, and if groundwater is within 3 m of the surface (Miller, 1996).

2.5.7 Electro-kinetic Remediation

Ground water remediation by using electric current via electro-osmosis, electro-migration and electrophoresis is called electro-kinetic remediation. In this method, electrodes are placed in the ground and a direct current electric field is applied across the contaminated soil. In strong electric field, positive ions migrate to the negatively charged cathode and negatively charged ions move to the positively charged anode. Non-ionic species will be transported along with the electro osmosis-induced water flow. The quantity and direction of contaminant migration depends on its concentration, soil type and structure, the mobility of contaminant ions, the interfacial chemistry and magnitude of the electroosmosis-induced flow velocity (Virkutyte et al., 2002). This remediation can be done effectively in clayey soils under both saturated and unsaturated conditions. Removing chromium as Cr (VI) is much efficient than as Cr (III) (Reddy and Parupudi 1997; 1999; Reddy and Chinthamreddy, 1999; Sah and Chen, 1998). Alkaline condition is favourable to chromium species. Therefore, alkaline reagents can be injected to enhance the remediation. The effectiveness of remediation depends on the co-existing metals, and oxidizing and reducing agents present in the soil (Haran et al., 1996). Presence of humic acid enhances the migration of chromium towards anode (Reddy and Chinthamreddy, 1999). The efficiency of remediation gets reduced due to increase in temperature when high voltage is applied. Presence of carbonate, hematite, large rocks and gravel can also reduce the efficiency of remediation.

2.5.8 Vitrification

Vitrification has been successful in treating coal ash, municipal incinerator ash and sludges generated in waste water treatment plants, and the same can be extended to the treatment of heavy metals also. This process produces eco-friendly by-products and aggregates for the construction, road aggregate, decorative home products, and for tennis court surfaces. Meegoda et al. (1999; 2000) performed demonstration tests on soils from two chromium contaminated sites using cold top ex-situ vitrification technology. The vitrification furnace had three movable molybdenum or carbon resistance-heating electrodes. Before adding the contaminated soil, the furnace was filled with silica sand and mulcoa and the electrodes were inserted into the mix to initiate heating to obtain stable operating conditions. The "Cold Top" condition was maintained by feeding the soil from the top through a soil auger system and the exhaust gas was treated with an air pollution control system. This process converts contaminated soils into an essentially monolithic, vitrified mass.

2.6 BIO-TRANSFORMATION

Bio-transformation of Cr (VI) is considered a novel transformation alternative for Cr (VI) contaminated soil and groundwater. Many bacterial species can use Cr (VI) as an electron acceptor and reduce soluble and toxic Cr (VI) compounds to less soluble and less toxic Cr (III) compounds. The versatility of bio-transformation in terms of aerobic/anaerobic, air/water/soil applications, availability of thousands of species of microbes makes this process a preferred alternative. This option is used especially when environmental impact, range of pollutants, costs, and feasibility is of prime concern. Groundwater bio-transformation can be done in two ways: (i) natural attenuation/Bio-stimulation, and (ii) bio-augmentation. Bio-stimulation is a natural process that uses indigenous microorganisms to degrade the pollutants. In case of Bio-augmentation, enriched efficient microorganisms are supplied to the contaminated site and are grown under optimum conditions. The schematic representation of a permeable reactive bio-barrier is shown in Fig. 2.6.

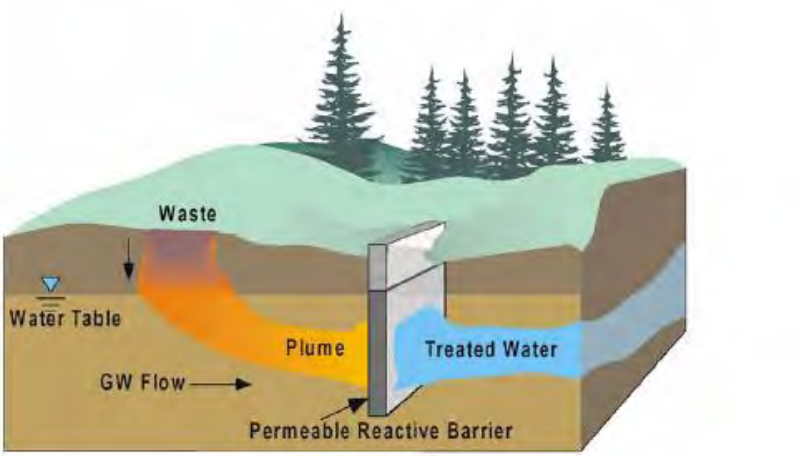

Fig. 2.6: Schematic representation of a permeable reactive bio-barrier

Many microbes were reported to reduce the Cr (VI) under a number of conditions and by a variety of species. Cr (VI) reduction mainly included representatives of the genera of Aeromonas, Escherichia, Pseudomonas, and Enterobacter. For the Cr (VI) reducing bacteria studied, two kinds of enzymatic mechanisms of Cr (VI) reduction have been proposed. The aerobic activity of Cr (VI) reduction is generally associated with a soluble protein fraction utilizing NADH as an electron donor either by necessity or for maximum activity. In most instances, the physiological functions of the electron flow to Cr (VI) through the soluble reductase have not been thoroughly examined. Bacterial respiration can utilize a number of inorganic compounds as terminal electron acceptors, including oxygen, nitrite, nitrate, sulfate, ferric and manganese. Organisms that are able to reduce Cr (VI) under aerobic conditions have been isolated by Bopp (1980), Ishibashi et al. (1990), Gopalan and Veeramani (1994), and Philip et al. (1998). Microbial reduction of Cr (VI) under aerobic process can be expressed as follows:

$$CrO_4^{2-} + 8H^+ + 3e^- \xrightarrow{CRB} Cr^{3+} + 4H_2O \xrightarrow{neutral\,pH} Cr(OH)_3(s) + 3H^+ + H_2O \qquad (2.1)$$

Romanenko and Korenkov (1977) were among the earliest researchers to isolate an organism from industrial wastewater, P. dechromaticans, which could use chromate and dichromate as terminal electron acceptors during anaerobic respiration. Labedeva and

Lyalikova (1979), Kvasnikov et al. (1985) and Gvozdyak et al. (1986) also identified number of organisms that utilize Cr (VI), generally chromate or dichromate, as a terminal electron acceptor during anaerobic respiration. The isolate of Streptomyces 3M obtained from the Cr (VI) contaminated soil could reduce 250 mg Cr (VI)/L in presence of glucose or NADH (Das and Chandra, 1990). Microbial chromium reduction activities were also found with bacteria from other Cr (VI) contaminated environments such as industrial sludge, industrial wastewaters and river sediments (Bopp, 1984; Kvasnikov et al, 1988; Gopalan and Veeramani, 1994).

Cr (VI) may also acts as a terminal electron acceptor through a membrane-bound reductase activity (Wang et al.,1989). Shen and Wang (1995) studied the biochemical characteristics and cellular location of Cr (VI) reductase as well as the possible involvement of the respiratory chain in Cr (VI) reduction activity. They have reported that the dissimilatory Cr (VI) reduction was mainly due to soluble reductase activity as a result of co-metabolism in E.coli ATCC-33456. The respiratory-chain linked electron transport was also involved in Cr (VI) reduction. The microbial reduction using acetate as electorn donor under anaerobic conditions can be expressed as

$$3CH_3COO^- + 8CrO_4^{2-} + 17H_2O \xrightarrow{CRB} 8Cr(OH)_3(s) + 6HCO_3^- + 13OH^- \quad (2.2)$$

There are evidences for both aerobic and anaerobic reduction of Cr (VI) by different microbes. P. ambigua G-1 reduced Cr(VI) rapidly during the early phase of the aerobic growth, from 150 to 60 mg Cr (VI)/L after 6h of cultivation (Horitisu et al., 1987) and there was no further significant reduction after 36h. Llovera et al. (1993) described that the strain of Agrobacterium radiobacter EPS-916 isolated from soil was sensitive to Cr (VI) under both aerobic and anaerobic conditions. However, the growing culture reduced 8.0 mg Cr (VI) /L anaerobically and only 2.6 mg Cr (VI)/L aerobically. The resting cells of this strain were able to reduce Cr (VI) completely at concentrations as high as 26 mg Cr (VI)/L.

P. fluorescencens LB-300 was isolated from chromium contaminated sediments of Upper Hudson river, New York (Bopp, 1980). The organism demonstrated plasmid-mediated chromate resistance above 1000 mg K_2 Cr_2 O_7/L and was capable of reducing Cr (VI) to Cr (III) both aerobically and anaerobically. Wang and Xiao (1995) isolated

Bacillus Sp. which could reduce Cr (VI) under aerobic conditions. Higher Cr (VI) reduction rates were observed with higher initial cell concentrations, but specific rate was higher at lower initial cell concentrations.

Chen and Hao (1996) had reported the Cr (VI) reduction by an anaerobically enriched mixed culture. Environmental factors including pH, temperature and other electron acceptor as well as waste characteristics affecting Cr (VI) removal capability were quantified. Komori et al. (1989), Chen and Hao (1996), Philip et al. (1998), and Ohtake et al. (1990), among others, have studied the effect of biomass density, initial Cr (VI) concentration, carbon source, pH, temperature, dissolved oxygen, oxidation reduction potential, presence of other oxyanions and other metal cations, on Cr (VI) reduction.

Earlier studies have identified many bacterial strains for the Cr (VI) reduction. However, the practical applications are limited by the facts that high initial concentrations of Cr (VI) can cause significant deactivation of the introduced microorganisms. Also, Cr (VI) polluted streams and soils often contain additional toxic compounds which severely inhibit Cr (VI) reduction. Komori et al. (1989) tried a dialysis bag reactor in which the cells of E. cloacae HOI were placed in a semi permeable bag that was submerged in the Cr (VI) containing solution. Fujie et al. (1994) tried to develop a fed batch reactor using E.cloacae HOI for the reduction of hexavalent chromium in which they added very small doses of Cr (VI) to reduce the toxic effects on the microbes. Chen and Hao (1997) have attempted Cr (VI) removal in an anaerobic hemostat fed with acetate containing medium. With the influent containing 26 mg/L Cr (VI), a nearly complete removal of Cr (VI) was achieved at dilution rates of 0.15 and 0.32/d at 20 ^{o}C and 35 ^{o}C, respectively. Philip et al. (1999) tried an immobilized microbial reactor employing Bacillus coagulans cells for the reduction of Cr (VI). As the Cr (VI) reduction capacity of the cells was limited, intermittent addition of fresh immobilized cells was required in order to maintain a high Cr (VI) reduction efficiency in the reactor.

2.7 TRANSPORT STUDIES

2.7.1 Transport of Cr (VI) without Biotransformation

2.7.1.1 Experimental Studies

Transport of heavy metals in subsurface media depends on their retention behaviour in soils. Fuller (1977), Alesii et al. (1980), Dowdy and Volk (1983), Ellis et al. (1983) Kabata-Pendias and Pendias (1984), and Selim (1990) studied the retention-release and leaching of heavy metals in soils. They observed that physical and chemical properties of soils influence the fate of heavy metals in the soil environment and their potential leaching to ground water supplies. Amacher et al. (1988) investigated the interactions and mobility of Cr (VI) in six varieties of soils using 4.4 cm diameter and 6.35 cm long columns. Kent et al. (1994) conducted tracer tests for Cr (VI), Se(VI), and dissolved oxygen in a shallow, sand and gravel aquifer with mildly reducing conditions. Loss of chromium occurred along with slight retardation of Cr (VI), probably due to reduction of Cr (VI) to Cr (III) and irreversible sorption of Cr (III). Kent et al. (1995) conducted field transport experiments in anoxic, sand and gravel aquifer using Br, Cr (VI), Se(VI), and other tracers. Within analytical errors, all mobile chromium was present as Cr (VI). Adsorption of chromium onto aquifer sediments caused retardation. Breakthrough curves for chromium had extensive tails. Friedly et al. (1995) conducted studies to obtain a quantitative description of the gradual disappearance of Cr (VI) from groundwater in a small scale field tracer test and in batch kinetic experiments using aquifer sediments under identical chemical conditions. Jardine et al. (1999) investigated the coupled hydrologic and geo-chemical processes on the fate and transport of Cr (VI) in undisturbed soil cores of 14.5 cm length and 8.5 cm diameter, obtained from a proposed solid waste dumping site. They showed that presence of surface bound natural organic matter under highly acidic field soils can significantly influence the mobility of Cr (VI). Guha et al. (2001) examined how the process of advection, dispersion, oxidation-reduction, and adsorption of Cr (VI) combine to affect the transport of Cr (VI) in the presence of β-MnO_2. Columns of length 4.2 cm and of diameter 1 cm were used to conduct the experiments, in which sand was coated with β-MnO_2. Weng et al. (2002) conducted similar studies for Cr (VI) transport to understand the leaching characteristics

of soils rich in chromate ore processing residue. Columns in their experiments were 1.9 cm in diameter and had a hydraulic head of 13 cm. Buczko et al. (2004) conducted similar studies for chromium transport in the unsaturated zone.

2.7.1.2 Mathematical models

Several mathematical models have been developed in the past to simulate the transport of Cr (VI) through saturated and unsaturated media. Sidle et al. (1977) were among the first to develop a mathematical model, using advection-dispersion equation, for the transport of Cu, Zn and Cd in a sludge-treated forest soil where sorption was assumed to be reversible and in nonlinear equilibrium. Amacher et al. (1988) proposed four general purpose multi-reaction, multi-site kinetic type models for describing the heavy metal retention and mobility mechanisms. Friedly et al. (1995) developed a model to obtain a quantitative description of the gradual disappearance of Cr (VI) from groundwater in a small scale field tracer test and in batch kinetic experiments using aquifer sediments under similar chemical conditions. Multi reaction transport model (MRTM) developed by Selim et al. (1990) was used to explain the data obtained from the column experiments. Jardine et al. (1999) simulated the experimental breakthrough curves of Cr (VI) in undisturbed soil cores using MRTM model developed by Selim et al. (1990). Guha et al. (2001) developed a model for the transport of Cr (III), Cr (VI) and dissolved oxygen. This model incorporates advection, dispersion and first order kinetic adsorption of the reduced and oxidized chromium species. Mayer et al. (2001) applied a multi-component reactive transport model to study the processes taking place in a permeable reactive barrier near Elizabeth City, North Carolina, U.S.A. The reactive barrier containing zero valent iron was emplaced to remediate groundwater contaminated by Cr (VI) and chlorinated solvents. Their model considered the treatment of contaminants, the reduction of other electron acceptors, microbially mediated sulphate reduction, the precipitation of secondary minerals and degassing of hydrogen gas, within the barrier. Transport model MIN3P was used by Mayer et al. (2001) to the site specific conceptual model to obtain the numerical simulation results. Results of the above study indicated that reactions other than remediation reactions may significantly affect the water

chemistry in the barrier. Weng et al. (2002) simulated the Cr (VI) leaching experiments using a one-dimensional transport model.

2.7.2 Transport of Cr (VI) with Biotransformation

2.7.2.1. Experimental studies

Cr (VI) bio-reduction and transport through the subsurface porous media is a highly dynamic process, which depends on the hydrogeology of the aquifer. Recently, Guha et al. (2003) conducted combined transport and biotransformation experiments in sand columns. This study focused on bio-reduction of Cr (VI) by Shewanella alga Simidu (BrY-MT) in the presence of pyrolusite (β -MnO2) coated sand. They monitored the breakthrough data for Cr (III), Cr (VI), lactate, and protein. Hossain et. al (2005a), and Alam et al. (2006) conducted column experiments to evaluate the effect of feed concentration on Cr (VI) reduction under fumarate reducing conditions. An overall Cr (VI) reduction of 20–45% was observed after its breakthrough for feed concentrations greater than 1.94 mg/L. No Cr (VI) or fumarate breakthrough was observed for feed Cr (VI) concentrations less than 1.32 mg/L.

2.7.2.2 Mathematical models

Several mathematical models, based on the numerical solution of advection-dispersion-reaction equation, are available for simulating the transport and biodegradation / biotransformation of organic and inorganic compounds in saturated and unsaturated media (Baveye and Valocchi, 1989; Kindred and Celia, 1989; Kinzelbach et al., 1991; Chen et al., 1992; Tebes-Stevens et al., 1998; Waddill and Widdowson, 1998; Chilakapati et al., 2000; Gwo et al., 2001; Brun and Engesgaard, 2002a, 2002b; Mayer et al., 2002; Boupha et al., 2004; Mohamed et al., 2005). Recently, Steefel et al. (2005) have presented a comprehensive review of the current status of reactive transport modelling. It may be noted here that only a few mathematical model studies, specifically addressing the transport and biotransformation of Cr (VI) in confined aquifers, have been conducted in the past. Recently, Guha (2004) developed a model that combined the transport and biotransformation of Cr (VI). This model accounts for (i) advective–dispersive transport of Cr (III), Cr (VI), lactate, and protein (mobile and immobile bacteria); (ii) first-order kinetic adsorption of Cr (III) and lactate; (iii) conversion of solid phase β- MnO2 to solid

phase MnOOH due to oxidation of Cr (III); and (iv) dual-Monod kinetics, where Cr (VI) is the electron acceptor and lactate is the electron donor. Hossain et al. (2005a) developed a transport model where reaction rate was represented by dual-enzyme reaction kinetics model for Cr (VI) reduction by MR-1. This model was used to estimate kinetic parameters from soil column data. It was found that the model predicted values were much smaller than those obtained from batch experiments. In a later study, Hossain et al. (2005b) developed a finite-element model for Cr (VI) transport and reduction by Shewanella Oneidensis MR-1 employing the dual-enzyme kinetic model. This model considered only one-dimensional transport of Cr (VI) with a sink term representing the reduction of Cr (VI) by MR-1. Separate equations for the transport of substrate and the microbial growth were not considered. The finite element model provided oscillation free numerical results for Peclet numbers less than 20 and Courant numbers less than one.

2.8 NUMERICAL TECHNIQUES FOR CONTAMINANT TRANSPORT MODELS

Advection-dispersion equation, combined with source/sink terms representing geochemical and biological reactions are generally used to describe the reactive solute transport in groundwater (Kindred and Celia, 1989; Herzer and Kinzelbach, 1989; Chiang et al., 1991; Zysset et al., 1994; Chilakapati et al. 2000). The governing system of equations consists of partial differential equations (PDEs) for transport coupled with algebraic equations, when the reactions are described by equilibrium conditions. On the other hand, PDEs for transport are coupled with the ordinary differential equations (ODEs) when the reactions are described by kinetic conditions (Kindred and Celia, 1989; Yeh and Tripathi, 1991; Clement et al., 1997; Chilakapati et al., 2000). Numerical solution of these governing equations is difficult, particularly when advection is dominant, and the reactions are described by non-linear ODEs. Numerical difficulties are also encountered while dealing with transport of large number of reacting components and large aquifers.

Numerical approaches used for solving the advection-dispersion-reaction equations can be broadly classified into two types: (i) Direct substitution approach or global implicit

approach, and (ii) Operator split approach or sequential approach. In the direct substitution approach, non-linear algebraic equations arising out of discretization of both transport and reaction equations are solved simultaneously using an appropriate iteration technique such as the Newton-Raphson method (Yeh and Tripathi, 1991). This approach typically involves the inversion of a large matrix during each Newton-Raphson iteration, and for each time step of computation. The size of the matrix depends upon the number of computational points in the domain, and the number of components being considered in the transport simulations. In the operator split or sequential approach, transport equations and reaction equations are decoupled and solved sequentially (Herzer and Kinzelbach, 1989; Kinzelbach et al.,1991; Yeh and Tripathi, 1991; Barry et al., 1996; Park and Kuo, 1996; Steefel and MacQuarri, 1996; Yeh et al., 2001; Bell and Binning, 2004). In the sequential iterative approach, the transport calculations and the reactive step calculations are coupled through iteration, while there is no coupling between the transport and reaction step calculations in the sequential non-iterative schemes. The main advantage of sequential iterative schemes is that a smaller set of equations need to be solved simultaneously during each time step calculation. This results in low computational cost per iteration.

Saaltink et al. (2000, 2001) compared the numerical behaviour of the above two approaches for reactive transport modelling. It was shown that the sequential iteration approach often requires very small time steps for convergence and thus results in excessive computation times for highly non-linear cases. Direct substitution approach is more robust in such cases. For very large domain problems, and where the reactions are not highly non-linear, direct substitution approach is not favourable. Split operator approach without iteration introduces an additional source of numerical error, referred to as split-operating error. This splitting error may be removed by adopting sequential iterative approach. However, usefulness of sequential iterative schemes depends upon the stability requirements and rate of convergence. Engesgaard and Kipp (1992) and Steefel and MacQuarrie (1996) reported that iterative schemes may not converge in certain cases. Kanney et al. (2003) used theoretical analysis and numerical experiments to investigate the convergence rate of the iterative split operator approach. It was shown that the convergence rate of the iterative split algorithm applied to non-linear reactive transport

problem is O (Δt^2). Carrayrou et al. (2004) compared the intrinsic operator-split errors for the sequential non-iterative and sequential iterative approaches for the solution of a reactive transport equation with a kinetic formulation of chemical phenomenon. They have developed analytical expressions of mass balance errors. It was shown that the symmetric sequential iterative scheme is the best among all the variants of operator split procedures studied by them. Tebes-Stevens et al. (1998) introduced an iterative two-step algorithm, which improves upon the convergence behaviour of traditional sequential iterative approach. Robinson et al. (2000) also introduced an alternative iterative solution, called the selective coupling method. In this approach, only the strongly coupled components are solved simultaneously, where as other components are decoupled.

Much of the recent research in the area of transport modelling dealt with correct numerical representation for highly advective flows and correct numerical representation of the highly non-linear reactive term. Classical first-order schemes for advective flow result in excessive numerical dissipation, while classical second order schemes result in numerical oscillations at the moving front. Putti et al., (1990) used a finite-volume method with high resolution upwind terms for solving the two-dimensional solute transport equation. Yeh and Tripathi (1991) used an iterative two step finite-element method. Srivastava and Yeh (1992) used a one-step backward particle tracking method for advective part in their finite-element model. Zysset et al. (1994) employed Galerkin finite-element scheme for the spatial integration and a central finite-differencing scheme for the temporal integration. An iterative two-step method is employed to link the transport part with the reaction part. Chilakapati et al. (2000) used a high resolution total variation diminishing (TVD) scheme for the advection sub-problem. Stefanovic and Stefan (2001) used an explicit semi-Lagrangian method for advective part, with higher order interpolation at the feet of the trajectories. Cirpka et al. (1999) presented a new cell-centered finite volume scheme, in which stream-line oriented grids were used to avoid artificial transverse mixing. Farthing and Miller (2001) investigated a large number of finite-volume schemes used for capturing sharp fronts. They also developed a one-dimensional model in which a finite-volume method is used for the advective module and central-differencing is used in the dispersive module.

2.9 OPTIMIZATION MODELS

"Simulation optimization" is a general term used to describe a family of optimization techniques which utilizes simulation models for the evaluation of objective and constraint functions. A wide variety of applications lend themselves to simulation optimization techniques, including engineering design optimization, optimization of stochastic systems, model calibration, and solution of inverse problems. In this context, "Simulation optimization" is the use of mathematical optimization techniques coupled with groundwater simulation models for flow and transport to determine optimal design parameters involved in a remediation process. Several methods are available for optimization in a simulation-optimization framework.

Simulated annealing mimics process in which a solid is initially heated up to its melting temperature and then is cooled down slowly so that all the particles arrange themselves in the state of minimum energy where crystallization occurs. In optimization, the objective function to be minimized represents the energy in the thermodynamic process, while the optimal solution corresponds to the crystal configuration. The basic concept lies in allowing the search procedure to move occasionally "uphill".

Genetic algorithm mimics the biological evolution based on Darwinist theory (survival of the fittest), where the strongest (or any selected) offspring in a generation are more likely to survive and reproduce. The method starts with a number of possible solutions, referred to as the first generation of the population. Each of the possible solutions is referred to as an individual, then encoded as either binary or real-coded string (called chromosome). For each individual, the objective function is evaluated. During the course of the search, new generations of individuals are reproduced from the old generations through random selection, crossover, and mutation based on certain probabilistic rules. The selection is in favor of those interim solutions with lower objective function values (in a minimization problem). Gradually, the population will evolve towards the optimal solution.

An artificial neural network (ANN) is a biological inspired computational system that (1) comprises individual processing or computational elements with associated memory,

(2) is interconnected in some information-passing topology, (3) operates largely in parallel, and (4) has some ability to adapt its functioning to its inputs and outputs. The belief that "intelligent" system might be developed from the collective behavior of many of these interconnected processing elements has led to the development of neural net models. In the context of optimal design and operation using a simulation-optimization model, neural networks are generally used to approximate the simulation model in the optimization model. This reduces the computational burden significantly. Basically, the ANN model acts as a surrogate for the simulation model. However, an optimization method is still needed to solve the optimization problem.

Optimal design of ground water remediation system has become an active area of research in the last several years Yoon and Shoemaker (1999). A variety of optimization methods have been used for this purpose. Computational performances of eight such optimization algorithms were compared by Yoon and Shoemaker (1999). Results showed that no one algorithm is consistently the most accurate on all the problems. Minsker and Shoemaker (1998) have developed an optimization technique for the design of in-situ bio-remediation system. They considered optimal design of a pump and treat system.

SOMOS has been developed by Shieh and Peralta, (2005). It is a powerful, broadly applicable, and adaptable family of Simulation/Optimization (S/O) modules for hydraulic and transport optimization. SOMOS can be used to optimize cleanup and containment of any plume that can be modeled by MODFLOW and MT3DMS. SOMOS employs wide ranges of constraints and objective functions (maximize mass removal, minimize mass remaining, minimize maximum concentration remaining, and minimize cost and many others). SOMOS includes genetic algorithm linked with tabu search, simulated annealing linked with tabu search, artificial neural network (ANN), and response function options. SOMOS has been used on many sites, but mostly pump and treat systems.

ASAP (Federal remediation technologies roundtable, 2008) provides rigorously optimized water resource and environmental management designs. This software package combines well-accepted simulation packages (*e.g.*, MODFLOW and MT3D) with

artificial neural network (ANN) and adaptive simulated annealing (ASA) techniques, ASAP provides formally optimized engineering designs which explicitly incorporate management goals and constraints.

ATOPT (Federal remediation technologies roundtable, 2008) is an advective control model that uses both contaminant path line and capture zone simulation to constrain plume capture designs. The advective transport model explicitly represents advective transport while neglecting dispersion and contaminant decay reactions. ATOPT couples MODFLOW and MODPATH, and allows constraints to be placed on advective transport, time to capture, hydraulic head, and pumping rates. Like many other optimization models, this model also has been applied for the case of pump and treat.

ModGA is a simulation-optimization model developed by Zheng and Wang (1999). It can be used for optimal design of groundwater hydraulic control and remediation systems under general field conditions. The model couples genetic algorithms (GA), a global search technique inspired by biological evolution, with MODFLOW and MT3D. MGO code, developed by Zheng (Federal remediation technologies roundtable, 2008), couples the MODFLOW and MT3D simulators with three global optimization methods, *i.e.*, genetic algorithm, simulated annealing, and tabu search, which are linked by a common input/output structure and integrated with a gradient-based optimization module to reduce the computational burden. Maskey et al, (2002) have developed a ground water remediation strategy using Global Optimization Algorithms. The remediation of groundwater contamination by pumping and injection is generally a long-term and costly strategy. Aquifer cleanup time is a highly nonlinear and non-convex function of pumping rates. The cleanup objective often involves minimizing or constraining the cleanup time or cleanup cost. Linear programming and nonlinear optimization cannot guarantee the global solution. In this study, four global optimization (GO) algorithms, including a popular genetic algorithm, were used to minimize both cleanup time and cleanup cost taking pumping rates and/or well locations as decision variables. Groundwater flow and particle-tracking models (MODFLOW and MODPATH) and a GO tool (GLOBE) were used. Real and hypothetical contaminated aquifers were considered for application. The

results were satisfactory and show that GO techniques can be widely applied in groundwater remediation strategy and planning.

Hu et al., (2006) have developed a dynamic predictive control system for in-situ bioremediation process. This control system includes an optimization tool that consists of a simulation model and an optimization function. The simulation model describes the fate and transport of subsurface contaminants, while the objective function is a constrained nonlinear function that has been implemented using Genetic Algorithms. The results indicate that the dynamic, simulation model can generate an appropriate control strategy and adjust control actions dynamically.

2.10 SUMMARY

Highly mobile and highly toxic Cr(VI) can be immobilised by reducing it to less toxic Cr(III). Several *in-situ* treatment options are available for this purpose. Among various technologies, bio-remediation appears to be more effective, economically viable, and environmentally friendly treatment option for Cr(VI) contaminated aquifers.

In the past three decades, many studies focused on batch experiments to understand biotransformation of Cr(VI) to Cr(III) by different microbes, under different environmental conditions. Many reports on Cr(VI) reduction by different microorganisms such as chromium reducing bacteria (CRB), iron reducing bacteria (IRB) and sulphate reducing bacteria (SRB) in presence of different electron donors are available. Most of these studies have dealt with only a specific microorganism and one or two inorganic compounds as sources / sinks of electrons. However, in nature, most of the water and wastewater systems contain different inorganic compounds and microbial flora. Thus, a proper understanding of the interaction between different inorganic compounds and microbial flora is essential for the design and appropriate management of any bio-remediation system. Also, biokinetic models are available only for individual systems like CRB, SRB, and IRB. To the best of authors‟ knowledge, no model is available to

describe the combined action of CRB, SRB and IRB in wastewaters / contaminated aquifers containing Cr(VI), sulphate and Fe(III).

Earlier, experiments have been conducted to understand the combined transport and geo-chemical processes pertaining to Cr(VI) in different soils through batch and continuous column studies. In the few combined transport and biotransformation studies, small laboratory scale columns (10 – 30 cm long) of uniform sand were used. These studies do not realistically represent the interplay between hydro-geology and chromium containment. Hence, it is essential to understand the effects of i) ground water velocity, ii) initial microbial concentration, and iii) aquifer soil characteristics on Cr(VI) containment. So far, no study has considered the effectiveness of Cr(VI) containment in confined aquifers using bio-barriers, which is one of the most commonly used treatment option for *in-situ* remediation. Also, no study using pilot scale experimental data has been reported to demonstrate the effectiveness of either the biobarrier or reaction zone technologies for Cr(VI) containment. These bench-scale and pilot scale studies are essential steps towards development of mathematical models.

A well developed mathematical model is also essential to predict Cr(VI) concentration in field scale systems, which can be used as a management tool for deciding the treatment option and for designing the optimal *in-situ* bioremediation. Literature review revealed that no work has been carried out on two-dimensional transport and biotransformation of Cr^{6+} in groundwater. Most of the earlier works concentrated on various treatment methods to be adopted and applied one-dimensional transport and biotransformation models. These models cannot be applied to study *in-situ* bio-remediation by funnel and gate systems, and reactive zone method.

Literature review also revealed that only recently attention has been focused on the mathematical modeling of transport and bio-transformation of Cr(VI) transport through confined aquifers. Although many generic simulation-optimization packages are available for optimal design of aquifer remediation strategies, most of them have been applied to the case of pump and treat method. Very few attempts are made on the optimal

design of trench type bio-barrier, especially for the containment of Cr(VI) in contaminated confined aquifers.

The aim and specific objectives of the current study are presented in the following chapter.

Chapter 3

AIM AND OBJECTIVES

3.1 AIM

The aim of the proposed research is to explore the ways and means of remediation of chromium contaminated aquifers through dissimilatory biotransformation of Cr (VI) to Cr (III).

3.2 OBJECTIVES

Objectives of the proposed study are:

1. Development of a mathematical model for the Cr (VI) transport in the aquifer under natural and engineered environments and to develop a management strategy for the effective bioremediation of contaminated aquifer.
2. Apply the software to chromium contaminated site at Ranipet, Tamilnadu, using the available field data, and study the viability of bio-remediation of this aquifer.
3. Identify the optimum environmental conditions for Cr (VI) reduction
4. Evaluation of the biokinetic parameters of the microbial system for use in the mathematical model.
5. Study the effects of: a) various carbon sources, b) inorganic ions like sulfate, nitrate and zero valent iron, on the biotic and abiotic reduction of Cr (VI)
6. Performance evaluation of the methodology through experimental studies on a lab-scale aquifer.
7. Demonstration of the technology on a pilot-scale system, depicting the field conditions of chromium contaminated site at Ranipet, Tamilnadu, as far as possible.
8. Have periodic meetings with CGWB scientists to disseminate the knowledge gained through the project, get feed back from them and modify the experimental and modeling work, if necessary.

Chapter 4

MATERIALS AND METHODS

Present work involves experimental and modeling studies for transport and biotransformation of Cr (VI) in aquifers. Experiments include both batch and continuous column studies. This chapter describes the details of materials used, instrumental methods employed, bench-scale and pilot scale column setup and experimental procedures adopted in the study.

4.1 MATERIALS

4.1.1 Chemicals and Glassware

All the chemicals used in this study were of analytical reagent (AR) grade and were supplied by Ranbaxy chemicals Ltd, Chennai, India. Glassware used in the present study were manufactured by M/S Borosil Glass Works Ltd. (Bombay, India) and marketed under the brand name „Borosil". They were washed with liquid soap (Ranklen Laboratory Detergent, Ranbaxy, India) followed by washing with tap water and distilled water. Glassware for adsorption study were finally immersed in the adsorbate metallic solution (1 mM) for 24 hours and washed with distilled water to eliminate any error being introduced due to the sorption of metals on glass in actual experiments. The list of instruments used in the present study is given in Table 4.1.

Table 4.1 Instruments Used for the Study

NAME OF THE INSTRUMENT	USED FOR	MODEL/MANUFACTURER SPECIFICATION
Centrifuge	Extraction of bacterial cultures, separation of liquid and solid phases.	Remi India limited. Spl centrifuge type R-23&R-24, India.
Environmental Shaker	Adsorption tests desorption tests, biokinetic/degradation studies and cultivation of	UNO scientific equipment's and services, India.

	bacteria.	
pH meter	pH measurements	Cyber scan 510, EUTECH Instrument, India.
COD digester	COD measurements	HACH Company, USA
Horizontal laminar flow Chamber	Bacterial inoculation, sterilization	Deepak Meditech Pvt. Ltd., India.
Electronic balance	Weighing	Mettler Toledo, China
Tech Comp 8500 UV/Visible double beam spectrophotometer	Bacterial cell density measurement	Tech Comp Ltd., Hong Kong.
Sonicator	Rupture the bacterial cells	VC 130PB, Sonics Vibra cell, USA.
Atomic absorption spectrometer	Analysis of inorganic compounds	Perkin Elimer, USA
Auto clave	Sterilizing growth media and glass wares	Gambakas intruments co., India
Flame Photometer CL-360	Analysis of Lithium	Elico Pvt. Ltd., India
Peristaltic Pump	Continuous column experiments	VSP-100-4C, Miclins India, Chennai, India
High Vaccum Pump	Filtering bacterial solution	Sulac, India
Cyber Scan DO 100	D.O. measurement in liquid	Eutech instruments, USA
Binocular Microscope vision 2000	Bacterial identification	Vision, USA

4.1.2 Water

All solutions were prepared either in fresh distilled water or de-ionized water as required. The average pH of the water used was around 7.0.

4.1.3 Soil

To isolate Cr (VI) reducing microbes, soil samples (150 g each) were collected from seven different locations of the contaminated site at Ranipet, Tamilnadu, India in clean polyethylene bags and preserved in a deep freezer (APNA Scientific Suppliers, Chennai).

Soils used in the bench scale study were collected from the I.I.T Madras campus, Chennai, India. They were surface soils collected from the unsaturated zone. Soils thus collected were sieved; the portions which passed through 4.75 mm were sterilized, cooled to room temperature and preserved in clean plastic containers for subsequent use. For sand column experiments, river sand which passed through 0.6 mm and retained in 0.425 mm sieves was washed thoroughly with distilled water and oven dried at 100^0C over night. Soil characteristics were analyzed as per the standard methods (BIS, 1989) and are presented in Table 4.2. The soils were classified and identified as per ASTM (American Society for Testing and Material) standards, as silty sand (SM, as per ASTM designation D 2487-00), and sand through sieve analysis and Atterberg‟s limit analysis. The organic matter content and specific gravity of the soil were determined by chromic acid method (IS 2720, (part 22, 1972)) and pyknometer method (IS 2720, (part 3/sec.1, 1987)).

Table 4.2: Soil Characteristics

S.No.	Properties	Value		
		Soil A	Soil B	Soil C
1	Clay content	3.1%	0%	6.19%
2	Silt content	11.35%	0%	22.70%
3	Sand content	85.55%	100%	71.11%
4	Specific gravity	2.6	2.63	2.543
5	Organic content	0.1%	0%	0.92%

6	Bulk density	1.6	1.41	1.6
7	Porosity	0.37	0.45	0.375

Soil used for pilot scale study was collected from Ranipet area, Tamil Nadu, India. The portion which passed through 4.75 mm sieve opening was used for the experiment. River sand which passed through 0.6 mm and retained in 0.425 mm sieve opening was used in the bio barrier. The soil and sand characteristics were analyzed as per the standard method and are presented in Table 4.3.

Table 4.3: Characteristics of Soil used for Pilot Scale study

Sl.No	Properties/Parameters	Soil
1	Clay (%)	8.5 %
2	Silt (%)	19.5 %
3	Sand (%)	72%
4	Organic content (%)	0.2%
5	Specific gravity	2.58
6	Bulk density (g/cc)	1.6
7	Porosity	0.38

4.1.4 Nutrient Media

The composition of nutrient medium (N1) used for bacterial growth was peptone 10 g, beef extract 2 g, yeast extract 1 g, and sodium chloride 5 g in 1 L of distilled water. The mineral medium (M1) for Cr (VI) reduction experiments consisted of K_2HPO_4 (0.03 g/L), KH_2PO_4 (0.05 g/L), $MgSO_4 \cdot 7H_2O$ (0.01 g/L), 0.01 g/L NaCl,NH_4Cl (0.03 g/L), NaCl (0.01 g/L), molasses (2 g/L), yeast extract 1g/L and 1 mL of trace element solution in 1 L of distilled water. Trace element solution consisted of $FeCl_2 \cdot 4H_2O$ (12.2 g/L), $MnCl_2 \cdot 4H_2O$ (4.09 g/L), $CoCl_2 \cdot 6H_2O$ (0.927 g/L), $ZnCl_2$ (0.37 g/L), $CuCl_2$ (0.61 g/L), $NaMoO_4 \cdot 2H_2O$ (0.579 g/L), H_3BO_3 (0.16 g/L), KI (0.148 g/L), $NiCl \cdot 6H_2O$ (0.067 g/L), and EDTA $Na_2 \cdot 4H_2O$ (6.5 g/L). The pH was maintained at 7 ± 0.2 by using HCl or

NaOH. All media were autoclaved at 120 ^{0}C and 15 psi for 15 min. and stored at room temperature until use. Ferric monosodium EDTA and sodium sulphate were used as Fe (III) and sulphate sources, respectively.

4.2 ANALYTICAL PROCEDURES

4.2.1 Liquid Phase Chromium Analysis

Cr (VI) concentration was determined by the diphenyl carbazide method (Reference number: 3500-Cr B colorimetric method) by measuring the absorbance. The diphenyl carbazide reacts with dichromate and oxidizes to diphenyl carbozone under acidic condition. The Cr^{6+} is reduced to Cr^{3+}. This Cr^{+3} reacts with diphenyl carbazone and forms the colored complex. The color intensity was measured at 540 nm absorbance using a UV-VIS Spectrophotometer (APHA, 1998). A standard graph was prepared between colour intensity vs Cr (VI) concentration. Cr (VI) concentration of an unknown sample was estimated using this calibration curve. In case of Cr (III), potassium permanganate was used to convert Cr (III) to Cr (VI), and Cr (VI) concentration was then determined as explained above. Total chromium concentration was analyzed using atomic absorption spectrometer (Perkin Elmer, USA), after acid digestion of the aqueous solution.

4.2.2 Extraction of Cr (VI) from Soil

Cr (VI) was extracted from soil by alkaline digestion method 3060A developed by USEPA (1996).

4.2.2.1 Reagents

(a) ***Digestion solution:*** 20.0 ± 0.05 g NaOH and 30.0 ± 0.05 g Na_2CO_3 were dissolved in distilled water in a one-liter volumetric flask and diluted to the mark. The solution was stored in a tightly capped polyethylene bottle at 20-25^{o}C and used for a month. The pH of the digestion solution was adjusted to a value greater than 11.5 each time before it was used.

(b) ***0.5 M K_2 HPO_4 /0.5 M KH_2 PO_4 buffer at pH 7:*** The phosphate buffer was prepared by dissolving 87.09 g K_2 HP O_4 and 68.04 g KH_2 PO_4 in 700 mL of distilled water, and diluted to 1 L

4.2.2.2 Extraction

2.5 ± 0.10 g of the field-moist sample was placed in a clean and labeled 250 mL digestion vessel and 50 mL ± 1 mL of digestion solution was added to each sample, along with approximately 400 mg of $MgCl_2$ and 0.5 mL of 1.0 M phosphate buffer. The samples were stirred continuously (unheated) for at least five minutes using an appropriate stirring device. Samples were heated up to 90-95^{o}C, then maintained at 90-95^{o}C for at least 60 minutes with continuous stirring, then cooled to room temperature and filtered through a 0.45µm membrane filter paper(Millipore, U.S.A.). pH of the solution was adjusted to 7.5 ± 0.5 by adding 5.0 M nitric acid solution slowly to the beaker drop wise. Solution was discarded and re-digestion was carried out whenever the pH of the digest deviated from the desired range. The sample was filtered through a 0.45 µm membrane filter paper (Millipore, U.S.A.) whenever there was a flocculent precipitate formation. These extracted samples were analyzed for hexavalent chromium by diphenyl carbazide method.

4.2.3 Extraction of Total Chromium from Soil

Total chromium in the soil was extracted as per Standard Methods (Reference number: 3030 G Nitric Acid-Sulfuric Acid Digestion) (APHA 1998). The soil sample was oven dried for 24 hours at 107^{0}C, then analyzed for the total chromium content. 5 grams of soil sample was taken in a conical flask of 250mL capacity. 10mL of concentrated sulphuric acid and 5 mL of concentrated nitric acid were added drop by drop and mixed well with a glass rod. The solution volume was made up to 100mL with distilled water and boiled for 10 minutes. This sample was centrifuged at 6000 rpm for 10 minutes and the supernatant was analyzed for total chromium.

4.2.4 Chemical Oxygen Demand (COD)

COD of liquid and soil samples were estimated as per standard methods (Reference Number 5220 Chemical Oxygen Demand) (APHA, 1998). Closed reflex method was

followed. Digestion was carried out in HACH COD digester (Model 45600, USA) fitted with temperature controller and timer. COD of the samples were determined to find the substrate utilization rate for Cr (VI) reduction. The digestion mixture consists of 1.5 mL standard potassium dichromate, 3.5 mL of digestion acid and 2.5 mL of sample (diluted according to the concentration of COD of sample). Digestion was done for 2 hours at a temperature of 150^0 C. The digested samples were cooled down to room temperature and titrated for excess dichromate against 0.01N ferrous ammonium sulphate (FAS) using ferroin indicator. A cold blank and a hot blank were employed. The COD of the sample was found against the hot blank.

4.2.5 COD estimation for samples containing Ferric EDTA

Since ferric monosodium EDTA is not completely oxidized during normal COD digestion, an extended digestion procedure was followed in which double strength $K_2Cr_2O_7$ was used (0.2N) and the digestion time was increased to 4 h to ensure complete oxidation of ferric EDTA.

4.2.6 Iron

Fe (II) and Fe(III) are analyzed by 1,10 phenanthroline colorimetric method (APHA, 1998). For the analysis of soluble Fe(II), 0.1 mL of sample was added to 0.8 mL of ammonium acetate buffer and 0.2 mL of phenanthroline (1 mg/mL). For Fe(III) analysis, 0.1 mL of sample was treated with 0.2 mL of hydroxylamine hydrochloride for 1 h to reduce Fe(III) to Fe(II) before adding 0.8 mL ammonium acetate (pH 4.8) buffer and 0.2 mL phenanthroline. The color was allowed to develop for 30 min. before the absorbance was measured at 510 nm using UV-VIS spectrophotometer (Techcom, UK).

4.2.7 Sulphate

Sulphate was analyzed by turbidimetric methods prescribed in standard methods (APHA, 1998). Before measuring sulphate, 2 mL of sample (the sulphide generated) was fixed by adding with 0.1mL NaOH (6N) and 0.2 mL zinc acetate (1M) in a 2 mL centrifuge tube. After that, the sample was spun for 5 min. at 7000 rpm to remove the precipitate and the supernatant was analyzed for sulphate. Measure 8 mL of sample or suitable portion diluted to 8 mL in a test tube. 2 mL of buffer solution (30g Magnesium chloride, 5g

sodium acetate, 1 g Potassium nitrate and 20 ml acetic acid in 500 ml and make up to 1 liter) was added to the sample. A pinch of barium chloride crystals was added while stirring and absorption was measured after 5± 0.5 min.

4.2.8 Measurement of Cell Density in Liquid Phase

Overnight cultures were centrifuged, and cell pellets were washed with physiological saline water thrice. This was followed by re-suspension in saline water and homogenization. The homogenized solution was used as stock solution. Different dilutions were made from the stock solution. A known volume of these solutions was filtered through 0.45 µm filter paper (Millipore, U.S.A.) to find out the dry weight of cells. Corresponding absorbance was measured at 440 nm using a spectrophotometer. This information was used to prepare a calibration curve between dry weight and absorbance. For unknown samples, the absorbance was measured at 440 nm and was converted to dry weight using absorbance versus dry weight calibration curve (Pelczar et al., 1993).

4.2.9 Microbial Quantification in Soil Phase

4.2.9.1 Protein estimation

The total protein of intact cells was determined according to the method of Herbert et al. (1971).

4.2.9.1.1Reagents:

1. Sodium carbonate: 5g of Na_2CO_3 was dissolved in 100 mL of distilled water.
2. Copper sulphate: 5g of Cu $SO_4.5H_2O$) was dissolved in 100 mL of 1% sodium potassium tartarate.
3. Alkaline copper reagent: To a 50 ml of reagent (1), 2 ml of reagent (2) was added and mixed. This reagent was prepared fresh every time just before use.
4. Folin-ciocalteu reagent: F.C. reagent was diluted with equal volume of distilled water just before use.
5. 1.0 N NaOH: 4g of NaOH was dissolved in 100 mL of distilled water

4.2.9.1.2 Procedure:

The cell suspension (0.5 mL) was mixed with 2 mL of 1.0 N NaOH and was kept in boiling water bath for 5 min. The contents were then cooled in cold water. To this, 5 mL of freshly prepared reagent (3) was added and allowed to stand for 30 min for the color development. Reagent blank containing 0.5 mL distilled water instead of bacterial suspension was treated in the same way. The optical density was measured at 750 nm using a spectrometer against the reagent blank. Known bacterial concentrations were used for preparing the calibration curve.

4.2.9.2 Bacterial cell count

The bacterial cell count was carried out as per standard procedure (Cappuccino and Sherman, 1996). It involves serial dilution in physiological saline water followed by plate count. Spread plate technique was adopted in the present study.

4.2.10 Lithium

Lithium was analyzed using flame photometer (Elico, India) at a wavelength of 670.8 nm as per standard methods (Reference Number 3500-Li B Flame Emission Photometric Method). Initially instrument was calibrated with 40 mg/L and 100 mg/L of lithium standard solutions and the samples were then injected. The concentration range which could be analyzed was 0.5 to 100 mg/L

4.2.11 Velocity Measurement

In continuous column experiments, flow rate was monitored with respect to time by collecting the water at the outlet for a minimum period of 10 minutes. The pore velocity was calculated from the above flow rate (Pore velocity = Flow rate / (Area of cross section x Porosity)).

4.3 EXPERIMENTAL METHODOLOGY

4.3.1 Enrichment and cultivation of Cr (VI) reducing bacterial strains

Cr (VI) reducing bacterial consortia was enriched from the soil samples collected from chromium contaminated site located in Ranipet, Tamilnadu, India. The soil was

contaminated with the chromium sludge discharged from chromate manufacturing industry. Five grams of soil sample was added to 100 mL of sterile growth media M1 with 10 mg/L of Cr (VI) and incubated in a shaking incubator for 24 h at 35 °C. After 1 day, when significant growth was observed, 1 mL of the supernatant of the slurry was transferred to 100 mL of fresh nutrient media (M1) and incubated at 35 °C. The consortia used for the Cr (VI) reduction was developed by a series of transfers at every 24 h by gradually increasing the Cr (VI) concentration. Once the enriched consortium was ready, they were incubated at 35 °C for 24 h and stored at 4 °C until further use.

4.3.2 Enrichment and cultivation of iron reducing bacterial strains

Wastewater was collected from municipal wastewater treatment plant, located at Chennai. The anaerobic sludge was enriched using a medium of 5.0 g ferric ammonium citrate (FAC), 0.5 g K_2HPO_4, 0.2 g $MgSO_4 \cdot 7H_2O$, and 0.01 g $CaCl_2 \cdot 2H_2O$, 1 mL of trace elements solution per litre at pH 7.0. The enrichment was performed by increasing the Fe (III) concentration by 1000 mg/L for every transfer into a fresh medium until 5 g/L concentration was attained in two months. The reactor was maintained as a source of inoculum for further experiments and media additions were performed only when necessary to produce sufficient biomass for inoculation.

4.3.3 Enrichment and cultivation of sulphate reducing bacterial strains

Enrichment of SRB was also carried out by using wastewater sample collected from municipal wastewater treatment plant, located at Chennai. The composition of the growth medium for enrichment of SRB consisted of 1.2 g/L sodium lactate, 3 g/L sodium citrate, 0.1 g/L yeast extract, 4.5 g/L Na_2SO_4, 0.06 g/L $CaCl_2 \cdot 2H_2O$, 1.0 g/L NH_4Cl, 0.5 g/L KH_2PO_4 ,2.0 g/L $MgSO_4 \cdot 7H_2O$, 0.5 g/L $FeSO_4 \cdot 7H_2O$, 0.3 g/L EDTA disodium salt and 1 mL of trace element solution and the volume was made up to 1 L with distilled water and pH of the solution was adjusted to 7±0.2. During enrichment, the COD to sulphate ratio was gradually increased from 1 to 1.5 over a period of two months. The enriched cultures were used in further experiments.

4.3.4 Batch Adsorption Study

Sorption equilibrium studies for Cr (VI) were used to estimate the adsorption coefficients for soils A, B and C. Adsorption kinetic study was conducted using 1g of sterilized soil and 100 mL of synthetic chromium contaminated water with 50 mg/L of Cr (VI) concentration in various reaction bottles. The reaction bottles were kept in a shaker at 140 rpm. The samples were withdrawn at time intervals of 5, 10, 15, 30, 60, 120, 180, 360, 420 and 480 min on self sacrificing mode. The samples were withdrawn from the reaction bottles, centrifuged and analyzed for residual Cr (VI) concentration. The equilibrium time obtained from the kinetic study was used for isotherm studies. For the isotherm studies, 1g of soil with 100 ml solution containing Cr (VI) was taken in several reaction bottles, and kept in a shaker for 6 hrs (pseudo-equilibrium time) at 140 rpm. The initial Cr (VI) concentrations employed were 2, 5, 10, 20, 30, 50, 100, 200, 300, 400, 500 mg/L. At the end of 6 h, the supernatant was separated and analyzed for Cr (VI) and total chromium. Similarly adsorption isotherm studies were conducted for Cr (III) and lithium. Lithium was used in continuous column studies as a tracer. Adsorption equilibrium studies were also conducted for Cr (VI) in presence of molasses and lithium.

4.3.5 Studies to Estimate Bio-kinetic Parameters

Different batch kinetic experiments were performed to evaluate various biokinetic parameters and rate constants. These experiments include (a) Cr (VI) reduction by CRB under aerobic conditions, (ii) Cr (VI) reduction by CRB, IRB, or SRB under anaerobic condition, (iii) Cr (VI) reduction by a mixture of IRB and CRB, or SRB and CRB under anaerobic condition, (iv) Cr (VI) reduction by a mixture of CRB, SRB, and IRB under anaerobic condition, (v) EDTA degradation studies using CRB, IRB or SRB. These experiments were conducted as follows. Predetermined amount of Cr (VI) and selected electron acceptor (Fe^{3+} or SO_4^{2-}) were added to mineral medium as per the requirement of each experiment. After autoclaving, Na_2S was added as per the requirement to remove dissolved oxygen. Then the medium was flushed with nitrogen to remove oxygen in the head space of reactor. Microbial cultures were then inoculated such that the initial concentration of solution was between 30 and 40 mg/L. An initial COD of 3100 to 3200 mg/L was maintained in all the experiments. Samples were withdrawn at pre-decided

time intervals and analyzed for Cr (VI), total chromium, biomass, COD, Fe (II), Fe (III), and sulphate concentrations.

All chemicals were analytical reagent (AR) grade supplied by Ranbaxy and Merck Pvt. Ltd. (India). Clean „Borosil" (India) make glassware was used for reagents preparation and volume measurements. Incubations were carried out at room temperature (30°C) without shaking for anaerobic and with shaking for aerobic. The contents of the aerobic flasks were in contact with the atmosphere since they were closed only with cotton plugs for sterility.

In presence of Cr (VI), specific growth rate of bacteria was assumed to follow the Monod"s equation with inhibition (Ohtake et al., 1990) as given below

$$\mu = \left(\frac{\mu_{max}\, S}{K_s + S}\right)\left(\frac{K_i}{K_i + Cr}\right) \qquad (4.1)$$

where μ_{max} = maximum specific growth rate [h^{-1}]; S= molasses concentration [COD mg /L]; Cr= chromium (VI) concentration [mg/L]; K_s = half-saturation constant [COD mg /L]; and K_i= chromium inhibition constant [mg Cr (VI)/L].

4.3.6 Continuous Column Study

4.3.6.1 Experimental Setup

The schematic of the bench scale experimental set up used in this study is shown in Fig. 4.1 (a). It was one m long and had a square cross section (10 cm × 10 cm). An overhead tank with provision for an adjustable head served as the inlet to the column. A porous plate was provided at the inlet in order to achieve a uniform entry of water into the soil. A collection reservoir was provided at the outlet. Water level in the outlet reservoir was maintained above the top of the soil column in order to maintain saturated conditions in the column. Sampling ports were provided on the sides at four different cross sections at distances 20 cm, 40 cm, 60 cm and 80 cm from the inlet, respectively. Four ports were provided at each cross-section as shown in Fig. 4.1 (b). Liquid samples were collected from these ports at regular time intervals using a syringe.

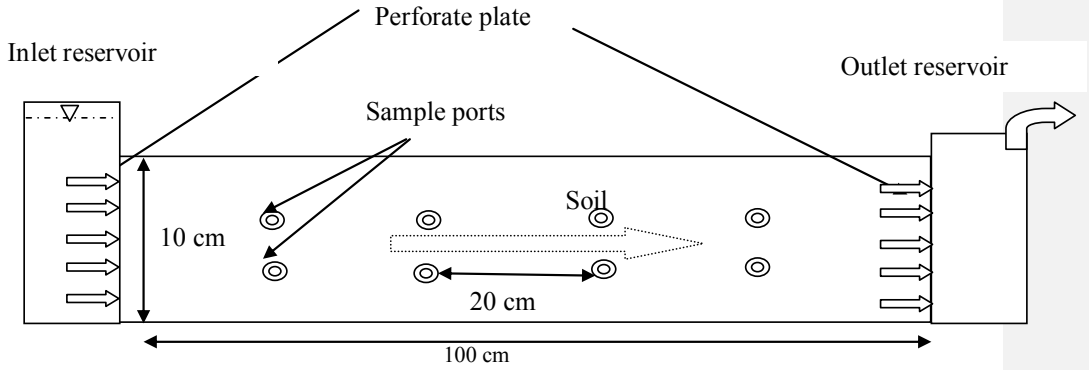

(a)

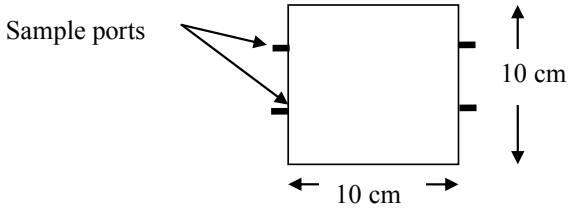

(b)

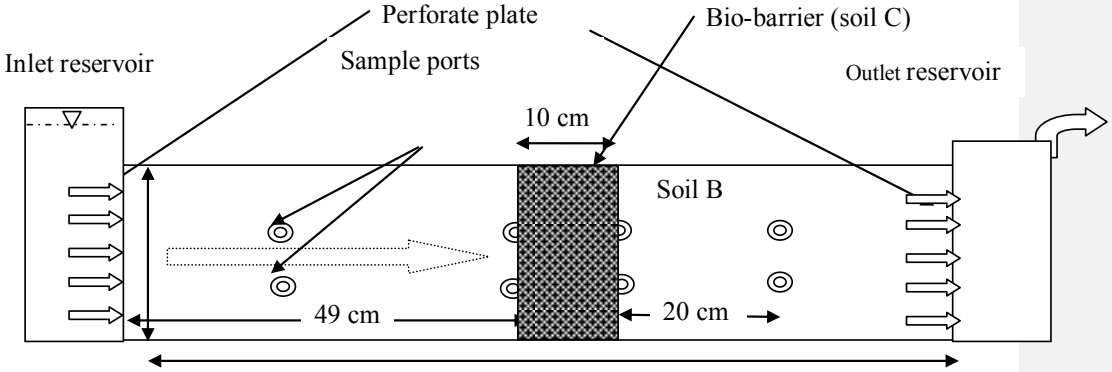

(c)

Fig. 4.1: Schematic of experimental setup

In case of bio-barrier experiments, the same experimental setup with slight modifications incorporating 4 more ports at 49 cm from the inlet was used. Figure 4.1(c) shows the schematic of the bench scale experimental set up used for bio-barrier studies.

The length of the column was one m and it had a 10 cm square cross section. The column was filled with sand from 0 to 50 cm, and again from 60 to 100 cm. To simulate the bio-barrier conditions, the portion between 50 to 60 cm was filled with Soil-C augmented with Cr (VI) reducing microbes. Sampling ports were provided on the sides at five different cross sections at distances 20 cm, 40 cm, 49 cm, 60 cm and 80 cm from the inlet, respectively. As shown in Fig. 4.1. (b), four ports were provided at each cross-section. A syringe was used to collect liquid samples from these ports at regular time intervals. Figure 4.2 shows a picture of the experimental set up used for bench-scale column studies.

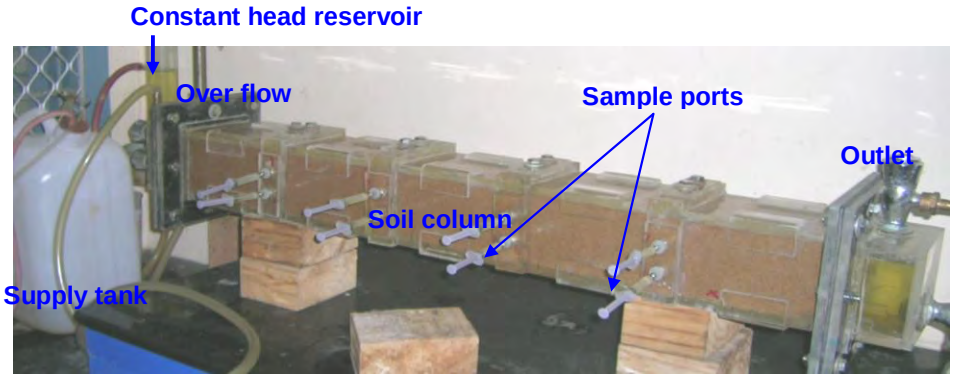

Fig. 4.2: Photograph of experimental setup

4.3.6.2 Transport studies without biotransformation

The prepared sterilized soil was filled in the column in 33 layers of approximately 3cm thickness. The column was compacted in vertical direction. Each layer was compacted with 25 blows of a 1.2 kg hammer falling from a 30 cm height, in order to get a more or less uniform compaction. The dry weight of the soil was measured before adding the required moisture and filling the column. This information was used to determine the bulk density of the soil. The porosity was determined using the formula relating the bulk density, and dry weight.

$$\phi = 1 - \rho_d / (G\rho_w) \quad (4.2)$$

Where ϕ = porosity of the medium; ρ_d = the dry density of soil (g/cm^3); ρ_w = the density of water (g/cm^3); and G = specific gravity. Constant heads were maintained in the head and tail tanks for 6-24 h (6 h for soil B and 24 h for soil C) to obtain a steady flow rate through the soil column. The flow rate was monitored with respect to time by collecting the water at the outlet. The pore velocity was calculated from the above flow rate (Pore velocity = Flow rate / (Area of cross section x Porosity)). Once steady state was attained, Cr (VI) contaminated water was introduced into the system through the head tank. Liquid samples were taken from the head tank and all the sampling ports at regular time intervals, and were analyzed for Cr (VI) concentration. Experiment was continued till the break-through occurred at the last sampling cross section. These experiments were conducted for Soil-C with a porosity of 0.36, for three different pore velocities of 22.4, 11.2 and 5.6 cm/h, respectively.

4.3.6.3 Transport studies with biotransformation

Transport studies with biotransformation were conducted in a similar manner, except that the soil was mixed with bacterial cells and mineral medium. The sterilized soil was mixed with highly concentrated cell suspension (the cells were already grown in the prescribed nutrient broth, centrifuged, washed and re-suspended in mineral medium) in mineral medium M2 without carbon source. Random samples were taken and checked for the uniformity in mixing. Once uniform mixing was achieved, the columns were packed with the soil as explained earlier. The column was fed with mineral medium (M2 without carbon source) until a steady state velocity was attained. The microbial concentration in column effluent was monitored continuously. After the attainment of constant velocity, the column was fed with medium containing 25mg/L of Cr (VI), molasses (approximately 2000 mg/L of COD) and lithium (50 mg/L) along with minerals. Samples were withdrawn from various sampling ports at regular intervals using syringes and were analyzed for Cr (VI), total chromium, COD and lithium. After the completion of column run, soil samples were taken from different ports and were analyzed for adsorbed Cr (VI), total chromium, COD, lithium and microbial concentration. These studies were conducted with three different soils namely soils A, B

and C as given in Table 4.2. For soil B, the studies were conducted with two different velocities (Table 4.4).

Table 4.4: Transport and Biotransformation Studies

Soil type	Initial pore velocity cm/h	Bacterial Conc. added mg/g	Column length (cm)
Soil A	7.32	0.0232	100
Soil B	6.67	0.0205	100
Soil B	1.16	0.0405	100
Soil C	5.83	0.0205	100
Bio-barrier studies			
			Bio-barrier thickness
Soil C	1.98	0.0205	10
Soil C	2.66	0.205	10

4.3.6.4 Transport studies with bio-barriers

Transport studies with bio-barriers were conducted in a manner similar to those without bio-barriers, except that a bio-barrier of 10 cm thickness was provided at a distance of 50 cm from the inlet. The 10 cm bio-barrier was filled with soil C mixed with microbes, where as the rest of the column was filled with soil B without any microbes. Also, four more sampling ports were provided at 49 cm from the inlet i.e., just at the starting of the bio-barrier. Two vents were provided for release of gasses generated in the bio-barrier. As in the column studies without bio-barriers, concentrations of microbes, substrate, Cr (VI), and lithium in liquid phase were monitored continuously at all the ports. Flow rate and microbial concentration were also monitored at the outlet. After the completion of column run, soil samples were taken from different ports and were analyzed for adsorbed Cr (VI), total chromium, COD, lithium and microbial concentration. These column studies with bio-barriers were conducted for two different initial microbial concentrations in the barrier. The experimental details for all the transport studies are presented in Table 4.4.

4.3.7 Head Loss Measurement

Piezometric head was measured using inclined piezometers, which were inserted at different ports in the column. Head loss between any two cross sections is the piezometric head difference between those two sections.

4.3.8 Measurement of Released Gas

Measurement of gas release was done by liquid displacement method. In this, a gas collection bottle filled with the saturated (3.5%) solution of NaCl was connected to the continuous column experimental set up such that the released gas could directly enter the bottle. The tip of the gas outlet tube was inserted into the bottle up to the bottom outlet where pressure was equal to atmospheric pressure. The amount of liquid displaced was equal to the amount of gas entered into the bottle.

4.4 PILOT SCALE STUDIES

4.4.1 Pilot scale studies for aquifer remediation using bio barrier

Two pilot scale reactors of size 3.0 x 1.0 x 0.5 m were fabricated using transparent 10 mm thick Acrylic sheets. Necessary support was given for the tank to hold the load. Two partitions were provided by inserting perforated sheets of adequate size at 25 cm distance from both the ends, and these portions were used as the inlet and the outlet chamber. Overflow provisions were made in both inlet and outlet chambers of the reactor so as to maintain constant head difference. The remaining portion of the reactor was filled with uncontaminated soil brought from Ranipet area.

In one of the reactors, R1, a 10 cm wide portion of the reactor, at 75 cm from the inlet end, was filled with sand containing Cr (VI) reducing biomass. This 10 cm layer containing biomass acted as the bio-barrier. On the other hand, in the other reactor, R2, used as the control reactor, this 10 cm portion was filled with only sand. Compaction has been done uniformly for each 10 cm height of soil while filling the reactor with soil. Water was allowed to pass continuously from inlet chamber of the reactor so that over flow occurs at outlet chamber. Inlet and outlet water levels were adjusted by opening the over flow line so that water flows from inlet chamber to outlet chamber.

A constant Darcy velocity of approximately 0.02 cm/h was maintained for flow of water through the reactor. Four sets of manometer provisions were made to assess the head distribution. Twenty monitoring wells, each of 6 mm diameters were provided on upstream and down stream sides of the bio barrier. Food and nutrients were supplied to the bio barrier at regular intervals. Once the steady state flow of water was achieved, Cr (VI) solution with a concentration of 50 mg/L was passed from the inlet chamber, and the water samples were collected from inlet and outlet chambers and from all the 20 monitoring wells periodically in order to assess the remediation potential of the bio barrier. The samples collected were analyzed for Cr (VI), total chromium, and COD. The schematic diagram of the reactor is shown in Fig. 4.3.

4.4.2 Reaction Zone Technology

Two pilot scale reactors of size 3.0 x 1.0 x 0.5 m were fabricated using transparent 10 mm thick Acrylic sheets. Necessary support was given for the tank to hold the load. Two partitions were provided by inserting perforated sheets of adequate size at 25 cm distance from both the ends, and these portions were used as the inlet and the outlet chamber. Overflow provisions were made in both inlet and outlet chambers of the reactor so as to maintain necessary head. The remaining portion of the reactor was filled with uncontaminated soil brought from Ranipet area. Compaction has been done uniformly for each 10 cm height of soil while filling the reactor with soil. Water was allowed to pass continuously from inlet chamber of the reactor so that over flow occurs at outlet chamber. Inlet and outlet water levels were adjusted by opening the over flow line so that water flows from inlet chamber to outlet chamber. A constant flow rate was maintained for flow of water through the reactor. In one of the reactors, R3, 2 injection wells of 10 mm diameter and in the other reactor, R4, 4 injection wells of 10 mm diameter were installed at a distance of 0.5 m from the inlet chamber.

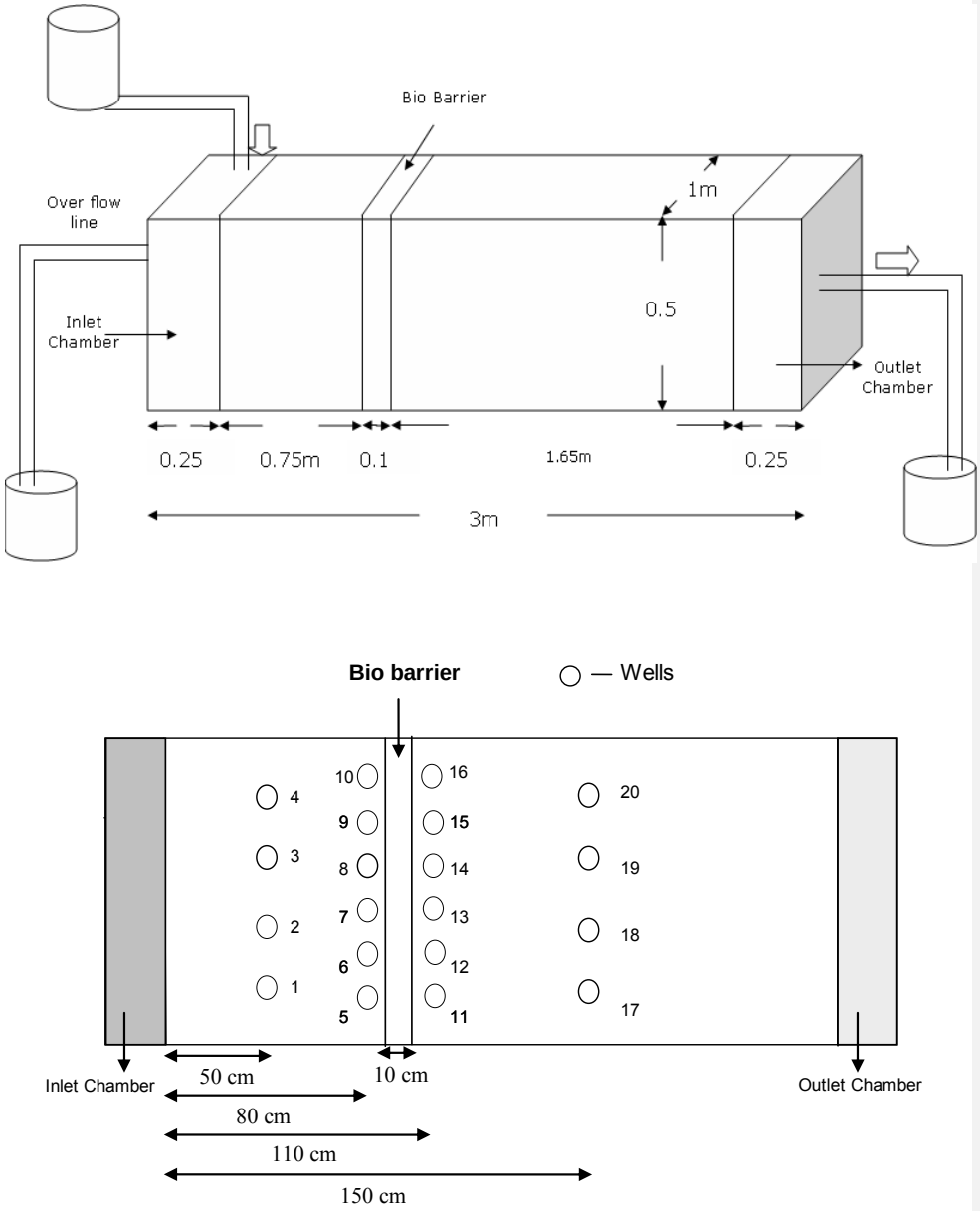

Fig. 4.3: Schematic of pilot scale reactor with Bio barrier

Monitoring wells of 6 mm diameter were installed in the upstream side and downstream side of the injection wells. 20 monitoring wells were provided in the reacto R3 and 27 monitoring wells were provided in the reactor R4 as shown in the Figs.4.4 (a), 4.4 (b) and 4.4 (c). Initially 200 ml of medium containing 100 gm of biomass (wet weight) and 100 gm of molasses were injected in each injection wells. Food and nutrients were supplied through the injection wells at regular intervals. Once the steady state flow of water was achieved, Cr(VI) solution with a concentration of 60 mg/L was passed from the inlet chamber, and the water samples were collected from inlet and outlet chambers and from all the monitoring wells periodically in order to assess the remediation potential. The samples collected were analyzed for Cr (VI), total chromium, and COD. On the 75th day inlet Cr (VI) concentration was increased to 250 mg/l in both the reactors and the performance was monitored.

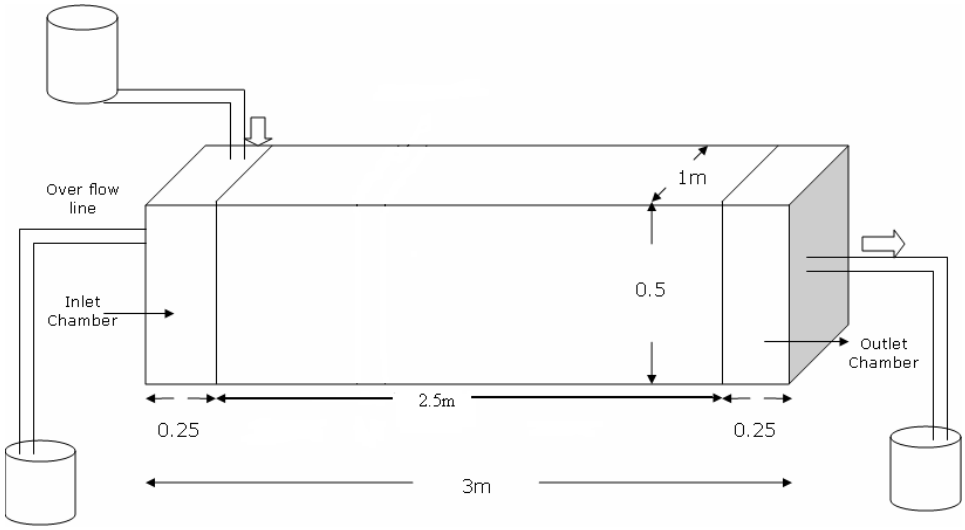

Fig. 4.4 (a): Schematic Diagram of the Reactor

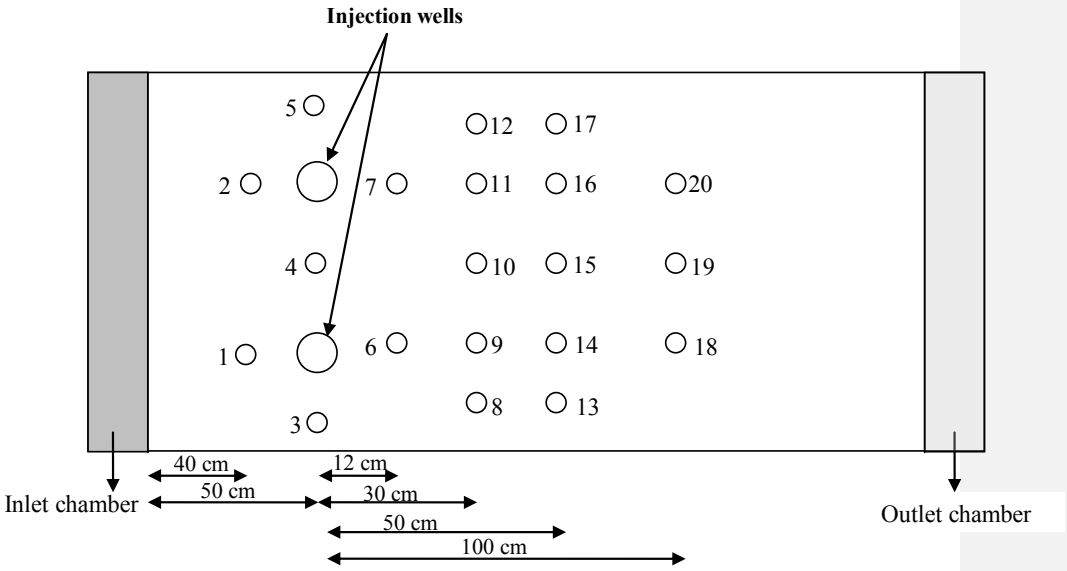

Fig. 4.4 (b): Injection and Monitoring wells in Reactor I

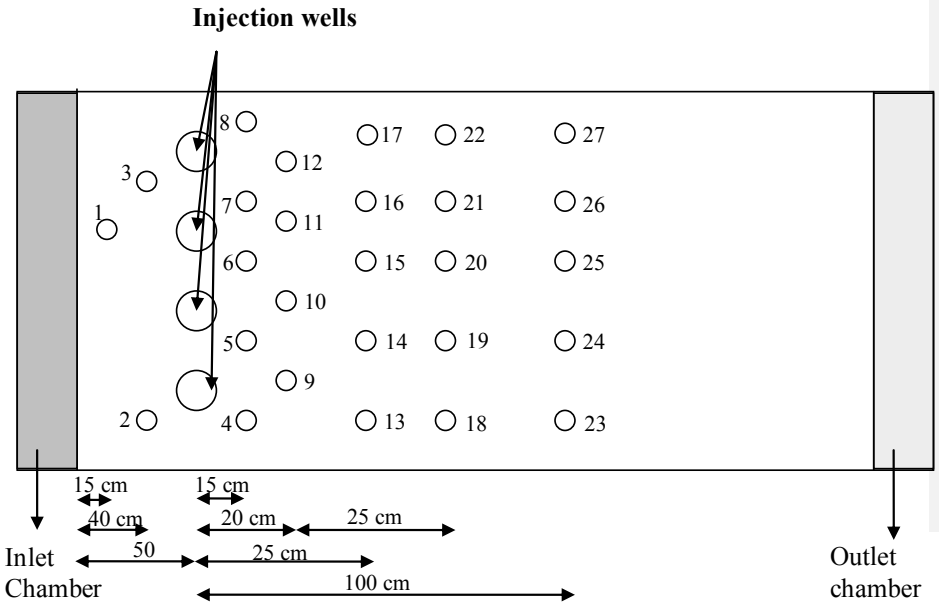

Fig. 4.4 (c): Injection and Monitoring wells in Reactor II

4.5 CLOSURE

Successful development of any mathematical model depends on the basic understanding of the process, which can be gained through carefully conducted experiments. Also, experimental data can be used for validation of proposed model. This chapter described the details of materials used, instrumental methods employed, bench-scale and pilot scale column setup and experimental procedures adopted in the study. Details of mathematical models are presented in the following chapter.

Chapter 5

MATHEMATICAL MODELS

In this study, two-dimensional mathematical models for transport and bio-transformation of Cr(VI) in confined and unconfined aquifers were developed. These models are based on the numerical solution of governing advection-dispersion-reaction equations. The model for bio-transformation module is first described, followed by a description of the one-dimensional transport model. The chapter ends with complete details of two-dimensional models.

5.1 MODEL FOR BIOTRANSFORMATION

5.1.1 Governing equations for microbial growth, COD and Cr(VI) reduction by single strain

A mathematical model was developed for the processes describing Cr(VI) reduction kinetics in batch systems by CRB, SRB and IRB, individually, under different conditions. The mathematical model not only describes the chromium reduction but also the temporal variations of substrate (COD) and biomass concentrations in the system. The model considered the inhibitory effect of Cr(VI) on the microbial growth. A simple Monod‟s inhibition model was considered in the present study to describe the Cr(VI) inhibition. The only other possible inhibitor present in the system was sulphide. Sulphide generated in the system could reduce either Cr(VI) or Fe(III) as soon as it is formed. Hence inhibition due to sulphide might not have been significant. Also, concentration of generated sulphide in the system at any time was much lower than the reported inhibition concentration (300 to 550 mg/L of sulphide is necessary to impart sulphide inhibition). Availability of sulphate / iron was unlimiting in the respective systems and therefore this was also not considered in the model. The model equations are:

$$\frac{dM_i}{dt} = M_i\left(\frac{\mu_{\max,i}S}{K_{s,i}+S}\right)\left(\frac{K_{in,i}}{K_{in,i}+Cr_6}\right) \quad \text{for i = } \textit{1,2, and 3} \tag{5.1}$$

$$\frac{dS}{dt} = M_i\left(\frac{1}{Y_T}\right)\left(\frac{\mu_{\max,i}S}{K_{s,i}+S}\right)\left(\frac{K_{in,i}}{K_{in,i}+Cr_6}\right) \text{ for i = } \textit{1,2, and 3} \tag{5.2}$$

$$\frac{dCr_6}{dt} = M_i(\eta)\left(\frac{1}{Y_T}\right)\left(\frac{\mu_{\max,i}S}{K_{s,i}+S}\right)\left(\frac{K_{in,i}}{K_{in,i}+Cr_6}\right) \text{ for i = } \textit{1,2, and 3} \tag{5.3}$$

where, M_i is bacterial biomass concentration in mg/L, subscript *i* represents the particular bacterial strain (*i* = 1 for CRB; *i* = 2 for SRB; *i* = 3 for IRB), S is concentration of residual substrate (organic matter, OM) in mg/L, Cr_6 is concentration of hexavalent chromium in mg/L, $\mu_{max,i}$ is the maximum specific growth rate for the bacterial strain *i*, $K_{i,i}$ is the chromium inhibition constant for bacterial strain *i* in mg/L, $K_{s,i}$ is the half saturation constant for bacterial strain *i* in mg/L, η_i is mg of Cr reduced/g of substrate utilized by bacterial strain *i*, $Y_{T,i}$ is the yield coefficient for bacterial strain *i*. Equations (1)–(3) are valid for kinetics of chromium reduction by each bacterial strain acting independently.

5.1.2 Governing equations for microbial growth, COD and Cr(VI) reduction by more than one bacterial strain

When more than one bacterial strain is present, it may be assumed that availability of substrate as well as chromium for that particular bacterial strain is proportional to the partial concentration of that bacterial strain (ratio of concentration of the particular bacterial strain to the total bacterial concentration). Implicit to this assumption is the absence of the symbiotic/asymbiotic effect of one strain on the other. With this assumption, following governing equations can be formulated for combined action of more than one bacterial strain:

$$\frac{dM}{dt} = \sum_i \frac{dM_i}{dt} \tag{5.4}$$

$$\frac{dS}{dt} = \sum_i \frac{dM_i}{dt}\left(\frac{1}{Y_{T,i}}\right) \tag{5.5}$$

$$\frac{dCr_6}{dt} = \sum_i \frac{dM_i}{dt}\left(\frac{\eta_i}{Y_{T,i}}\right) \tag{5.6}$$

$$M = \sum_i M_i \tag{5.7}$$

$$S = \sum_i S_i \tag{5.8}$$

$$Cr_6 = \sum_i Cr_{6,i} \tag{5.9}$$

$$S_i = S\left(\frac{M_i}{M}\right) \tag{5.10}$$

$$Cr_{6,i} = Cr_6\left(\frac{M_i}{M}\right) \tag{5.11}$$

$$\frac{dM_i}{dt} = \frac{M_i.\mu_{\max,i}.S\left(\frac{M_i}{M}\right)}{K_{s,i} + S\left(\frac{M_i}{M}\right)}\left(\frac{K_{i,i}}{K_{i,i} + Cr_6\left(\frac{M_i}{M}\right)}\right) \tag{5.12}$$

5.1.3 Solution for differential equations by Euler finite difference method

The model for bio-transformation was validated using the batch experimental data. For this purpose, equations (5.4)-(5.12) were solved by a simple explicit Euler finite-difference method (programmed using MATLAB 2006b) as given below to determine the concentrations of biomass, substrate, and Cr(VI) at time t+Δt, from the known values at time t.

$$M_i(t+\Delta t) = M_i(t) + \frac{M_i(t) * \Delta t * \mu_{\max,i} * S(t)\left(\frac{M_i(t)}{M(t)}\right) * K_{i,i}}{\left(K_{s,i} + S(t)\left(\frac{M_i(t)}{M(t)}\right)\right)\left(K_i + Cr_6(t)\left(\frac{M_i(t)}{M(t)}\right)\right)} \tag{5.13}$$

$$M(t+\Delta t) = \sum_i M_i(t+\Delta t) \tag{5.14}$$

$$S(t+\Delta t) = \sum_i S(t)\left(\frac{M_i(t)}{M(t)}\right) - \left(M_i(t+\Delta t) - M_i(t)\right)\left(\frac{1}{Y_{t,i}}\right) \tag{5.15}$$

$$Cr_6(t+\Delta t) = \sum_i Cr_6(t)\left(\frac{M_i(t)}{M(t)}\right) - \left(M_i(t+\Delta t) - M_i(t)\right)\left(\frac{\eta_i}{Y_{t,i}}\right) \tag{5.16}$$

The model equations were also solved using classical Fourth-Order Runge Kutta method (programmed using MATLAB 2008a). Results obtained using both Runge Kutta and Euler methods matched very well. A very small value of computational time step, Δt, was taken in all simulations, based on grid convergence test.

5.2 ONE-DIMENSIONAL MODEL FOR TRANSPORT WITHOUT BIOTRANSFORMATION

In this section, the formulation of a mathematical model for transport of hexavalent chromium in contaminated confined aquifers is described. The proposed model is applicable for one-dimensional transport in a homogeneous aquifer.

5.2.1 Governing Equation

The governing equation for the one-dimensional advective-dispersive transport, along with adsorption, of any pollutant such as Cr(VI) through saturated soils under steady state flow conditions is given as (Bear and Verruijt, 1990)

$$\frac{\partial Cr_6}{\partial t} = D_h \frac{\partial^2 Cr_6}{\partial x^2} - v\frac{\partial Cr_6}{\partial x} - \frac{\rho_b \partial S_a}{\phi \partial t} \tag{5.17}$$

where, Cr_6 = concentration of the contaminant in solution (mg/L); D_h = coefficient of hydrodynamic dispersion (cm^2/h); x = distance from the inlet (cm); t = time from the start of transport (h); v = pore water velocity (cm/h); ρ_b = bulk density of the soil (g/cm^3); S_a = mass of the Cr (VI) on the soil (adsorbed / precipitated etc.) per unit mass of soil (mg/g); ϕ = porosity of the medium. In Eq. (5.17), the last term on the right hand side represents all the chemical reactions (adsorption, ion exchange, precipitation and complexation) occurring between the soil surface and the solute during the transport process, which is described in this study using a simple non-linear adsorption isotherm.

Batch equilibrium studies indicated that Freundlich isotherm fits well with the experimental data, and therefore, this isotherm was adopted for use in the transport equation.

$$S_a = K_f Cr_6^{\frac{1}{n}} \tag{5.18}$$

where, K_f (L/mg) and 1/n (dimensionless) are Freundlich coefficient and constant, respectively. Substitution of Eq. (5.18) in Eq. (5.17) results in the following:

$$R_{Cr6}\frac{\partial Cr_6}{\partial t} = D_h \frac{\partial^2 Cr_6}{\partial x^2} - v\frac{\partial Cr_6}{\partial x} \tag{5.19}$$

where, R_{Cr6} = retardation coefficient and is given by

$$R_{Cr6} = 1 + \frac{\rho_b}{n\phi} K_f Cr_6^{\left(\frac{1}{n}-1\right)} \tag{5.20}$$

5.2.2 Numerical Solution

In this study, Eq. (5.19) was solved using an implicit-explicit numerical method because of its better numerical stability characteristics. The advection term was discritized using an Essentially Non-Oscillating (ENO) scheme in which MINMOD limiter was employed for suppressing the numerical oscillations so that the model could be applied to even

highly advective flows. The dispersion term was discritized using the central finite-differences.

With reference to Fig. 5.1, the finite-difference analog of the Eq. (5.19) at any finite difference node "i" can be written as below.

$$(R_{Cr6})_i^t\left[\frac{Cr_{6_i}^{\,t+\Delta t}-Cr_{6_i}^{\,t}}{\Delta t}\right]=D_h\theta\left[\frac{Cr_{6_{i+1}}^{\,t+\Delta t}-2Cr_{6_i}^{\,t+\Delta t}+Cr_{6_{i-1}}^{\,t+\Delta t}}{\Delta x^2}\right]+D_h(1-\theta)\left[\frac{Cr_{6_{i+1}}^{\,t}-2Cr_{6_i}^{\,t}+Cr_{6_{i-1}}^{\,t}}{\Delta x^2}\right] \quad (5.21)$$
$$-\theta v\left[\frac{Cr_{6i+1/2}^{\,t+\Delta t}-Cr_{6i-1/2}^{\,t+\Delta t}}{\Delta x}\right]-(1-\theta)v\left[\frac{Cr_{6i+1/2}^{\,t}-Cr_{6i-1/2}^{\,t}}{\Delta x}\right]$$

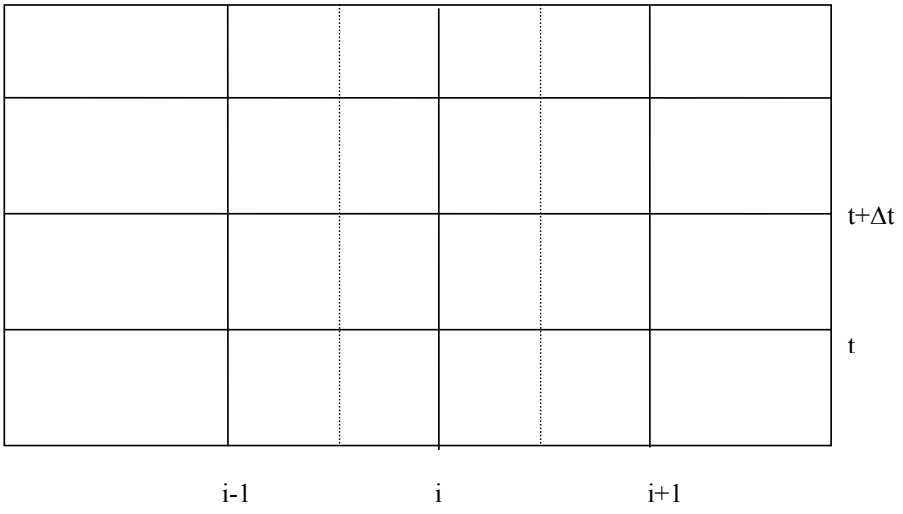

Fig. 5.1: Finite-difference grid

In Eq. (5.21), subscript „i" denotes the value at node i and the superscript t denotes the value at time t. It may be noted that the values of concentrations and R_{Cr6} at time t are treated as known quantities, and the values of concentrations at time t+Δt at all nodes i = 1 to N (N= total number of nodes) are treated as unknown quantites, which need to be determined. In Eq. (5.21), $Cr_{6_{i+1/2}}$ are determined using the following equation.

$$Cr_{6i+1/2} = Cr_{6i} + \delta Cr_{6i}/2 \tag{5.22}$$

where, δCr_{6i} is determined using the MINMOD function as given below.

$$\delta Cr_{6i} = Min\,\mathrm{mod}\left(Cr_{6i+1} - Cr_{6i}, Cr_{6i} - Cr_{6i-1}\right) \tag{5.23}$$

$$\text{Minmod(a,b)} = \begin{cases} a & if\ |a| < |b| \quad and \quad ab > 0 \\ b & if\ |b| < |a| \quad and \quad ab > 0 \\ 0 & if \quad ab \le 0 \end{cases}$$

substitution of Eqs. (5.22) and (5.23) in Eq. (5.21) yields

$$\begin{aligned} &\left[-\frac{D_h\theta\Delta t}{\Delta x^2\left(R_{Cr6}\right)_i^t} - \frac{v\theta\Delta t}{\Delta x\left(R_{Cr6}\right)_i^t}\right] Cr_{6i-1}^{\,t+\Delta t} + \left[1 + \frac{2D_h\theta\Delta t}{\Delta x^2\left(R_{Cr6}\right)_i^t} + \frac{v\theta\Delta t}{\Delta x\left(R_{Cr6}\right)_i^t}\right] Cr_{6i}^{\,t+\Delta t} + \left[-\frac{D_h\theta\Delta t}{\Delta x^2\left(R_{Cr6}\right)_i^t}\right] Cr_{6i+1}^{\,t+\Delta t} \\ &= Cr_{6i}^{\,t} + \frac{D_h(1-\theta)\Delta t}{\Delta x^2\left(R_{Cr6}\right)_i^t}\left[Cr_{6i+1}^{\,t} - 2Cr_{6i}^{\,t} + Cr_{6i-1}^{\,t}\right] - \frac{v(1-\theta)\Delta t}{\Delta x\left(R_{Cr6}\right)_i^t}\left[Cr_{6i+1/2}^{\,t} - Cr_{6i-1/2}^{\,t}\right] - \frac{v\theta\Delta t}{\Delta x\left(R_{Cr6}\right)_i^t}\left[\delta Cr_{6i}^{\,t+\Delta t} - \delta Cr_{6i-1}^{\,t+\Delta t}\right] \end{aligned} \tag{5.24}$$

Equation (5.24) when written for all the nodes i = 2 to N-1 along with the upstream and downstream boundary conditions forms a tri-diagonal matrix equation. In this study, inlet concentration was specified as the upstream boundary condition, while a zero gradient condition was applied at the downstream boundary. This matrix equation can be solved easily using the Thomas algorithm (Press et al. 2002). However, an iteration procedure is required for the solution because of the presence of $\delta Cr_{6i}^{\,t+\Delta t}$ and $\delta Cr_{6i-1}^{\,t+\Delta t}$ on the right hand side of Eq. (5.24). In this study, concentrations at the time level t+Δt were assumed and $\delta Cr_{6i}^{\,t+\Delta t}$ and $\delta Cr_{6i-1}^{\,t+\Delta t}$ were evaluated using the Eq. (5.23), and substituted on the right hand side of Eq. (5.24). Equation (5.24) was then solved for better estimates of $Cr_{6i}^{\,t+\Delta t}$, and this procedure was iterated upon till convergence. It may be noted here that the incorporation of retardation involved a lag of one time step because R_{Cr6} was estimated using the values at time level t. This did not introduce significant error since the R_{Cr6} value was not very high in the present study. θ is the implicit time weighing

factor ($0< \theta<1$). θ =0, 0.5 and 1.0 give rise to the explicit Euler, Crank-Nicolson (second order accurate), and fully implicit (first order accurate) schemes. In this study, θ = 0.65 was used to obtain oscillation free results. The numerical accuracy of the adapted mathematical model was validated by comparing the numerical results with the analytical solution (Freeze and Cherry, 1979) for the case when the retardation coefficient is constant.

5.3 ONE-DIMENSIONAL MODEL FOR TRANSPORT WITH BIO TRANSFORMATION

5.3.1 Governing Equations

Mathematical model for the transport accounted for the advective-dispersive-reactive transport of three aqueous species: Li, Cr(VI) and substrate (molasses). Lithium, a conservative pollutant, was used as a tracer. Therefore, Li transport data could be used to determine the dispersion coefficient The column experiments showed that Cr(III) formed due to biotransformation of Cr(VI) did not remain in the liquid phase and it was either precipitated and retained or adsorbed on to the soil matrix almost immediately. The liquid samples collected from all the 16 ports and the outlet tank did not contain any Cr(III). Therefore, Cr(III) transport was not included in the mathematical model.

In the column experiments, there was washout of microbes during the initial stabilization. During this period, water with only mineral medium was allowed to pass through the column till steady state flow conditions were achieved. The amount of washout depended upon the soil. There was more wash out of microbes in columns with sand as compared to those in columns with soil. It may be noted that although there was washout during the stabilization period, the liquid samples taken from 16 ports as well as the outlet tank did not contain significant amount of microbes, once the stabilization was achieved. Therefore, it was assumed that the microbes were immobile and attached to the soil matrix. Only the microbial growth equation was considered and the transport of microbes in the liquid phase was neglected.

It may be noted that in an earlier study on bio-geochemical transport of Cr(VI) through sand columns, Guha (2004) used a similar approach to model the transport and

transformation of Cr(VI). However, in that model, it was assumed that some bacteria were mobile and some were immobile. Also, a double Monod"s kinetic equation was used for microbial growth, in which both Lactate (electron donor) and Cr(VI) (electron acceptor) were treated as substrates. In this study, the Monod"s equation with inhibition was used to model the microbial growth. Batch studies indicated that molasses (substrate) concentration was un-limiting, while Cr(VI) concentration used was much above the inhibition concentration (3.06 mg/L). Also, the batch studies indicated that not all the molasses present was available for microbial utilization. Therefore, the concept of utilizable substrate (Ribesa et al., 2004) was adapted in the model for microbial growth rate. Another modification made to the usual microbial growth rate equation was the introduction of a parameter, λ, which is similar to the microbial metaboloic potential factor used by other researchers (Murphy, 1997; Guha, 2004).

The governing advection-dispersion-reaction equations for one dimensional transport of lithium, hexavalent chromium, substrate, and microbes can be written as follows:

$$\frac{\partial Li}{\partial t} + v\frac{\partial Li}{\partial x} = D_h \frac{\partial^2 Li}{\partial x^2} \tag{5.25}$$

$$R_{Cr6}\frac{\partial Cr_6}{\partial t} + v\frac{\partial Cr_6}{\partial x} = D_h \frac{\partial^2 Cr_6}{\partial x^2} - R_{\sin kCr6} \tag{5.26}$$

$$R_s \frac{\partial S}{\partial t} + v\frac{\partial S}{\partial x} = D_h \frac{\partial^2 S}{\partial x^2} - R_{\sin kS} \tag{5.27}$$

$$R_{\sin kS} = \frac{dS}{dt} \tag{5.28}$$

$$\frac{dS}{dt} = \frac{\lambda \mu M}{Y} \tag{5.29}$$

$$\mu = \left(\frac{\mu_{\max} Su}{K_s + Su}\right)\left(\frac{K_i}{K_i + Cr_6}\right) \quad = 0 \ \ if \quad Su < 0 \tag{5.30}$$

$$Su = S - 0.63\,S_T \tag{5.31}$$

$$\frac{1}{M}\left(\frac{dM}{dt}\right) = \lambda(\mu - k_d) \tag{5.32}$$

$$R_{\sin kCr6} = \frac{M\lambda\eta\mu}{Y} \tag{5.33}$$

in which, Li = lithium concentration in the liquid medium (mg/L); Cr_6 = hexavalent chromium concentration in the liquid medium (mg/L); S = molasses concentration in the liquid medium (mg/L); M = bacterial concentration expressed as mg/L of liquid in the column; Su = utilizable concentration of molasses (mg/L); S_T = total inlet molasses concentration (mg/L); v = pore water velocity (cm/h); R_{Cr6} = retardation coefficient for hexavalent chromium; R_s = retardation coefficient for substrate; $R_{sinkCr6}$ = sink term for hexavalent chromium due to biotransformation; R_{sinkS} = sink term for substrate due to microbial utilization; μ = specific growth rate (1/h); μ_{max} = maximum specific growth rate (1/h); k_d = decay constant (1/h); Y = observed yield coefficient; η = efficiency factor for chromium reduction with respect to substrate utilization; λ = a proportionality constant which takes care of the differences in the microbial growth in a suspended batch system and attached continuous system. It also implicitly accounts for metabolic retardation due to starving in the stabilization and acclimatization periods. In the present model, the pore velocity, v is obtained by dividing the Darcy velocity, U by the porosity of the soil column, ϕ. The coefficient of dispersion, D_h is obtained by multiplying the pore velocity, v with the dispersivity, α_L. Computation of the retardation coefficients for hexavalent chromium and substrate is based on the equilibrium adsorption studies.

5.3.2 Assumptions in the Model

The basic assumptions made in deriving the model can be summarized as follows.

1. The flow in the column is one-dimensional.
2. The porous medium is homogeneous, and the porosity remains constant through out the study period.
3. Adsorption is assumed to occur under equilibrium conditions.

4. The model is based on the "macroscopic modeling" of microbiological reactions. This is a single phase model where all the microorganisms present in a given control volume are equally exposed to the substrate concentration prevailing in the bulk liquid volume (Baveye and Valocchi, 1989).
5. The microbes are immobile.
6. The contaminant is toxic and has inhibitory effect on microbial growth rate.
7. The Monod"s equation with inhibition describes the microbial growth.
8. Only a fraction of substrate is available for Cr(VI) reduction.
9. Cr(III) generated due to biotransformation is either adsorbed or precipitated and retained on the soil matrix.
10. The temperature is constant.

5.3.3 Numerical Technique

A sequential iterative technique was used to solve the non-linear partial differential equations (Herzer and Kinzelbach, 1989; Yeh and Tripathi, 1991; Steefel and MacQuarrie, 1996). In this approach, the advection part was discretized based on the Monotone Upwind Scheme for Conservation Laws (MUSCL)(Van Leer, 1977a, 1977b) which is globally second order accurate and non oscillatory. Diffusive part was approximated by the second order central difference. Finite difference approximations of Eqs. (5.26) and (5.27) can be written, with reference to the finite difference grid shown in Fig. 5.1, as follows.

$$(R_{Cr6})_i^t\left[\frac{Cr_{6i}^{\,t+\Delta t}-Cr_{6i}^{\,t}}{\Delta t}\right]=D_h\theta\left[\frac{Cr_{6i+1}^{\,t+\Delta t}-2Cr_{6i}^{\,t+\Delta t}+Cr_{6i-1}^{\,t+\Delta t}}{\Delta x^2}\right]+D_h(1-\theta)\left[\frac{Cr_{6i+1}^{\,t}-2Cr_{6i}^{\,t}+Cr_{6i-1}^{\,t}}{\Delta x^2}\right]$$
$$-\theta v^{t+\Delta t}\left[\frac{Cr_{6i+1/2}^{\,t+\Delta t}-Cr_{6i-1/2}^{\,t+\Delta t}}{\Delta x}\right]-(1-\theta)v^t\left[\frac{Cr_{6i+1/2}^{\,t}-Cr_{6i-1/2}^{\,t}}{\Delta x}\right]-\theta\left(R_{\sin kCr6}\right)_i^{t+\Delta t}-(1-\theta)\left(R_{\sin kCr6}\right)_i^t \quad (5.34)$$

$$(R_s)_i^t\left[\frac{S_i^{\,t+\Delta t}-S_i^{\,t}}{\Delta t}\right]=D_h\theta\left[\frac{S_{i+1}^{\,t+\Delta t}-2S_i^{\,t+\Delta t}+S_{i-1}^{\,t+\Delta t}}{\Delta x^2}\right]+D_h(1-\theta)\left[\frac{S_{i+1}^{\,t}-2S_i^{\,t}+S_{i-1}^{\,t}}{\Delta x^2}\right]$$
$$-\theta v^{t+\Delta t}\left[\frac{S_{i+1/2}^{t+\Delta t}-S_{i-1/2}^{t+\Delta t}}{\Delta x}\right]-(1-\theta)v^t\left[\frac{S_{i+1/2}^{t}-S_{i-1/2}^{t}}{\Delta x}\right]-\theta\left(R_{\sin kS}\right)_i^{t+\Delta t}-(1-\theta)\left(R_{\sin kS}\right)_i^t \quad (5.35)$$

In Eqs. (5.34) and (5.35),

$$\left(R_{\sin kCr6}\right)_i^t = \frac{M_i^t \lambda \eta \mu_i^t}{Y} \tag{5.36}$$

$$\mu_i^t = \left(\frac{\mu_{\max} Su_i^t}{K_s + Su_i^t}\right)\left(\frac{K_i}{K_i + Cr_{6i}^t}\right) \tag{5.37}$$

$$Su_i^t = S_i^t - 0.63\, S_T \tag{5.38}$$

$$\left(R_{\sin kS}\right)_i^t = \frac{M_i^t \lambda \mu_i^t}{Y} \tag{5.39}$$

$$\left(R_{\sin kCr6}\right)_i^{t+\Delta t} = \frac{M_i^{t+\Delta t} \lambda \eta \mu_i^{t+\Delta t}}{Y} \tag{5.40}$$

$$\mu_i^{t+\Delta t} = \left(\frac{\mu_{\max} Su_i^{t+\Delta t}}{K_s + Su_i^{t+\Delta t}}\right)\left(\frac{K_i}{K_i + Cr_{6i}^{t+\Delta t}}\right) \tag{5.41}$$

$$Su_i^{t+\Delta t} = S_i^{t+\Delta t} - 0.63\, S_T \tag{5.42}$$

$$\left(R_{\sin kS}\right)_i^{t+\Delta t} = \frac{M_i^{t+\Delta t} \lambda \mu_i^{t+\Delta t}}{Y} \tag{5.43}$$

$$M_i^{t+\Delta t} = M_i^t \lambda \Delta t\left(\mu_i^{t+\Delta t} - k_d\right) + M_i^t \tag{5.44}$$

Equations 5.34 and 5.35 can be rearranged as shown below.

$$\begin{aligned}\beta_3 Cr_{6i-1}^{t+\Delta t} + \beta_2 Cr_{6i}^{t+\Delta t} + \beta_1 Cr_{6i+1}^{t+\Delta t} = \beta_4 Cr_{6i-1}^{t} + \beta_5 Cr_{6i}^{t} + \beta_6 Cr_{6i+1}^{t} - \theta\omega_1^{t+\Delta t}\left[\frac{\delta Cr_{6i}^{t+\Delta t}}{2} - \frac{\delta Cr_{6i-1}^{t+\Delta t}}{2}\right] \\ -(1-\theta)\omega_1^{t}\left[\frac{\delta Cr_{6i}^{t}}{2} - \frac{\delta Cr_{6i-1}^{t}}{2}\right] - \theta\Delta t\left(R_{\sin kCr6}\right)_i^{t+\Delta t} - (1-\theta)\Delta t\left(R_{\sin kCr6}\right)_i^{t}\end{aligned} \tag{5.45}$$

$$\begin{aligned}\beta_3 S_{i-1}^{t+\Delta t} + \beta_7 S_i^{t+\Delta t} + \beta_1 S_{i+1}^{t+\Delta t} = \beta_4 S_{i-1}^{t} + \beta_8 S_i^{t} + \beta_6 S_{i+1}^{t} - \theta\omega_1^{t+\Delta t}\left[\frac{\delta S_i^{t+\Delta t}}{2} - \frac{\delta S_{i-1}^{t+\Delta t}}{2}\right] \\ -(1-\theta)\omega_1^{t}\left[\frac{\delta S_i^{t}}{2} - \frac{\delta S_{i-1}^{t}}{2}\right] - \theta\Delta t\left(R_{\sin kS}\right)_i^{t+\Delta t} - (1-\theta)\Delta t\left(R_{\sin kS}\right)_i^{t}\end{aligned} \tag{5.46}$$

where,

$$\beta_1 = \theta(-\omega_2^{t+\Delta t}) \tag{5.47}$$

$$\beta_2 = \theta(\omega_1^{t+\Delta t} + 2\omega_2^{t+\Delta t}) + R_{Cr6}{}^{t} \tag{5.48}$$

$$\beta_3 = \theta(-\omega_1^{t+\Delta t} - \omega_2^{t+\Delta t}) \tag{5.49}$$

$$\beta_4 = (1-\theta)(\omega_1^{t} + \omega_2^{t}) \tag{5.50}$$

$$\beta_5 = (1-\theta)(-\omega_1^{t} - 2\omega_2^{t}) + R_{Cr6}{}^{t} \tag{5.51}$$

$$\beta_6 = (1-\theta)(\omega_2^{t}) \tag{5.52}$$

$$\beta_7 = \theta(\omega_1^{t+\Delta t} + 2\omega_2^{t+\Delta t}) + R_s{}^{t} \tag{5.53}$$

$$\beta_8 = (1-\theta)(-\omega_1^{t} - 2\omega_2^{t}) + R_s{}^{t} \tag{5.54}$$

$$\omega_1 = \frac{\Delta t}{\Delta x} v \tag{5.55}$$

$$\omega_2 = D_h \frac{\Delta t}{(\Delta x)^2} \tag{5.56}$$

Equations 5.45 and 5.46, when written for all the nodes in the domain, along with the upstream and downstream boundary conditions, form two tri-diagonal matrices. In these equations, all the variables with superscript "t" are known, while the solution is sought for the variables with superscript "t+Δt", by solving the matrix Eqs. (5.45) and (5.46). Solution of these matrix equations is not straight forward because these two equations are coupled through the sink terms, and the presence of $\delta Cr_{6i}{}^{t+\Delta t}$ and $\delta S_i{}^{t+\Delta t}$ on the right hand side. Following iterative procedure was used to determine the concentrations at the time level t+Δt.

To start with, concentrations of Cr(VI), substrate, and microbes at the time level t+Δt are assumed. Values of $\delta Cr_{6i}{}^{t+\Delta t}$, $\delta Cr_{6i\text{-}1}{}^{t+\Delta t}$, $R_{\sin kCr6}^{t+\Delta t}$, $\delta S_i^{t+\Delta t}$, $\delta S_{i-1}^{t+\Delta t}$ and $R_{\sin kS}^{t+\Delta t}$ were

evaluated and substituted on the right hand side of Eq. (5.45) and Eq (5.46), respectively. These equations were then solved for better estimates of $Cr_{6i}^{t+\Delta t}$, $S_i^{t+\Delta t}$, and $M_i^{t+\Delta t}$. Absolute values of the differences in the assumed and estimated concentrations of Cr(VI) and substrate were calculated and the maximum error was determined. If the maximum error was more than a pre-specified tolerance value, once again the above procedure for getting better estimates was followed. These iterations were continued until the differences in the assumed and estimated values were less than the tolerance limit. Once the values of variables at time t+Δt were determined, same procedure was followed to estimate concentrations at t +2Δt, using the values at the time level at t+Δt. This procedure was repeated till the last time step was reached. It may be noted here that the incorporation of retardation involved a lag of one time step because R_{Cr6} and R_s were estimated using the values at time level t. This did not introduce significant error since R_{Cr6} and R_s values were not very high in the present study. The above algorithm gives numerically stable and oscillation free results when the following criterion for computational time step is satisfied.

$$\Delta t = \frac{C_n \cdot \Delta x}{u} \tag{5.57}$$

in which, C_n = Courant number. C_n is taken less than one for suppressing numerical oscillations. Fig. 5.2 shows the flow chart for the numerical algorithm.

It may be noted here that also a one-dimensional transport and transformation model was developed (details not presented here) in which the biotransfomation module corresponds to biotransformation by CRB, IRB, and SRB in presence of Fe and sulphates. The biotrnasformation module is same as that presented in section 5.1.

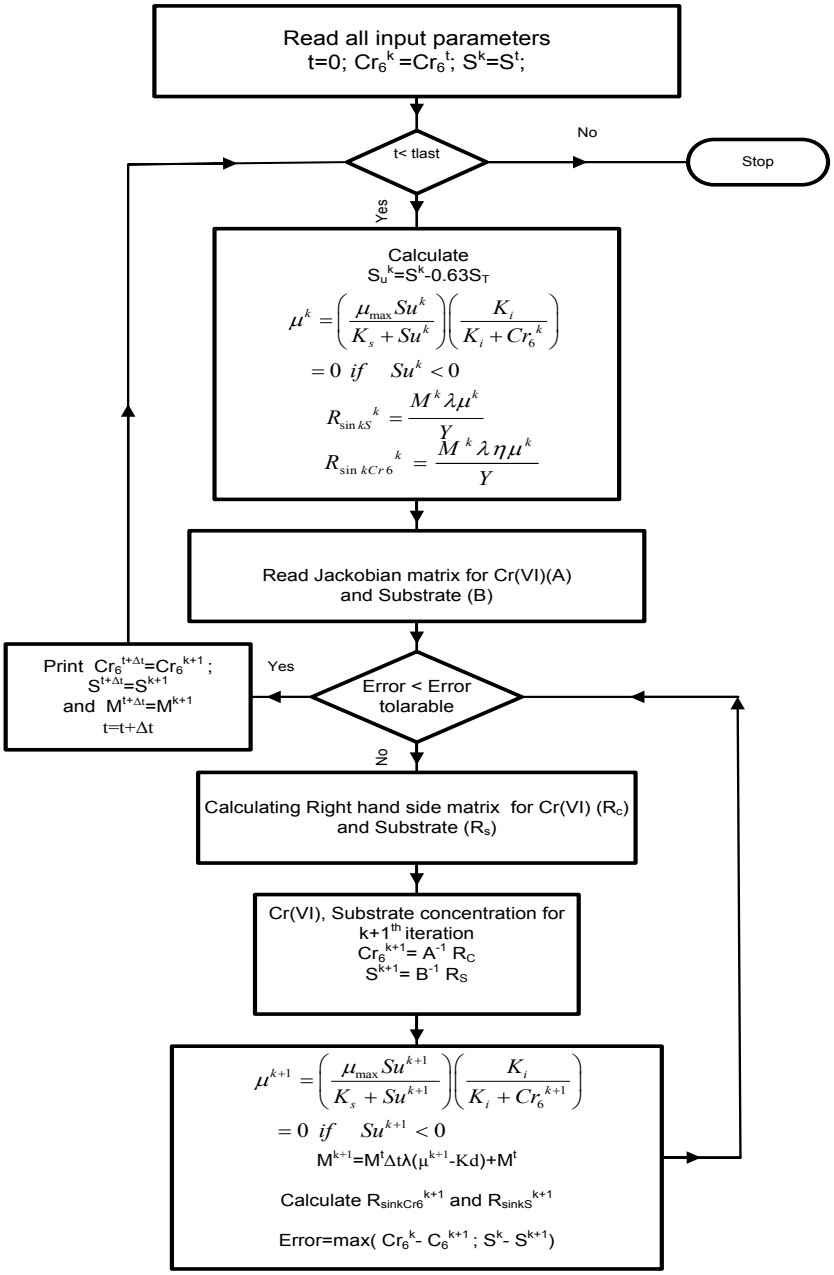

Fig. 5.2: Flow chart of solving procedure of one-dimensional model for transport with bio transformation

5.4 TWO-DIMENSIONAL MODEL FOR TRANSPORT WITH BIO TRANSFORMATION

5.4.1 Governing Equations for Confined Aquifers

The governing equations used in two-dimensional mathematical model for transport and biotransformation of Cr^{6+} in contaminated confined aquifers are described in this section. Mathematical model for the transport accounts for the advective-dispersive-reactive transport, along with adsorption and source/sink terms of four species: Li, Cr^{6+}, molasses (S) and mobile bacteria (M_m); reactive equation for immobile bacteria (M_i); and ground water flow equations.

Lithium, a conservative pollutant, is used as a tracer. Therefore, Li transport data can be used to determine the dispersive coefficients. Only Cr^{6+} transport is used in the model since many earlier column experiments showed that Cr^{3+} is immobile. Bacteria is divided into both mobile (M_m) and immobile (M_i) parts. For both these bacteria, molasses (S) is required for growth.

For adsorption, we get an extra term in our transport equation (i.e., $\frac{\rho_b \partial S_a}{\Phi \partial t}$). But in our transport equation we replace it with a retardation coefficient, which can be calculated assuming an isotherm. Batch equilibrium studies indicated that Freundlich isotherm fits well with the experimental data, and therefore, this non-linear isotherm was adopted for use in the transport equation. $\left\langle S_a = K_f C^{(1/n)} \right\rangle$. After using this isotherm, the resultant transport equation has the following retardation coefficient in the rate of change in the control volume term $\left\langle R_C = 1 + \frac{\rho_b}{n\Phi} K_f C^{(1/n)-1} \right\rangle$.

The Monad"s equation with inhibition is used to model the microbial growth. In many situations, molasses (substrate) concentration could be un-limiting, while Cr^{6+} concentration could be much above the inhibition concentration (3.06 mg/L). Also, the batch studies indicated that not all the molasses present may be available for microbial

utilization. Therefore, concept of utilizable substrate (Ribesa et al., 2004) is adapted in the model for the microbial growth rate. Another modification made to the usual microbial growth rate equation is the introduction of a parameter, λ, which is similar to the microbial metabolic potential factor used by other researchers (Guha, 2004).

The ground water flow equations for two-dimensional flow are written for saturated confined aquifers, including source/sink term for recharge/pumping.

5.4.1.1 Two-dimensional reactive transport equations

$$R_{cr}\frac{\partial Cr}{\partial t}+\hat{A}\,(Cr)=\hat{D}\,(Cr)-\frac{\eta\lambda\mu M}{\gamma} \tag{5.58}$$

$$R_s\frac{\partial S}{\partial t}+\hat{A}(S)-\frac{S_j q_j}{n}=\hat{D}(S)-\frac{\lambda\mu M}{\gamma} \tag{5.59}$$

$$\frac{\partial M_m}{\partial t}+\hat{A}(M_m)-\frac{M_j q_j}{n}=\hat{D}(M_m)+\lambda M_m\mu_m-\frac{\rho_b}{\Phi}K_m(M_m-M_i) \tag{5.60}$$

$$\frac{dM_i}{dt}=\lambda M_i\mu_i+\frac{\rho_b}{\Phi}K_m\left(M_m-M_i\right) \tag{5.61}$$

$$\mu_m=\left(\frac{\mu_{\max}S_u}{K_s+S_u}\right)\left(\frac{K_{im}}{K_{im}+Cr}\right)$$
$$=0\quad if\quad S_u<0 \tag{5.62}$$

$$\mu_i=\left(\frac{\mu_{\max}S_u}{K_s+S_u}\right)\left(\frac{K_{ii}}{K_{ii}+Cr}\right)$$
$$=0\quad if\quad S_u<0 \tag{5.63}$$

$$S_u=S-1000 \tag{5.64}$$

$$\mu=\frac{M_m\mu_m+M_i\mu_i}{M} \tag{5.65}$$

$$M=M_m+M_i \tag{5.66}$$

$$R_{cr}=1+\frac{\rho_b}{n_c\Phi}K_{cr}\left(Cr\right)^{(1/n_c)-1} \tag{5.67}$$

$$R_s=1+\frac{\rho_b}{n_s\Phi}K_{ss}\left(S\right)^{(1/n_s)-1} \tag{5.68}$$

$$\hat{A} = \frac{\partial}{\partial x}(u \quad) + \frac{\partial}{\partial y}(v \quad) \tag{5.69}$$

$$\hat{D} = \frac{\partial}{\partial x}\left[D_{xx} \frac{\partial}{\partial x} + D_{xy} \frac{\partial}{\partial y} \right] + \frac{\partial}{\partial y}\left[D_{yx} \frac{\partial}{\partial x} + D_{yy} \frac{\partial}{\partial y} \right] \tag{5.70}$$

5.4.1.2 Two-dimensional ground water flow equations

$$\frac{\partial}{\partial x}\left(K_x \frac{\partial h}{\partial x} \right) + \frac{\partial}{\partial y}\left(K_y \frac{\partial h}{\partial y} \right) - q_j = S_S \frac{\partial h}{\partial t} \tag{5.71}$$

$$u'' = -K_x \frac{\partial h}{\partial x} \tag{5.72}$$

$$v'' = -K_y \frac{\partial h}{\partial y} \tag{5.73}$$

$$u = \frac{u'}{\Phi} \tag{5.74}$$

$$v = \frac{v'}{\Phi} \tag{5.75}$$

where, x- longitudinal distance from the reference point; y- transverse distance from the reference point; t- time from the start of the transport; Li - Lithium concentration in the liquid medium (mg/l); Cr - hexavalent chromium concentration in the liquid medium (mg/l); S - molasses concentration in the liquid medium (mg/l); M_m - mobile bacterial concentration in the liquid medium (mg/l); M_i - immobile bacterial concentration expressed as mg/l of liquid in the column; M - total bacterial concentration expressed as mg/l; M_j - bacterial concentration added to aquifer through wells expressed as mg/l; S_u - utilizable concentration of molasses (mg/l); S_T - total inlet molasses concentration (mg/l); S_j - molasses concentration added to aquifer through wells expressed as mg/l; R_{Cr} - retardation coefficient for hexavalent chromium; R_S - retardation coefficient for substrate; $K_{ss}, K_{cr}, n_s, n_{cr}$ - Freundlich coefficients (l/mg) and constants (dimensionless) respectively for substrate and chromium; μ_m - specific growth rate of mobile bacteria; μ_i - specific growth rate of immobile bacteria; μ - specific growth rate of total bacteria;

μ_{max} - maximum specific growth rate; Y - observed yield coefficient; η - efficiency factor for chromium reduction with respect to substrate utilization; λ - a proportionality constant which takes care of the differences in the microbial growth in a suspended batch system and attached continuous system (it also implicitly accounts for metabolic retardation due to starving in the stabilization and acclimatization periods); K_s - half saturation constant of the substrate in Monad‟s equation; K_{im} - inhibition constant due to mobile bacteria; K_{ii} - inhibition constant due to immobile bacteria; $\hat{A}$ - advection operator; $\hat{D}$ - dispersion operator; D_{ij} - dispersion in i^{th} direction due to the change in the concentration in the j^{th} direction; K_i - permeability of soil in i^{th} direction; Q_j - recharge rate expressed as discharge per unit area (m/s); q_j - recharge rate expressed as discharge per unit volume $\left(s^{-1}\right)$; S_s - specific storage of the confined aquifer; h- piezometric head in the aquifer; u- pore velocity in x-dir; v- pore velocity in y-dir; u‟- Darcy velocity in x-dir; v‟- Darcy velocity in y-dir; Φ - porosity of the soil medium; ρ_b - bulk density of the soil medium $\left(g/cm^3\right)$.

5.4.1.3 Assumptions

The basic assumptions made in deriving the model are as follows:

- The flow in the aquifer is two-dimensional
- Soil medium is heterogeneous and anisotropic
- Aquifer is confined, aquifer thickness is more or less constant, and the porosity remains constant through out the medium
- Adsorption is assumed to occur under equilibrium conditions
- This model is based on the “macroscopic modeling” of microbiological reactions. This is a single phase model where all the micro organisms present in a given control volume are equally exposed to the substrate concentration prevailing in the bulk liquid volume (Baveye and Valocchi, 1989)
- Contaminant is toxic and has inhibitory effect on the microbial growth rate
- The Monod‟s equation with inhibition describes the microbial growth.
- Only a fraction of substrate is available for Cr^{6+} reduction

- Cr^{3+} generated due to biotransformation is either adsorbed or precipitated and retained on the soil matrix.
- Temperature is constant.

5.4.2 Governing Equations for Unconfined Aquifers

The governing equations used in two-dimensional mathematical model for transport and biotransformation of Cr^{6+} in contaminated unconfined aquifers are described in this section.

5.4.2.1 Two-dimensional reactive transport equations

$$R_{cr}\frac{\partial Cr}{\partial t}+R_{hcr}\frac{\partial h}{\partial t}+\hat{A}(Cr) = \hat{D}(Cr)-\frac{\eta\lambda}{\gamma}\mu hM \tag{5.76}$$

$$R_s\frac{\partial S}{\partial t}+R_{hs}\frac{\partial h}{\partial t}+\hat{A}(S)-\frac{S_jQ_j}{n}=\hat{D}(S)-\frac{\lambda\mu Mh}{\gamma} \tag{5.78}$$

$$h\frac{\partial M_m}{\partial t}+M_m\frac{\partial h}{\partial t}+\hat{A}(M_m)-\frac{M_jQ_j}{n} = \hat{D}(M_m)+\lambda h\mu_m M_m-\frac{\rho_b}{\Phi}K_m(M_m-M_i)h \tag{5.79}$$

$$\frac{d(M_ih)}{dt} = \lambda h\mu_iM_i+\frac{\rho_b}{\Phi}K_m(M_m-M_i)h \tag{5.80}$$

$$\mu_m=\left(\frac{\mu_{\max}S_u}{K_s+S_u}\right)\left(\frac{K_{im}}{K_{im}+Cr}\right) \tag{5.81}$$
$$=0 \quad if \quad S_u<0$$

$$\mu_i=\left(\frac{\mu_{\max}S_u}{K_s+S_u}\right)\left(\frac{K_{ii}}{K_{ii}+Cr}\right) \tag{5.82}$$
$$=0 \quad if \quad S_u<0$$

$$S_u=S-1000 \tag{5.83}$$

$$\mu=\frac{M_m\mu_m+M_i\mu_i}{M} \tag{5.84}$$

$$M=M_m+M_i \tag{5.85}$$

$$R_{cr}=h\left(1+\frac{\rho_b}{n_{cr}\phi}K_{cr}cr^{\frac{1}{n}-1}\right) \tag{5.86}$$

$$R_{hcr}=cr\left(1+\frac{\rho_b}{\phi}K_{cr}cr^{\frac{1}{n}-1}\right) \tag{5.87}$$

$$R_S = h\left(1+\frac{\rho_b}{n_S\phi}K_S S^{\frac{1}{n}-1}\right) \tag{5.88}$$

$$R_{hcr} = S\left(1+\frac{\rho_b}{\phi}K_S S^{\frac{1}{n}-1}\right) \tag{5.89}$$

$$\hat{A} = \frac{\partial}{\partial x}(uh(\ )) + \frac{\partial}{\partial y}(vh(\ )) \tag{5.90}$$

$$\hat{D} = \frac{\partial}{\partial x}\left[D_{xx}h\frac{\partial(\ )}{\partial x} + D_{xy}h\frac{\partial(\ )}{\partial y}\right] + \frac{\partial}{\partial y}\left[D_{yx}h\frac{\partial(\ )}{\partial x} + D_{yy}h\frac{\partial(\ )}{\partial y}\right] \tag{5.91}$$

5.4.2.2 Two-dimensional ground water flow equations

$$\frac{\partial}{\partial x}\left(K_x h\frac{\partial h}{\partial x}\right) + \frac{\partial}{\partial y}\left(K_y h\frac{\partial h}{\partial y}\right) - Q_j = S_y\frac{\partial h}{\partial t} \tag{5.92}$$

$$u'' = -K_x\frac{\partial h}{\partial x} \tag{5.93}$$

$$v'' = -K_y\frac{\partial h}{\partial y} \tag{5.94}$$

$$u = \frac{u'}{\Phi} \tag{5.95}$$

$$v = \frac{v'}{\Phi} \tag{5.96}$$

In the above equations, S_y is the specific yield of the unconfined aquifer. Assumptions behinf the model for unconfined aquifer are same as those for confined aquifer. In addition, it is assumed that Dupuit"s assumption is valid for unconfined aquifer.

5.4.3 Governing Equations for Simplified Transport and Transformation Model

In the present study, a simplified model for transport and chromium reduction was also developed, based on the following assumptions:

1. bacteria is immobile;
2. net growth rate of bacteria is zero i.e, chromium reduction is by resting cells, which consume substrate for only metabolism and not for growth;

3. chromium reduction can be described by a first-order reaction in which reduction is proportional to the concentration of bacteria at that location, and this reaction rate constant depends on Cr(VI) concentration;
4. substrate consumption is related to the chromium reduction by a constant factor;
5. chromium reduction occurs only when bacteria and substrate are present.

Thus the simplified model considers the advection-dispersion-reaction equations for only hexavalaent chromium and the substrate. The transport equations for an unconfined aquifer are given below:

$$R_{cr}\frac{\partial Cr}{\partial t}+R_{hcr}\frac{\partial h}{\partial t}+\hat{A}(Cr) \;=\; \hat{D}(Cr)-\lambda hM\left[\frac{K_i}{\frac{K_i}{Cr}+Cr}\right] \tag{5.97}$$

$$R_S\frac{\partial S}{\partial t}+R_{hS}\frac{\partial h}{\partial t}+\hat{A}(S)-S_j q_j \;=\; \hat{D}(S)-\frac{\lambda hM}{\eta}\left[\frac{K_i}{\frac{K_i}{Cr}+Cr}\right] \tag{5.98}$$

$$R_{cr}=h\left(1+\frac{\rho_b}{n_{cr}\phi}K_{cr}Cr^{\frac{1}{n}-1}\right) \tag{5.99}$$

$$R_{hcr}=Cr\left(1+\frac{\rho_b}{\phi}K_{cr}Cr^{\frac{1}{n}-1}\right) \tag{5.100}$$

$$R_S=h\left(1+\frac{\rho_b}{n_S\phi}K_S S^{\frac{1}{n}-1}\right) \tag{5.101}$$

$$R_{hcr}=S\left(1+\frac{\rho_b}{\phi}K_S S^{\frac{1}{n}-1}\right) \tag{5.102}$$

$$\hat{A}=\frac{\partial}{\partial x}(uh(\;))+\frac{\partial}{\partial y}(vh(\;)) \tag{5.103}$$

$$\hat{D}=\frac{\partial}{\partial x}\left[D_{xx}h\frac{\partial(\;)}{\partial x}+D_{xy}h\frac{\partial(\;)}{\partial y}\right]+\frac{\partial}{\partial y}\left[D_{yx}h\frac{\partial(\;)}{\partial x}+D_{yy}h\frac{\partial(\;)}{\partial y}\right] \tag{5.104}$$

In the above equations, λ is a reaction rate constant and K_i represents the inhibition to microbial activity due to Cr(VI) concentration. The model for microbial reduction for Cr(VI) gives a reduction rate of zero when Cr(VI) concentration is zero, and it is once again zero when Cr(VI) concentration is infinity due to inhibition effect.

5.4.4 Numerical Technique

In previous sub-sections, mathematical models for simulating the two-dimensional transport and biotransformation of Cr^{6+} in aquifers are presented. These mathematical models consist of a set of partial differential equations and solving these equations requires numerical techniques. Therefore, in this sub-section, the numerical methods used for solving different partial differential equations in the mathematical model are discussed. First, the numerical technique for groundwater flow is discussed and the second part discusses the numerical technique used for Cr^{6+} transport and biotransformation.

5.4.4.1 Numerical Technique for Groundwater Flow Equations

The governing equation for groundwater flow is discretized by Crank-Nicolson Scheme. The dispersion part in the differential equation is approximated using second order central difference. Finite-volume method is used to discretize these equations. In the finite-volume method, the aquifer is divided into a number of cells, and for each cell the law of conservation of mass for water is used to arrive at these equations. The discretized equations are applicable for all cells and they form a system of non-linear equations. So, for solving this system of non-linear equations, Newton-Raphson method is used. The numerical method is explained with particular reference to model for unconfined aquifers presented in section 5.4.2.

The discretized equation for equation 5.92 is:

$$(1-\theta)\left(\frac{Kx_{i+1/2,j}\left(\frac{h^t_{i+1,j}-h^t_{i,j}}{\Delta x}.\frac{h^t_{i+1,j}+h^t_{i,j}}{2}\right)-Kx_{i-1/2,j}\left(\frac{h^t_{i,j}-h^t_{i-1,j}}{\Delta x}.\frac{h^t_{i,j}+h^t_{i-1,j}}{2}\right)}{\Delta x}\right.$$

$$\left.+\frac{Ky_{i,j+1/2}\left(\frac{h^t_{i,j+1}-h^t_{i,j}}{\Delta y}.\frac{h^t_{i,j+1}+h^t_{i,j}}{2}\right)-Ky_{i,j-1/2}\left(\frac{h^t_{i,j}-h^t_{i,j-1}}{\Delta y}.\frac{h^t_{i,j}+h^t_{i,j-1}}{2}\right)}{\Delta y}\right)$$

$$+\theta\left(\frac{Kx_{i+1/2,j}\left(\frac{h^{t+\Delta t}_{i+1,j}-h^{t+\Delta t}_{i,j}}{\Delta x}.\frac{h^{t+\Delta t}_{i+1,j}+h^{t+\Delta t}_{i,j}}{2}\right)-Kx_{i-1/2,j}\left(\frac{h^{t+\Delta t}_{i,j}-h^{t+\Delta t}_{i-1,j}}{\Delta x}.\frac{h^{t+\Delta t}_{i,j}+h^{t+\Delta t}_{i-1,j}}{2}\right)}{\Delta x}\right.$$

$$\left.+\frac{Ky_{i,j+1/2}\left(\frac{h^{t+\Delta t}_{i,j+1}-h^{t+\Delta t}_{i,j}}{\Delta y}.\frac{h^{t+\Delta t}_{i,j+1}+h^{t+\Delta t}_{i,j}}{2}\right)-Ky_{i,j-1/2}\left(\frac{h^{t+\Delta t}_{i,j}-h^{t+\Delta t}_{i,j-1}}{\Delta y}.\frac{h^{t+\Delta t}_{i,j}+h^{t+\Delta t}_{i,j-1}}{2}\right)}{\Delta y}\right)$$

$$+\left(\frac{(1-\theta)\cdot Q^t_{i,j}+\theta\cdot Q^{t+\Delta t}_{i,j}}{\Delta x.\cdot\Delta y}\right)\quad=\quad S_y\left(\frac{h^{t+\Delta t}_{i,j}-h^t_{i,j}}{\Delta t}\right)\qquad(5.105)$$

Equation 5.105 can be written for all the cells (i,j) in the computational domain. These equations are suitably modified for boundary cells to account for boundary conditions. Equation (5.105), when written for all the cells in the domain, forms a set of non-linear equations in the unknowns $h_{i,j}$, and when Newton-Raphson methods is applied, a set of linear equations are formed and it is an iterative method, and the system of linear equations is solved using the Jacobi iteration method. The solution from these equations is the head at each cell in the aquifer. From values of head, velocities in the x and y

directions can be calculated using Darcy"s equation. Equations 5.93 and 5.94 are discretized as:

$$u''^{t}_{i+1/2,j} = -K^{\ t}_{x\,i+1/2,j} \cdot \frac{h^{t}_{i+1,j} - h^{t}_{i,j}}{\Delta x} \tag{5.106}$$

$$v''^{t}_{i+1/2,j} = -K^{\ t}_{y\,i,j+1/2} \cdot \frac{h^{t}_{i,j+1} - h^{t}_{i,j}}{\Delta y} \tag{5.107}$$

5.4.4.2 Numerical Technique for Transport and Biotransformation of Cr^{6+}

Governing equations for transport and biotransformation of Cr^{6+} are also discretized by Crank-Nicolson Scheme. In the partial differential equations, the advection part is discretized using Essentially Non-Oscillating Scheme with minmod limiter, and dispersion part is approximated by the second order central difference. Here also, finite-volume method is used to discretize these equations. In the finite-volume method, the aquifer is divided into a number of cells, and for each cell the law of conservation of mass for chromium, substrate and bacteria are used to arrive at these equations.

Here, the system of partial differential equations needs to be solved, and the discretized equations form systems of non-linear equations. So, for solving these systems of non-linear equations, sequential iterative technique is used. The contaminant transport equations, i.e., from equations 5.76 to 5.91, are discretized as shown below:

$$R_{cr\,i,j}^{\ t}\left(\frac{Cr_{i,j}^{t+\Delta t} - Cr_{i,j}^{t}}{\Delta t}\right)$$

$$+\left(\frac{1-\theta}{\Delta x}\right)\left[Cr_{i+1/2,j}^{t} \cdot U_{i+1/2,j}^{t} - Cr_{i-1/2,j}^{t} \cdot U_{i-1/2,j}^{t}\right] + \left(\frac{\theta}{\Delta x}\right)\left[Cr_{i+1/2,j}^{t+\Delta t} \cdot U_{i+1/2,j}^{t+\Delta t} - Cr_{i-1/2,j}^{t+\Delta t} \cdot U_{i-1/2,j}^{t+\Delta t}\right]$$

$$+\left(\frac{1-\theta}{\Delta y}\right)\left[Cr_{i,j+1/2}^{t}\cdot V_{i,j+1/2}^{t}-Cr_{i,j-1/2}^{t}\cdot V_{i,j-1/2}^{t}\right]+\left(\frac{\theta}{\Delta y}\right)\left[Cr_{i,j+1/2}^{t+\Delta t}\cdot V_{i,j+1/2}^{t+\Delta t}-Cr_{i,j-1/2}^{t+\Delta t}\cdot V_{i,j-1/2}^{t+\Delta t}\right]$$

$$=\left(\frac{1-\theta}{\Delta x}\right)\left[D_{xxi+1/2,j}^{t}\cdot\frac{Cr_{i+1,j}^{t}-Cr_{i,j}^{t}}{\Delta x}+D_{xyi+1/2,j}^{t}\cdot\frac{Cr_{i+1,j+1}^{t}+Cr_{i,j+1}^{t}-Cr_{i+1,j-1}^{t}-Cr_{i,j-1}^{t}}{4\cdot\Delta y}\right.$$

$$\left.-D_{xxi-1/2,j}^{t}\cdot\frac{Cr_{i,j}^{t}-Cr_{i-1,j}^{t}}{\Delta x}-D_{xyi-1/2,j}^{t}\cdot\frac{Cr_{i,j+1}^{t}+Cr_{i-1,j+1}^{t}-Cr_{i,j-1}^{t}-Cr_{i-1,j-1}^{t}}{4\cdot\Delta y}\right]$$

$$+\left(\frac{\theta}{\Delta x}\right)\left[D_{xxi+1/2,j}^{t+\Delta t}\cdot\frac{Cr_{i+1,j}^{t+\Delta t}-Cr_{i,j}^{t+\Delta t}}{\Delta x}+D_{xyi+1/2,j}^{t+\Delta t}\cdot\frac{Cr_{i+1,j+1}^{t+\Delta t}+Cr_{i,j+1}^{t+\Delta t}-Cr_{i+1,j-1}^{t+\Delta t}-Cr_{i,j-1}^{t+\Delta t}}{4\cdot\Delta y}\right.$$

$$\left.-D_{xxi-1/2,j}^{t+\Delta t}\cdot\frac{Cr_{i,j}^{t+\Delta t}-Cr_{i-1,j}^{t+\Delta t}}{\Delta x}-D_{xyi-1/2,j}^{t+\Delta t}\cdot\frac{Cr_{i,j+1}^{t+\Delta t}+Cr_{i-1,j+1}^{t+\Delta t}-Cr_{i,j-1}^{t+\Delta t}-Cr_{i-1,j-1}^{t+\Delta t}}{4\cdot\Delta y}\right]$$

$$+\left(\frac{1-\theta}{\Delta y}\right)\left[D_{yxi,j+1/2}^{t}\cdot\frac{Cr_{i+1,j+1}^{t}+Cr_{i+1,j}^{t}-Cr_{i-1,j+1}^{t}-Cr_{i-1,j}^{t}}{4\cdot\Delta x}+D_{yyi,j+1/2}^{t}\cdot\frac{Cr_{i,j+1}^{t}-Cr_{i,j}^{t}}{\Delta y}\right.$$

$$\left.-D_{yxi,j+1/2}^{t}\cdot\frac{Cr_{i+1,j}^{t}+Cr_{i+1,j-1}^{t}-Cr_{i-1,j}^{t}-Cr_{i-1,j-1}^{t}}{4\cdot\Delta x}+D_{yyi,j+1/2}^{t}\cdot\frac{Cr_{i,j}^{t}-Cr_{i,j-1}^{t}}{\Delta y}\right]$$

$$+\left(\frac{\theta}{\Delta y}\right)\left[D_{yxi,j+1/2}^{t+\Delta t}\cdot\frac{Cr_{i+1,j+1}^{t+\Delta t}+Cr_{i+1,j}^{t+\Delta t}-Cr_{i-1,j+1}^{t+\Delta t}-Cr_{i-1,j}^{t+\Delta t}}{4\cdot\Delta x}+D_{yyi,j+1/2}^{t+\Delta t}\cdot\frac{Cr_{i,j+1}^{t+\Delta t}-Cr_{i,j}^{t+\Delta t}}{\Delta y}\right.$$

$$\left.-D_{yxi,j+1/2}^{t+\Delta t}\cdot\frac{Cr_{i+1,j}^{t+\Delta t}+Cr_{i+1,j-1}^{t+\Delta t}-Cr_{i-1,j}^{t+\Delta t}-Cr_{i-1,j-1}^{t+\Delta t}}{4\cdot\Delta x}+D_{yyi,j+1/2}^{t}\cdot\frac{Cr_{i,j}^{t+\Delta t}-Cr_{i,j-1}^{t+\Delta t}}{\Delta y}\right]$$

$$-\frac{(1-\theta)\cdot\eta\cdot\lambda}{\gamma}\cdot\mu_{i,j}^{t}\cdot M_{i,j}^{t}-\frac{\theta\cdot\eta\cdot\lambda}{\gamma}\cdot\mu_{i,j}^{t+\Delta t}\cdot M_{i,j}^{t+\Delta t}\qquad(5.108)$$

$$R_{Si,j}^{\ t}\left(\frac{S_{i,j}^{t+\Delta t}-S_{i,j}^{t}}{\Delta t}\right)$$

$$+\left(\frac{1-\theta}{\Delta x}\right)\left[S_{i+1/2,j}^{t}\cdot U_{i+1/2,j}^{t}-S_{i-1/2,j}^{t}\cdot U_{i-1/2,j}^{t}\right]+\left(\frac{\theta}{\Delta x}\right)\left[S_{i+1/2,j}^{t+\Delta t}\cdot U_{i+1/2,j}^{t+\Delta t}-S_{i-1/2,j}^{t+\Delta t}\cdot U_{i-1/2,j}^{t+\Delta t}\right]$$

$$+\left(\frac{1-\theta}{\Delta y}\right)\left[S^{t}_{i,j+1/2}\cdot V^{t}_{i,j+1/2}-S^{t}_{i,j-1/2}\cdot V^{t}_{i,j-1/2}\right]+\left(\frac{\theta}{\Delta y}\right)\left[S^{t+\Delta t}_{i,j+1/2}\cdot V^{t+\Delta t}_{i,j+1/2}-S^{t+\Delta t}_{i,j-1/2}\cdot V^{t+\Delta t}_{i,j-1/2}\right]$$

$$=\left(\frac{1-\theta}{\Delta x}\right)\left[D^{t}_{xxi+1/2,j}\cdot\frac{S^{t}_{i+1,j}-S^{t}_{i,j}}{\Delta x}+D^{t}_{xyi+1/2,j}\cdot\frac{S^{t}_{i+1,j+1}+S^{t}_{i,j+1}-S^{t}_{i+1,j-1}-S^{t}_{i,j-1}}{4\cdot\Delta y}\right.$$

$$\left.-D^{t}_{xxi-1/2,j}\cdot\frac{S^{t}_{i,j}-S^{t}_{i-1,j}}{\Delta x}-D^{t}_{xyi-1/2,j}\cdot\frac{S^{t}_{i,j+1}+S^{t}_{i-1,j+1}-S^{t}_{i,j-1}-S^{t}_{i-1,j-1}}{4\cdot\Delta y}\right]$$

$$+\left(\frac{\theta}{\Delta x}\right)\left[D^{t+\Delta t}_{xxi+1/2,j}\cdot\frac{S^{t+\Delta t}_{i+1,j}-S^{t+\Delta t}_{i,j}}{\Delta x}+D^{t+\Delta t}_{xyi+1/2,j}\cdot\frac{S^{t+\Delta t}_{i+1,j+1}+S^{t+\Delta t}_{i,j+1}-S^{t+\Delta t}_{i+1,j-1}-S^{t+\Delta t}_{i,j-1}}{4\cdot\Delta y}\right.$$

$$\left.-D^{t+\Delta t}_{xxi-1/2,j}\cdot\frac{S^{t+\Delta t}_{i,j}-S^{t+\Delta t}_{i-1,j}}{\Delta x}-D^{t+\Delta t}_{xyi-1/2,j}\cdot\frac{S^{t+\Delta t}_{i,j+1}+S^{t+\Delta t}_{i-1,j+1}-S^{t+\Delta t}_{i,j-1}-S^{t+\Delta t}_{i-1,j-1}}{4\cdot\Delta y}\right]$$

$$+\left(\frac{1-\theta}{\Delta y}\right)\left[D^{t}_{yxi,j+1/2}\cdot\frac{S^{t}_{i+1,j+1}+S^{t}_{i+1,j}-S^{t}_{i-1,j+1}-S^{t}_{i-1,j}}{4\cdot\Delta x}+D^{t}_{yyi,j+1/2}\cdot\frac{S^{t}_{i,j+1}-S^{t}_{i,j}}{\Delta y}\right.$$

$$\left.-D^{t}_{yxi,j+1/2}\cdot\frac{S^{t}_{i+1,j}+S^{t}_{i+1,j-1}-S^{t}_{i-1,j}-S^{t}_{i-1,j-1}}{4\cdot\Delta x}+D^{t}_{yyi,j+1/2}\cdot\frac{S^{t}_{i,j}-S^{t}_{i,j-1}}{\Delta y}\right]$$

$$+\left(\frac{\theta}{\Delta y}\right)\left[D^{t+\Delta t}_{yxi,j+1/2}\cdot\frac{S^{t+\Delta t}_{i+1,j+1}+S^{t+\Delta t}_{i+1,j}-S^{t+\Delta t}_{i-1,j+1}-S^{t+\Delta t}_{i-1,j}}{4\cdot\Delta x}+D^{t+\Delta t}_{yyi,j+1/2}\cdot\frac{S^{t+\Delta t}_{i,j+1}-S^{t+\Delta t}_{i,j}}{\Delta y}\right.$$

$$\left.-D^{t+\Delta t}_{yxi,j+1/2}\cdot\frac{S^{t+\Delta t}_{i+1,j}+S^{t+\Delta t}_{i+1,j-1}-S^{t+\Delta t}_{i-1,j}-S^{t+\Delta t}_{i-1,j-1}}{4\cdot\Delta x}+D^{t}_{yyi,j+1/2}\cdot\frac{S^{t+\Delta t}_{i,j}-S^{t+\Delta t}_{i,j-1}}{\Delta y}\right]$$

$$-\frac{(1-\theta)\cdot\lambda}{\gamma}\cdot\mu^{t}_{i,j}\cdot M^{t}_{i,j}-\frac{\theta\cdot\lambda}{\gamma}\cdot\mu^{t+\Delta t}_{i,j}\cdot M^{t+\Delta t}_{i,j} \tag{5.109}$$

$$\left(\frac{M_{mi,j}{}^{t+\Delta t}-M_{mi,j}{}^{t}}{\Delta t}\right)$$

$$+\left(\frac{1-\theta}{\Delta x}\right)\left[M_{mi+1/2,j}{}^{t}\cdot U^{t}_{i+1/2,j}-M_{mi-1/2,j}{}^{t}\cdot U^{t}_{i-1/2,j}\right]+\left(\frac{\theta}{\Delta x}\right)\left[M_{mi+1/2,j}{}^{t+\Delta t}\cdot U^{t+\Delta t}_{i+1/2,j}-M_{mi-1/2,j}{}^{t+\Delta t}\cdot U^{t+\Delta t}_{i-1/2,j}\right]$$

$$+\left(\frac{1-\theta}{\Delta y}\right)\left[M^{\ t}_{mi,j+1/2}\cdot V^{t}_{i,j+1/2}-M^{\ t}_{mi,j-1/2}\cdot V^{t}_{i,j-1/2}\right]+\left(\frac{\theta}{\Delta y}\right)\left[M^{\ t+\Delta t}_{mi,j+1/2}\cdot V^{t+\Delta t}_{i,j+1/2}-M^{\ t+\Delta t}_{mi,j-1/2}\cdot V^{t+\Delta t}_{i,j-1/2}\right]$$

$$\begin{aligned}=\ & \left(\frac{1-\theta}{\Delta x}\right)\left[D^{t}_{xxi+1/2,j}\cdot\frac{M^{\ t}_{mi+1,j}-M^{\ t}_{mi,j}}{\Delta x}+D^{t}_{xyi+1/2,j}\cdot\frac{M^{\ t}_{mi+1,j+1}+M^{\ t}_{mi,j+1}-M^{\ t}_{mi+1,j-1}-M^{\ t}_{mi,j-1}}{4\cdot\Delta y}\right.\\ & \left.-D^{t}_{xxi-1/2,j}\cdot\frac{M^{\ t}_{mi,j}-M^{\ t}_{mi-1,j}}{\Delta x}-D^{t}_{xyi-1/2,j}\cdot\frac{M^{\ t}_{mi,j+1}+M^{\ t}_{mi-1,j+1}-M^{\ t}_{mi,j-1}-M^{\ t}_{mi-1,j-1}}{4\cdot\Delta y}\right]\end{aligned}$$

$$\begin{aligned}& +\left(\frac{\theta}{\Delta x}\right)\left[D^{t+\Delta t}_{xxi+1/2,j}\cdot\frac{M^{\ t+\Delta t}_{mi+1,j}-M^{\ t+\Delta t}_{mi,j}}{\Delta x}+D^{t+\Delta t}_{xyi+1/2,j}\cdot\frac{M^{\ t+\Delta t}_{mi+1,j+1}+M^{\ t+\Delta t}_{mi,j+1}-M^{\ t+\Delta t}_{mi+1,j-1}-M^{\ t+\Delta t}_{mi,j-1}}{4\cdot\Delta y}\right.\\ & \left.-D^{t+\Delta t}_{xxi-1/2,j}\cdot\frac{M^{\ t+\Delta t}_{mi,j}-M^{\ t+\Delta t}_{mi-1,j}}{\Delta x}-D^{t+\Delta t}_{xyi-1/2,j}\cdot\frac{M^{\ t+\Delta t}_{mi,j+1}+M^{\ t+\Delta t}_{mi-1,j+1}-M^{\ t+\Delta t}_{mi,j-1}-M^{\ t+\Delta t}_{mi-1,j-1}}{4\cdot\Delta y}\right]\end{aligned}$$

$$\begin{aligned}& +\left(\frac{1-\theta}{\Delta y}\right)\left[D^{t}_{yxi,j+1/2}\cdot\frac{M^{\ t}_{mi+1,j+1}+M^{\ t}_{mi+1,j}-M^{\ t}_{mi-1,j+1}-M^{\ t}_{mi-1,j}}{4\cdot\Delta x}+D^{t}_{yyi,j+1/2}\cdot\frac{M^{\ t}_{mi,j+1}-M^{\ t}_{mi,j}}{\Delta y}\right.\\ & \left.-D^{t}_{yxi,j+1/2}\cdot\frac{M^{\ t}_{mi+1,j}+M^{\ t}_{mi+1,j-1}-M^{\ t}_{mi-1,j}-M^{\ t}_{mi-1,j-1}}{4\cdot\Delta x}+D^{t}_{yyi,j+1/2}\cdot\frac{M^{\ t}_{mi,j}-M^{\ t}_{mi,j-1}}{\Delta y}\right]\end{aligned}$$

$$\begin{aligned}& +\left(\frac{\theta}{\Delta y}\right)\left[D^{t+\Delta t}_{yxi,j+1/2}\cdot\frac{M^{\ t+\Delta t}_{mi+1,j+1}+M^{\ t+\Delta t}_{mi+1,j}-M^{\ t+\Delta t}_{mi-1,j+1}-M^{\ t+\Delta t}_{mi-1,j}}{4\cdot\Delta x}+D^{t+\Delta t}_{yyi,j+1/2}\cdot\frac{M^{\ t+\Delta t}_{mi,j+1}-M^{\ t+\Delta t}_{mi,j}}{\Delta y}\right.\\ & \left.-D^{t+\Delta t}_{yxi,j+1/2}\cdot\frac{M^{\ t+\Delta t}_{mi+1,j}+M^{\ t+\Delta t}_{mi+1,j-1}-M^{\ t+\Delta t}_{mi-1,j}-M^{\ t+\Delta t}_{mi-1,j-1}}{4\cdot\Delta x}+D^{t}_{yyi,j+1/2}\cdot\frac{M^{\ t+\Delta t}_{mi,j}-M^{\ t+\Delta t}_{mi,j-1}}{\Delta y}\right]\end{aligned}$$

$$+(1-\theta)\cdot\lambda\cdot\mu^{\ t}_{mi,j}\cdot M^{\ t}_{mi,j}+\theta\cdot\lambda\cdot\mu^{\ t+\Delta t}_{mi,j}\cdot M^{\ t+\Delta t}_{mi,j}$$

$$-(1-\theta)\cdot\frac{\rho_b}{\Phi}\cdot K_m\cdot(M^{\ t}_{mi,j}-M^{\ t}_{ii,j})-\theta\cdot\frac{\rho_b}{\Phi}\cdot K_m\cdot(M^{\ t+\Delta t}_{mi,j}-M^{\ t+\Delta t}_{ii,j}) \tag{5.110}$$

$$\begin{aligned}\frac{M^{\ t+\Delta t}_{ii,j}-M^{\ t}_{ii,j}}{\Delta t}=&(1-\theta)\cdot\lambda\cdot\mu^{\ t}_{ii,j}\cdot M^{\ t}_{ii,j}+\theta\cdot\lambda\cdot\mu^{\ t+\Delta t}_{ii,j}\cdot M^{\ t+\Delta t}_{ii,j}\\ &+(1-\theta)\cdot\frac{\rho_b}{\Phi}\cdot K_m\cdot(M^{\ t}_{mi,j}-M^{\ t}_{ii,j})+\theta\cdot\frac{\rho_b}{\Phi}\cdot K_m\cdot(M^{\ t+\Delta t}_{mi,j}-M^{\ t+\Delta t}_{ii,j})\end{aligned} \tag{5.111}$$

$$\mu_{mi,j}^{\ t} = \left(\frac{\mu_{\max} \cdot S_{ui,j}^{\ t}}{K_s + S_{ui,j}^{\ t}}\right) \cdot \left(\frac{K_{im}}{K_{im} + Cr_{i,j}^{t}}\right) \tag{5.112}$$

$$\mu_{ii,j}^{\ t} = \left(\frac{\mu_{\max} \cdot S_{ui,j}^{\ t}}{K_s + S_{ui,j}^{\ t}}\right) \cdot \left(\frac{K_{ii}}{K_{ii} + Cr_{i,j}^{t}}\right) \tag{5.113}$$

$$S_{ui,j}^{\ t} = S_{i,j}^{t} - 0.63 \cdot S_t \tag{5.114}$$

$$\mu_{i,j}^{t} = \frac{M_{mi,j}^{\ t} \cdot \mu_{mi,j}^{\ t} + M_{ii,j}^{\ t} \cdot \mu_{ii,j}^{\ t}}{M_{i,j}^{t}} \tag{5.115}$$

$$M_{i,j}^{t} = M_{mi,j}^{\ t} + M_{ii,j}^{\ t} \tag{5.116}$$

$$R_{cri,j}^{\ t} = 1 + \frac{\rho_b}{n_c \Phi} K_{cr} \left(Cr_{i,j}^{t}\right)^{\frac{1}{n_c}-1} \tag{5.117}$$

$$R_{Si,j}^{\ t} = 1 + \frac{\rho_b}{n_S \Phi} K_S \left(S_{i,j}^{t}\right)^{\frac{1}{n_S}-1} \tag{5.118}$$

In these equations, all the variables with superscript "t" are known, while the variables with superscript "$t + \Delta t$"are unknown. All the above equations are written for all the nodes (i,j). At first, the solutions for chromium, substrate and bacteria are found for advection-dispersion- adsorption, with reactive terms evaluated using the estimated values. Then the reactive terms are reevaluated using the results from previous iteration, and the equations for chromium, substrate and mobile bacteria are again solved to get better results. Iterations are carried out until the difference in the concentrations between the iterations is less than the tolerance limits. The flowchart in Fig. 5.3 shows the algorithm for finding concentrations at every time step.

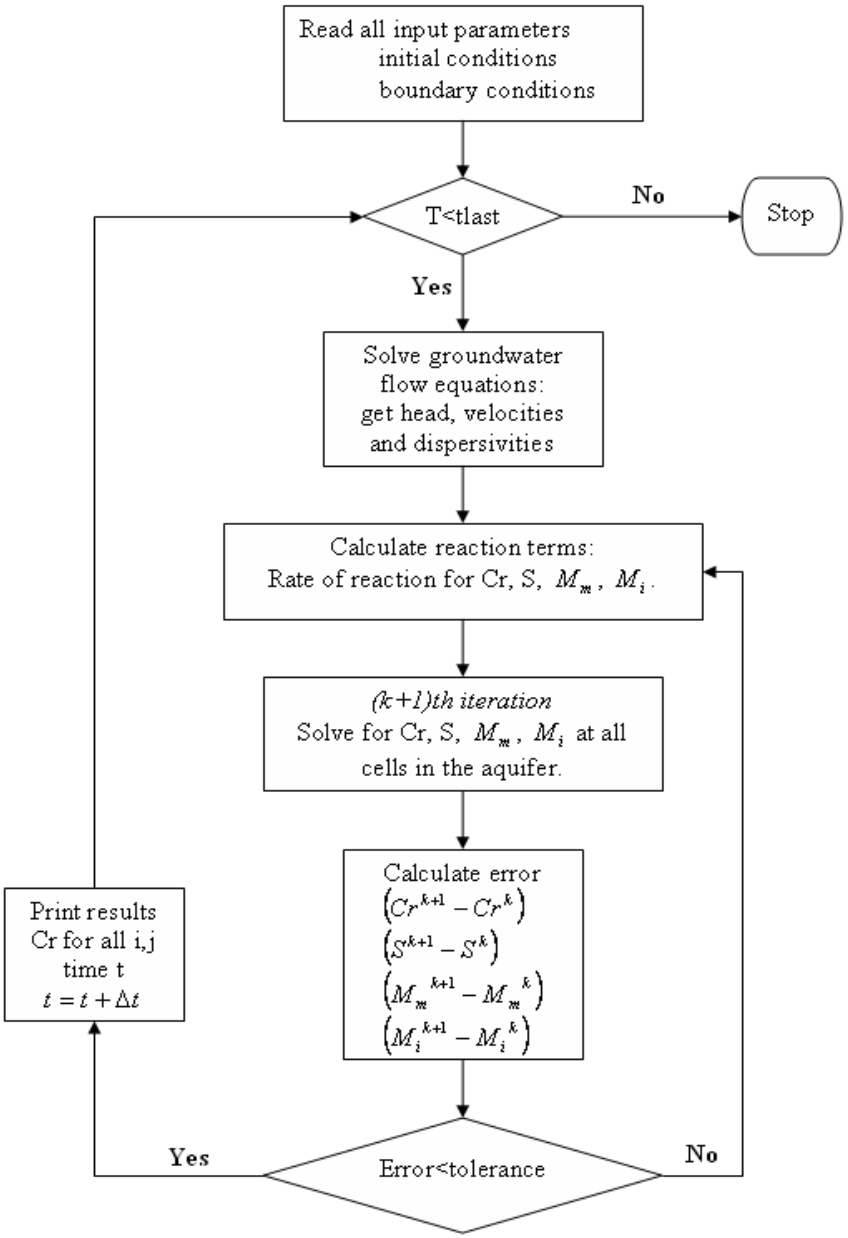

Fig. 5.3: Flow chart of solving procedure of two-dimensional model for transport with bio transformation

5.5 MANAGEMENT MODEL

Any bioremediation system which uses either a bio-barrier technology or reaction zone technology, the design and operation variables need to be determined in such a way that the target containment is achieved with least cost, while taking note of many constraints (both physical and managerial). In this section, a methodology is described for developing management models which use a formal simulation-optimization framework for the design and operation of *in situ* bioremediation systems for remediation of aquifers contaminated with hexavalent chromium. The methodology is described with respect to the containment of a Cr(VI) plume in a one-dimensional confined aquifer using a passive bio-barrier technology. Same concepts can be used for designing bio-barriers in two-dimensional systems and reaction zone technologies.

In any bio-augmentation system which uses a trench type passive bio-barrier, the design variables are length (along the flow direction), L, width (across the flow direction), W, and depth, D of the barrier, initial microbial concentration, M_0 in the barrier, and the substrate (electron donor / electron acceptor), S_0, to be provided for the microbial growth. For a one-dimensional system such as that considered in this section, barrier is assumed to extend for the entire width, and depth of the plume. Hence, only L, M_0, and S_0 are considered as decision variables in the optimization model. These variables are determined such that the total cost including the capital cost of trenching, cost of providing the initial microbial population in the barrier, and the operational cost of injecting the substrate through out the period of remediation, is a minimum.

While designing the bio-barrier, it should be ensured that the length of the barrier is not lesser than a minimum value, and not greater than a maximum value because of construction and space requirements. Also, the initial microbial concentration is not allowed to exceed a maximum value in order to prevent the clogging of the barrier during the remediation period. The remediation period is taken as that time after which the Cr(VI) concentration on the downstream side of the barrier is less than the allowable limit of 0.05 mg/l. Lower and higher limits can also be put on the inlet substrate concentration, if required. Besides these, the main management constraint to be satisfied is that the

concentration of Cr(VI) at the control point, on the downstream side of the bio-barrier, should be within the specified limit at all time ***t*** greater than or equal to a specified time. This time is equal to the time of travel for Cr(VI) plume to the control point, in case of a slug discharge and if there is no remediation. In case of contamination due to a continuous source, the above time is specified by the user, depending upon the source characteristics, and / or the longevity of the bio-barrier.

5.5.1 Formulation of the Optimization Problem

The optimization problem can be stated as follows:

Objective function

$$\text{Min } Z_1 = C_1 \cdot A \cdot L + \frac{C_2 \cdot M_0 \cdot A \cdot L \cdot \phi \cdot 1000}{10^6} + \frac{C_3 \cdot S_0 \cdot Q \cdot T \cdot 1000}{10^6} \qquad (5.119)$$

where, Z_1 = total cost of bio-barrier; C_1 = cost of trenching per m^3 of soil; A = cross sectional area in m^2; L = length of the bio-barrier in m; C_2 = cost of microbes per kg; M_0 = Initial microbial concentration in mg/L; ϕ = porosity ; C_3 = cost of substrate per kg; S_0 = inlet concentration of substrate in mg/L; Q = groundwater flow rate in m^3/h; and T= Time for which the substrate is applied for remediation in hours.

Constraints

Following constraints have to be satisfied while minimizing the objective function.

1. $[C_{cr6}]_{outlet} <= 0.05 mg/l \quad \forall$ t>= T

   The concentration of Cr (VI) at the outlet of the bio-barrier should be less than or equal to the specified minimum value at all times **t** greater than or equal to the time specified for remediation, T. A maximum acceptable concentration of 0.05 mg/l (50 µg / l) for chromium in drinking water has been established on the basis of health considerations.

2. $L_{\min} < L < L_{\max}$

   Length of the bio-barrier should be within limits.

3. $M_{0\min} < M_0 < M_{0\max}$

Initial microbial concentration in the bio-barrier should be within limits.

4. $S_{0\min} < S_0 < S_{0\max}$

   Input substrate concentration at the beginning of the bio-barrier should be within limits.

5. $[C_{Cr6}]_{outlet} = f(M_0, S_0, L,$ hydro-geologic conditions, Bio-kinetic parameters). This relationship is represented by the Cr(VI) transport and bio-transformation equations in the simulator.

In the present study, the design problem is solved as a simulation-optimization problem, wherein the optimization model makes several function calls to the simulation model. The simulation model (presented in section 5.2) is used to determine the Cr(VI) concentration at the control point, given the values of the decision variables (M_0, S_0, and L), the hydro-geological conditions of the aquifer (pore velocity, soil characteristics), the bio-kinetic parameters, and the initial Cr(VI) concentration. In the simulation model, the governing advection-dispersion-reaction equations for one dimensional transport of hexavalent chromium, and substrate through a confined aquifer, and the microbial growth equation are numerically solved.

5.5.2 Optimization Technique

A Genetic Algorithm (GA) is used for solving the combined simulation-optimization problem in the present study because of nonlinearity involved in the design problem. Gradient based methods are proven to be not so robust for solving nonlinear design problems where the number of parameters involved is more than two.

Genetic Algorithms (Goldberg 1989) are non-deterministic search/optimization methods that utilize the theories of evolution and natural selection to solve an optimization problem within a complex solution space. Unlike the traditional search methods such as the Gradient methods (which use the gradient of a function to guide the direction of search), and the Enumerative methods (which work within a finite search space), a GA conducts random walk through the search space while saving the best.

The classical GA works with a coding of the parameter set and not with the parameter itself. It discretises the space, even though the function is continuous, by using the string coding of variables. The GA works with a population, i.e. a set of solutions, instead of a single solution at a time and thus is more likely to arrive at a global minimum when there are more than one local minimum present in the search space. Genetic algorithms do not get stuck in local minimum, which may be the case with traditional methods.

In a GA, initially a population of specified size (population size) is generated using a random generator. This is known as the initial population. It consists of a set of binary numbers of a given string length. These strings are decoded to their corresponding parameter values depending on the range within which they are expected to lie. This solution is evolved through to the next generation by operating it with the three basic genetic algorithm operators: (i) selection (reproduction), (ii) crossover, and (iii) mutation.

In Reproduction, a mating pool is created whose members are selected based on a selection process, which involves the calculation of the objective function (the simulator subroutine is used for this purpose), the fitness values and some statistical calculations for each solution in the population. The principle of "Survival of the Fittest" is implemented. Depending on the fitness value of each solution, the stronger ones are selected for further operations while the weaker ones are discarded. Procedures known as "tournament selection" method, "roulette wheel" method, and "stochastic remainder roulette wheel" method are available for creating the mating pool. The selection process used in the present study is the roulette wheel method.

Now, crossover takes place among randomly chosen pairs from the mating pool. With a bias of a crossover probability (P_c), it is determined whether the pair will undergo crossover. A biased coin with the probability P_c is flipped and if the outcome is "true", then a site is chosen randomly in the strings as the crossover site. The bits from the right side of the cross over site from the parent-1 and the parent-2 are swapped to generate two new children. Crossover is responsible for the creation of new solutions or new decision vectors.

In the mutation step, each bit in a string is altered, i.e. a zero is changed to a one, and vice versa, depending on the probability of mutation P_m. A biased coin with the probability P_m is flipped and the outcome is "true", then the bit is altered. This operation is performed for each bit in a string, and for all strings in the population. Typically, the value of P_m is very small. Mutation creates a point in the neighborhood of the current point (solution), thereby allowing a local search around that solution. Mutation is used to maintain diversity in the population.

The population obtained after performing the above operations is known as the new population. By decoding these new strings, we get the new solution set. If the end condition is not satisfied this new set is used to generate another new population using the procedure outlined earlier. The population in the new generation will be better than the population in the earlier generations. GA terminates after looping over the user specified number of generations. It gives a large number of sets of the parametric variables, unlike the traditional methods in which only the final solution is reported. One can select any one of these sets, depending on the required fitness value that is usually unique for a given set.

The pseudo code for the classical GA is presented below (Bilkent, 2000).

1. **[Start]** A random population of „n" chromosomes i.e. suitable decision vectors (solutions) for the problem, are generated.

2. **[Fitness]** The fitness of each chromosome in the population is evaluated. This is achieved by calling the simulation subroutine for each decision vector, evaluating the constraints (if any), and then determining the value of objective function. If it is a minimization problem, the fitness = $\frac{1}{1+OF}$ where, OF= objective function. If it is a maximization problem, fitness = OF.

3. **[New population]** Following steps are repeated on the entire existing population, and a new population whose size is same as the size of the existing population is created.

~~3.1~~ **[Selection]** Two parent chromosomes are selected from the population according to their fitness value. The better the fitness, the greater is the chance to be selected.

~~3.2~~ **[Crossover]** With a probability of crossover (P_c), the parent chromosomes are crossed over to form two new children. If no crossover was performed, children (offspring) are an exact copy of the parents.

~~3.3~~ **[Mutation]** With a probability of mutation (P_m), mutation is performed on the new offspring at each position in the chromosome.

~~3.4~~ **[Accepting]** The new offspring is placed in a new population.

4. **[Replace]** The newly generated population is used for a further run of algorithm.
5. **[Test]** If the end condition is satisfied, stop and return the best solution in current population.
6. **[Loop]** The process is repeated (from steps 2 to 5) until the end condition is satisfied.

The block diagram showing the interaction between the simulation and optimization modules is presented in Fig 5.4.

Formatted: Bullets and Numbering

Formatted: Bullets and Numbering

Formatted: Bullets and Numbering

Formatted: Bullets and Numbering

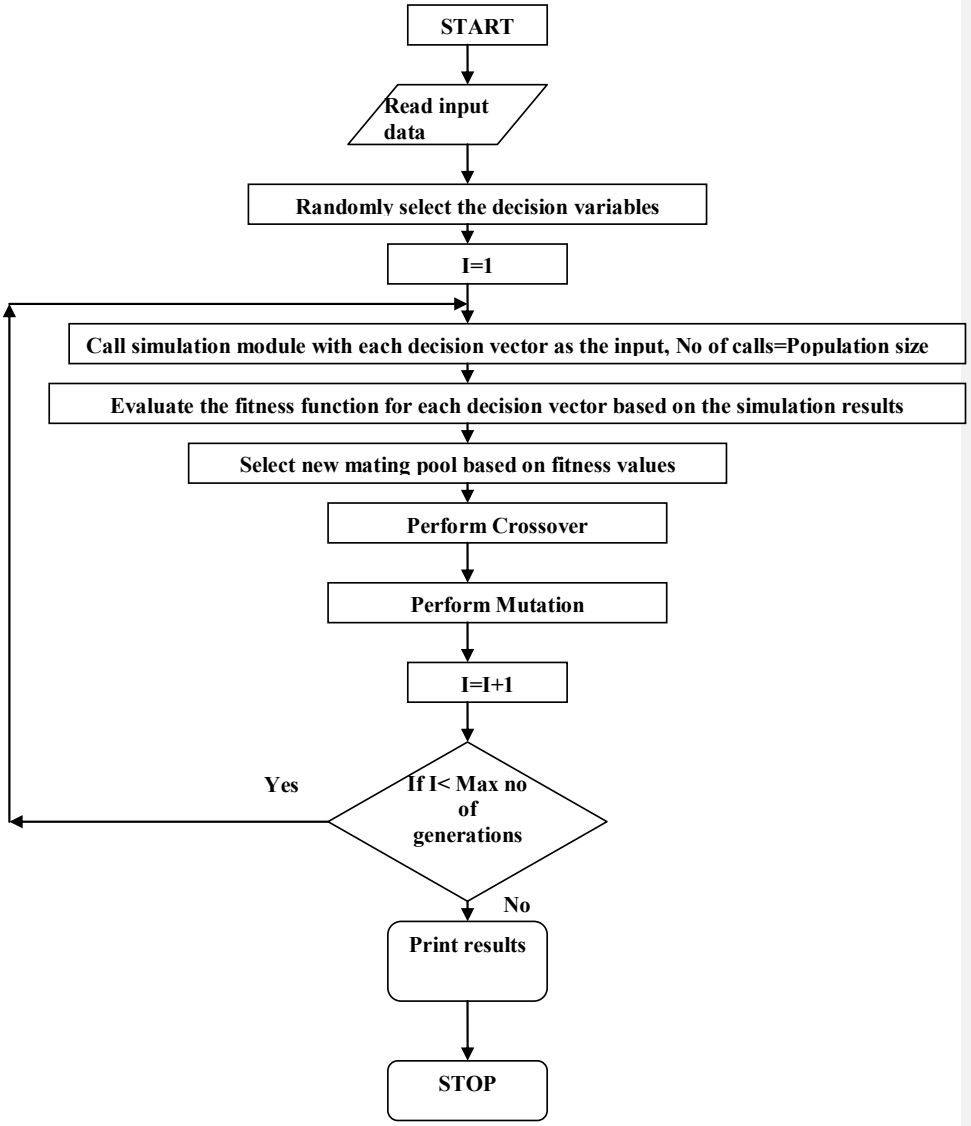

Fig. 5.4: Flow chart for the simulation-optimization framework

The important parameters of a GA are the population size, number of generations and the probabilities of crossover and mutation. All these have to be given as an input by the user and vary depending on the problem. The number of generations to be considered depends strongly on the number of decision variables. Practically, the computational over burden also dictates the selection of the number of generations. In the present work, the Genetic Algorithm provided in the MATLAB tool box is used for solving the simulation-optimization problem. In this, the probability of mutation and the probability of cross over are chosen automatically.

Advantages of Genetic Algorithms

Some of the advantages of genetic algorithms over other traditional optimization methods (Goldberg, 1989) are:

1. GAs work with coding of parameter set, not the parameters themselves.
2. GAs search from a population of points, not from a single point.
3. GAs use only objective function information, not derivatives or other auxiliary knowledge.
4. GAs use probabilistic transition rules, not deterministic rules.
5. GAs can solve a multimodal problem very easily.

Penalty Function Approach

The classical GA presented in the earlier section is designed for application to an unconstrained optimization problem. However, its application to a constrained optimization problem is not straight forward. In the constrained optimization problem, the constraints pertaining to lower and upper bounds on the decision variables L, M_0 and S_0 are easily implemented through the specification of maximum and minimum values of the decision variables, which in any case are needed for decoding of the strings representing the variable. However, there is an inequality constraint on the concentration of Cr(VI) at the end of the bio-barrier. Implementation of this constraint is done using the penalty function approach. In this approach, a constrained optimization problem is transformed to an unconstrained problem by associating a penalty with all constraint

violations, and changing the value of objective function accordingly. For this purpose, the objective function is written as:

Minimize

$$OF = Z_1 + B \tag{5.120}$$

where, Z_1 is the total cost involved and B is the penalty factor. In the above equation, B is assigned a non-zero constant value if the inequality constraint on the concentration of Cr(VI) at the end of the bio-barrier is violated. Increase in the objective function value corresponding to a particular decision vector reduces the chance of survival of that decision vector in the next generation. This ensures that only those decision vectors that nearly satisfy the constraints remain in the population at the end of the run. A very high value of 10^{10} is used for B in the present study so that a heavy penalty is levied when this constraint is violated.

5.5.3 Non-Dimensional Parameters for Optimal Design

It is convenient if charts, which show the interrelationship between design variables (L, M_0, and S_0) and non-dimensional system characteristics, are available to aid the design. The idea of non-dimensionalization of governing equations is to combine all the variables involved in the present problem into a few non-dimensional parameters, and to study interrelationship between them. In this study, variations of optimal cost (Z_1), length of the bio-barrier (L), microbial concentration (M_0) and inlet substrate concentration (S_0) corresponding to the optimal design are studied with respect to these non-dimensional parameters. Here we assume that only one type of microbes is used. Hence, bio-kinetic parameters are taken as constant. For the sake of simplicity in explaining the concept, it is also assumed that the flow is steady, uniform and one-dimensional. The non-dimensional governing equations are:

$$R_{dc} \cdot \frac{\partial C^*}{\partial t^*} + \frac{\partial C^*}{\partial x^*} = \frac{\partial^2 C^*}{\partial x^{*2}} - R^*_{\sin kC} \tag{5.121}$$

$$R_{ds} \frac{\partial S^*}{\partial t^*} + \frac{\partial S^*}{\partial x^*} = \frac{\partial^2 S^*}{\partial x^{*2}} - R^*_{\sin kS} \tag{5.122}$$

$$R^*_{\sin kC} = \pi_5 \cdot \lambda \cdot M^* \left[\frac{S^*}{\pi_2 + S^*}\right] \cdot \left[\frac{\pi_3}{\pi_3 + C^*}\right] \tag{5.123}$$

$$R^*_{\sin kS} = \pi_4 \cdot \lambda \cdot M^* \left[\frac{S^*}{\pi_2 + S^*}\right] \cdot \left[\frac{\pi_3}{\pi_3 + C^*}\right] \tag{5.124}$$

$$\frac{1}{M^*} \cdot \frac{dM^*}{dt^*} = \pi_1 \cdot \lambda \cdot \left[\frac{S^*}{\pi_2 + S^*}\right] \cdot \left[\frac{\pi_3}{\pi_3 + C^*}\right] \tag{5.125}$$

where

$$C^* = \frac{C}{C_0}; \quad x^* = \frac{x}{\alpha_L}; \quad t^* = \frac{t}{\alpha_L} \cdot u; \quad S^* = \frac{S}{C_0}; \quad M^* = \frac{M}{C_0} \tag{5.126}$$

$$\pi_1 = \frac{\mu_{\max} \cdot \alpha_L}{u} \tag{5.127}$$

$$\pi_2 = \frac{K_s}{C_0} \tag{5.128}$$

$$\pi_3 = \frac{K_i}{C_0} \tag{5.129}$$

$$\pi_4 = \pi_1 \cdot \left(\frac{1}{Y}\right) \cdot \left(\frac{1}{C_0}\right) \cdot C_0 \tag{5.130}$$

$$\pi_5 = \pi_4 \cdot \eta \tag{5.131}$$

The transport and bio-transformation of Cr(VI) depends upon the flow characteristics and bio-kinetics of the microbes used. Flow characteristics are determined by pore velocity and longitudinal dispersivity. The bio-kinetic parameters of the system are represented by the maximum specific growth rate, μ_{max}, half saturation constant, K_s, yield coefficient, Y, and inhibition constant, K_i. For given type of microbes, these parameters are constant. Similarly η and λ are also constants for a given system. Therefore, the non-dimensional parameters π_2 and π_3 are constant for given conditions. The non-dimensional parameter

π_1 incorporates the relative effect of microbial growth and transport on pollutant containment. Optimal design values of L, M_0, and S_0 are determined as function of this parameter π_1, for given microbial and soil system. The plots between the design variables and π_1 indicate how the design changes depending upon the transport conditions.

5.6 CLOSURE

In this chapter, details of proposed mathematical models for chromium reduction by a mixture of bacteria, and one-dimensional and two-dimensional transport and transformation models are presented. Governing equations and numerical methods for solving them have been presented. It has been explained how a "simulation-optimization" framework may be used to formulate a management model for obtaining optimal design and operation values for the decision variables.

Chapter 6

RESULTS AND DISCUSSION – EXPERIMENTAL STUDIES

6.1 BIOREMEDIATION OF CHROMIUM (VI): OPTIMIZATION OF OPERATING PARAMETERS UNDER LABORATORY CONDITIONS

6.1.1 Screening of microbes for chromium (VI) reduction

Bacterial cultures isolated from seven locations of the contaminated site were screened based on their Cr (VI) reduction capacity. Kinetics of Cr (VI) reduction was carried out under aerobic conditions with an initial Cr (VI) concentration of 50mg/L for all the seven strains and the results are presented in Figures 6.1 and 6.2. The bacterial strains employed for the present study is tabulated in Table 6.1. Among the seven strains screened, H1, the strain isolated from a clay mat near the old effluent treatment plant (ETP) shows highest Cr (VI) reduction potential. This strain was used for further studies.

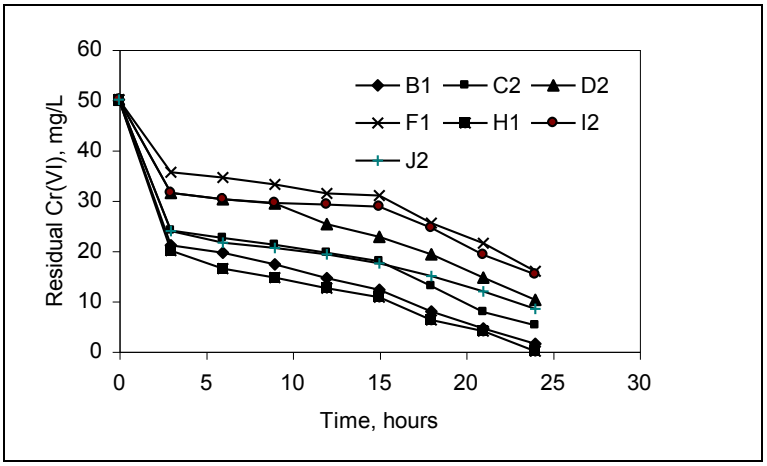

Fig. 6.1: Kinetics of Cr (VI) reduction by different bacterial strains

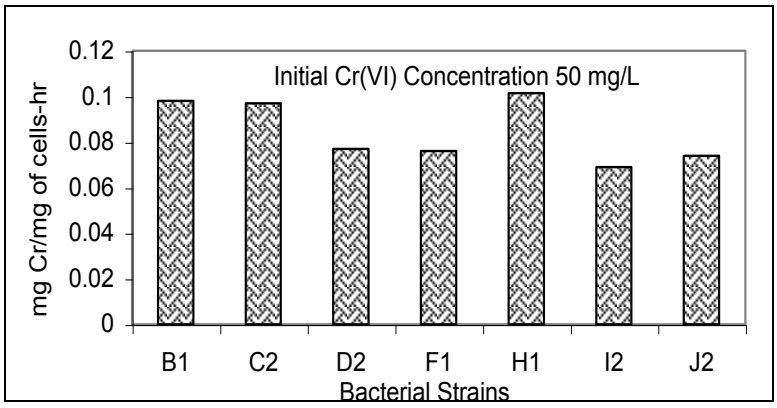

Fig. 6.2: Specific Cr (VI) reduction rate for different bacterial strains

Table 6.1: Bacterial strains employed for the present study

Sl. No.	Sample location	Strain name
1	Open well inside the factory premises	B2
2	Grass root sample outside the premises (eastern side)	C2
3	Grass root sample outside the premises (southern side)	D2
4	Grass root sample in the SIPCOT drain	F1
5	Sample from mat formation near ETP	H1
6	Sample from waste dump site (eastern side)	I2
7	Sample from waste dump site (western side)	J2

The strain which had a history of exposure to high Cr (VI) concentration has exhibited an excellent Cr (VI) reduction potential. The environmental stress might have forced the strain to develop an effective detoxification mechanism to survive in the adverse condition. It was also reported that many microorganisms isolated from the contaminated

sites showed high resilience to a toxicant and hence, better pollution remediation potential (Wang et al., 1989; Bopp and Echrlich, 1998; Bader et al., 1996, Philip et al., 1998). The specific Cr (VI) reduction potential was also higher for bacterial strain H1 (Fig 6.2). Bacterial strains B1 and C2 also showed high specific chromium reduction.

6.1.2 Effect of initial Cr(VI) concentration on Cr(VI) reduction

In order to determine the effect of initial Cr (VI) concentration on microbial Cr (VI) reduction, studies were carried using H1 bacterial strain with different initial Cr (VI) concentrations (50-400 mg/L) under aerobic condition and the results are presented in Fig 6.3 (a). The specific growth rates with respect to different Cr (VI) concentrations are presented in Fig 6.3 (b).

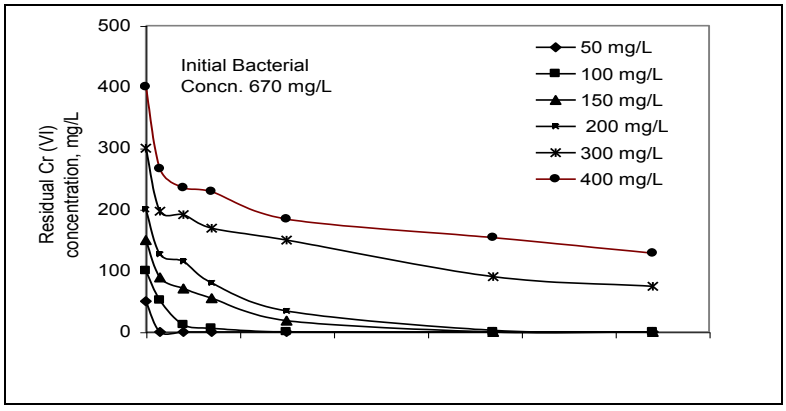

Fig. 6.3 (a): Effect of initial Cr (VI) concentration on Cr (VI) reduction

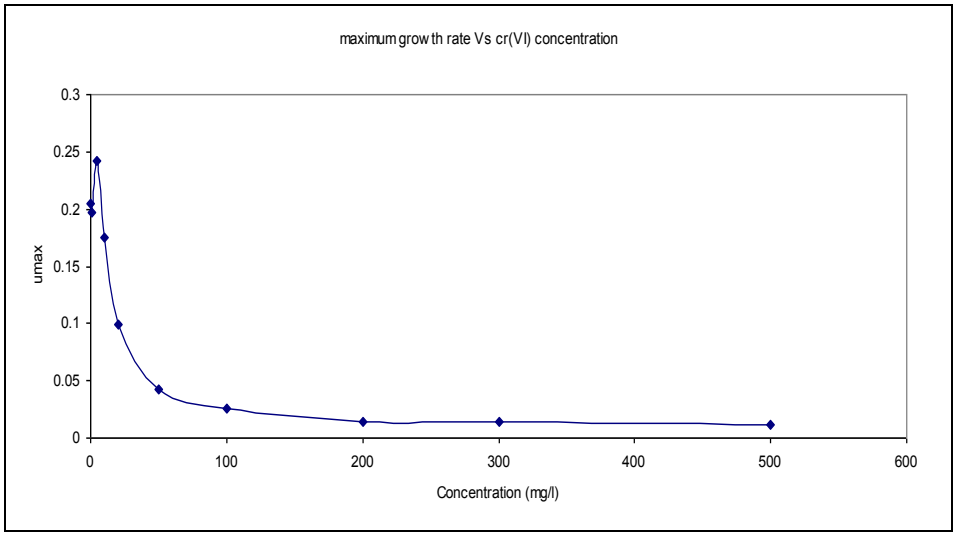

Fig. 6.3 (b): Effect of initial Cr (VI) concentration on maximum specific growth rate

The initial bacterial cell concentration was 670mg/L. The time required for complete reduction of Cr (VI) increased with the initial Cr (VI) concentrations. Complete Cr (VI) reduction was achieved in 3 hours for initial Cr (VI) concentration of 50mg/L; for a high Cr (VI) concentration of 200mg/L, it took 108 hours. Beyond this Cr (VI) concentration, the complete Cr (VI) reduction was not observed. The specific Cr (VI) reduction rate for various concentrations of Cr (VI) is given in Fig 6.4.

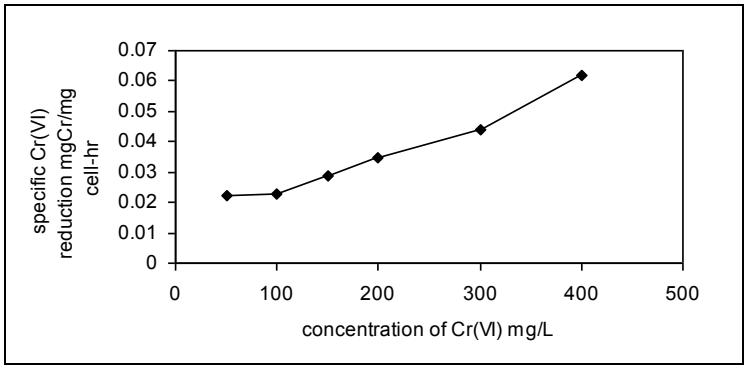

Fig 6.4: Specific Cr(VI) reduction rate for different initial Cr(VI) concentrations

The specific Cr (VI) reduction rate increased with the initial Cr (VI) concentration. Even at high initial Cr (VI) concentration of 400 mg/L, Cr (VI) was still reduced at a high specific rate (0.062 mg/mg cell-hr). These results also showed that isolated microbial consortium was able to sustain a Cr (VI) concentration in the range of 400 mg/L without much adverse effect. This is an important observation especially when *in-situ* bioremediation is contemplated. The microbes are able to reduce/remediate Cr (VI) even at higher concentrations though it takes a long time. The cell yield was very low at high Cr (VI) concentrations due to the inhibition effect (Fig 6.3 b). This may be the reason for high specific Cr (VI) reduction rate at higher initial Cr VI) concentrations.

6.1.3 Effect of pH

pH plays an important role in most of the biological systems. The preferable pH range in such systems is 6-8. The effect of pH on Cr (VI) reduction was studied for a wide range of pH 4-10 under aerobic conditions. The results are shown in Fig. 6.5. At neutral pH, the Cr (VI) reduction was found to be 100% within three hours when an initial Cr (VI) concentration of 50 mg/L was exposed to a bacterial concentration of 670 mg/L. The reduction decreased with either increase or decrease of pH from neutral. Here, entire Cr (VI) was in liquid phase and when bioremediation of Cr (VI) for clean up of contaminated soils is opted, then, adsorption and desorption characteristics of Cr (VI) as influenced by pH may determine the performance of the system. It was reported that Cr (VI) could be desorbed from soil at a faster rate at elevated pH values (Wang et al., 2002).

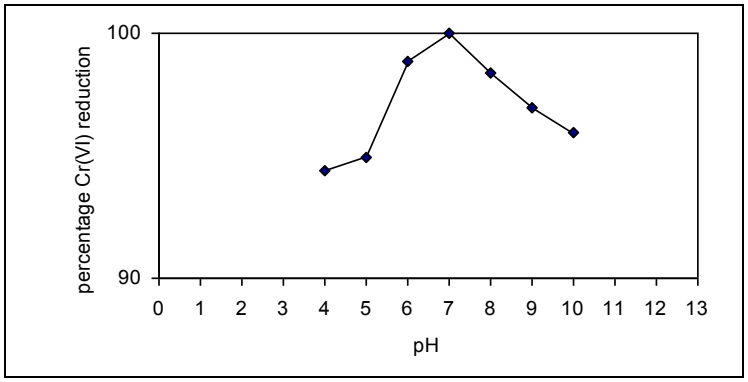

Fig 6.5: Effect of pH on Cr (VI) Reduction

6.1.4 Cr (VI) reduction in aerobic and anaerobic conditions

Bioremediation of Cr (VI) was studied under aerobic and anaerobic conditions with an initial Cr (VI) concentration of 50mg/L and the results are shown in Fig 6.6. It was observed that under aerobic conditions, Cr (VI) reduction was high. However, as large areas have to be bioremediated under field condition, provision of aeration may not be economically feasible. Therefore, the anaerobic reduction/bioremediation option is evaluated further though it is slightly less efficient (90%) than the aerobic system.

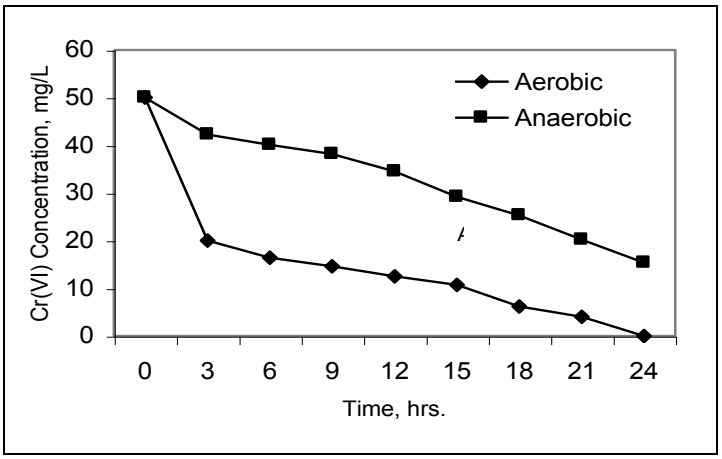

Fig. 6.6: Cr (VI) reduction in aerobic and anaerobic conditions

6.1.5 Conclusions

The present study focuses on the ability of a mixed population of microbial culture isolated from hexavalent chromium contaminated site to biotransform Cr (VI). Batch and continuous experiments were carried out to study the biotransformation pattern of Cr (VI) with molasses as the electron donor. Among the bacterial strains isolated from seven different locations of the contaminated site, the bacterial strain (H1) which was isolated from a clay mat near the effluent treatment plant (ETP) showed high Cr (VI) reduction potential.

6.2 EXPERIMENTAL STUDIES ON Cr(VI) REDUCTION BY CRB, SRB AND IRB, INDIVIDUALLY AND IN COMBINATION

6.2.1 Kinetics of chromium reduction by CRB in aerobic conditions

Chromium reduction studies were carried out using CRB under aerobic conditions. The microbial strains used for the study were enriched and isolated from a chromium contaminated soil collected from Ranipet, Tamilnadu, India. Concentrations of biomass, COD and Cr (VI) were monitored with respect to time. In these studies, initial concentration of Cr (VI) was varied from 0 to 100 mg/L, whereas the initial COD concentration was kept at 3040 mg/L. Initial biomass concentration in all the experiments was equal to 30 mg/L. Results of these studies are presented in Figs. 6.7(a) - 6.7 (c).

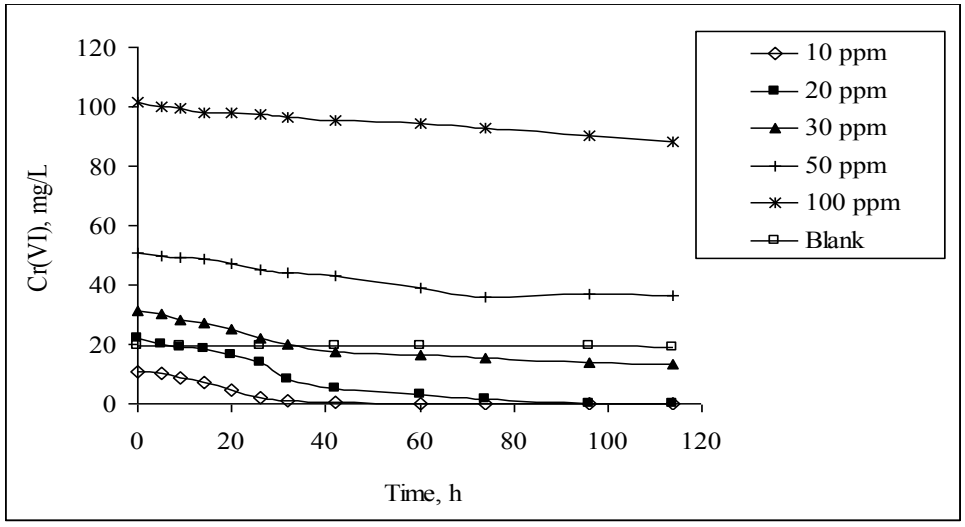

Fig. 6.7 (a): Kinetics of Cr (VI) reduction by CRB for different initial Cr (VI) concentrations under aerobic conditions

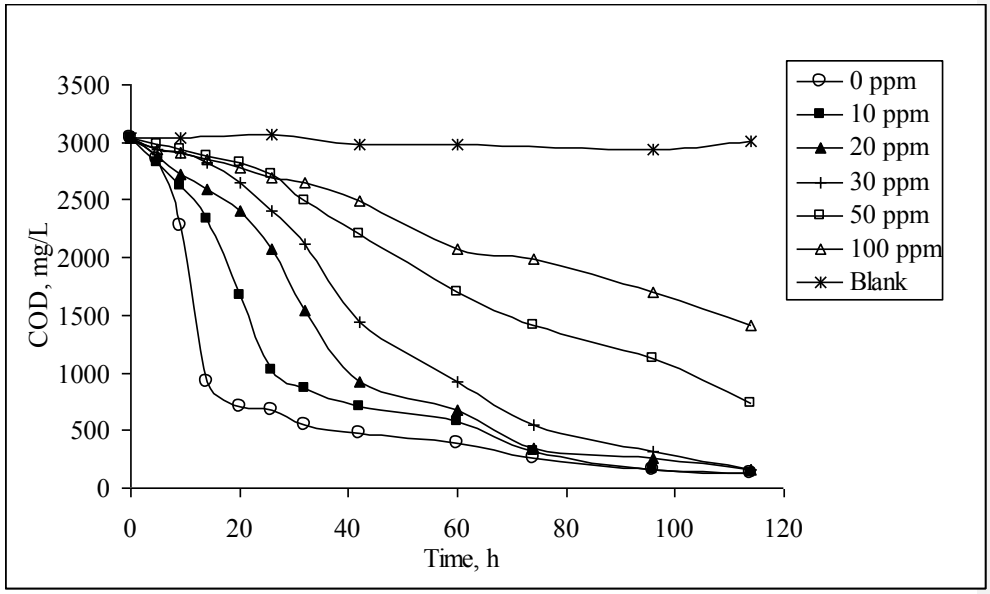

Fig. 6.7 (b): Kinetics of substrate utilization by CRB for different initial Cr (VI) concentrations under aerobic conditions

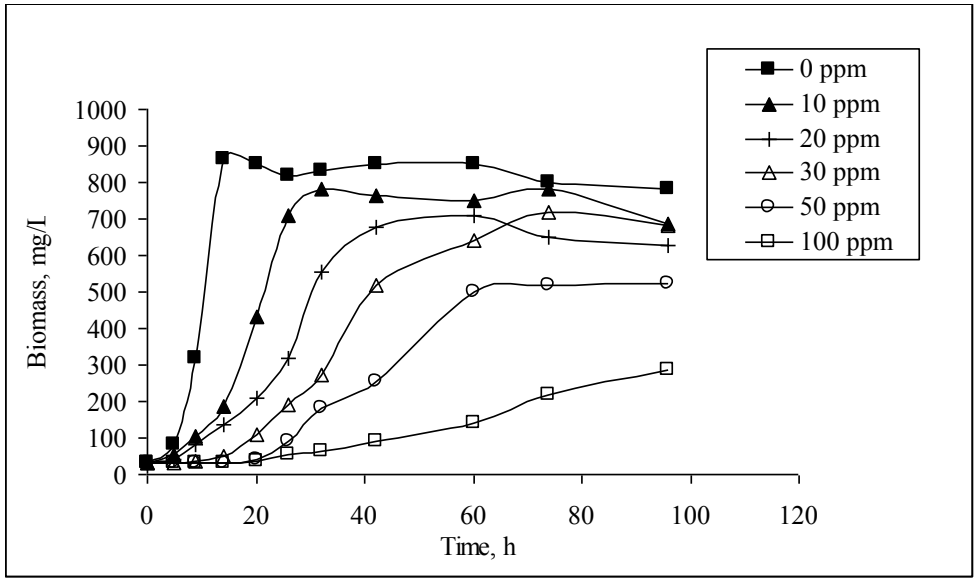

Fig. 6.7 (c): Growth curve of CRB with different initial Cr (VI) concentrations under aerobic conditions

It can be seen from the results (Fig. 6.7 a) that the chromium reduction was complete up to a concentration of 20 mg/L within 70 h, in aerobic conditions. Cr (VI) reduction occurred for higher concentrations also although it was not complete. COD removal also followed a similar trend. The COD removal rate was very fast up to 50 h, for a Cr (VI) concentration of 30 mg/L. At higher Cr (VI) concentrations, the rate of COD removal was reduced (Fig 6.7 b). This may be due to the inhibitory effect of Cr (VI) on the CRB. Similar results were reported by other researchers also (Philip et al., 1998, Gopalan and Veeramani 1994, Campos et al., 1995). The inhibition effect is clear from the biomass concentrations in the systems (Fig 6.7 c). Maximum biomass concentration of 900 mg/L was achieved in the system with zero Cr (VI) concentration. There was slight reduction in maximum biomass concentration up to a Cr (VI) concentration of 30 mg/L and the effect was very significant beyond 50 mg/L.

6.2.2 Kinetics of chromium reduction by CRB in facultative anaerobic conditions

Chromium reduction studies were carried out using CRB under facultative anaerobic conditions, keeping all other experimental conditions same as in aerobic system. Results from these experiments are presented in Figs. 6.8 (a) – 6.8 (c). It can be observed that Cr (VI) reduction rate was faster under anaerobic conditions for low concentrations of Cr (VI) (Fig. 6.8 a). However, the rate decreased significantly for high concentrations of Cr (VI). COD removal efficiency was lesser in anaerobic conditions (Fig. 6.8 b) as compared to removal efficiency in aerobic conditions. The inhibition effect is clear from the biomass concentrations shown in Fig. 6.8 (c). The inhibition effect was more in anaerobic system as compared to aerobic system. This is also evident in the COD removal efficiency of the system. Maximum biomass concentration of 300 mg/L was achieved in the system with zero Cr (VI) concentration, which was much lower than that for aerobic system. Also, there was practically no growth in the system with a Cr (VI) concentration of 100 mg/L.

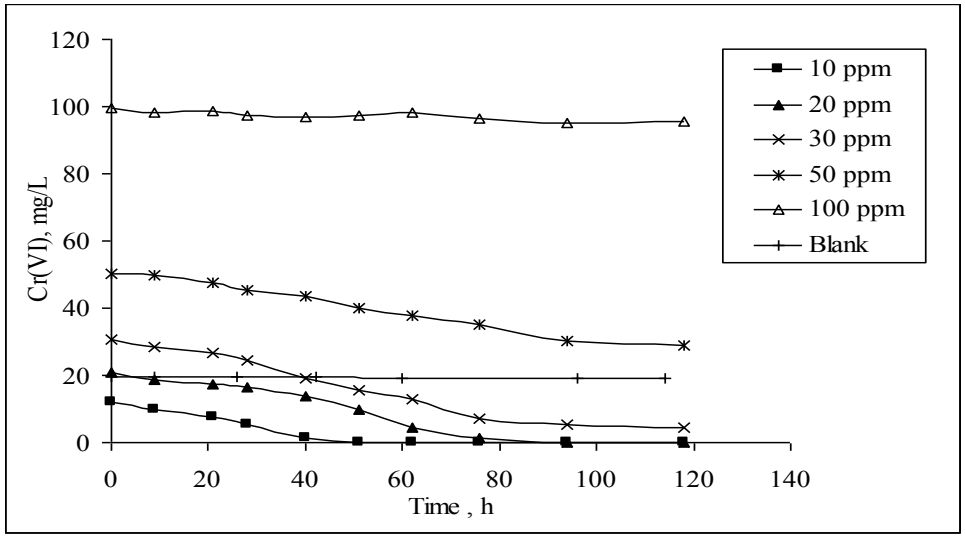

Fig. 6.8 (a): Kinetics of Cr (VI) reduction by CRB for different initial Cr (VI) concentrations under facultative anaerobic conditions

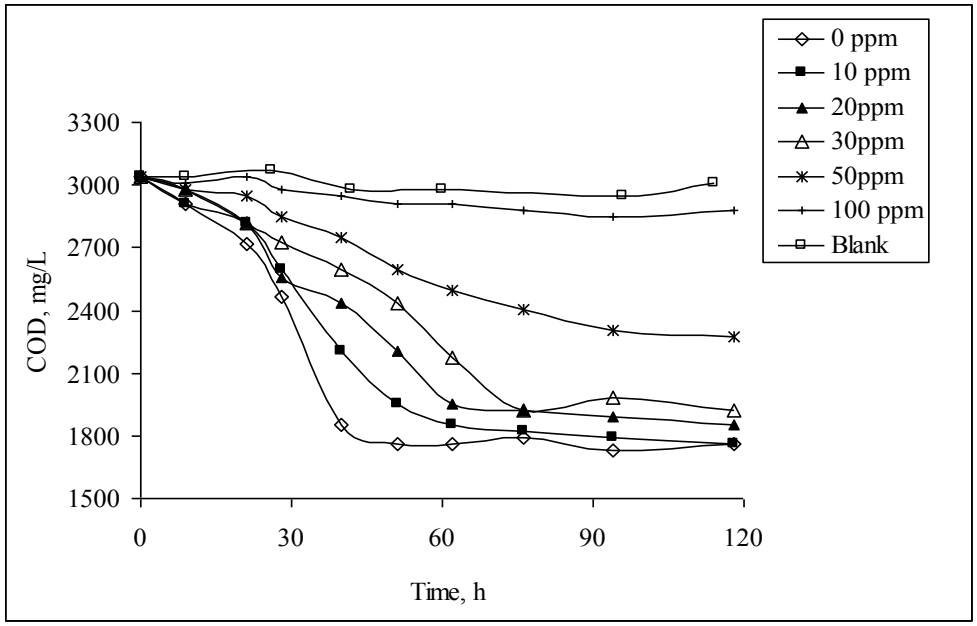

Fig. 6.8 (b): Kinetics of substrate utilization by CRB for different initial Cr (VI) concentrations under facultative anaerobic conditions

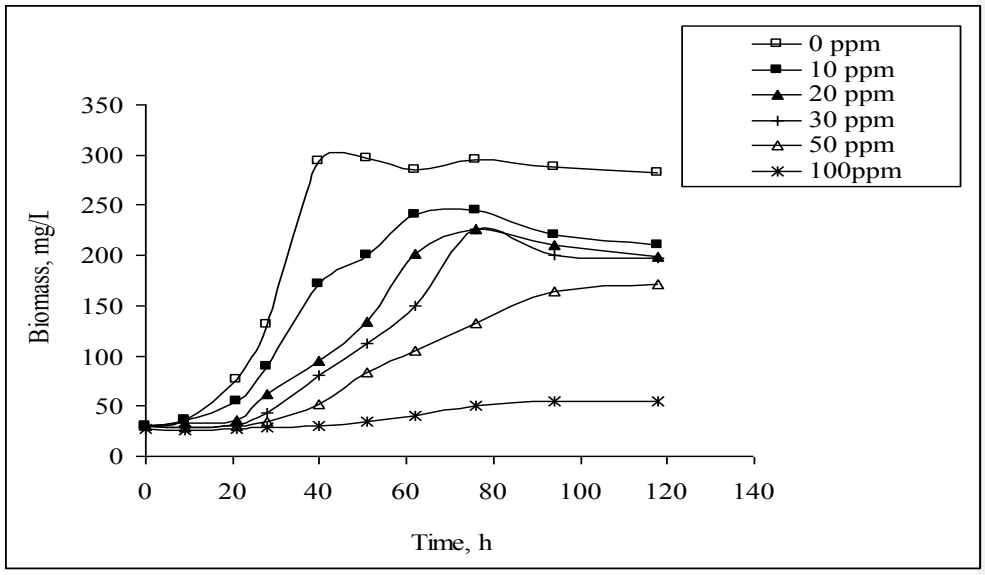

Fig. 6.8 (c): Growth curve of CRB with different initial Cr (VI) concentrations under facultative anaerobic conditions

6.2.3 Kinetics of chromium reduction by SRB

Chromium reduction studies were carried out using SRB under strict anaerobic conditions. The microbial strains used for the study were enriched and isolated from municipal wastewater. Concentrations of biomass, COD, SO_4^{2-} and Cr (VI) were monitored with respect to time. In these studies, initial concentration of Cr (VI) was varied from 0 to 50 mg/L, where as the COD concentration was kept constant at 3072 mg/L. Initial biomass concentration in all the experiments was equal to 28 mg/L. The effect of sulphate concentration on the microbes was studied by varying the sulphate concentration from 0 to 2000 mg/L. However, for all Cr (VI) reduction studies, sulphate concentration was taken as 1000 mg/L. Results of these studies are presented in Figs. 6.9 (a) – 6.9 (d).

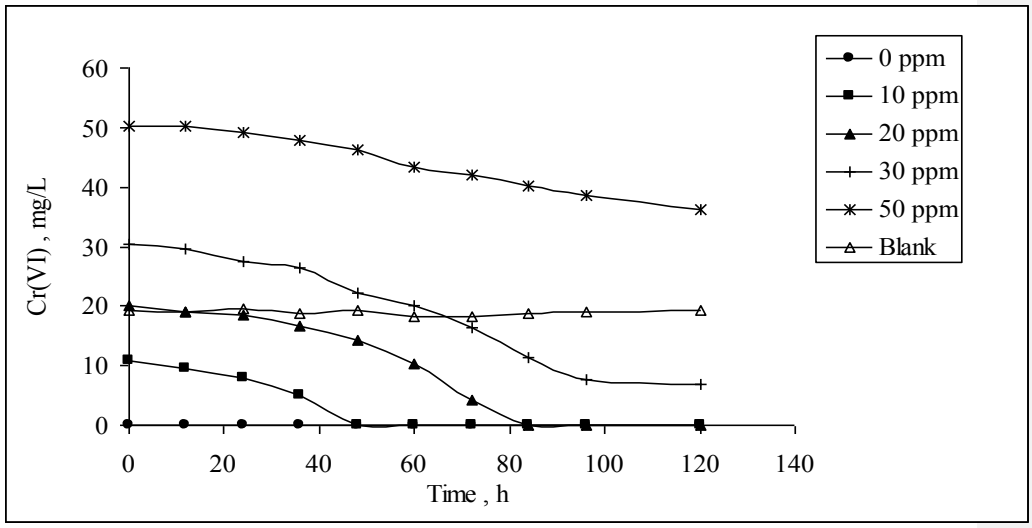

Fig. 6.9 (a): Kinetics of Cr (VI) reduction by SRB for different initial Cr (VI) concentrations under anaerobic conditions

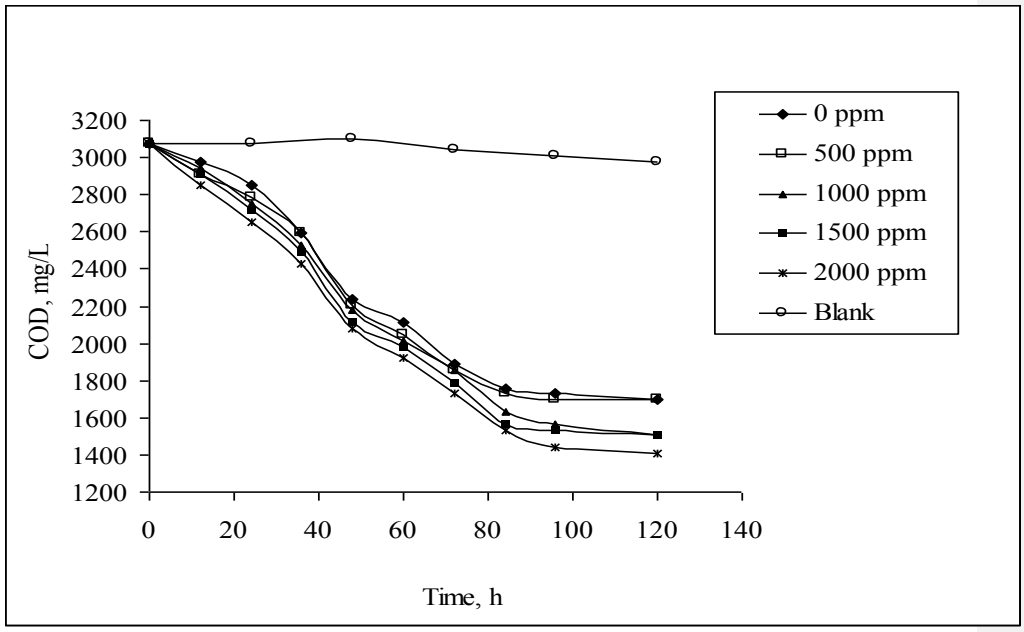

Fig. 6.9 (b) (i): Kinetics of COD reduction by SRB for different initial sulphate concentrations under anaerobic conditions

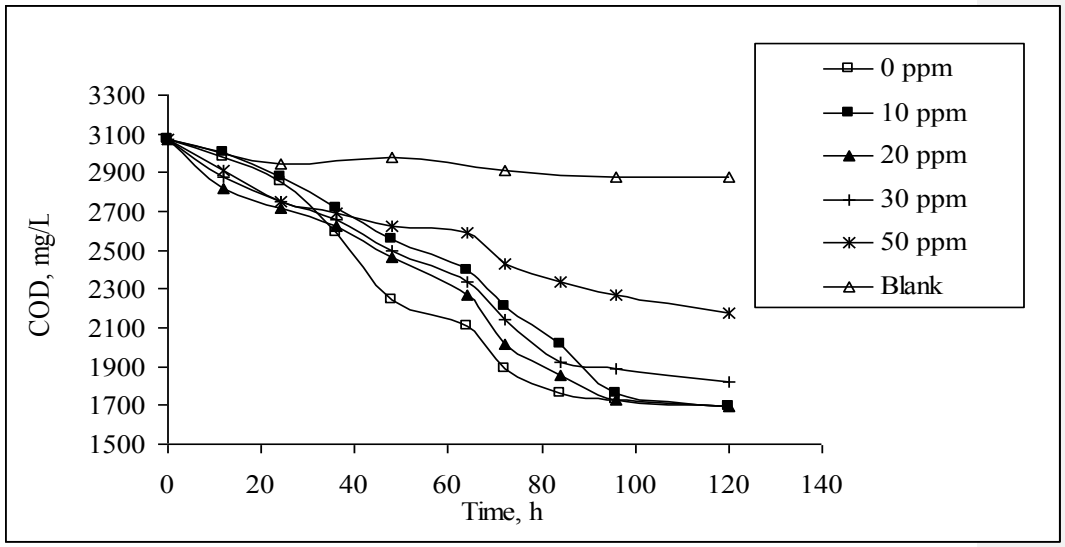

Fig. 6.9 (b) (ii): Kinetics of COD reduction by SRB for different initial Cr (VI) concentrations under anaerobic conditions

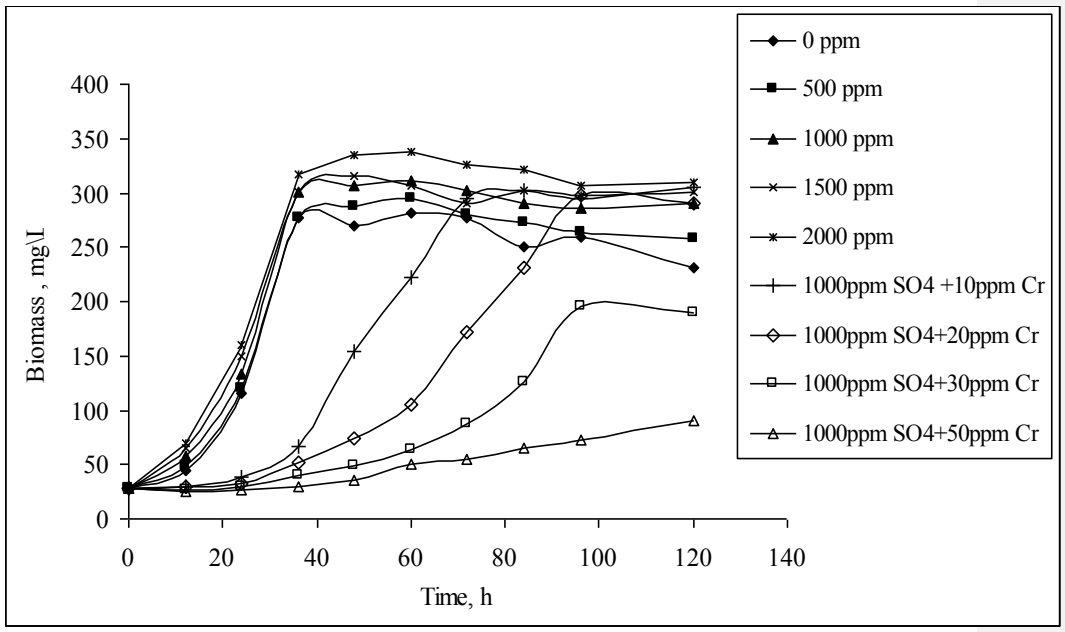

Fig. 6.9 (c): Growth curve of SRB with different initial sulphate and Cr (VI) concentrations under anaerobic conditions

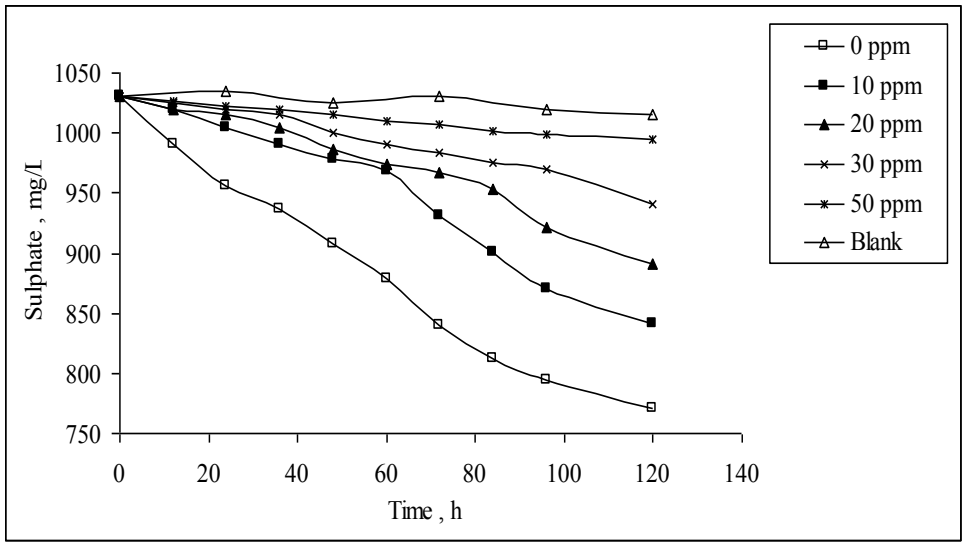

Fig. 6.9 (d) (i): Kinetics of sulphate reduction by SRB for different initial Cr (VI) concentrations under anaerobic conditions

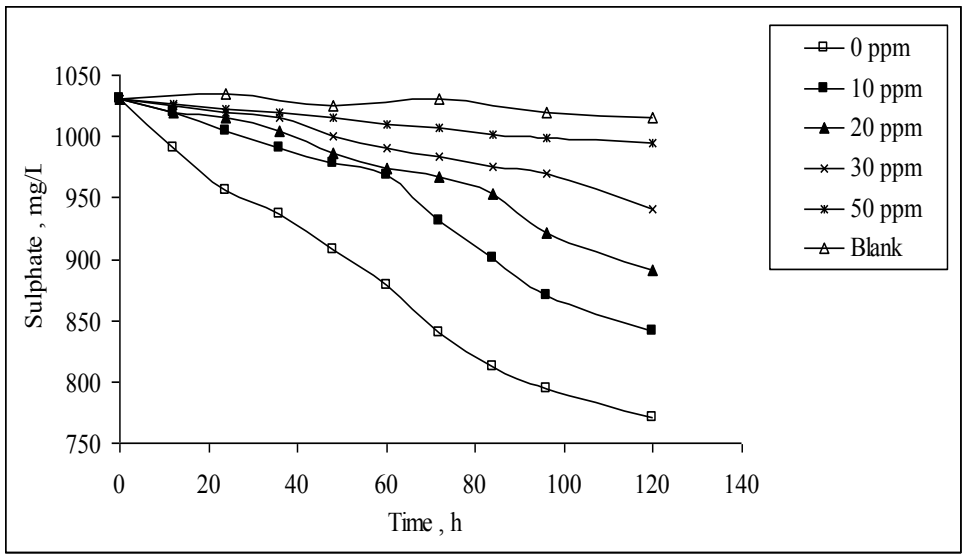

Fig. 6.9 (d) (ii): Kinetics of sulphate reduction by SRB for different initial Cr (VI) concentrations under anaerobic conditions

Kinetics of Cr (VI) by the SRB is presented in (Fig. 6.9 (a)). It can be seen from this figure that although complete reduction of chromium occurred for concentrations less

than 20 mg/L, the time taken was much longer (80 h) compared to that by CRB in both aerobic and anaerobic conditions. The reduction was not significant at higher Cr (VI) concentrations. The COD reduction efficiency was almost the same irrespective of sulphate concentration (up to 1000 mg/L), when Cr (VI) was absent in the system (Fig. 6.9 (b) (i)). However, the presence of Cr (VI) affected the COD removal efficiency of the SRB significantly (Fig. 6.9 (b) (ii)). The rate of sulphate reduction remained constant irrespective of sulphate concentration in the absence of Cr (VI) (Fig. 6.9 (d) (i)). However, the sulphate reduction rate reduced significantly as the Cr (VI) concentration in the system was increased (Fig. 6.9 (d) (ii)). These results indicate that SRB is highly sensitive to Cr (VI). As expected, growth rate of SRB also decreased as the Cr (VI) concentration increased (Fig. 6.9 (c)).

6.2.4 Kinetics of chromium reduction by IRB

Chromium reduction studies were carried out using IRB under anaerobic conditions. The microbial strains used for the study were enriched and isolated from soils exposed to iron filings. Studies were conducted by using Fe (III). Concentrations of biomass, COD, iron (Fe (II) and Fe (III)) and Cr (VI) were monitored with respect to time. In these studies, initial concentration of Cr (VI) was varied from 0 to 50 mg/L, whereas the COD concentration was kept constant at 3040 mg/L. Initial biomass concentration in all the experiments was equal to 30 mg/L, and iron concentration was varied from 0 to 1600 mg/L. Results of these studies are presented in Fig. 6.10.

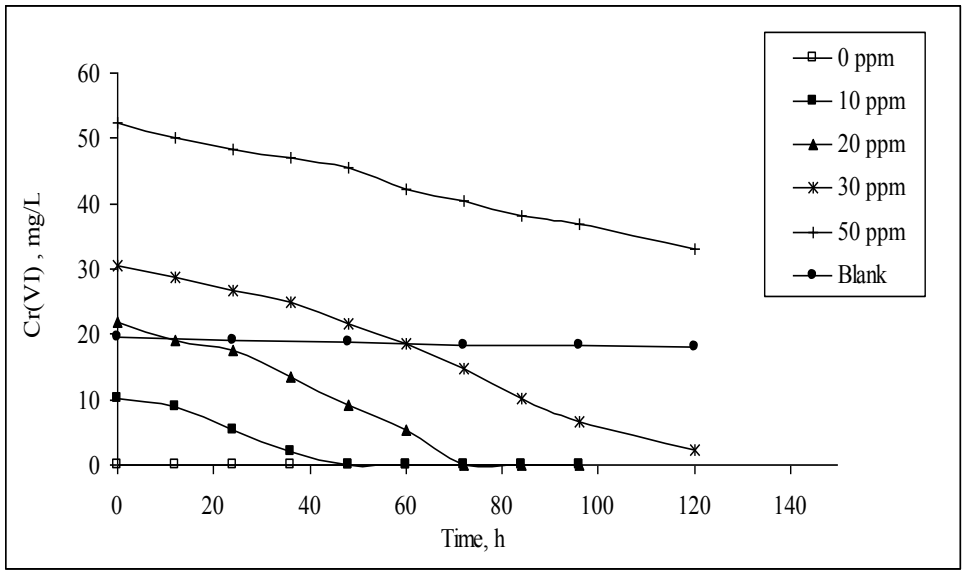

Fig. 6.10 (a): Kinetics of Cr (VI) reduction by IRB for different initial Cr (VI) concentrations under anaerobic conditions (Initial Fe (III) concentration = 800 mg/L)

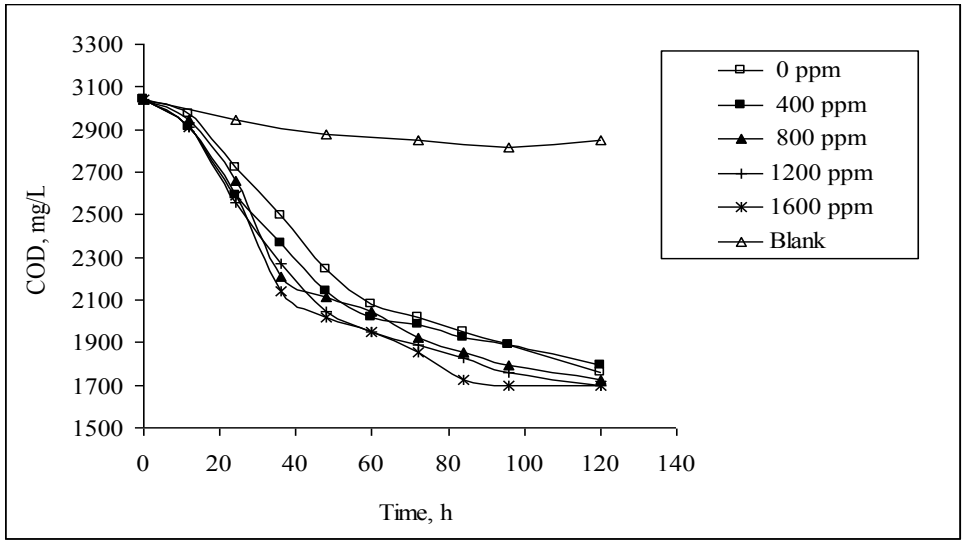

Fig. 6.10 (b) (i): Kinetics of COD reduction by IRB for different initial iron concentrations under anaerobic conditions (Initial Cr (VI) concentration = 20 mg/L)

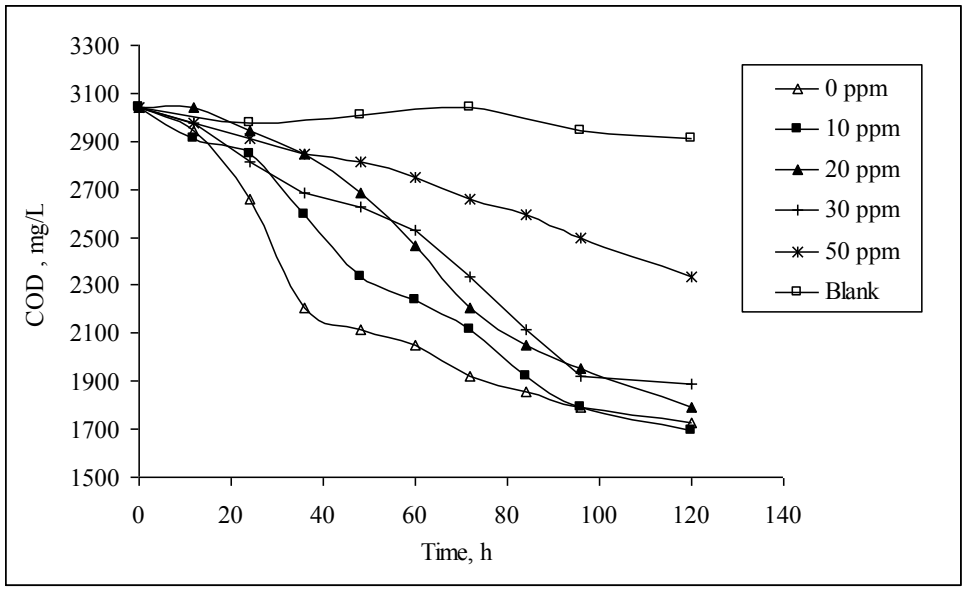

Fig. 6.10 (b) (ii): Kinetics of COD reduction by IRB for different initial Cr (VI) concentrations under anaerobic conditions (Initial Fe (III) concentration = 800 mg/L)

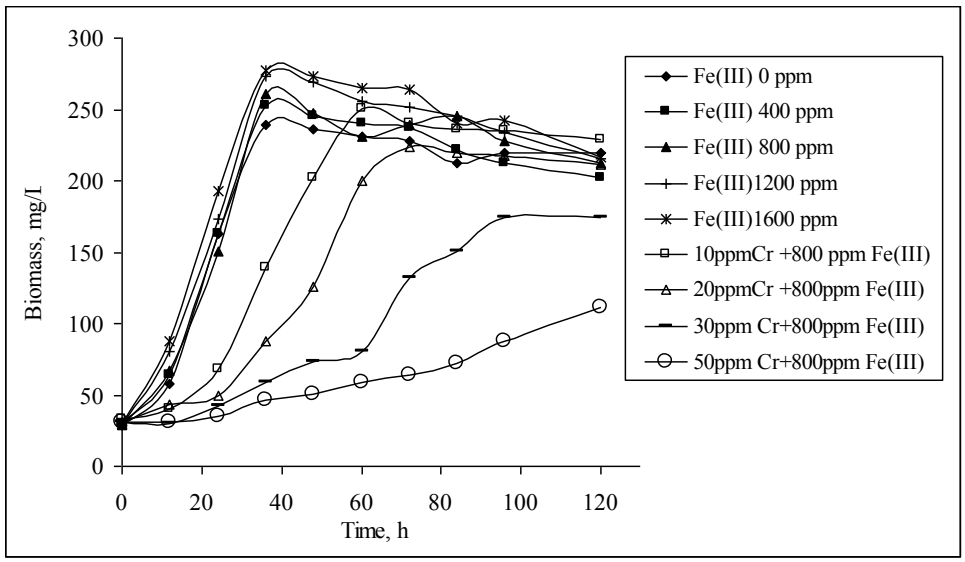

Fig. 6.10 (c): Growth curve of IRB with different initial Cr (VI) and Fe (III) concentrations under anaerobic conditions

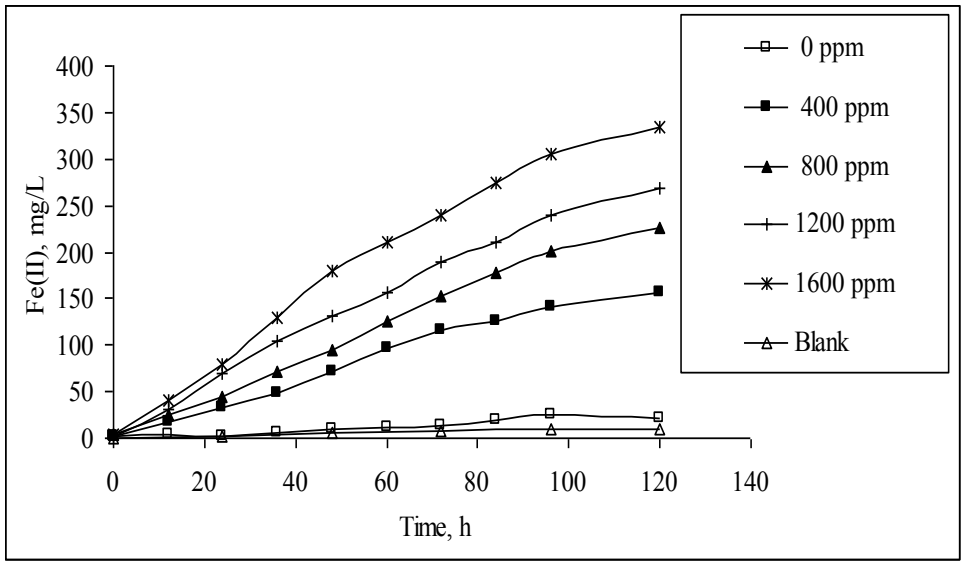

Fig. 6.10 (d) (i): Kinetics of Fe (II) generation by IRB for different initial Fe (III) concentrations under anaerobic conditions

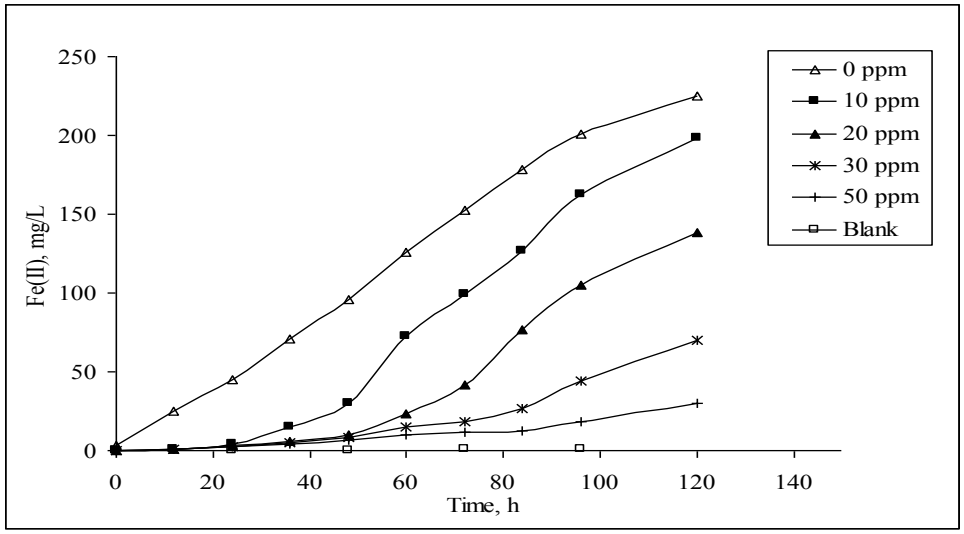

Fig. 6.10 (d) (ii): Kinetics of Fe (II) generation by IRB for different initial Cr (VI) concentrations under anaerobic conditions (Initial Fe (III) concentration = 800 mg/L)

The kinetics of chromium reduction by IRB in presence of 800 mg/L of Fe (III) is presented in Fig.10 (a). Growth of IRB and COD reduction were maximum when the Fe (III) concentration was 1600 mg/L (Fig.6.10 (c) and 6.10 (b) (i)). It can be seen from Fig. 6.10 (a) that the Cr (VI) reduction was complete within 70 h for initial concentrations of chromium up to 20 mg/L. Although Cr (VI) reduction occurred for a high initial Cr (VI) concentration (50 mg/L), the reduction was not complete. This could be due to the inhibition effect of Cr (VI) on the IRB. Results of these studies have shown that IRB is also sensitive to chromium like SRB and CRB. This is also evident from the COD removal efficiency (Fig. 6.10 (b) (ii)), biomass growth (Fig.6.10 (c)), and Fe (II) generation (Fig. 6.10 (d) (ii)).

Fe (III) was supplied to the system as ferric EDTA. Apart from the external carbon source, EDTA also contributes to the COD of the system. In order to assess the effect of excess COD on Cr (VI) reduction, microbial growth kinetic studies were conducted using different microorganisms and EDTA as sole carbon source. The results showed that EDTA utilization and the microbial growth were insignificant. This shows that additional COD contributed by EDTA did not have any effect on Cr (VI) reduction. The biokinetic parameters for CRB, SRB and IRB are tabulated in Table 6.2.

Table 6.2: Biokinetic parameters for CRB, SRB and IRB

Parameter	CRB Aerobic	CRB Anaerobic	SRB Anaerobic	IRB Anaerobic
μ_{max} (1/h)	0.35	0.09	0.11	0.09
μ_{max} (1/d)	8.42	2.13	2.53	2.08
Ks	120	80	180	220
Ki	5.49	7.68	7.12	7.42
η	0.009	0.020	0.028	0.036
Y_T	0.40	0.22	0.24	0.27

6.2.5 Kinetics of chromium reduction by a consortium of CRB and SRB

Chromium reduction studies were carried out using a consortium of CRB and SRB under anaerobic conditions. Concentrations of biomass, COD, sulphate and Cr (VI) were monitored with respect to time. In these studies, initial concentration of Cr (VI) was varied from 0 to 50 mg/L, whereas the COD concentration was kept constant at 3104 mg/L. Initial biomass concentration in all the experiments was equal to 40 mg/L. Sulphate concentration was varied from 0 to 2000 mg/L. Results of these studies are presented in Figs. 6.11 (a) – 6.11 (d).

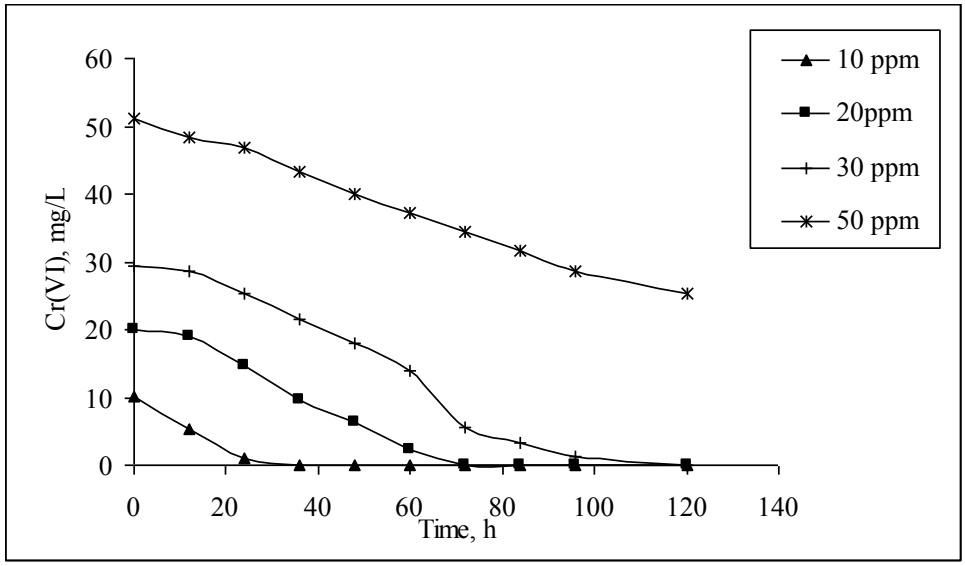

Fig. 6.11 (a) (i): Kinetics of Cr (VI) reduction by a consortium of CRB and SRB for different initial chromium concentrations (Initial sulphate concentration = 1000 mg/L)

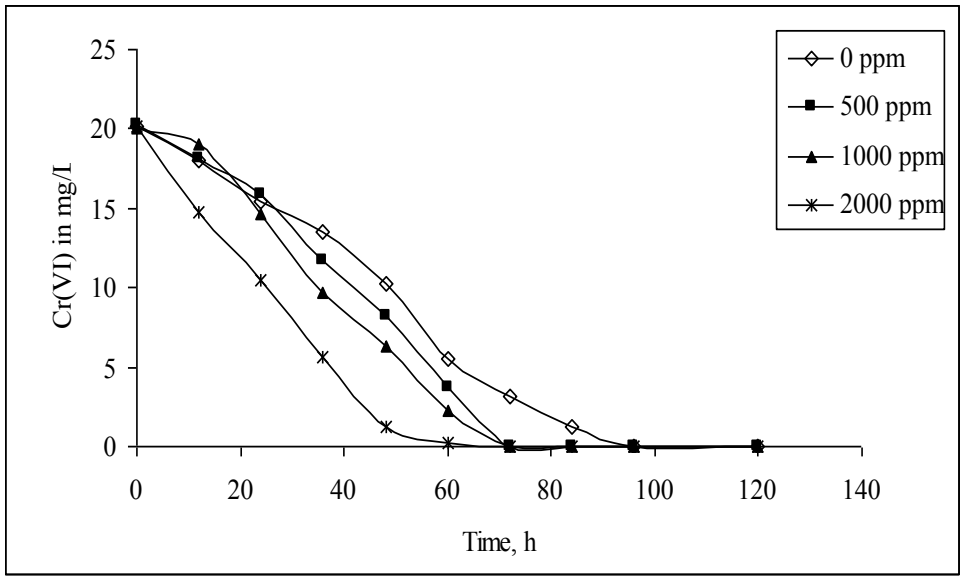

Fig. 6.11 (a) (ii): Kinetics of Cr (VI) reduction by a consortium of CRB and SRB for different initial sulphate concentrations

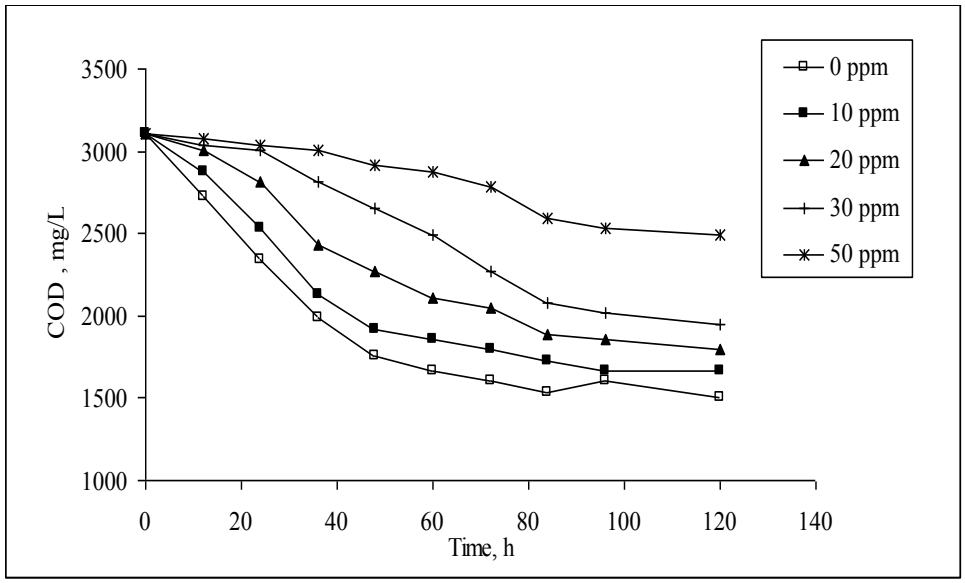

Fig. 6.11 (b) (i): Kinetics of COD removal by a consortium of CRB and SRB for different initial chromium concentrations (Initial sulphate concentration = 1000 mg/L)

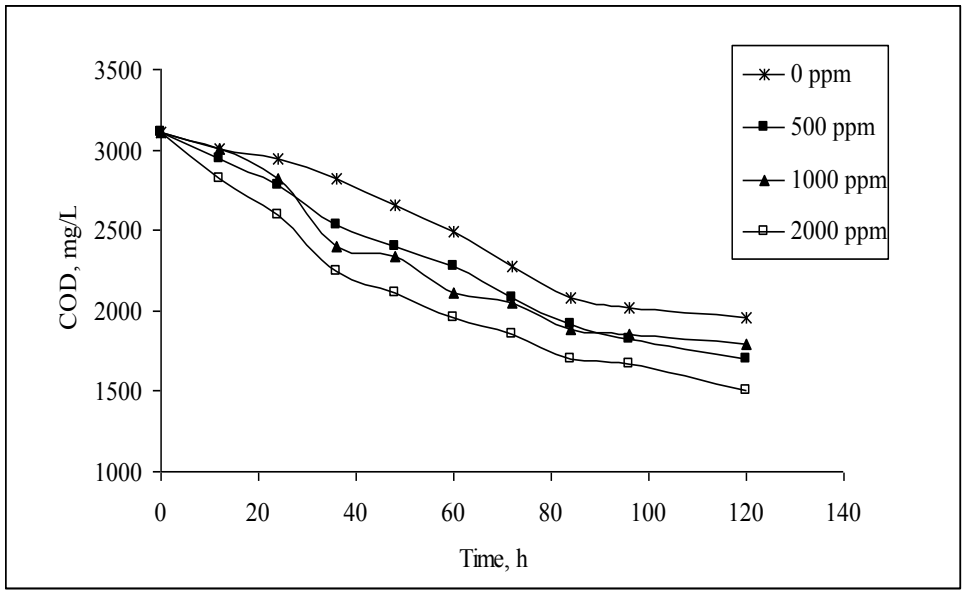

Fig. 6.11 (b) (ii): Kinetics of COD removal by a consortium of CRB and SRB for different initial sulphate concentrations (Initial Cr (VI) concentration = 20 mg/L)

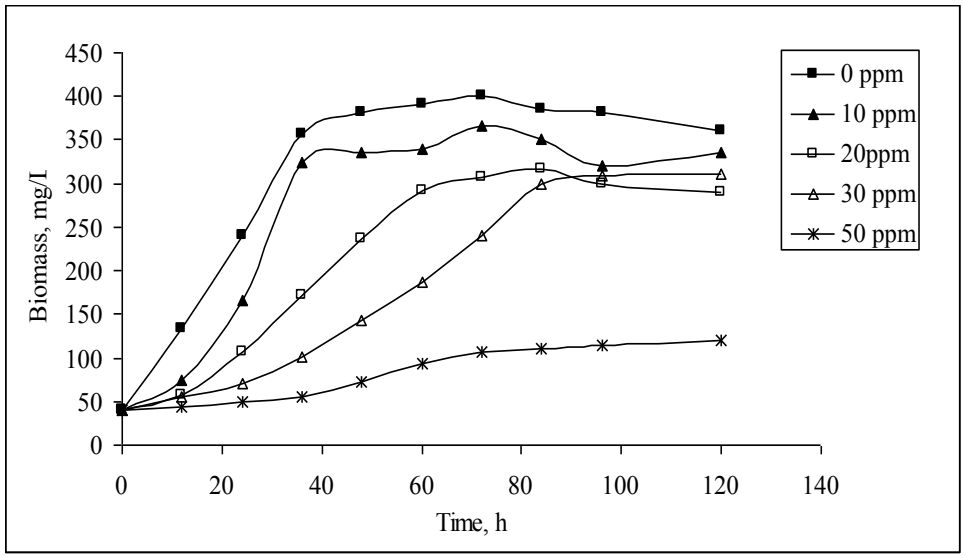

Fig. 6.11 (c) (i): Growth kinetics of a consortium of CRB and SRB for different initial chromium concentrations (Initial sulphate concentration = 1000 mg/L)

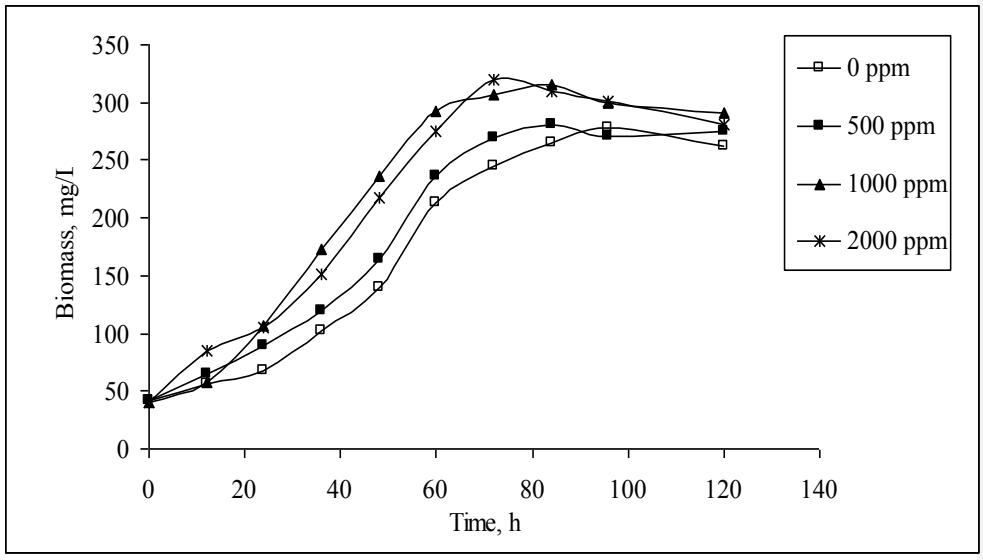

Fig. 6.11 (c) (ii): Growth kinetics of a consortium of CRB and SRB for different initial sulphate concentrations (Initial Cr (VI) concentration = 20 mg/L)

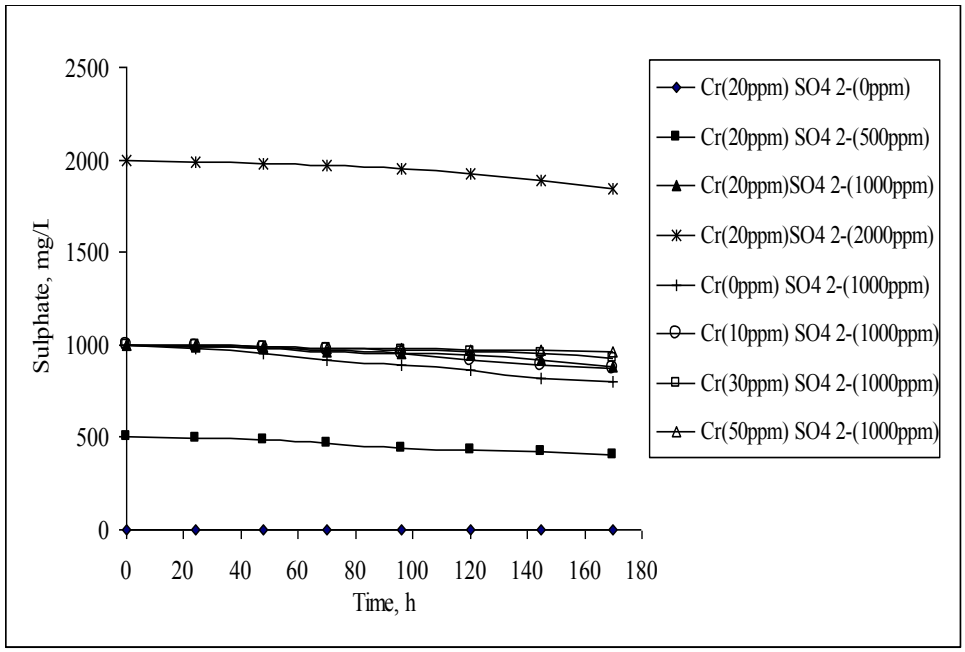

Fig. 6.11 (d): Kinetics of sulfate reduction by a consortium of CRB and SRB for different initial Cr (VI) and sulphate concentrations

It can be seen from Fig. 6.11 (a) (i) that the chromium reduction was complete up to a concentration of 30 mg/L within 110 h, with an initial sulfate concentration of 1000 mg/L in the system. Cr (VI) reduction was complete at lower sulfate concentrations also though it took relatively longer time to achieve this (Fig. 6.11 (a) (ii)). Cr (VI) reduction occurred for higher concentrations also although it was not complete. COD removal also followed a similar trend (Figs. 6.11 (b) (i) and 6.11 (b) (ii)). At higher Cr (VI) concentrations, the rate of COD removal was reduced. This could be due to the inhibitory effect of Cr (VI) on CRB and SRB as observed in the experiments for individual cultures. The inhibition effect is clear from the biomass concentrations in the systems (Figs. 6.11 (c) (i) and 6.11 (c) (ii)). Maximum biomass concentration of 400 mg/L was achieved in the system with zero Cr (VI) concentration and a sulphate concentration of 1000 mg/L. There was slight reduction in maximum biomass concentration up to a Cr (VI) concentration of 30 mg/L and the effect was very significant when the concentration was more than 50 mg/L. The rate of sulphate reduction was very low irrespective of sulphate concentration (Fig. 6.11 (d)).

6.2.6 Kinetics of chromium reduction by a consortium of CRB and IRB

Chromium reduction studies were carried out using a consortium of CRB and IRB under anaerobic conditions. Concentrations of biomass, COD, Fe (II), Fe (III) and Cr (VI) were monitored with respect to time. In these studies, initial concentration of Cr (VI) was varied from 0 to 50 mg/L, whereas the COD concentration was kept constant at 3072 mg/L. Initial biomass concentration in all the experiments was equal to 39 mg/L. Sulphate concentration was varied from 0 to 1600 mg/L. Results of these studies are presented in Figs. 6.12 (a) – 6.12 (d).

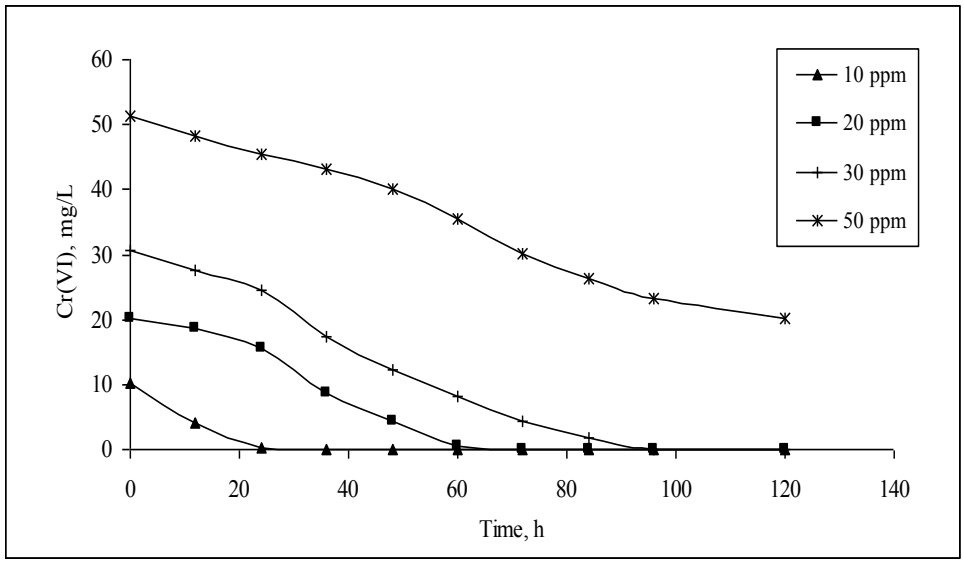

Fig. 6.12 (a) (i): Kinetics of Cr (VI) reduction by a consortium of CRB and IRB for different initial chromium concentrations (Initial Fe (III) concentration = 800 mg/L)

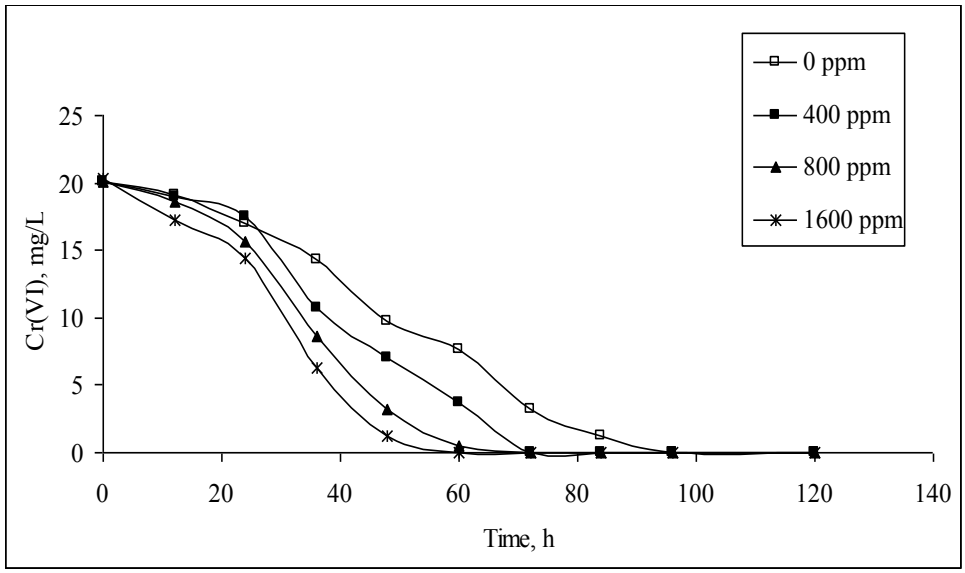

Fig. 6.12 (a) (ii): Kinetics of Cr (VI) reduction by a consortium of CRB and IRB for different initial Fe (III) concentrations (Initial Cr (VI) concentration = 20 mg/L)

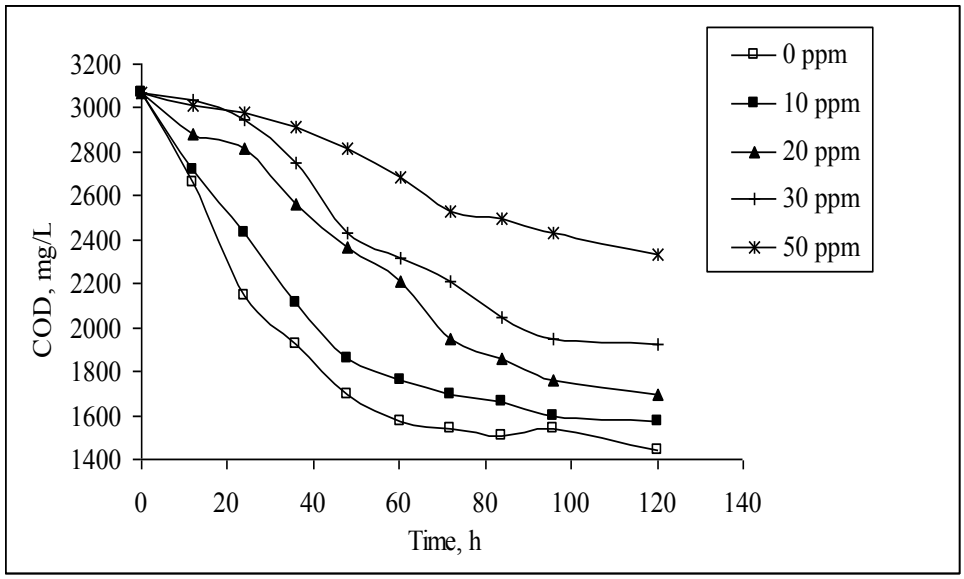

Fig. 6.12 (b) (i): Kinetics of COD removal by a consortium of CRB and IRB for different initial chromium concentrations (Initial Fe (III) concentration = 800 mg/L)

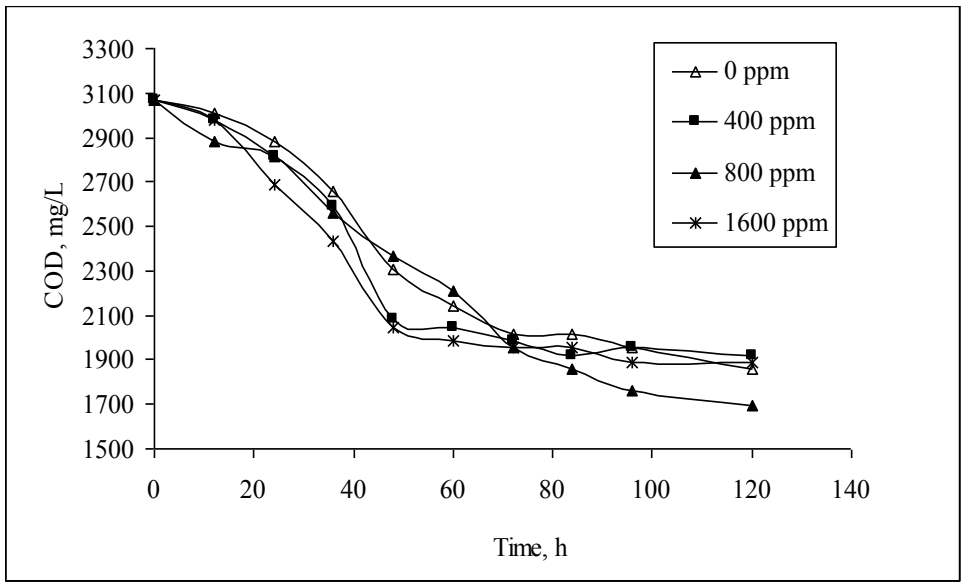

Fig. 6.12 (b) (ii): Kinetics of COD removal by a consortium of CRB and IRB for different initial Fe (III) concentrations (Initial Cr (VI) concentration = 20 mg/L)

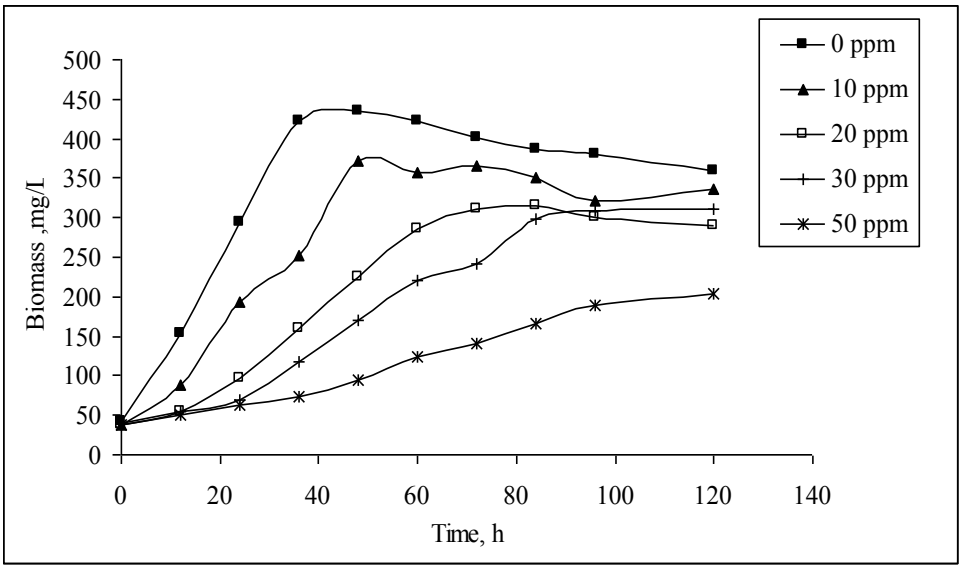

Fig. 6.12 (c) (i): Growth kinetics of a consortium of CRB and IRB for different initial Cr (VI) concentrations (Initial Fe (III) concentration = 800 mg/L)

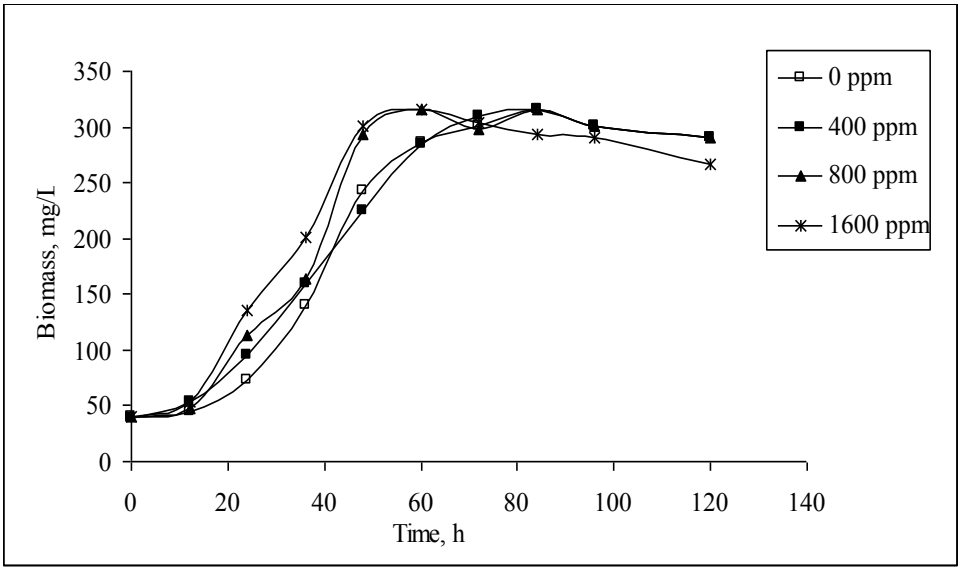

Fig. 6.12 (c) (ii): Growth kinetics of a consortium of CRB and IRB for different initial Fe (III) concentrations (Initial Cr (VI) concentration = 20 mg/L)

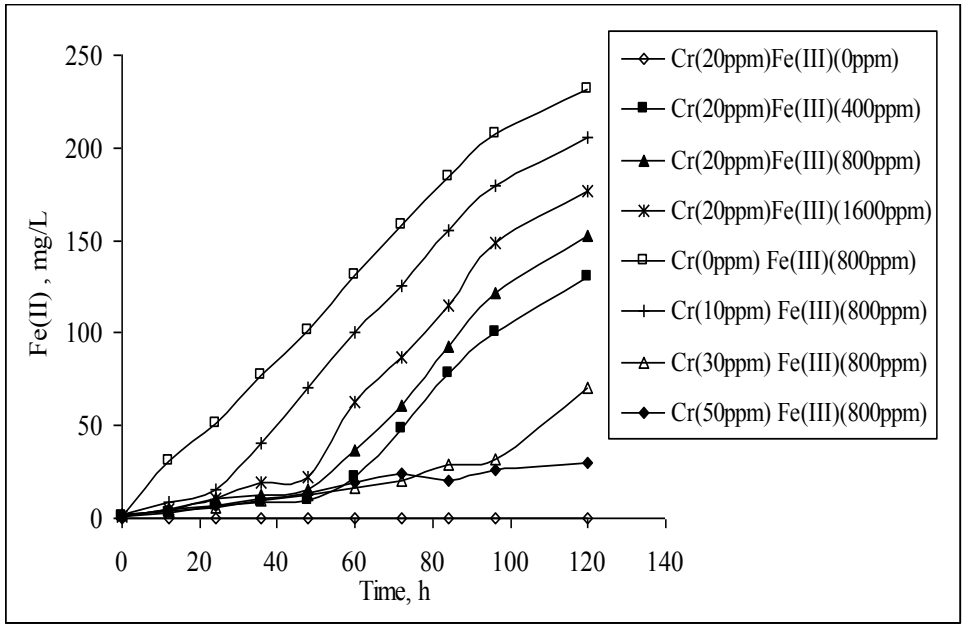

Fig. 6.12 (d): Kinetics of Fe (II) generation by a consortium of CRB and IRB for different initial Cr (VI) and Fe (III) concentrations

It can be seen from Fig. 6.12 (a) (i) that the chromium reduction was complete up to a concentration of 30 mg/L within 100 h, with an initial Fe (III) concentration of 800 mg/L in the system. Cr (VI) reduction was complete at lower Fe (III) concentrations also though it took relatively longer time to achieve this (Fig. 12 (a) (ii)). Cr (VI) reduction occurred for higher concentrations also although it was not complete. COD removal also followed a similar trend (Figs. 6.12 (b) (i) and 6.12 (b) (ii)). At higher Cr (VI) concentrations, the rate of COD removal was reduced. This could be due to the inhibitory effect of Cr (VI) on CRB and IRB as observed in the experiments for individual cultures. The inhibition effect is clear from the biomass concentrations in the systems (Figs. 6.12 (c) (i) and 6.12 (c) (ii)). Maximum biomass concentration of 450 mg/L was achieved in the system with zero Cr (VI) concentration and a Fe (III) concentration of 800 mg/L. There was slight reduction in maximum biomass concentration up to a Cr (VI) concentration of 30 mg/L and the effect was very significant when the concentration was

more than 50 mg/L. As expected, Fe (II) generation was very high when Cr (VI) was not present in the system and it significantly reduced when Cr (VI) concentration in the system was high (Fig. 6.12 (d)).

6.2.7 Kinetics of chromium reduction by a consortium of CRB, SRB and IRB

Chromium reduction studies were carried out using a consortium of CRB, SRB and IRB under anaerobic conditions. Concentrations of biomass, COD, Fe (II), Fe (III), sulphate and Cr (VI) were monitored with respect to time. In these studies, initial concentration of Cr (VI) was varied from 0 to 50 mg/L, whereas the COD concentration was kept constant at 3040 mg/L. Initial biomass concentration in all the experiments was equal to 37 mg/L. Sulphate and Fe (III) concentrations were maintained at 500 mg/L and 400 mg/L, respectively. Experiments were also conducted with sulphate and Fe (III) concentrations at 1000 mg/L and 800 mg/L, respectively. Results of these studies are presented in Figs. 6.13 (a) – 6.13 (e).

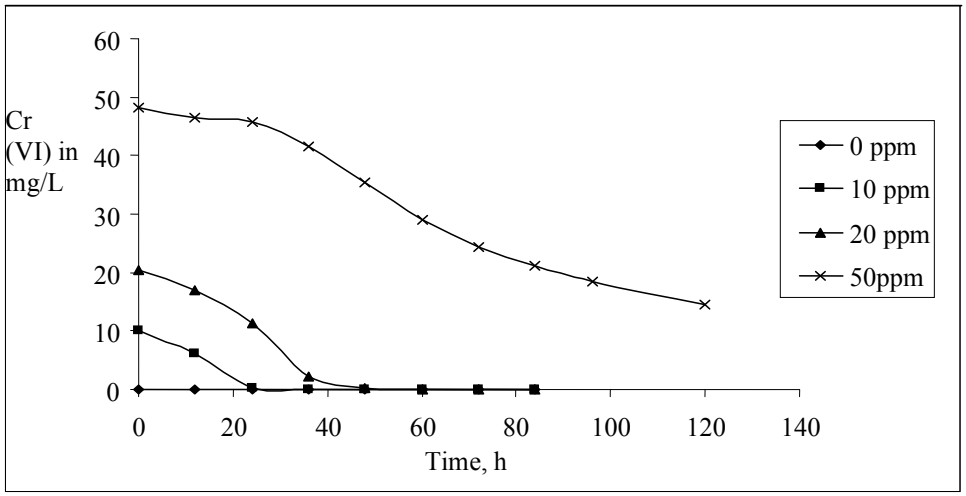

Fig. 6.13 (a): Kinetics of Cr (VI) reduction by a consortium of CRB, SRB and IRB for different initial chromium concentrations (Initial Fe (III) concentration = 400 mg/L, Initial sulphate concentration = 500 mg/L)

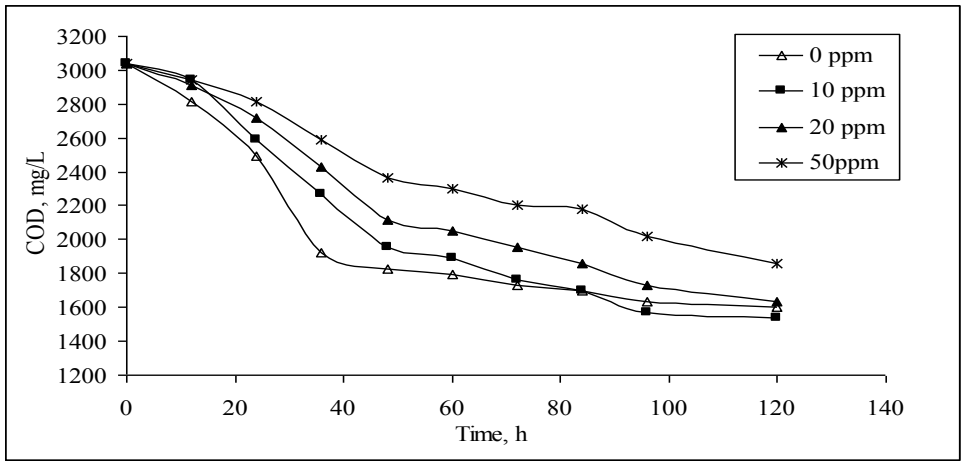

Fig. 6.13 (b): Kinetics of COD reduction by a consortium of CRB, SRB and IRB for different initial chromium concentrations (Initial Fe (III) concentration = 400 mg/L, Initial sulphate concentration = 500 mg/L)

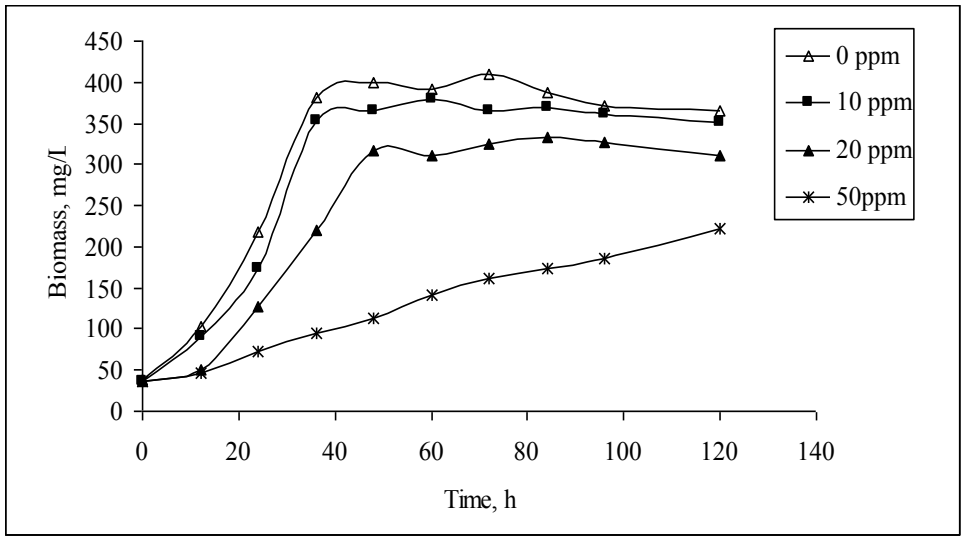

Fig. 6.13 (c): Growth kinetics of a consortium of CRB, SRB and IRB for different initial chromium concentrations (Initial Fe (III) concentration = 400 mg/L, Initial sulphate concentration = 500 mg/L)

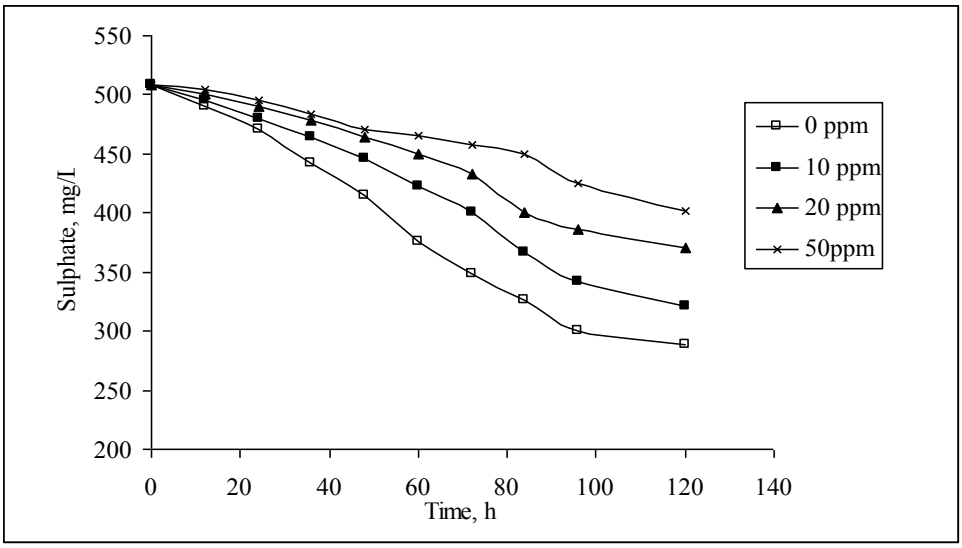

Fig. 6.13 (d): Kinetics of sulphate reduction by a consortium of CRB, SRB and IRB for different initial chromium concentrations (Initial Fe (III) concentration = 400 mg/L, Initial sulphate concentration500 mg/L)

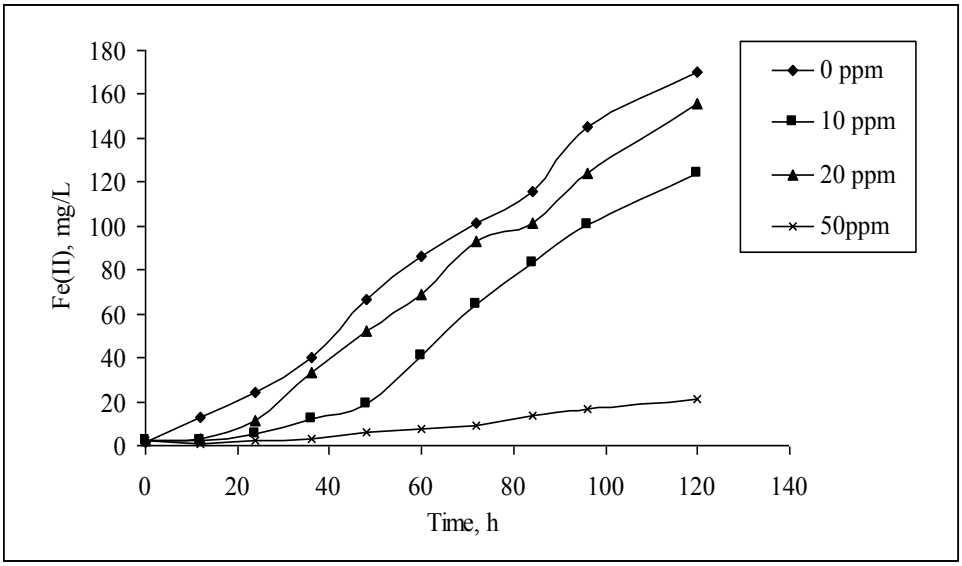

Fig. 6.13 (e): Kinetics of Fe (II) generation by a consortium of CRB, SRB and IRB for different initial chromium concentrations (Initial Fe (III) concentration = 400 mg/L, Initial sulphate concentration 500 mg/L)

It can be seen from Fig. 6.13 (a) that the chromium reduction was complete up to a concentration of 20 mg/L within 40 h, with an initial Fe (III) concentration of 400 mg/L and initial sulphate concentration of 500 mg/L in the system. Cr (VI) reduction occurred for higher concentrations also although it was not complete. COD removal also followed a similar trend (Fig. 6.13 (b)). At higher Cr (VI) concentrations, the rate of COD removal was reduced. This could be due to the inhibitory effect of Cr (VI) on CRB, SRB and IRB as observed in the experiments for individual cultures. The inhibition effect is clear from the biomass concentrations in the systems (Fig. 6.13 (c)). Maximum biomass concentration of 400 mg/L was achieved in the system with zero Cr (VI) concentration, a Fe (III) concentration of 400 mg/L, and a sulphate concentration of 500 mg/L. There was slight reduction in maximum biomass concentration up to a Cr (VI) concentration of 20 mg/L and the effect was very significant when the concentration was more than 50 mg/L. As expected, Fe (II) generation was very high when Cr (VI) was not present in the system and it was significantly reduced when Cr (VI) concentration in the system was high (Fig. 6.13 (e)). Sulphate reduction also followed the same trend (Fig. 6.13 (d)).

6.3 BENCH SCALE COLUMN EXPERIMENTS: CONTAINMENT OF Cr(VI) IN CONFINED AQUIFERS BY BIOTRANSFORMATION

6.3.1 Batch adsorption studies

Adsorption studies were conducted to understand the role of adsorption on the transport/ containment of Cr (VI) and Cr (III) in contaminated aquifers. Kinetics of adsorption of Cr (VI), Cr (III), Li and COD on the soil matrix were studied using batch experiments. Adsorption studies were conducted at a pH equal to 4.0 to 5.0 to avoid precipitation. Adsorption was very fast during the initial few minutes and attained a pseudo-equilibrium state at approximately t=6 hrs. Usually it takes days to attain the true equilibrium. Therefore, t=6 hrs is used as the equilibrium time for all the isotherm studies. Figs 6.14, 6.15 and 6.16 show the adsorption isotherms for Cr (VI), Cr (III) and Li, respectively for soil A. In all these figures, Freundlich isotherm was used for fitting the experimental data because soil is a heterogeneous medium with different functional groups. Table 6.3

shows the Freundlich coefficient (K_f), exponent (1/n) and the corresponding correlation coefficient for all the isotherms.

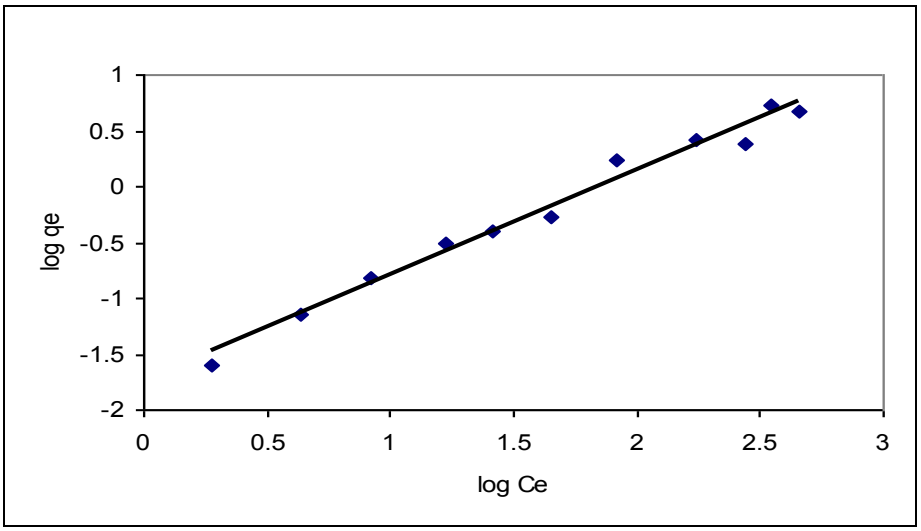

Fig. 6.14: Freundlich adsorption isotherm for Cr(VI) for soil A (pH - 4.2 to 5.0, C_0 - 1.0 to 500 mg/L)

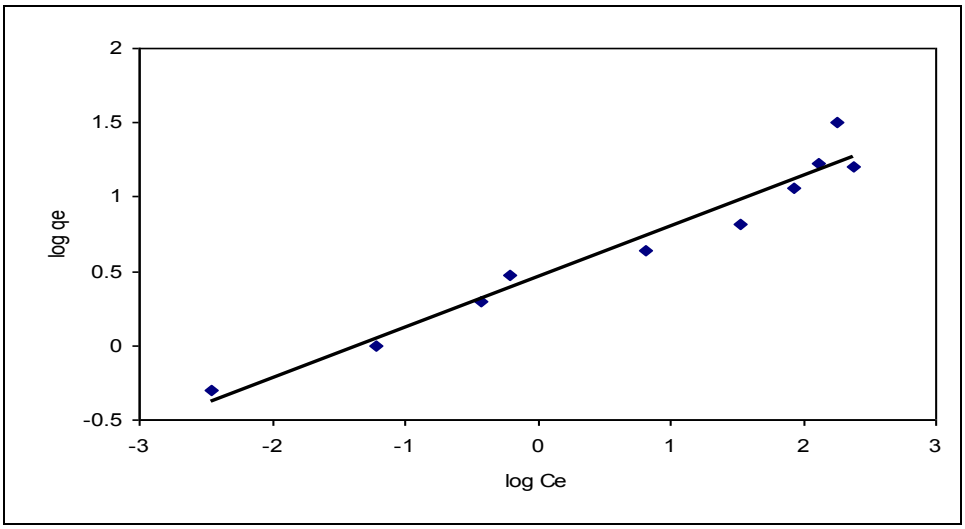

Fig. 6.15: Freundlich adsorption isotherm for Cr(III) for soil A (pH - 4.0 to 5.0, C_0 - 1.0 to 500 mg/L)

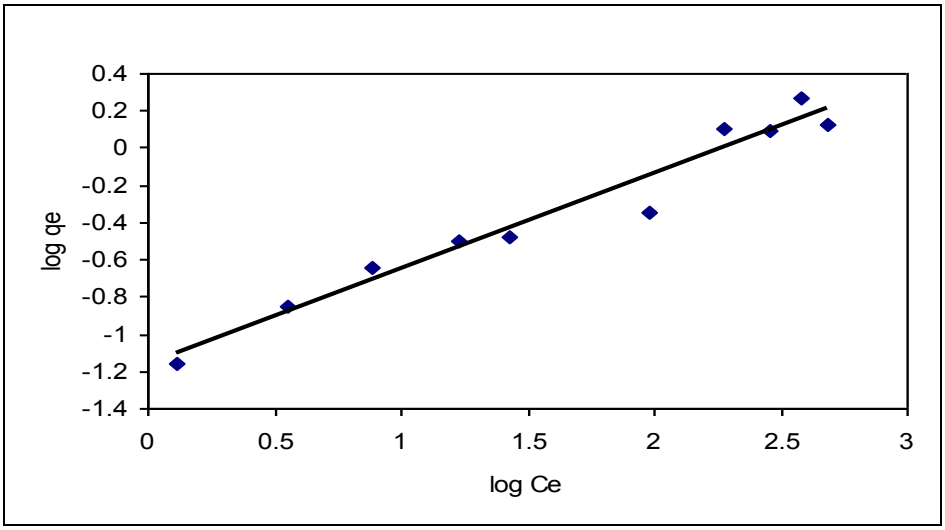

Fig. 6.16: Freundlich adsorption isotherm for Lithium for soil A (pH - 4.0 to 5.0, C_0 – 1.0 to 500 mg/L)

Table 6.3: Isotherm constants for soil adsorption

	Freundlich Isotherm		
	K_f	**1/n**	**r^2**
Soil A			
Cr(VI)	0.01798	0.9445	0.98
Cr(III)	2.9	0.339	0.96
Li	0.068061	0.5128	0.96
Cr(VI) in presence of Molasses and lithium			
Soil A	0.012303	1.9135	0.96
Soil B	0.010325	1.0512	0.94
Molasses in presence of Cr(VI) and lithium			
Soil A	0.055017	0.764	0.95
Soil B	0.050687	0.7575	0.90
Cr(III) in presence of Molasses and lithium (pH = 7.0)			
Soil A	0.1667	4.628	0.859

Soil B	0.734	5.778	0.933
Cr(III) in presence of Molasses and Lithium			
Soil A	0.1979	0.704	0.855
Soil B	0.0257	0.8443	0.983

It can be seen that adsorption of Cr (III) is much higher than Cr (VI) as expected. The residual Cr (VI) concentration and total chromium concentration in liquid phase were almost same in case of Cr (VI) isotherm studies. Adsorption of Li is almost negligible, indicating that it is a conservative pollutant, which servers as a tracer to determine dispersion characteristics. Adsorption studies were also conducted for Cr (VI) and Cr (III) in presence of COD and Li to understand the interference of these components on adsorption as it is a non-selective process. High adsorption of Cr (III) was observed when the pH was adjusted to 7.0, which was the pH of the mineral medium used for column studies. This high value is due to the precipitation of Cr (III). It is difficult to differentiate between the adsorption, precipitation, ion exchange and polymerization processes. Also, the focus of this work is on containment of chromium. Hence, all these reactions are considered together as "adsorption" in this study.

6.3.2 Batch biotransformation studies

Kinetics of Cr (VI) biotransformation by the enriched microbial culture isolated from contaminated soils was conducted. These results are presented in Fig. 6.17. The enriched microbes were able to reduce Cr (VI) even when the initial Cr (VI) concentration was as high as 500 mg/L. The Cr (VI) reduction was faster at low Cr (VI) initial concentrations. At higher concentrations of Cr (VI), microbial growth might have been inhibited. Measured residual COD values (results not shown) indicated that the system was working under substrate unlimiting conditions with an initial COD value of 2000 mg/L. In an earlier study, control experiments with Cr (VI) and molasses without any microbes had shown that the abiotic Cr (VI) reduction was less than 2% (Ramakrishna and Philip, 2005).

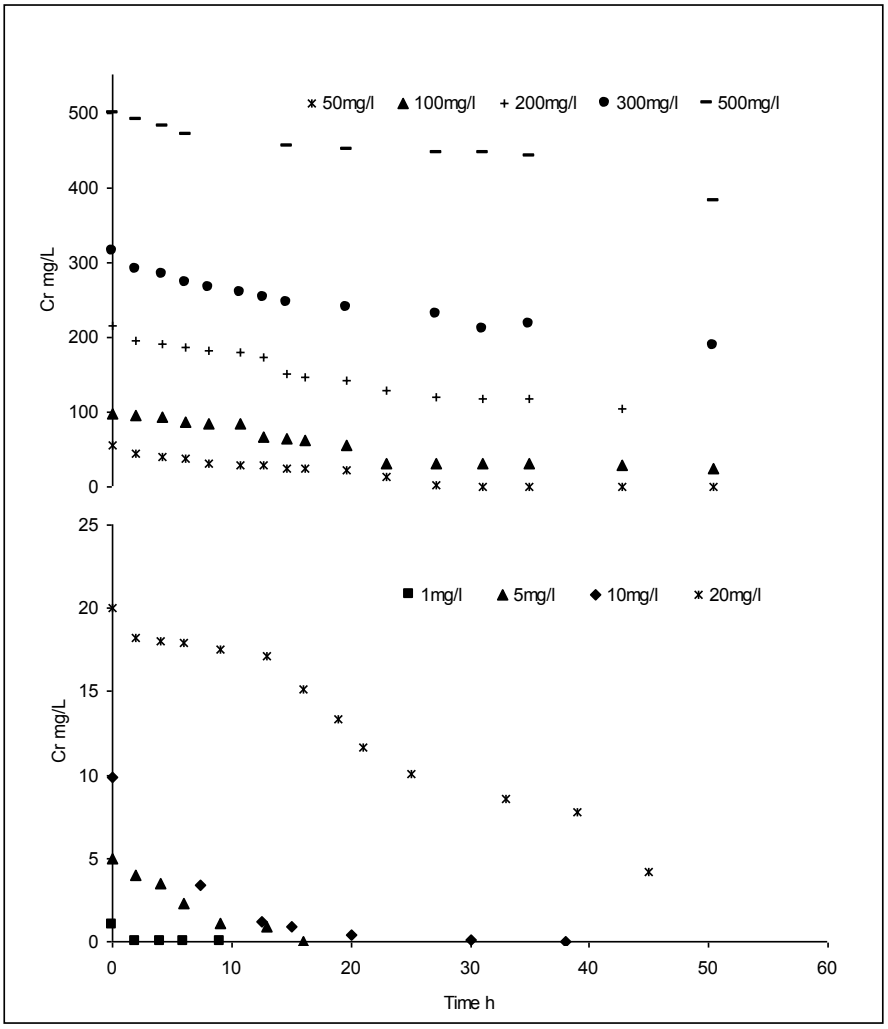

Fig. 6.17: Kinetics of Cr(VI) reduction for different initial Cr(VI) concentration(pH - 7, Cr (VI) concentration - 1 to 500 mg/L)

6.3.3 Studies to estimate Biokinetic Parameters

Data from bio-kinetic studies conducted without chromium were used to determine μ_{max} and K_s in Monod"s equation for bacterial growth. Lineweaver-burk plots (Benefield and Randall, 1982) were used for this purpose, and μ_{max}=0.5846/h and K_s=3835 mg/L (as COD) were determined. Experiments for microbial growth rate in the presence of

chromium were then used to determine the inhibition constant K_i and it was found to be equal to 11.46 mg/L of Cr (VI). The yield coefficient, Y_T and decay constant K_d were found to be equal to 0.2615 and 0.091 h^{-1}, respectively.

6.3.4 Transport studies with no biotransformation

To study the role of biotransformation in the containment of Cr (VI) in aquifers, it is essential to understand the transport of Cr (VI) without any biotransformation, considering only the adsorption. These transport studies were conducted for Soil A, with three different pore velocities. Figs. 6.18 (a) to 6.18 (d) present the break-through curves for Cr (VI) at 20, 40, 60 and 80 cm ports, respectively. Each figure shows the variation of Cr (VI) concentration in liquid phase with respect to time for different pore velocities. It is clear from these figures that the dispersion effect is more predominant than the advection effect when the pore velocity is low, as expected. The maximum Cr (VI) concentration at 80 cm port was almost equal to the inlet concentration when the pore velocity was equal to 11.2 cm/h. Further, the maximum Cr (VI) concentration at 80 cm port was almost equal to the inlet concentration even when the pore velocity was as low as 5.6 cm/h. Break-through curves for both Cr (VI) and Li at 80 cm port for a pore velocity of 22.4 cm/hr (not shown here) matched closely, indicating that the adsorption and hence retardation of Cr (VI) is insignificant. This is also evident from the adsorption isotherm constants for Cr (VI) and Li presented in Table 6.3. Therefore, it can be inferred that adsorption alone cannot significantly retard Cr (VI) transport in the aquifer. Model based parameter estimation using the advection-dispersion equation for Cr (VI) accounting for retardation showed that the dispersivity in these studies was equal to 4.46 cm. The dispersion coefficient varied linearly with pore velocity.

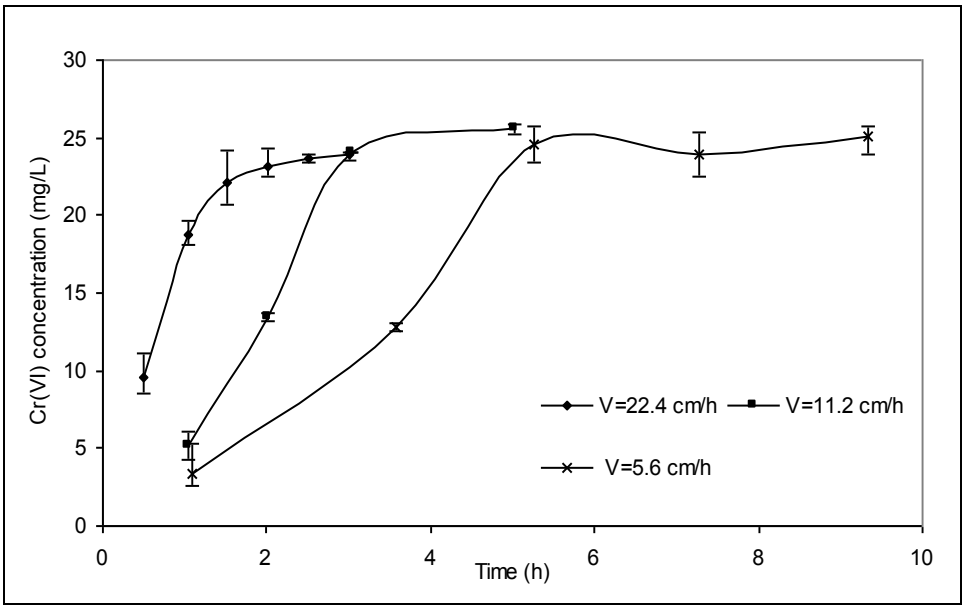

Fig. 6.18 (a): Breakthrough curve at 20cm port for different pore velocities; No biotransformation (pH - 6.7 to 7.0, Inlet Cr(VI) concentration- 25 mg/L)

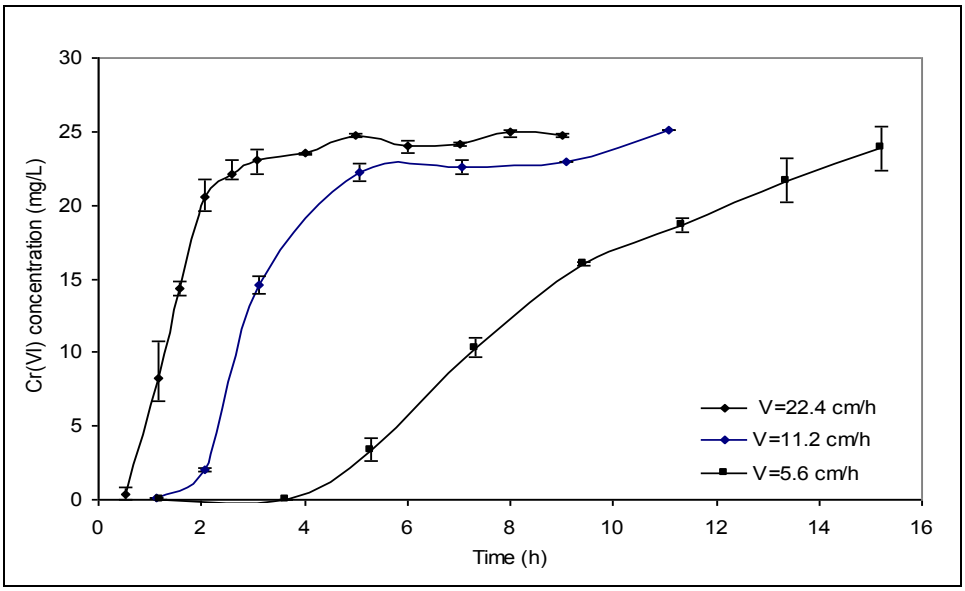

Fig. 6.18 (b): Breakthrough curve at 40cm port for different pore velocities; No biotransformation (pH - 6.7 to 7.0, Inlet Cr(VI) concentration- 25 mg/L)

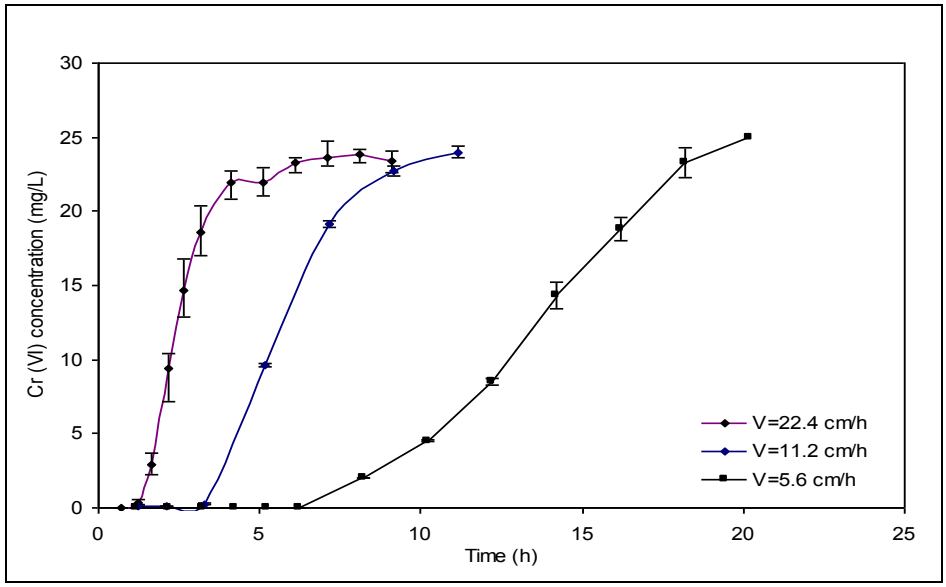

Fig. 6.18 (c): Breakthrough curve at 60cm port for different pore velocities; No biotransformation (pH - 6.7 to 7.0, Inlet Cr (VI) concentration- 25 mg/L)

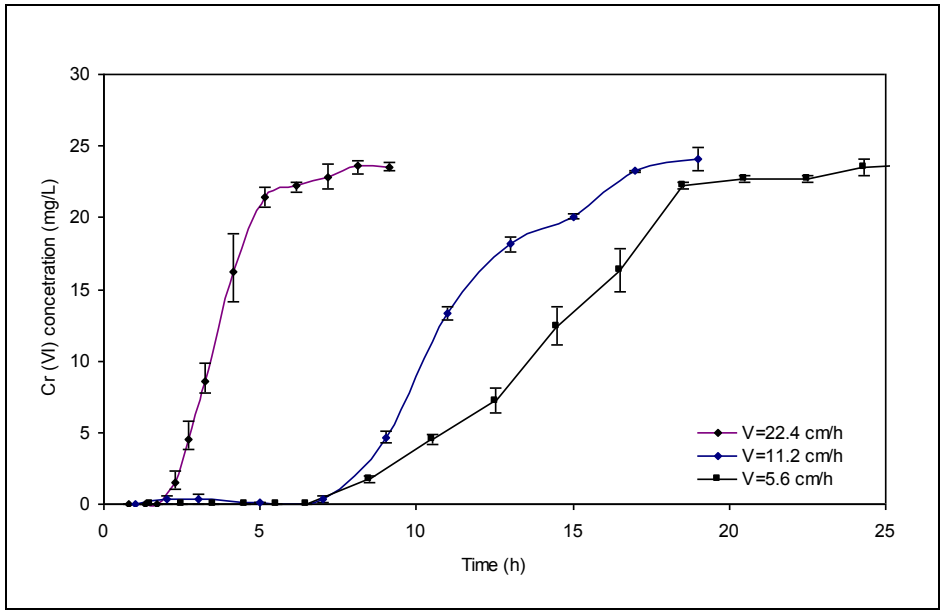

Fig. 6.18 (d): Breakthrough curve at 80cm port for different pore velocities; No biotransformation (pH - 6.7 to 7.0, Inlet Cr (VI) concentration- 25 mg/L)

6.3.5 Transport studies with bio-transformation

Bench scale experiments were conducted for transport along with bio-transformation in saturated, confined aquifer systems. Different soil types and different pore velocities were used as shown in Tables 6.4 and 6.5. The pH of the systems was monitored intermittently. The values were in the range of 6.2-7.2. In an earlier study on bioremediation of soil by authors (Jeyasingh and Philip, 2005; Ramakrishna and Philip, 2005), it was found that biotransformation of Cr (VI) to Cr (III) was most effective in the pH range of 6-8.

Table 6.4: Different soil types and its characteristics

S. No.	Properties	Value (mass %)	
		Soil A	Soil B
1	Clay content	6.19%	0%
2	Silt content	22.70%	0%
3	Sand content	71.11%	100%
4	Specific gravity	2.543	2.635
5	Organic Content	0.92%	ND
6	Bulk Density (g/c.c)	1.41	1.60
7	Porosity	0.45	0.375
8	pH	6.59	6.6

Table 6.5: Different pore velocities

Run No.	Soil type	Initial pore velocity, cm/h	Initial bacterial concentration added, mg/g
1	Soil A	5.833	0.0205
2	Soil B (Run-1)	6.67	0.0205
3	Soil B (Run-2)	1.16	0.0405

6.3.5.1 Cr (VI) containment with and without bio-transformation

Figs. 6.19 (a) and 6.19 (b) present Cr (VI) break-throughs in the confined aquifer in soil A, with and without bio-transformation respectively. These figures present the break-through curves at 20, 40 and 60 cm ports. It may be noted that the initial pore velocity for both the runs was approximately equal to 5.6 cm/h. However, in the case of experiment with bio-transformation, the pore velocity reduced with respect to time. It might have been due to the change in the permeability resulting from gas release and microbial growth. Water level in the upstream head tank was adjusted periodically to obtain approximately an average pore velocity of 2.3 cm/h. The pore velocity variation with time is also shown in Fig. 6.19 (a). It can be observed from Fig. 6.19 (b) that, in the experiment without bio-transformation, the break-through (≈95% of initial concentration) occurred at 9 hrs, 15 hrs 20 hrs and 25 hrs at 20, 40, 60 and 80 cm ports, respectively.

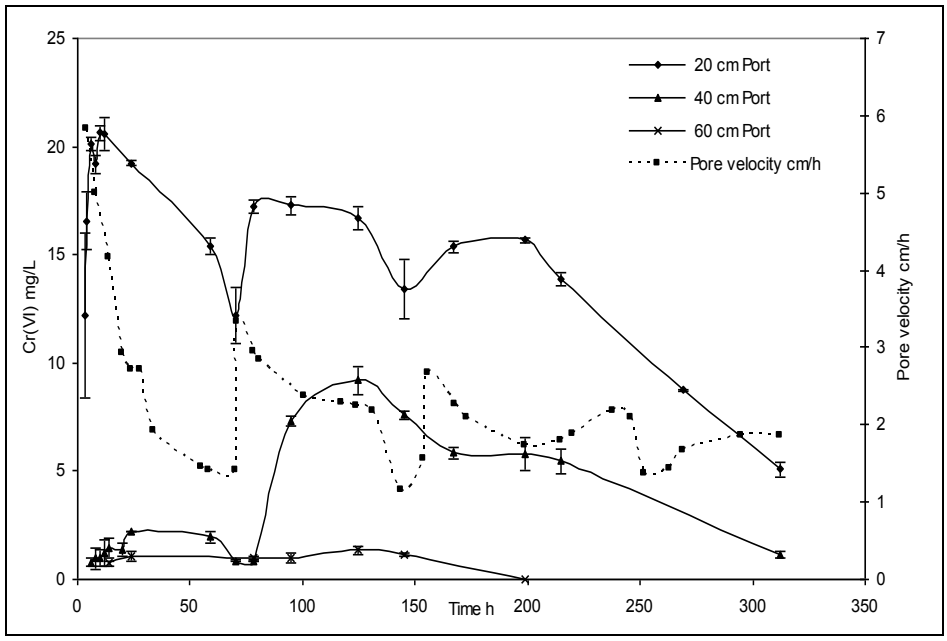

Fig. 6.19 (a): Cr (VI) break-through curve with biotransformation in soil A (pH - 6.2 to 7.2, Inlet Cr (VI) concentration- 25 mg/L)

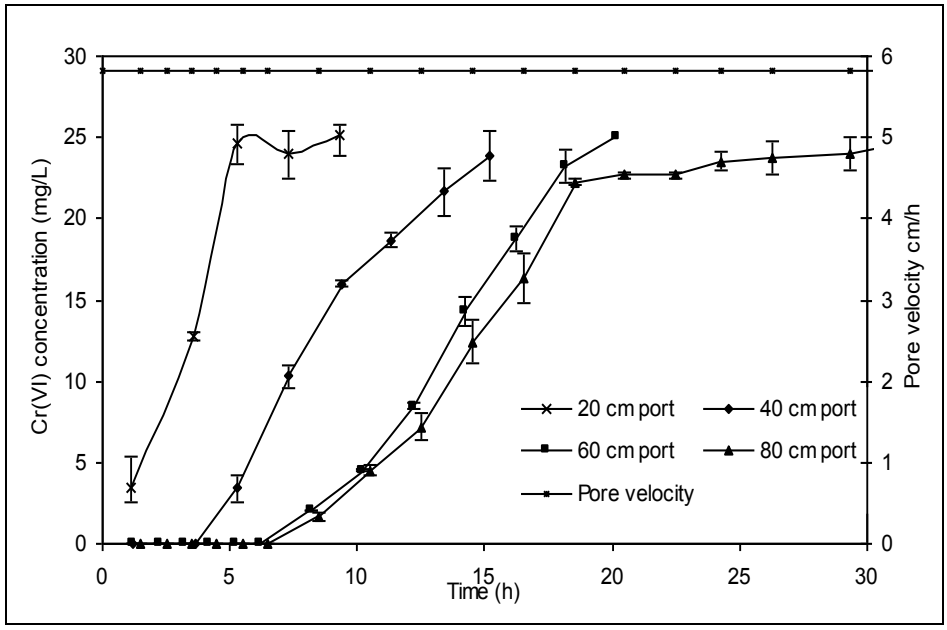

Fig. 6.19 (b): Cr (VI) break-through curve without biotransformation in soil A (pH - 6.7 to 7.0, Inlet Cr (VI) concentration- 25 mg/L)

In the case of experiment with bio-transformation, even though break-through occurred at 10 h at the 20 cm port, the Cr (VI) concentration reduced drastically in the next 300 h. In the same experiment, the maximum concentration at 40 cm port was only 8 mg/L (≈33% of initial concentration) and it occurred at time t = 125 h. The maximum concentration in 60 cm port never exceeded 1 mg/L (≈4% of initial concentration). There was no significant reduction of the Cr (VI) by molasses as discussed in an earlier work (Ramakrishna and Philip, 2005). The transport experiments without biotransformation showed very little containment of Cr (VI) in the soil column. Moreover, adsorption equilibrium studies with soil and molasses showed insignificant adsorption of Cr (VI) though there was some adsorption of Cr (III) (Table 6.3). This clearly indicates the effectiveness of bio-transformation on hexavalent chromium containment in contaminated aquifers.

In the case of column study with biotransformation, break-through of Cr (VI) at 20 cm port occurred almost at the same time as that in column without biotransformation. This might be due to the acclimatization period of microbes present in the system. As the microbes got acclimatized, the rate of biotransformation and hence the containment of Cr (VI) increased. This is clearly evident from the results for ports 40 cm and 60 cm. Cr (VI) was contained completely within 80 cm as the bio-barrier distance through which Cr (VI) transport occurred was more.

6.3.5.2 Effect of velocity and cell concentration on biotransformation

Figs. 6.20 (a) to 6.20 (d) present the variation of Cr (VI) concentration at 20, 40, 60 and 80 cm ports, respectively, for the case of transport and bio-transformation experiments in soil B. Results for two different pore velocities of 6.67 cm/h and 1.16 cm/h are presented in these figures. It is clear that the effect of bio-transformation on Cr (VI) containment is significant in the case of low pore velocity. Here, although break-through did occur, the Cr (VI) concentration reduced to zero subsequently. In case of high pore velocity, break-through of Cr (VI) occurred much earlier and also the maximum concentration was almost equal to the inlet concentration even after 150 hrs.

Pore velocity had a significant effect on bacterial retention on the soil matrix. Initially, the columns were operated with only mineral medium until steady state flow conditions were attained (6 hours). High pore velocity resulted in significant bacterial cell wash out during this initial period. The bacterial concentration reduced from 0.021 to 0.005 mg/g in the case of column with high pore velocity, while it reduced from 0.04 to 0.027 mg/g in the case of column with low pore velocity. Thus column with low pore velocity had an advantage over the column with high pore velocity since the rate of any biological activity depends upon the biomass concentration. Cr (VI) containment in the case of column with low pore velocity was delayed to some extent because the bacteria introduced to the system might have taken time to get acclimatized. It can be seen from Figs. 6.20 (a) to 6.20 (d) that the rate of Cr (VI) containment increased with respect to time because of corresponding increase in biomass concentration in the system. It is clear from these results that initial biomass concentration as well as the pore velocity plays a significant role in Cr (VI) containment in contaminated aquifers.

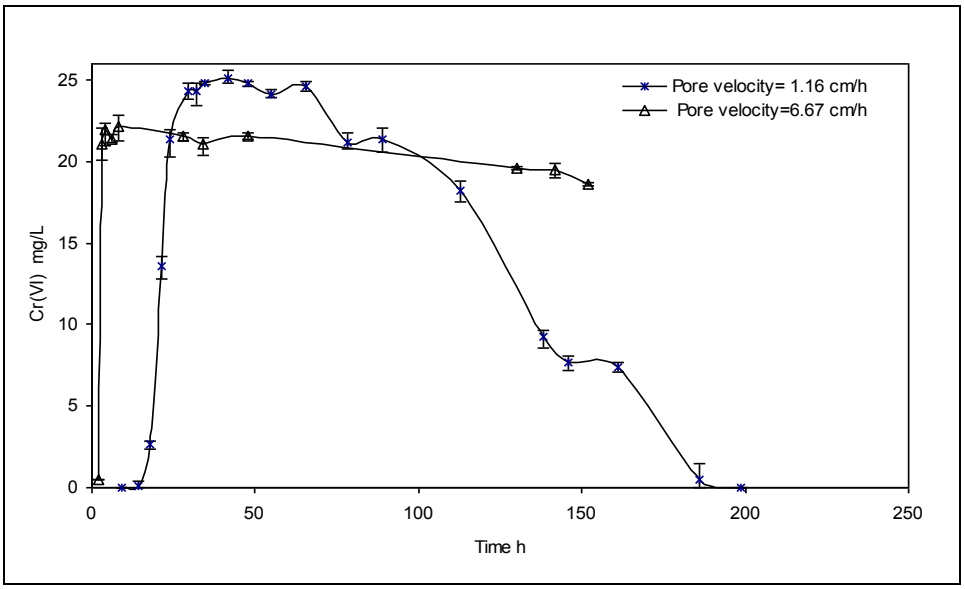

Fig. 6.20 (a): Cr (VI) break-through curve at 20 cm port in soil B; with bio-transformation (pH - 6.2 to 7.2, Inlet Cr(VI) concentration- 25 mg/L)

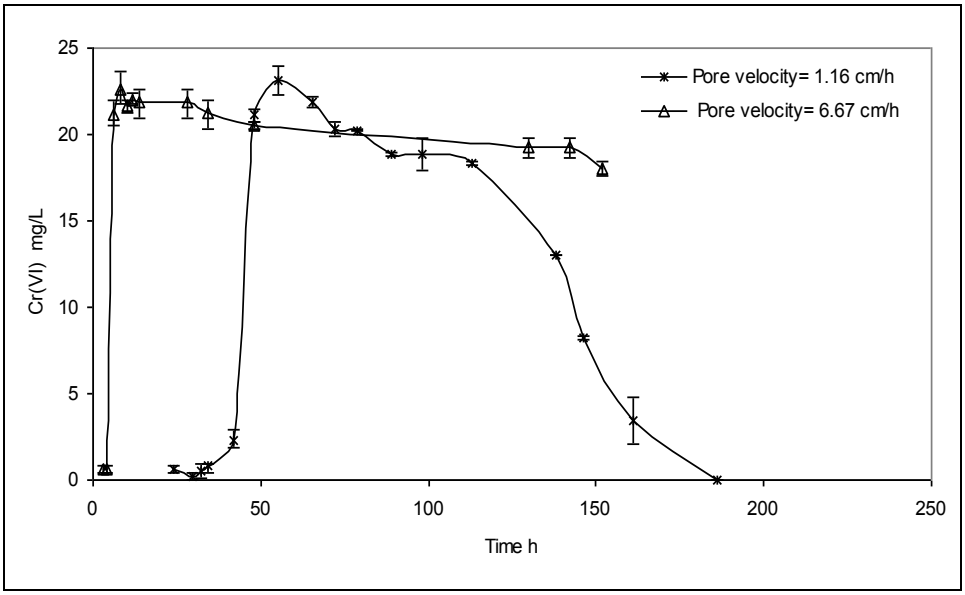

Fig. 6.20 (b): Cr (VI) break-through curve at 40 cm port in soil B; with bio-transformation (pH - 6.2 to 7.2, Inlet Cr(VI) concentration- 25 mg/L)

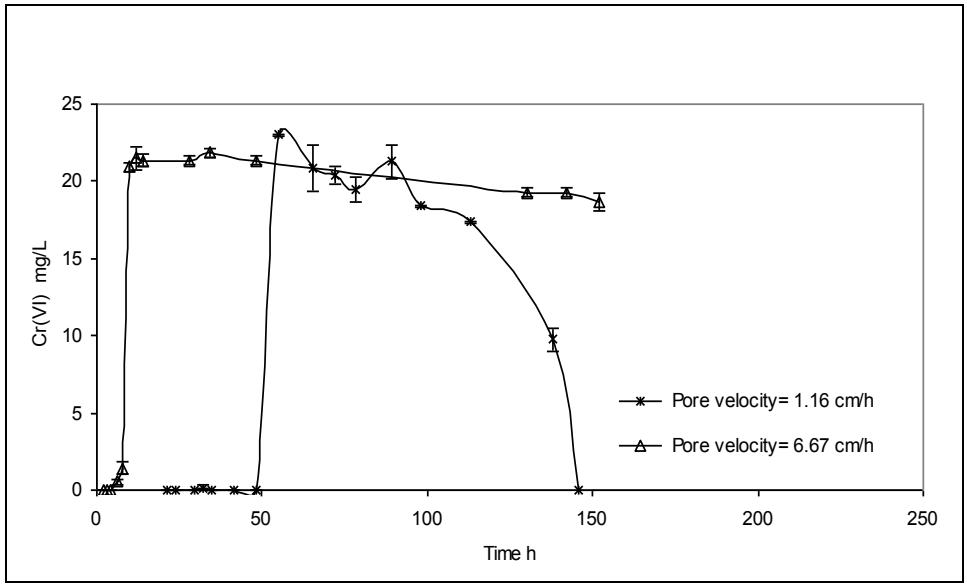

Fig. 6.20 (c): Cr (VI) break-through curve at 60 cm port in soil B; with bio-transformation (pH - 6.2 to 7.2, Inlet Cr (VI) concentration- 25 mg/L)

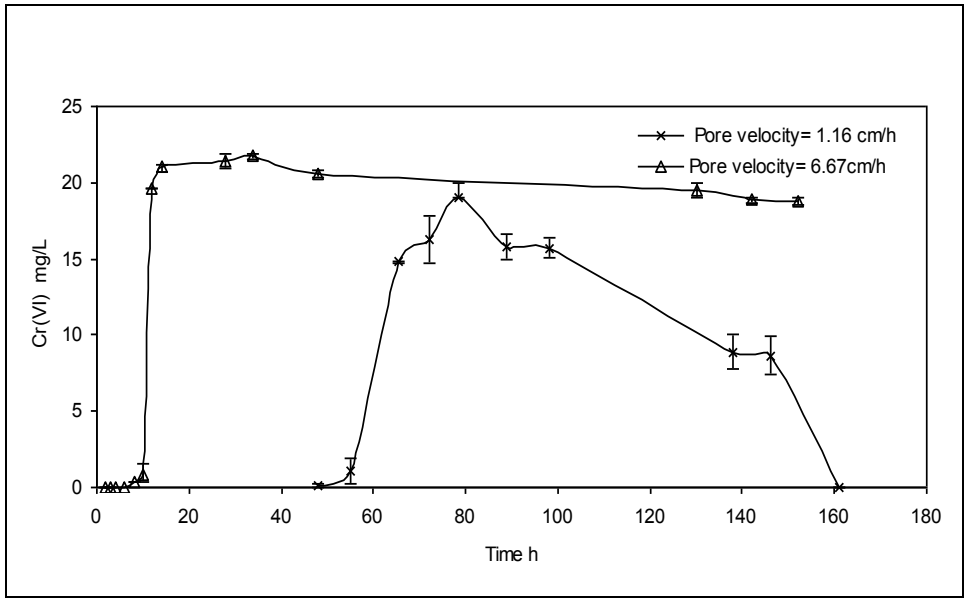

Fig. 6.20 (d): Cr (VI) break-through curve at 80 cm port in soil B; with bio-transformation (pH - 6.2 to 7.2, Inlet Cr (VI) concentration- 25 mg/L)

Mass balance was made for the system with respect to substrate and chromium. These results are summarized in Tables 6.6 and 6.7. Following equations were used for this purpose.

Mass balance equation for substrate:

Total COD entered – Total COD left + COD present in the system

= COD consumed by bacteria + COD adsorbed by soil

$$\int_0^t (\mathrm{COD_i} - \mathrm{COD_o})\mathrm{Q_{out}}dt + \int_0^t (\mathrm{COD_i} - \mathrm{COD_{av}})\mathrm{dt} * \mathrm{V_s} + COD_b * V_c = T\mathrm{COD_{bact(ana+cata)}} + \mathrm{TCOD_{soil}} - TCOD_{bact(ana)} \quad (6.3)$$

where, COD_i = inlet COD, COD_o = outlet COD, COD_{av} = average COD of the samples, V_s = volume of the samples, V_c = volume of the column, $TCOD_{bact(ana+cata)}$ = total COD consumed by bacteria for metabolism, $TCOD_{soil}$ = total COD of soil, and $TCOD_{bact(ana)}$ = total COD consumed for bacterial anabolism.

Mass balance equation for total chromium:

Total Cr (VI) entered – Total Cr left = Total Cr retained in the column

$$\int_0^t (\mathrm{Cr(VI)_i} - \mathrm{Cr_o})\mathrm{Q_{out}}dt + \int_0^t (\mathrm{Cr(VI)_i} - \mathrm{Cr_{av}})\mathrm{dt} * \mathrm{V_s} = Total\ Cr * V_c \quad (6.4)$$

where, $Cr(VI)_i$ = inlet Cr (VI) concentration, Cr_o = outlet total Cr concentration, and Cr_{av} = average total Cr concentration of the samples. It can be seen from these tables that mass balances for Cr and COD are satisfactory (±7% Error).

Table 6.6: Substrate Mass balance

Soil	$TCOD_{bact(ana)}$ (mg)	$TCOD_{bact(cat)}$ (mg)	$TCOD_{bact(ana+cata)}$ (mg)	$TCOD^*V_c$ (mg)	COD_b*V_c (mg)	$\int_0^t (COD_i - COD_o)Q_{out}dt$ (mg)	$\int_0^t (COD_i - COD_{av})dt * V_s$ (mg)	Left hand Side of Eq. (3) (mg)	Right Hand side of Eq. (3) (mg)
Soil A	5511.7	15445.36	20957.06	36650.88	26853.12	19812	2122.01	48787.13	52096.24
Soil B (Run-1)	1588.16	4450.47	6038.63	8842.08	0	13746.84	440.69	14187.53	13292.55
Soil B (Run-2)	2801.78	7851.4	10653.18	5967.75	0	13203	643	13647.53	13819.15

Table 6.7: Total Chromium Mass balance

Soil	$\int_0^t (Cr(VI)_i - Cr_o)Q_{out}dt$ (mg)	$\int_0^t (Cr(VI)_i - Cr_{av})dt * V_s$ (mg)	Left hand Side of Eq. (6.4), (mg)	Total Cr * V_c Right Hand Side of Eq. (6.4), (mg)
Soil A	605.3	34.3	639.6	621.27
Soil B (Run-1)	195.52	10.07	205.58	218.63
Soil B (Run-2)	400	8.53	408.53	438.5

6.3.5.3 Cr (VI) containment in aquifer with different soils

Figs. 6.19 (a) and 6.21 show the variation of concentration of Cr (VI) with time for the transport and biotransformation in soils A and B, respectively. Cr (VI) concentrations at 20, 40 and 60 cm ports are shown in these figures. Though initial bacterial concentrations and initial pore water velocities were approximately the same in both the experiments (bacterial conc ≈ 0.0295 mg/g and pore water velocity ≈ 6 cm/h), Cr (VI) was effectively contained in aquifer with soil A, where as there was only negligible containment in the case of aquifer with soil B. This was because there was more bacterial retention in soil A (concentration ≈ 0.0148 mg/g) compared to that in soil B (concentration ≈ 0.0053 mg/g), at the start of biotransformation process. It may be inferred from these results that it is easier to contain Cr (VI) in silty aquifers as compared to sandy aquifers.

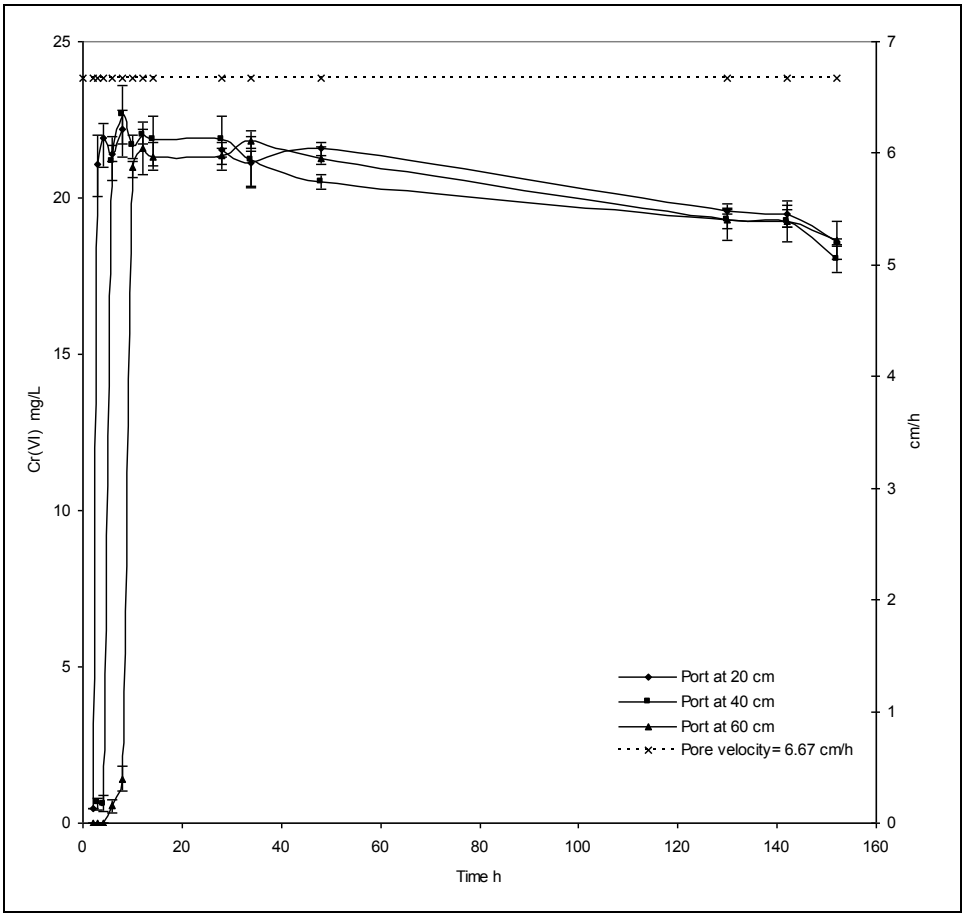

Fig. 6.21: Cr (VI) breakthrough curve in soil B for pore velocity=6.67 cm/h; with biotransformation (pH - 6.2 to 7.2, Inlet Cr(VI) concentration- 25 mg/L)

6.3.6 Strategies for Cr (VI) containment in contaminated aquifers

Results from the present study shed light on the strategies to be adopted for containing Cr (VI) in aquifers. It can be inferred that it is a better choice to utilize pump and treat technology in case of sandy aquifers with high hydraulic gradients in ground water levels. Pore velocities in such cases would be very high and it would be hard to retain the biomass on the soil matrix. Subsequently, the advective effect would be more

predominant than the bio-transformation effect, potentially leading to ineffective containment in case of in-situ strategies.

The in-situ biotransformation strategy can be adopted for silty aquifers. Initial biomass concentration is a significant parameter in this case. It can be inferred from this study that it is a better choice to utilize bio-augmentation to have effective faster containment. This bio-augmentation can be implemented using a bio-barrier of a short width transecting the flow path. Based on the results of this study, width of the bio-barrier could be as small as 1 m if the Cr (VI) concentration is in the range of 1 to 25 mg/L.

6.4. PILOT SCALE STUDIES FOR THE BIOREMEDIATION OF Cr(VI) CONTAMINATED AQUIFERS USING BIOBARRIER AND REACTIVE ZONE METHODS

6.4.1 Pilot scale studies for aquifer remediation using bio-barrier technology

Samples from the wells located on the upstream and downstream sides of the reactor with biobarrier (R_1) and wells in the control reactor (R_2) were collected at regular intervals and analyzed for Cr (VI), total Cr and COD. Temporal variations of Cr (VI) concentrations in wells 1, 2, 3 and 4 (at a distance of 50 cm from the inlet on the upstream side of the barrier) are shown in Figs. 6.22 (a) and 6.22 (b), for R_1 and R_2, respectively. Temporal variations of Cr (VI) concentrations in wells 5, 6, 7, 8, 9 and 10 (at a distance of 80 cm from the inlet on the upstream side of the barrier) for R_1 and R_2 are presented in Figs. 6.23 (a) and 6.23 (b), respectively. Cr (VI) concentrations in wells 11–16 (110 cm from the inlet on the downstream side of the barrier) and in wells 17-20 (150 cm from the inlet on the downstream side of the barrier) in R_1 and R_2 are shown in Figs. 6.24 and 6.25, respectively. It can be observed from Figs. 6.24 (a) and 6.25 (a) that even after 180 days, Cr (VI) concentration was zero in wells located downstream of the biobarrier. On the other hand, the Cr (VI) plume reached wells 17-20 in the control reactor after 50 days Fig. 6.25 (b) and the Cr (VI) concentration reached the maximum value of 43 mg/L after 125 days.

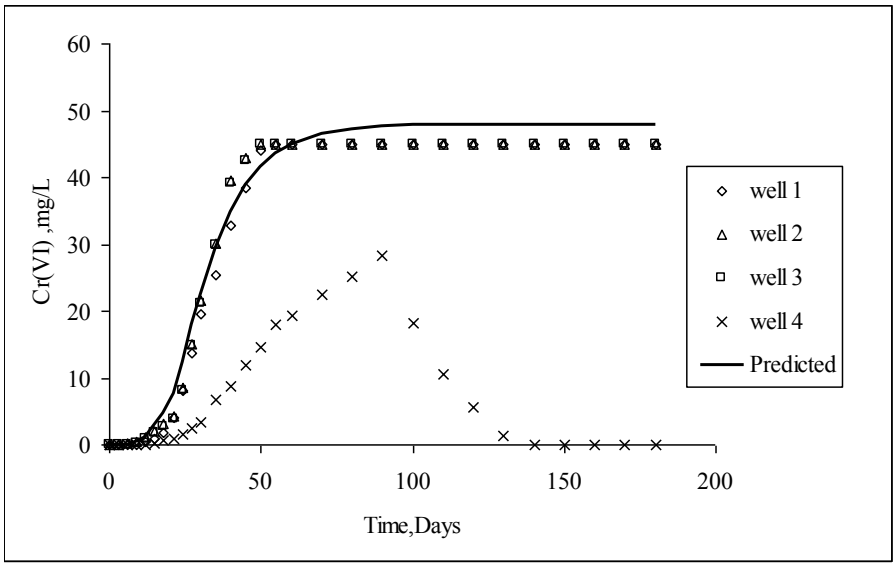

Fig. 6.22a.Experimental results showing temporal variation of Cr(VI) concentration in wells 1,2,3, and 4 (at a distance of 50 cm from inlet) in reactor R1

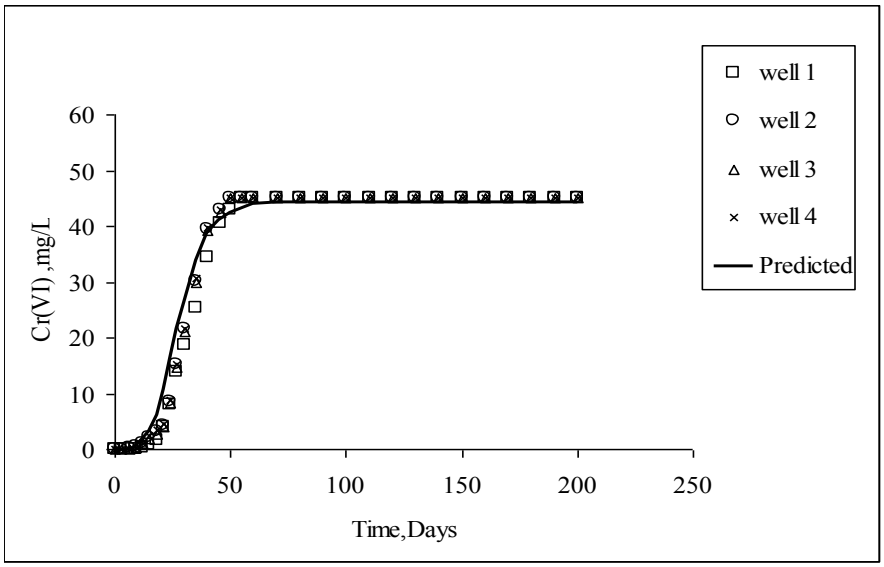

Fig. 6.22b Experimental results showing temporal variation of Cr(VI) concentration in wells 1, 2, 3, and 4 (at a distance of 50 cm from inlet) in reactor R2

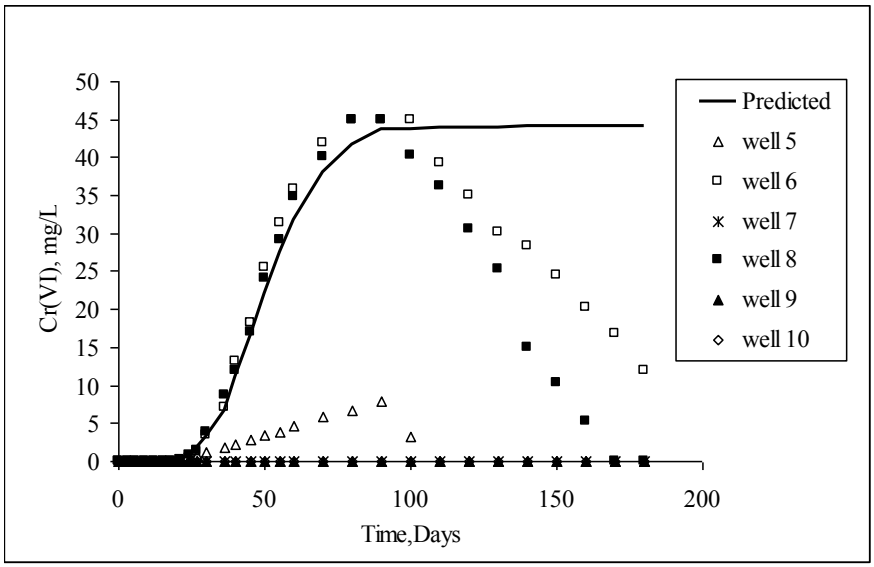

Fig. 6.23a Experimental results for temporal variation of Cr(VI) concentration in wells 5, 6, 7, 8, 9, and 10 (at a distance of 80 cm from inlet) in reactor R1

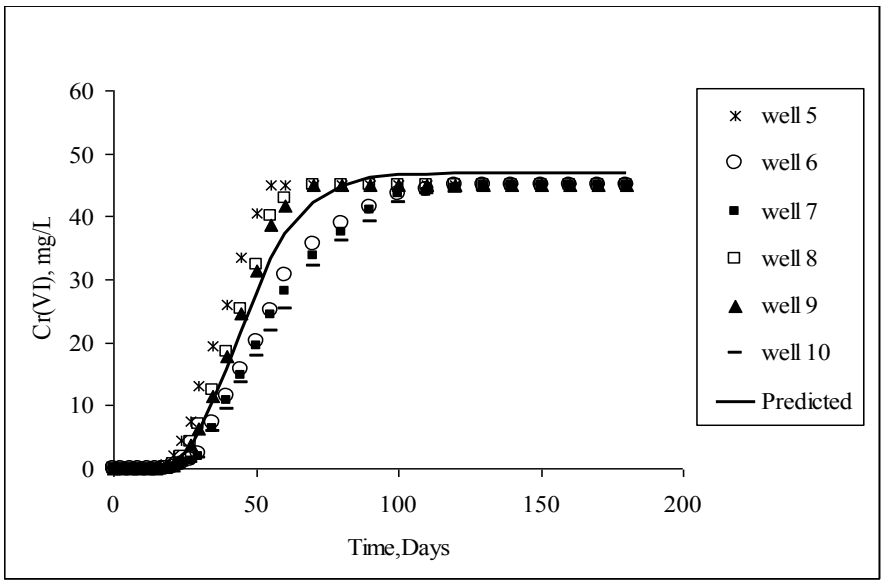

Fig. 6.23b Experimental results showing temporal variation of Cr(VI) concentration in wells 5,6,7,8,9, and10 (at a distance of 80 cm from inlet) in reactor R2

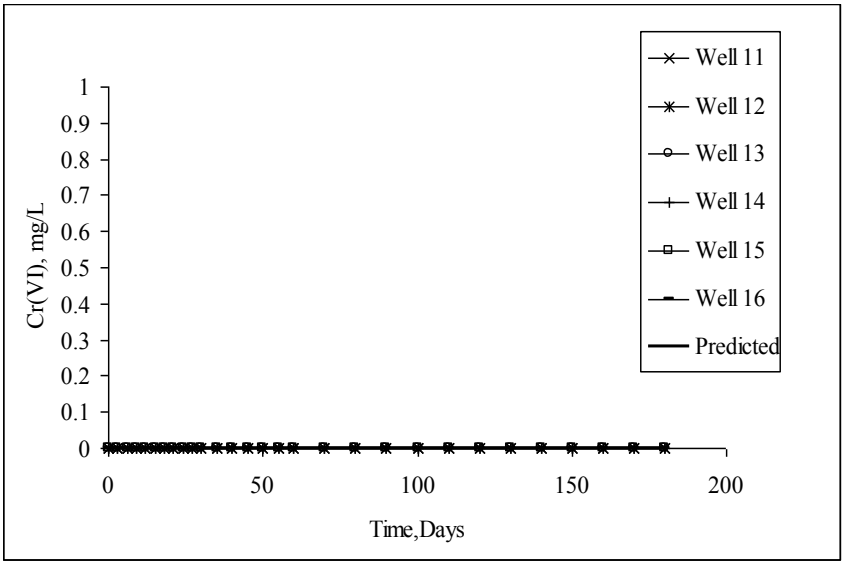

Fig. 6.24a Experimental results for temporal variation of Cr(VI) concentration in wells 11-16 (at a distance of 110 cm from inlet) in reactor R1

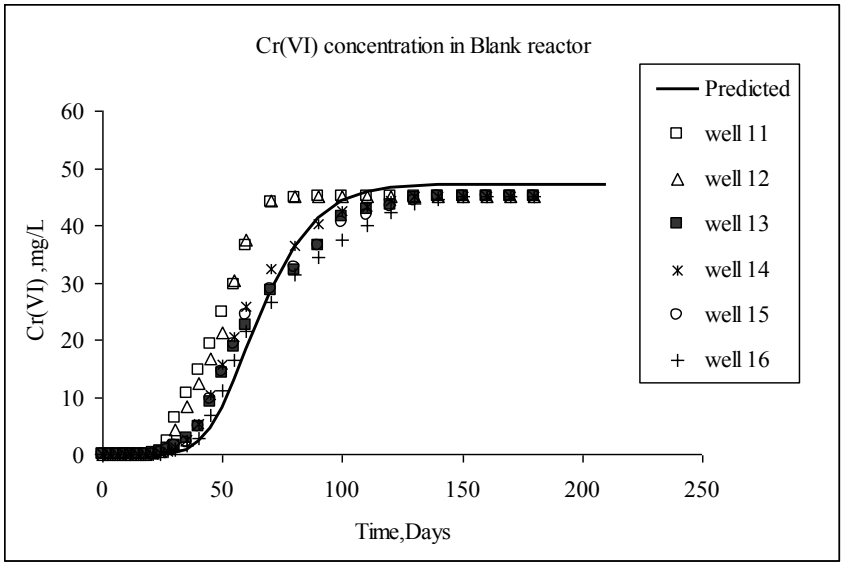

Fig. 6.24b Experimental results showing temporal variation of Cr(VI) concentration in wells 11-16 (at a distance of 110 cm from inlet) in reactor R2

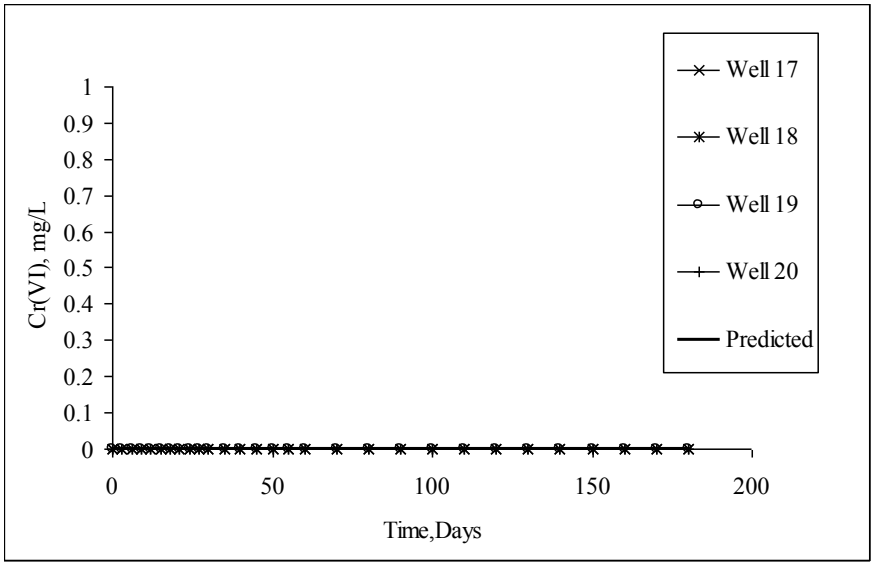

Fig. 6.25a Experimental and results for temporal variation of Cr(VI) concentration in wells 17-20 (at a distance of 150 cm from inlet) in reactor R1

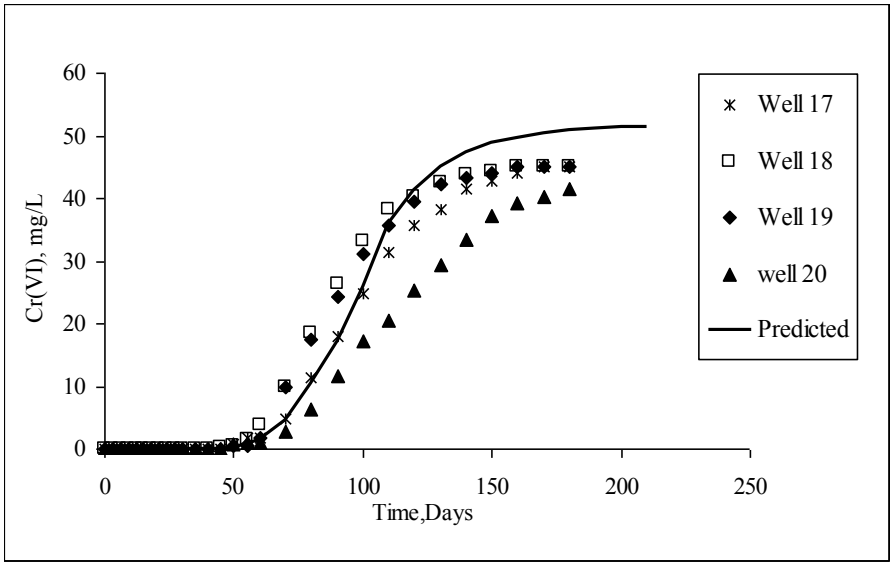

Fig. 6.25b Experimental results for temporal variation of Cr(VI) concentration in wells 17-20 (at a distance of 150 cm from inlet) in reactor R2

It can be observed from Fig. 6.23 (a) that chromium concentrations in wells 5, 7, 9 and 10 were almost zero at all times, while Cr (VI) concentrations in wells 6 and 8 increased initially to a high value of 45 mg/L, but reduced subsequently. Although these wells are located on the upstream side of the biobarrier, bioremediation had occurred in this stretch (only 10 cm upstream of biobarrier). This bioremediation could be due to upstream dispersion of bacteria and molasses from the biobarrier. It may be noted that the flow velocities were very low (pore velocity = 0.06 cm/h) in the experiment and there could have been some upstream movement of bacteria and dispersion of molasses. Same effect was observed also at well 4, which was located close to the wall. Growth of bacteria on the upstream side of the biobarrier was also evident from visual observation. These results show that the biobarrier technology is successful in remediating the Cr (VI) contaminated aquifer.

6.4.2 Pilot scale studies for aquifer remediation using reactive zone technology

6.4.2.1 Two injection wells

Samples from various monitoring wells in the reactors were collected at regular intervals and analyzed for Cr(VI), total chromium and COD. Temporal variations of Cr(VI) concentrations in wells 1 and 2 in the reactor R3 (located at a distance of 40 cm from the inlet on the upstream side of injection wells) are shown in Fig. 6.26a, while the same for wells 3–5 (located in line with the injection wells) is shown in Fig. 6.26b. Cr(VI) concentrations in wells located on the downstream side (in wells 6-20) are shown in Fig. 6.26c. It can be observed from these figures that for an inlet Cr(VI) concentration of 60 mg/L, the Cr(VI) plume did not pass the line of injection wells. This clearly indicates that the reactive zone created around the injection wells was effective in containing the Cr(VI) plume. However, when the inlet concentration of Cr(VI) was increased to 250 mg/L on the 75^{th} day, the plume passed beyond the line of injection wells, and the concentrations in the observation wells 3-20 (Figs. 6.26b and 6.26c) increased with time.

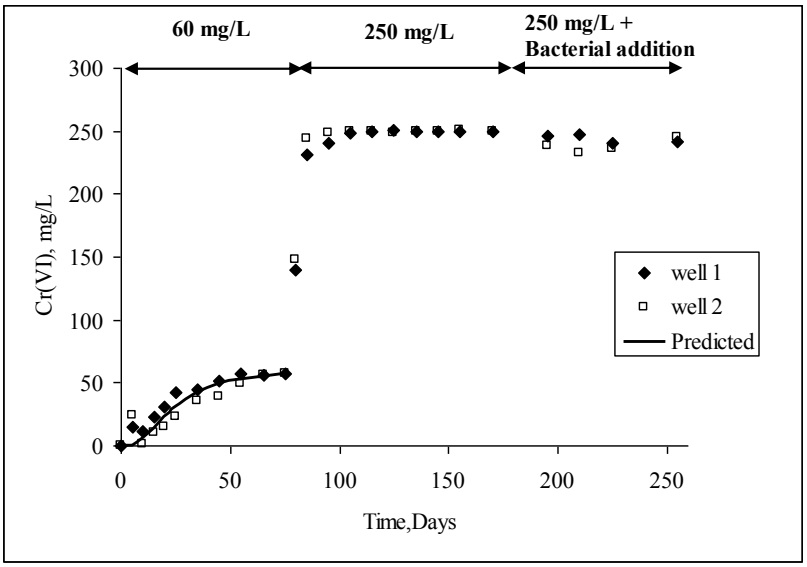

Fig. 6.26a Experimental results for temporal variation of Cr(VI) concentration in wells 1 and 2 (at a distance of 40 cm from inlet) in reactor R3

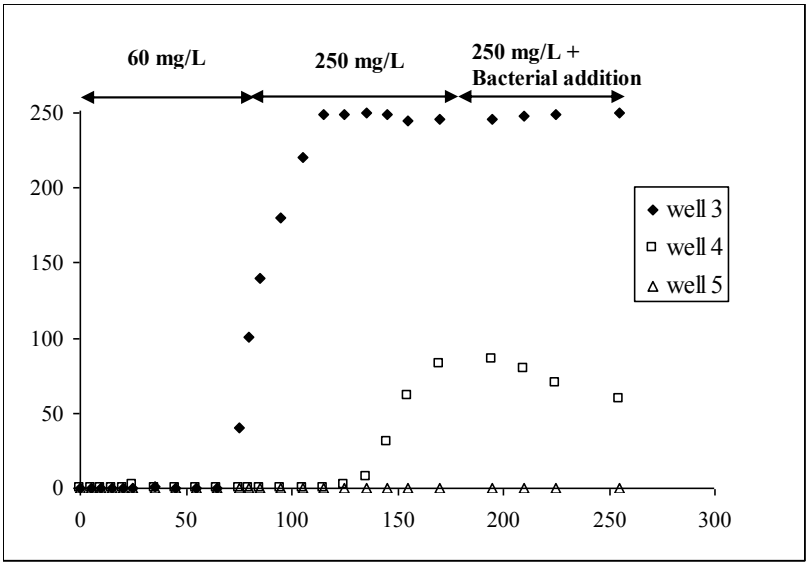

Fig. 6.26b Experimental results for temporal variation of Cr(VI) concentration in wells 3, 4 and 5 (at a distance of 50 cm from inlet) in reactor R3

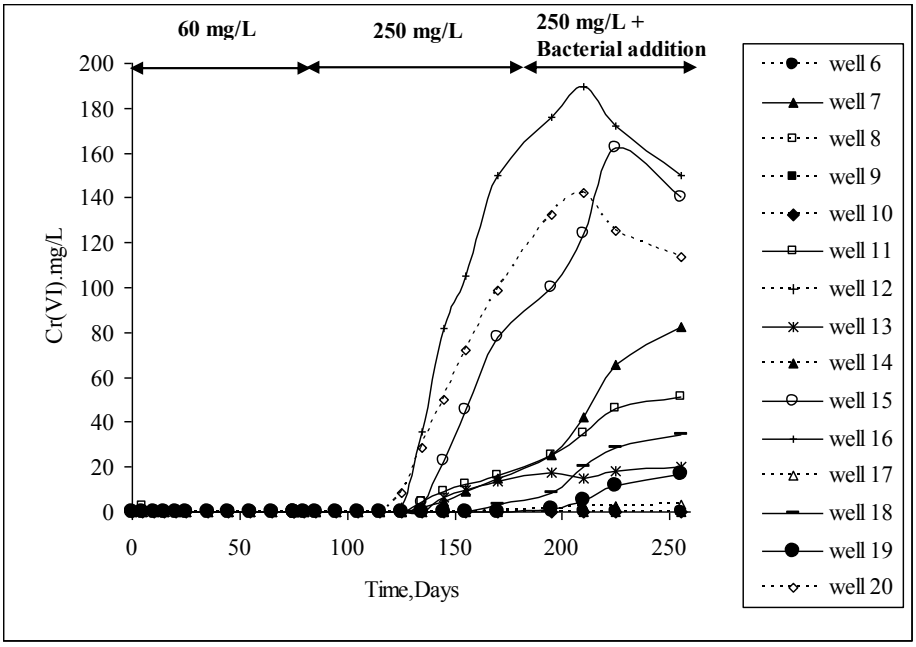

Fig. 6.26c Experimental results showing temporal variation of Cr(VI) concentration in all wells from 6-20 in reactor R3

This could be due to the inhibitory effect of high concentrations of Cr(VI). In order to contain the plume even for high concentrations of Cr(VI), more chromium reducing bacteria (concentration = 50 g wet weight in each well) were introduced into the reactor through injection wells on 175th day. It is evident from Figs. 6.26b and 6.26c that the above strategy did not work well in containing the plume, although Cr(VI) concentrations in most of the wells showed a decreasing trend after the addition of extra biomass.

6.4.2.2 Four injection wells

Temporal variation of Cr(VI) concentrations in well 1 in the reactor R4 (located at a distance of 15 cm from the inlet on the upstream side of injection wells) is shown in Fig. 6.27a, while the same for wells 2 – 3 (located at a distance of 40 cm from the inlet on the upstream side of injection wells) is shown in Fig. 6.27b. Cr(VI) concentrations in wells located on the downstream side (in wells 4-27) are shown in Fig. 6.27c to .

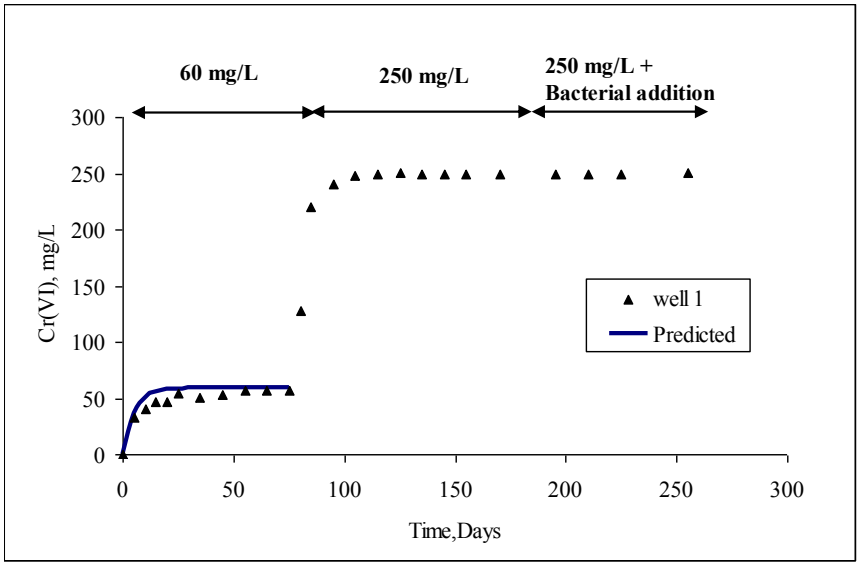

Fig. 6.27a Experimental results for temporal variation of Cr(VI) concentration in well 1 (at a distance of 15 cm from inlet) in reactor R4

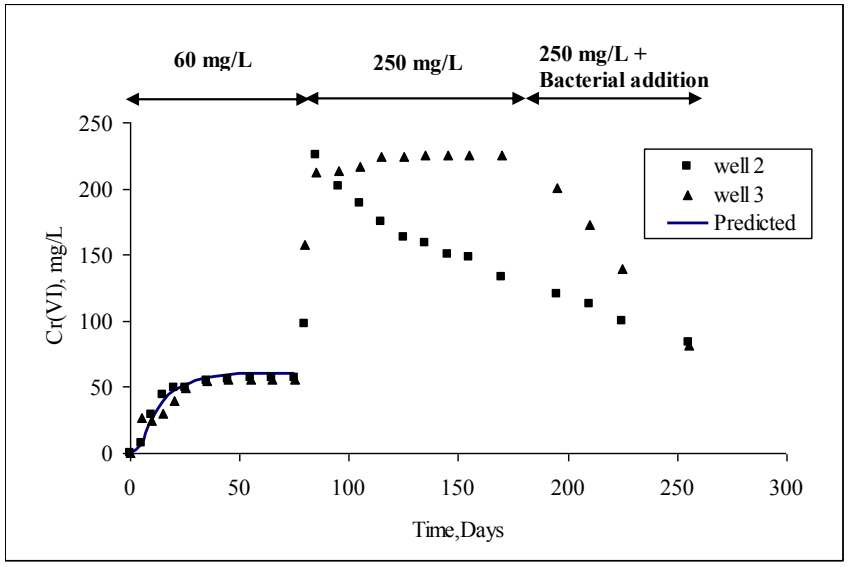

Fig. 6.27b Experimental results for temporal variation of Cr(VI) concentration in wells 2 and 3 (at a distance of 40 cm from inlet) in reactor R4

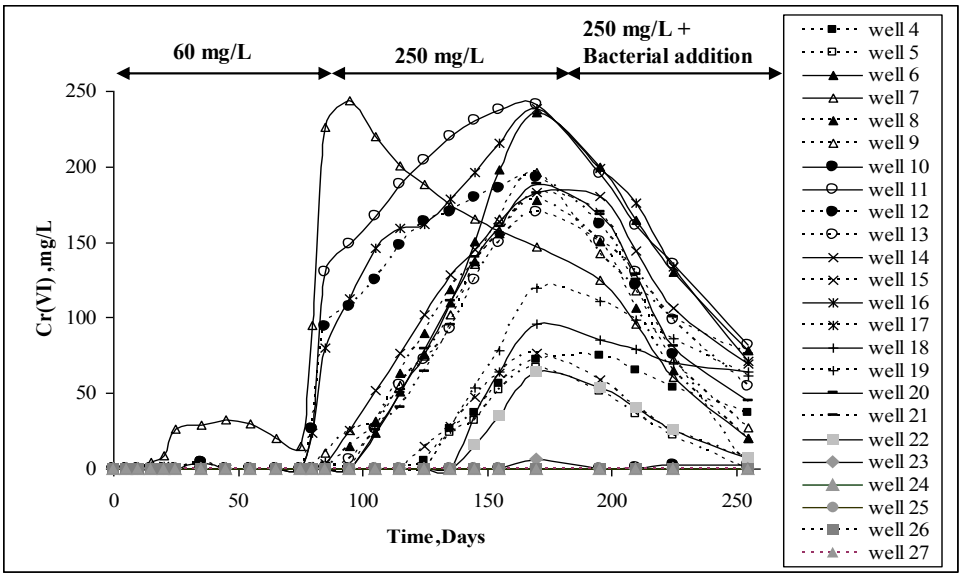

Fig. 6.27c Experimental results for temporal variation of Cr(VI) concentration at all wells from 4-27 in reactor R4

As for the case of reactor with two injection wells, the Cr(VI) plume did not pass the line of injection wells (Fig. 6.27c) for an inlet Cr(VI) concentration of 60 mg/L, indicating that the reactive zone created around the injection wells was effective in containing the Cr(VI) plume. However, when the inlet concentration of Cr(VI) was increased to 250 mg/L on the 75th day, the plume passed beyond the line of injection wells, and the concentrations in the observation wells 4-27 (Fig. 6.27c) showed an increasing trend. As explained earlier, this could be due to the inhibitory effect of high concentrations of Cr(VI). As for the case of R3, more chromium reducing bacteria (concentration = 50 g wet weight in each well) were introduced into the reactor through injection wells on 175 day in order to contain the plume even for high concentrations of Cr(VI). It is evident from Fig. 6.27c that the above strategy worked well in containing the plume. Cr(VI) concentrations in most of the wells decreased significantly after the addition of extra biomass. This decrease in Cr(VI) concentration in R4 was much more than that in reactor R3, indicating that at least 4 injection wells are needed to effectively create a reaction barrier to contain plumes with high Cr(VI) concentration, in the system studied.

6.5 FIELD SCALE STUDY

Based on the results obtained as part of the present study sponsored by the MoWR, a new project has been sponsored by the Central Pollution Control Board. This new project involves field demonstration for bioremediation of chromium contaminated soils and aquifer in Ranipet area. A brief outline of this project and sample results obtained so far are presented here for the sake of completeness. Details of the study can be obtained either from the authors or from CPCB (the sponsoring agency) on request.

In the chromium contaminated site at Ranipet in Tamilnadu, at the premises of Tamilnadu Chromates and Chemicals Limited (TCCL), the solid waste of about 2.2 lakh tons, generated over a period of 20 years from the manufacture of sodium bichromate and basic chromium sulphate, was dumped within the factory premises in an area of 2 hectares. Due to high porosity of the soil around the plant area, leachate containing Cr(VI) contaminated the soil and water environment in the nearby areas. Water samples collected within 2 km downstream of the plant have shown Cr(VI) concentration in the range of 50 to 200 mg/L. The factory is not in operation for the past 14 years and no action has been taken by the management to control leachate. As the surrounding area is polluted with hexavalent chromium, there is an urgent need for the remediation of this contaminated site.

There has been an initiative from Central Pollution Control Board (CPCB), in collaboration with Tamilnadu Pollution Control Board (TNPCB) and IIT Madras to develop and implement a remediation strategy for the area of Ranipet in Vellore District of Tamil Nadu. A three-year plan for this site envisages detailed investigations leading to a systematic study of the affected site, contaminant transport, evaluation of strategies for site remediation, groundwater restoration, and direct remediation activities. For the first phase of this project, the CPCB requested IIT Madras to undertake a field level demonstration project for bioremediation of Cr(VI) contaminated soil and aquifer in Ranipet.

Objective of this study is demonstration of the bioremediation technology for the treatment of sludge and Cr(VI) contaminated aquifer at Ranipet, Tamilnadu. The scope of the study includes the following:

1. Remediation of at least 5 tons of chromium sludge in the vicinity of Tamilnadu Chromates and Chemicals Limited (TCCL) at the site;

2. Demonstration of in-situ bioremediation of Cr(VI) contaminated aquifer in a 5 m ×5 m area of aquifer in the vicinity of Tamilnadu Chromates and Chemicals Limited (TCCL), Ranipet, by injection well - reactive zone technology;

Methodology adopted for *insitu* bioremediation of aquifer is presented below. Four injection wells and an array of monitoring wells (Total 9) were installed in the designated 5 m × 5 m area in the TCCL compound (Fig. 6.28). One pumping well was also installed at a distance of 10 m from the line of injection wells. The monitoring and pumping wells extended the entire depth of aquifer (approximately 20 m below ground level) at the corresponding location. Sufficient quantity of enriched microbes, along with appropriate amount of molasses and nutrients, were injected into the aquifer through the injection well No. 5. After 15 days bacteria were injected through well no 6 and well no.3. Details of injection are given in Table 6.8. The microbes which were injected have been enriched and isolated from the very same site at Ranipet. The fate and transport of chromium (both Cr(VI) and Cr(III)), molasses were monitored. Results for aquifer remediation are discussed briefly here.

Enriched microbes (2.5 kg) and molasses (25 kg) were injected into the aquifer through well No. 5 on 10th December 2009. The injection was carried out using a 2 HP pump. Water samples were collected from all the fourteen wells and analyzed for Cr(VI), Total Chromium and COD concentrations before and after the injection with respect to time . These results are presented in Figs 6.29-6.31. It is clear from the results that Cr(VI) concentration in all the wells before injection were in the range of 92-155 mg/L. It is clear from these results that Cr(VI) reduction occurred in most of the wells surrounding the injection wells. The remediation was more significant in wells 7, 8, 9, 10 and 12,

which are on the downstream side of the injection well. Cr(VI) concentrations in wells 5, 7, 8, 9 and 12 reduced to less than 2 mg/L within 17 days. It may be noted that well Nos.12 is situated 5 m downstream of the injection well 5. Well No. 7 is situated at 1 m away from well No. 5 whereas well Nos. 8 and 9 are situated 3 m away from the injection well. During the remediation, we have not carried out any pumping in order to increase the flow rate. Cr(VI) concentration even in well no14 which is situated at 10 m away from the injection well is reduced below detection limit.

Table 6.8 Details of aquifer remediation process

S.NO	Date	Time, d	Injection at well no	Bacteria injected (in L) Conc 50g/L	Molasses (kg)	Samples taken
	7.12.2009					14 samples
	9.12.2009					14 samples
	10.12.2009		5	40	10	14 samples
	11.12.2009					14 samples
	12.12.2009					
	14.12.2009					14 samples
	23.12.2009					14 samples
	25.12.2009		5	40	10	14 samples
	27.12.2009					14 samples
	3.01.2010		6	40	7.5	14 samples
	10.01.2010		6	40	7.5	14 samples
	13.01.2010					14 samples
	18.01.2010					14 samples
	23.01.2010					14 samples
	24.1.2010		3	35	5	
	28.01.2010					14 samples
	02.01.2010		3	40	10	
	02.01.2010		5		7.5	
	02.01.2010		6		7.5	
	03.02.2010					14 samples
	09.02.2010					14 samples

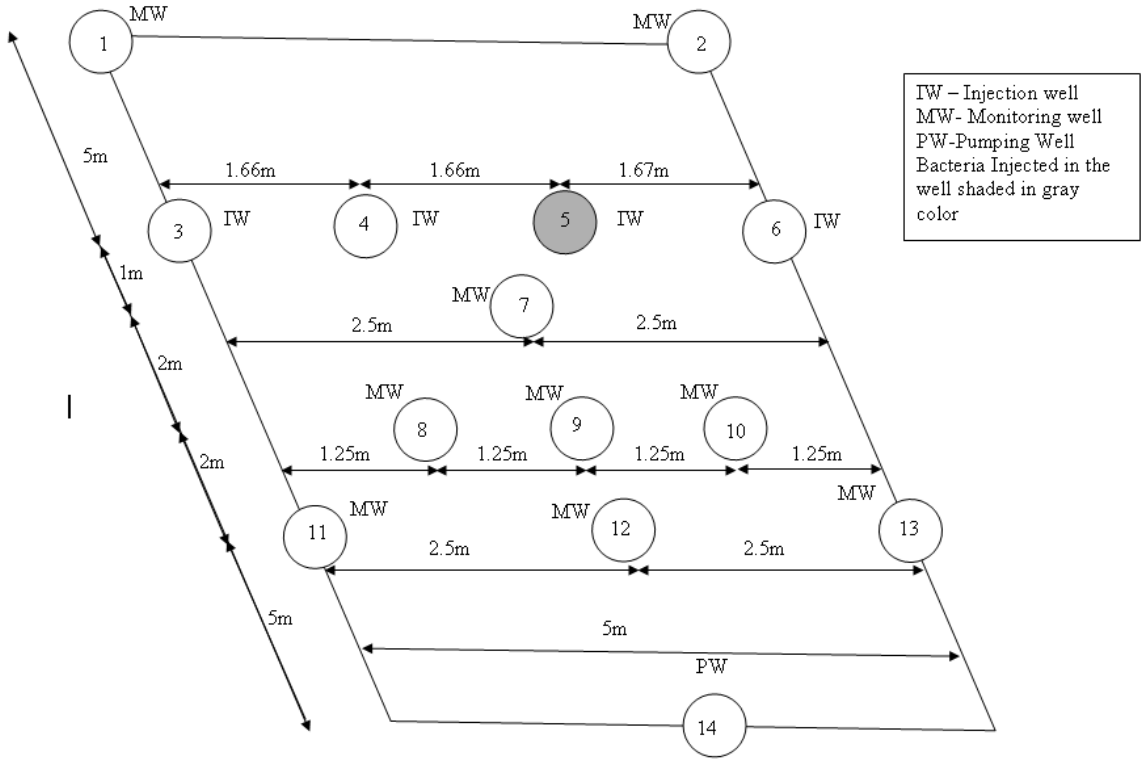

Fig. 6.28 Well Locations

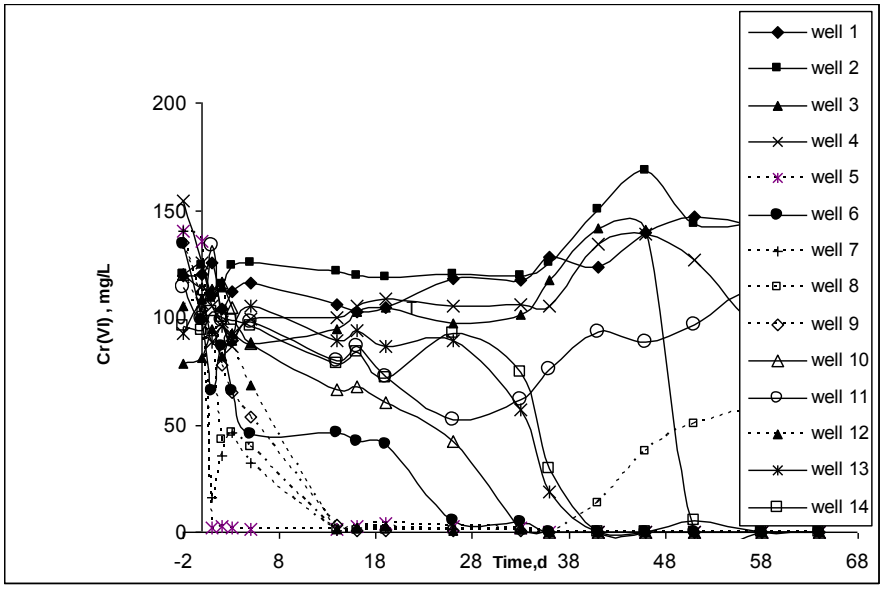

Fig. 6.29 Variation of Cr(VI) concentration with respect to time in aquifer

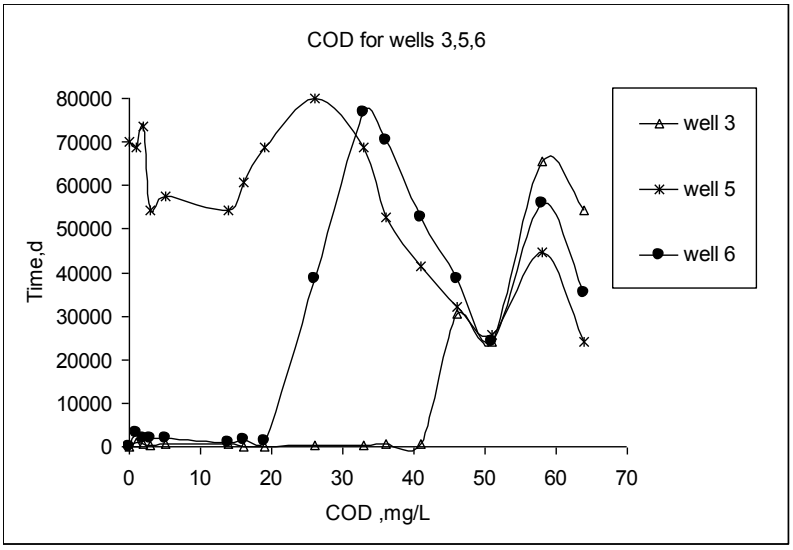

Fig. 6.30 Variation of COD with respect to time in aquifer

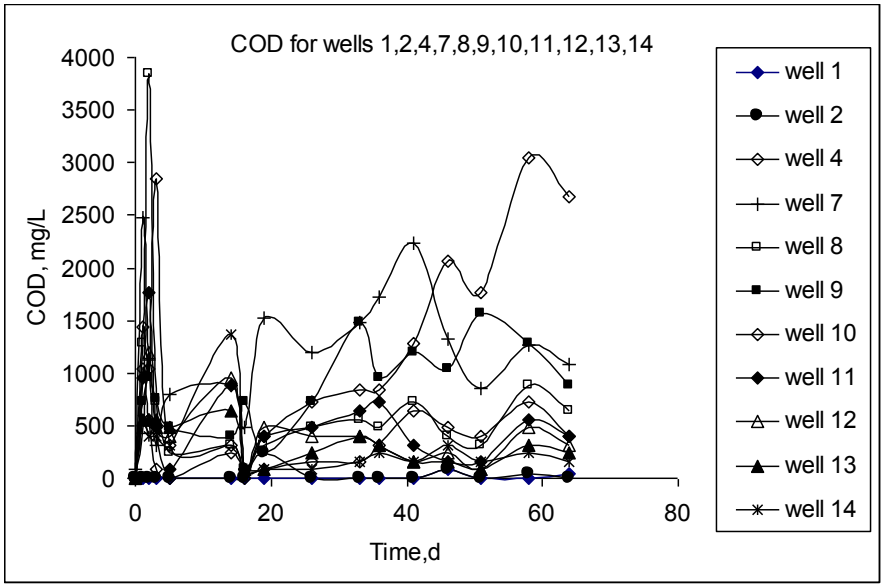

Fig. 6.31 Variation of COD with respect to time in aquifer

6.6 CLOSURE

In this chapter, the experimental results obtained from batch, bench scale and pilot scale studies have been presented and discussed. First set of batch studies focused on the ability of a mixed population of microbial culture isolated from hexavalent chromium contaminated site to biotransform Cr (VI). Batch and continuous experiments were carried out to study the biotransformation pattern of Cr(VI) with molasses as the electron donor. Among the bacterial strains isolated from seven different locations of the contaminated site, the bacterial strain (H1) which was isolated from a clay mat near the effluent treatment plant (ETP) showed high Cr(VI) reduction potential. Effects of initial Cr(VI) concentration and pH on Cr(VI) reduction were studied. Cr(VI) reduction under both aerobic and anaerobic conditions was studied.

In the second set of batch studies, different bacterial cultures, CRB, SRB and IRB, were enriched and isolated from contaminated soils. These cultures were used for Cr(VI) reduction studies, individually and in combination. Studies were conducted with

different initial Cr(VI), SO_4^{2-} and Fe(III) concentrations. Biokinetic parameters such as μ_{max}, K_s, Y_T and K_i for individual cultures were evaluated. Biokinetic parameters evaluated from one set of experiments for individual cultures were utilized in developing the mathematical model for Cr(VI) reduction by a combination of microbes. Experimental data from the other batch experiments was used for validating the model.

Batch adsorption and bench scale column transport studies indicated that it may not be possible to contain Cr(VI) in aquifers using only adsorption. Bench scale transport and biotransformation studies showed that biotransformation is an effective way of chromium containment in contaminated aquifers. Most significant parameters in the containment of Cr(VI) through biotransformation are pore water velocity and the initial bio-mass concentration. Containment is more effective in aquifers with silty soils. Bio-barriers of relatively small thickness with bio-augmentation can effectively contain the Cr(VI) in saturated confined aquifers.

Pilot scale studies with biobarriers revealed that even after 180 days, Cr(VI) concentration was zero in wells located downstream of the biobarrier and at the outlet, whereas in the blank reactor Cr(VI) concentration in the outlet reached the maximum of 43 mg/L. Experiments also revealed that even after 75 days, Cr(VI) concentration was zero in almost all wells located downstream of the injection wells and at the outlet in both the reactors for 2 and 4 injection wells , for an inlet Cr(VI) concentration of 60 mg/L. However, Cr(VI) reduction potential decreased when the Cr(VI) concentration was increased to 250 mg/L after 75^{th} day because of the inhibitory effect of high concentrations of Cr(VI). Addition of extra microbes through injection wells showed Cr(VI) reduction again, even though the Cr(VI) concentration was very high. 4 injection well system showed better performance than the two injection well system. The experimental results clearly show that both the bio barrier and reaction zone technologies can be successfully employed for remediating the Cr(VI) contaminated aquifer.

Data from batch, bench scale and pilot scale studies was utilized in developing, calibrating and validating mathematical models.

Chapter 7

RESULTS AND DISCUSSION – MODELING STUDIES

Experimental data obtained from batch, bench-scale and pilot scale column studies were presented and discussed in the previous chapter. These experimental data were used to calibrate and validate the proposed mathematical models. Results from these modeling studies are presented and discussed in this chapter.

7.1 MODEL FOR BIOTRANSFORMATION

7.1.1 Calibration and validation for chromium reduction by single consortium

The proposed mathematical model for chromium reduction under different conditions using a single consortium (CRB/IRB/SRB) is calibrated and validated using the experimental data. The governing equations were solved using an explicit Euler method. A grid convergence test was first performed and was found that a computational time step of $\Delta t = 10$ minutes was adequate to obtain convergent results. Results from this study are presented in this section. Experimental data for chromium reduction by CRB under aerobic conditions with an initial chromium concentration of 20 mg/L was used for calibration and obtaining the bio-kinetic parameters. Figs. 7.1(a), (b) and (c) show the matching between the experimental results and the model fitted results from this calibration study for chromium reduction by CRB. The biokinetic parameters are summarized in Table 7.1. The same biokinetic constants obtained from calibration are used to predict the chromium reduction, COD consumption and microbial growth for different initial chromium concentrations. Figs. 7.2(a), (b) and (c) show the model predicted chromium reduction by CRB, COD consumption and microbial growth, respectively, for different initial Cr(VI) concentrations (10, 30, 50, 100 mg/L). It can be observed from these figures that the proposed model predicts the chromium reduction by CRB very well.

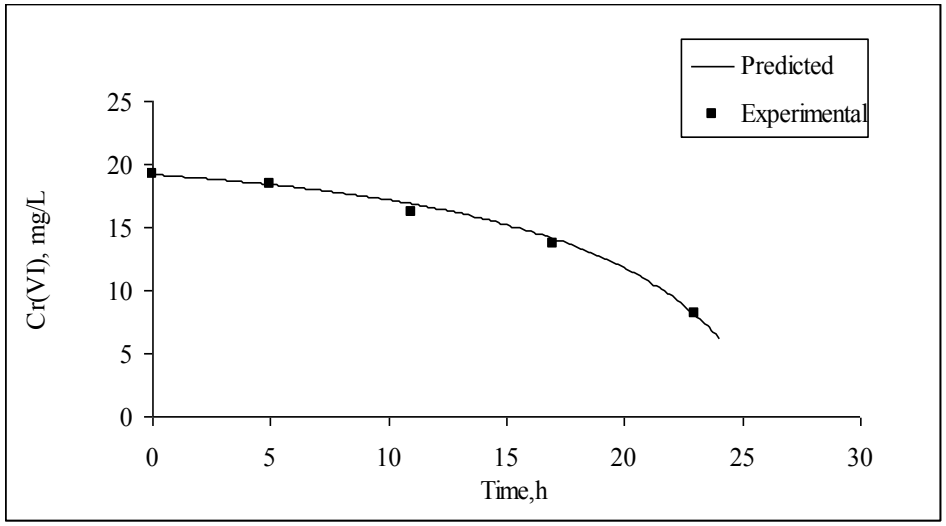

Fig. 7.1 (a): Experimental and model fitted Cr (VI) reduction by CRB under aerobic conditions

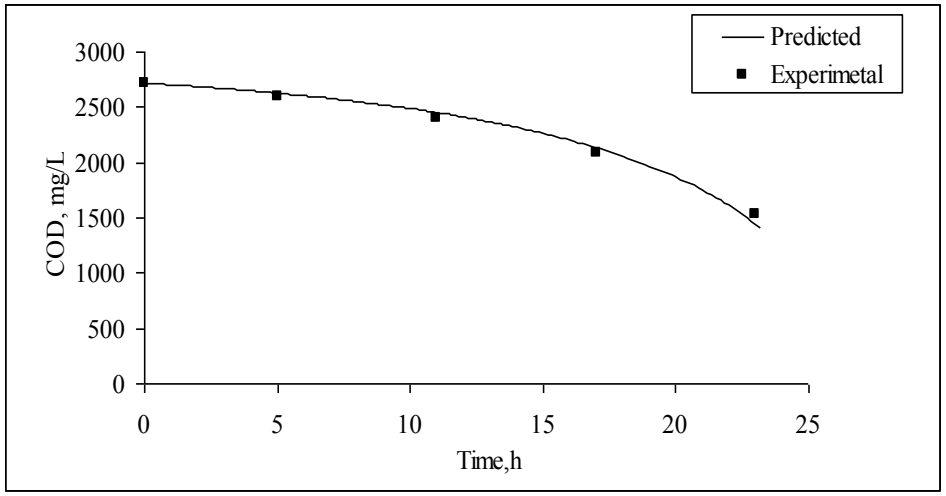

Fig. 7.1 (b): Experimental and model fitted COD consumption by CRB under aerobic conditions

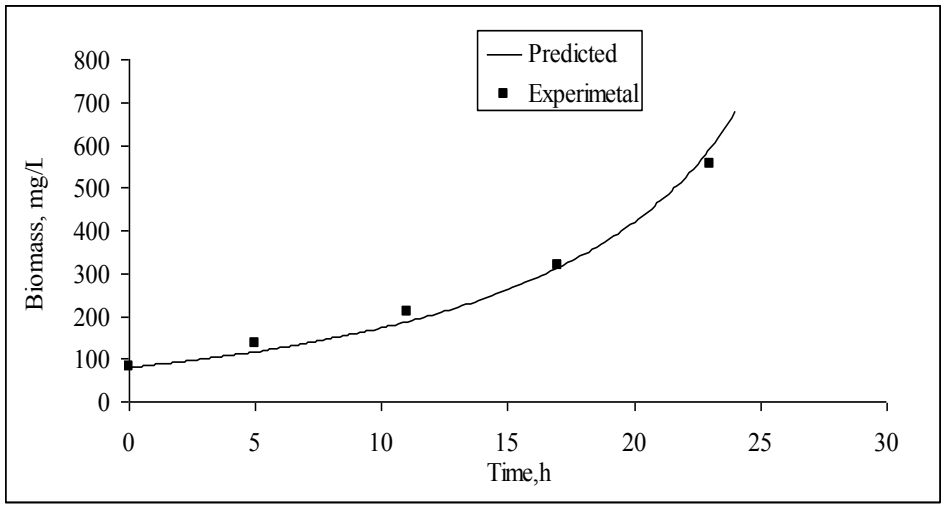

Fig. 7.1 (c): Experimental and model fitted growth of CRB under aerobic conditions

Table 7.1: Biokinetic parameters for CRB, SRB and IRB from Batch Experiments

Parameter	CRB Aerobic	CRB Anaerobic	SRB Anaerobic	IRB Anaerobic
μ_{max} (1/h)	0.35	0.09	0.11	0.09
μ_{max} (1/d)	8.42	2.13	2.53	2.08
Ks	120	80	180	220
Ki	5.49	7.68	7.12	7.42
η	0.009	0.020	0.028	0.036
Y_T	0.40	0.22	0.24	0.27

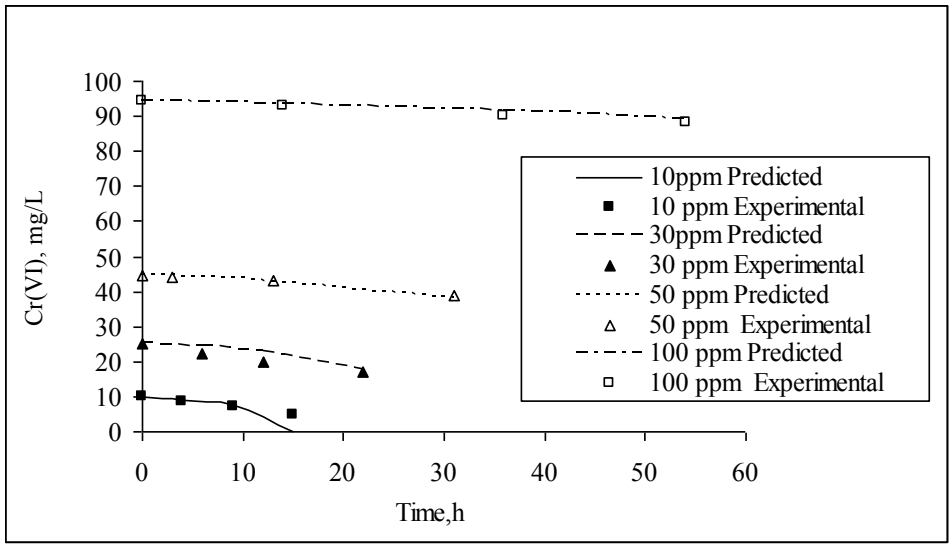

Fig. 7.2 (a): Experimental and model predicted Cr (VI) reduction by CRB under aerobic conditions for different initial Cr (VI) concentrations

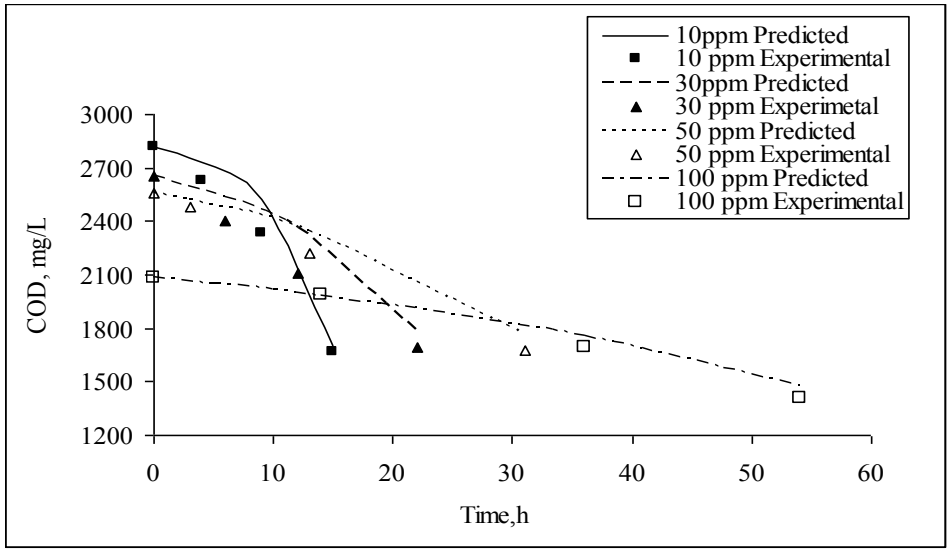

Fig. 7.2 (b): Experimental and model predicted COD consumption by CRB under aerobic conditions for different initial Cr (VI) concentrations

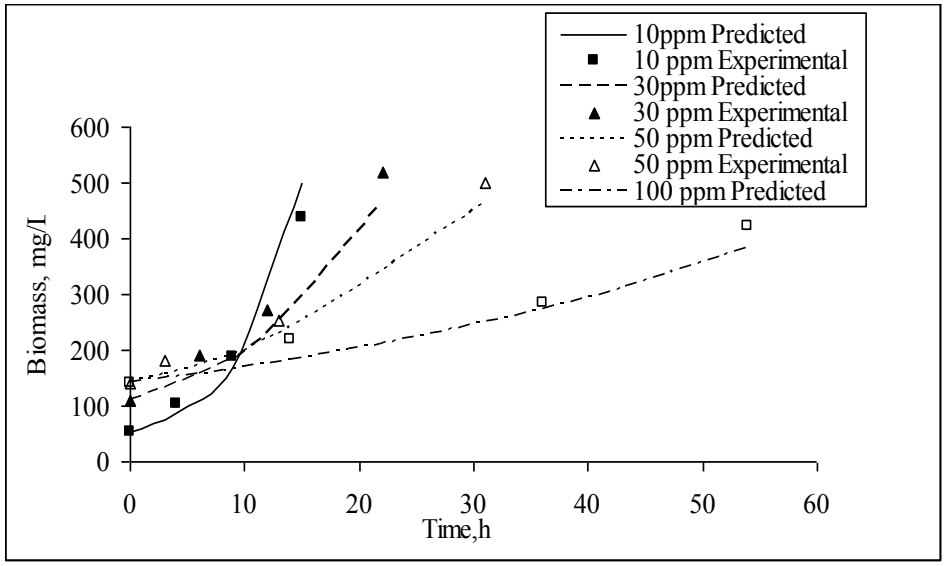

Fig. 7.2 (c): Experimental and model predicted growth of CRB under aerobic conditions for different initial Cr (VI) concentrations

In this study, the model performance was statistically evaluated using the dimensionless modified coefficient of efficiency, E.

$$E = 1 - \frac{\sum_{i=1}^{N}\left[\left|E(t_i) - O(t_i)\right|\right]}{\sum_{i=1}^{N}\left|O(t_i) - \overline{O}\right|} \qquad (7.1)$$

where $E(t_i)$ is the numerically simulated value of a variable at time t_i, $O(t_i)$ is the observed value of the same variable at time t_i, and $\overline{O}$ is the mean value of the observed variable. E varies between -∞ to 1.0, the higher values indicating better model prediction. As suggested by Kohne et al. (2006), a positive value of E represents an "acceptable" simulation whereas E > 0.5 represents a "good" simulation. E equal to one indicates a "perfect" simulation. Values of E for all the simulations carried out in this study are presented in Table 7.2. The E value for chromium reduction by CRB ranges from 0.53 to 0.93, for different initial chromium concentrations. This indicates good performance of

Table 7.2: Modified Coefficients of Efficiency (E) Obtained while Evaluating Model Performances

Cr(VI) concentration	10 mg/L			20 mg/L			30 mg/L			50 mg/L			100 mg/L		
	Biomass	COD	Cr(VI)	Biomass	Biomass	COD	Cr(VI)	COD	Cr(VI)	Biomass	COD	Cr(VI)	Biomass	COD	Cr(VI)
CRB Aerobic	0.7722	0.7644	0.7584	0.8075	0.7206	0.6295	0.5302	0.7886	0.8096	0.9315	0.8702	0.9291	0.8902	0.8616	0.708
CRB Anaerobic	0.9220	0.7665	0.7486	0.7129	0.7977	0.7017	0.6546	0.8197	0.5307	0.9047	0.8365	0.889	*	*	*
SRB Anaerobic	0.8181	0.6664	0.8341	0.7902	0.9367	0.6561	0.8287	0.8312	0.789	0.8514	0.7322	0.8995	-	-	-
IRB Anaerobic	0.7794	0.5954	0.7641	0.8182	0.7358	0.6181	0.7593	0.4128	0.5847	0.8492	0.7971	0.6825	-	-	-
CRB+SRB Anaerobic	0.5996	0.4052	0.8746	0.8217	0.967	0.8416	0.8522	0.4373	0.4405	0.9326	0.8613	0.7188	-	-	-
CRB+IRB Anaerobic	0.8830	0.7883	0.8425	0.8091	0.8582	0.8986	0.7506	0.8326	0.4372	0.9171	0.7743	0.8485	-	-	-
CRB+SRB+IRB (Fe 400ppm ,Sulphate 500 ppm) Anaerobic	0.7449	0.3531	0.9779	0.7625	-	-	-	0.5300	0.7938	0.8834	0.7325	0.8354	-	-	-
CRB+SRB+IRB (Fe 800ppm, Sulphate 1000ppm) anaerobic	0.7741	0.4232	0.9081	0.8459	-	-	-	0.5169	0.6072	0.7989	0.7978	0.7165	-	-	-

* No growth was observed during Experiments
- Experiments were not conducted

the proposed mathematical model. Similar calibration and validation studies were carried out for chromium reduction by CRB, IRB and SRB under anaerobic conditions. The biokinetic parameters obtained from the calibration are given in Table 7.1. The dimensionless modified coefficient of efficiency, E for different calibration as well as validation studies are presented in Table 7.2. The E values for all the validation studies are greater than 0.5, indicating a good performance of the proposed mathematical model.

It was observed that the model performance for lower concentrations was not as good. In the model, it was assumed that the inhibition can be represented through one single value of K_i, using Monod"s inhibition model. This may not represent the inhibition correctly for lower Cr(VI) concentrations. Satisfactory results were obtained in the initial stages even in cases of low initial Cr(VI) concentrations, but the performance deteriorated with time as the Cr(VI) reduction progressed. During the later stages, microbial growth predicted by the proposed model was higher than the observed growth indicating that the inhibition model did not represent the mechanism appropriately. It may be noted here that Guha (2004) used a double substrate model, rather than an inhibition model, for chromium reduction by a single culture. Cr(VI) concentrations in the study by Guha (2004) were low. Finally, experimental and analytical errors could also contribute to the mismatch.

Kinetic parameters for Monod-type equations often have linear correlations between them. It was shown by Liu and Zachara (2001) that the bio-kinetic parameters depend on the initial conditions in the experiment and they suggested ways to find the experimental conditions for which the bio-kinetic parameters do not show significant variation. This issue was not addressed in the present study while determining the kinetic parameters. The objective of the present study was to maximize the chromium reduction, and the biokinetic parameters were determined for experimental conditions corresponding to the optimal environmental conditions (such as substrate concentration and initial biomass concentration) which result in maximum Cr (VI) reduction. Such data will be useful for developing management models.

7.1.2 Validation of Model for Chromium Reduction by a Combination of Consortiums

7.1.2.1 CRB and SRB

Biokinetic parameters obtained from batch studies for single consortium are used for the validation of the mathematical model for chromium reduction, COD consumption, and biomass growth by a consortium of CRB and SRB. It may be noted that though sulphate reduction during the process was monitored, no attempt was made to model this. It was assumed that sulphate was unlimiting and the inhibition effect was not very significant. Model predicted and experimental data for chromium reduction, COD consumption and biomass growth for different initial chromium concentrations are presented in Figs. 7.3 (a), (b) and (c), respectively. The dimensionless modified coefficients of efficiency, E are presented in Table 7.2. The E values for the above validation studies are greater than 0.5, indicating a good performance of the proposed mathematical model. As in the case of single consortium, the performance of the model was better for higher concentrations of Cr (VI) as compared to lower concentrations. It can be clearly observed from Figs. 7.3 (b), and 7.3 (c) that the performance of the model in predicting the COD consumption and biomass growth deteriorated especially after all the Cr (VI) in the system was reduced. This may be because bacterial culture which is acclimatized to reducing Cr (VI) behaves differently when Cr (VI) availability is limited. The proposed model does not consider the limiting effect of Cr (VI) availability.

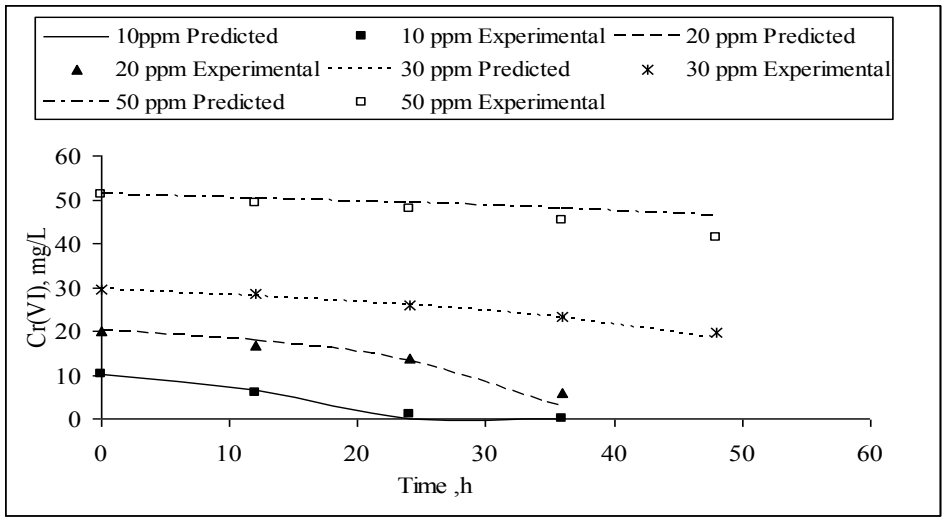

Fig. 7.3 (a): Experimental and model predicted Cr (VI) reduction by CRB and SRB under anaerobic conditions for different initial Cr (VI) concentrations (Initial sulphate concentration = 1000 mg/L)

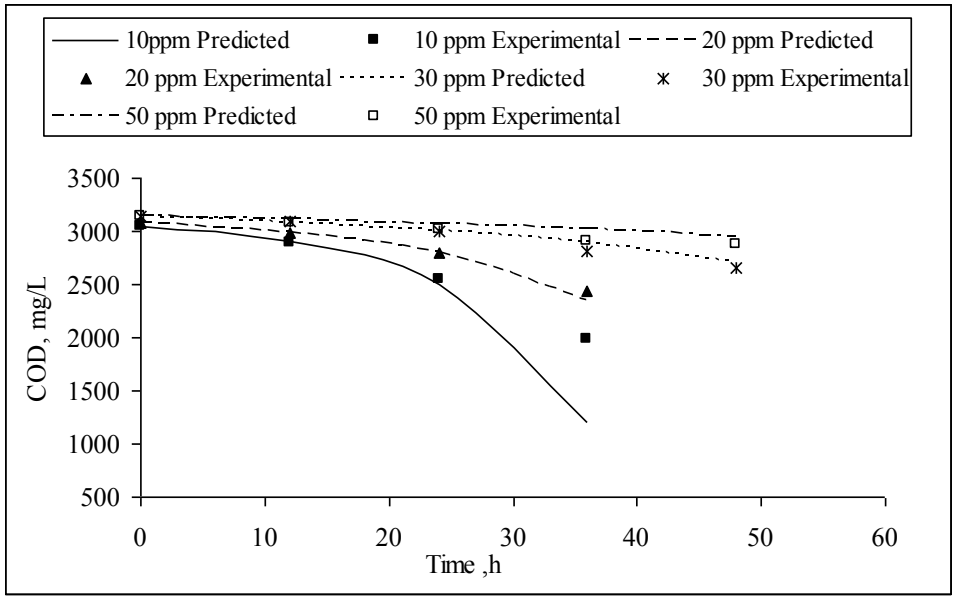

Fig. 7.3 (b): Experimental and model predicted COD consumption by CRB and SRB under anaerobic conditions for different initial Cr (VI) concentrations (Initial sulphate concentration = 1000 mg/L)

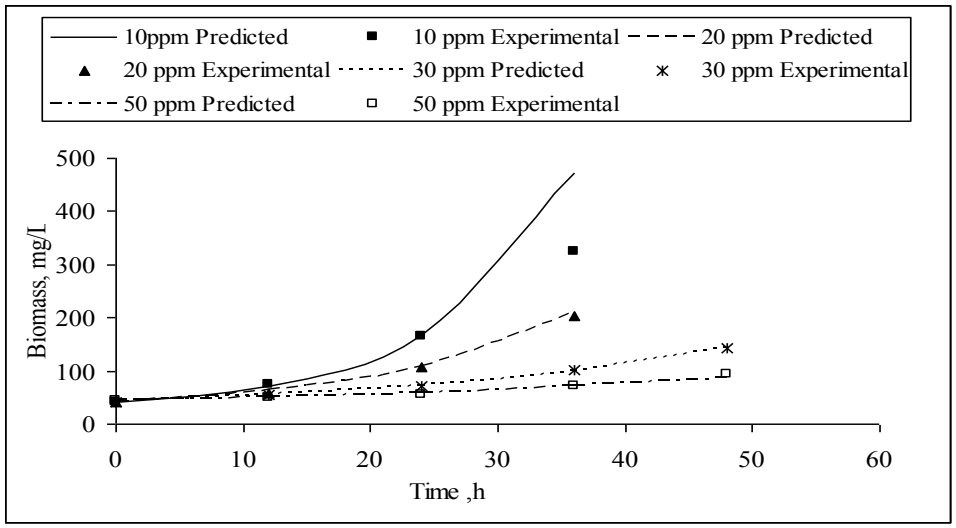

Fig. 7.3 (c): Experimental and model predicted growth of CRB and SRB under anaerobic conditions for different initial Cr (VI) concentrations (Initial sulphate concentration = 1000 mg/L)

7.1.2.2 CRB and IRB

Biokinetic parameters obtained from batch studies for single consortium are used for the validation of the mathematical model for chromium reduction, COD consumption, and biomass growth by a consortium of CRB and IRB. It may be noted that though Fe (II) generation during the process was monitored no attempt was made to model this. It was assumed that Fe (III) was unlimiting and the inhibition effect was insignificant. Model predicted and experimental data for chromium reduction, COD consumption and biomass growth for different initial chromium concentrations are presented in Figs. 7.4 (a), (b) and (c), respectively. The dimensionless modified coefficients of efficiency, E are presented in Table 7.2. The E values for the above validation studies are greater than 0.5, indicating a good performance of the proposed mathematical model.

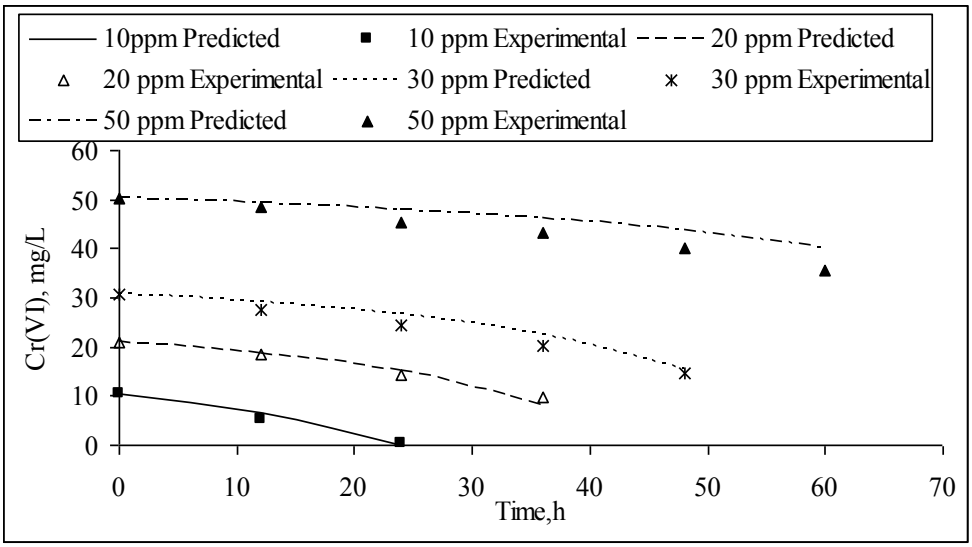

Fig. 7.4 (a): Experimental and model predicted Cr(VI) reduction by CRB and IRB under anaerobic conditions for different initial Cr(VI) concentrations (Initial Fe(III) concentration = 800 mg/L)

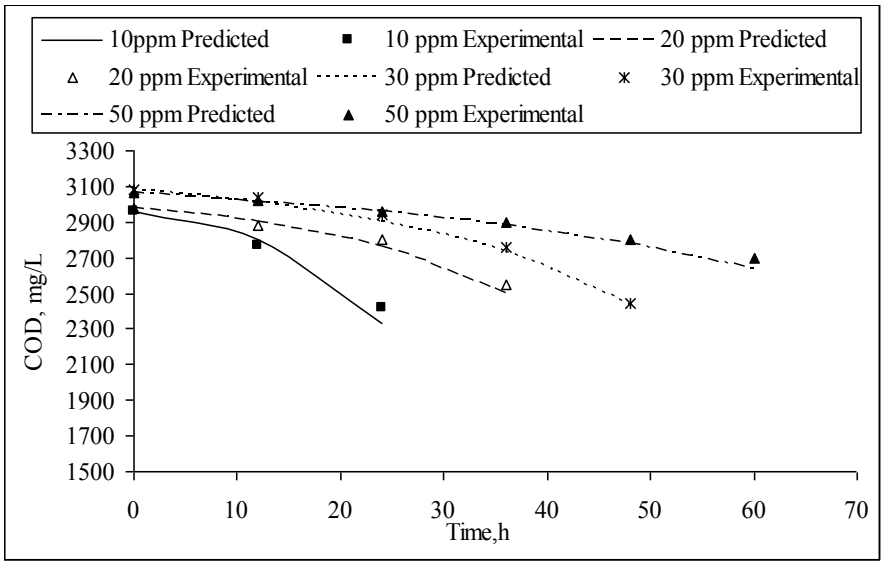

Fig. 7.4 (b): Experimental and model predicted COD consumption by CRB and IRB under anaerobic conditions for different initial Cr(VI) concentrations (Initial Fe(III) concentration = 800 mg/L)

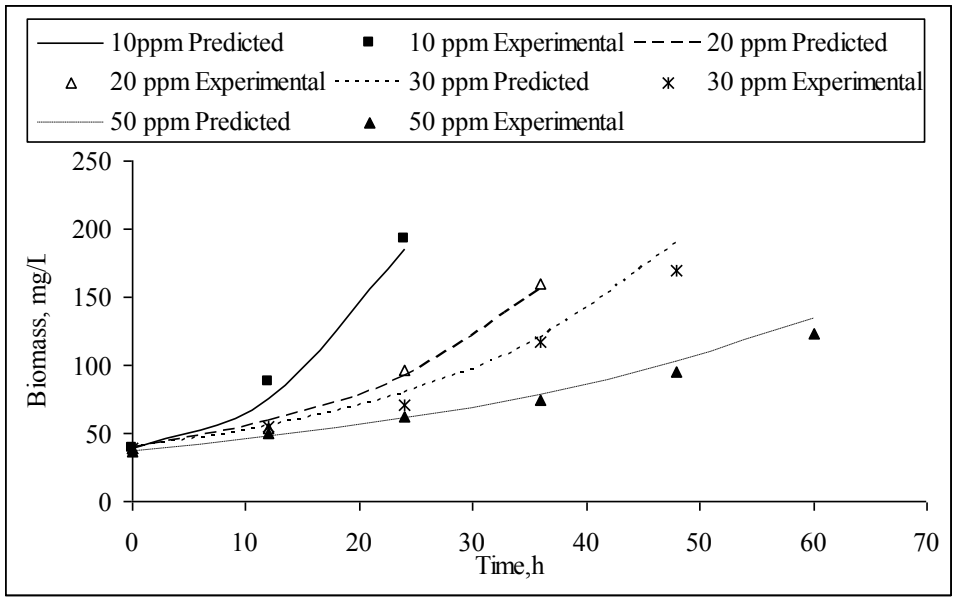

Fig. 7.4 (c): Experimental and model predicted growth of CRB and IRB under anaerobic conditions for different initial Cr(VI) concentrations (Initial Fe(III) concentration = 800 mg/L)

7.1.2.3 CRB, SRB and IRB

Biokinetic parameters obtained from batch studies for single consortium are used for the validation of the mathematical model for chromium reduction, COD consumption, and biomass growth by a consortium of CRB, SRB and IRB. Model predicted and experimental data for chromium reduction, COD consumption and biomass growth for different initial chromium concentrations are presented in Figs. 7.5 (a), (b) and (c), respectively. The dimensionless modified coefficients of efficiency, E are presented in Table 7.2. The E values for the above validation studies are greater than 0.5, indicating a good performance of the proposed mathematical model. Model validation was also carried out for different initial sulphate and Fe(III) concentrations. E values for these set of studies also are presented in Table 7.2.

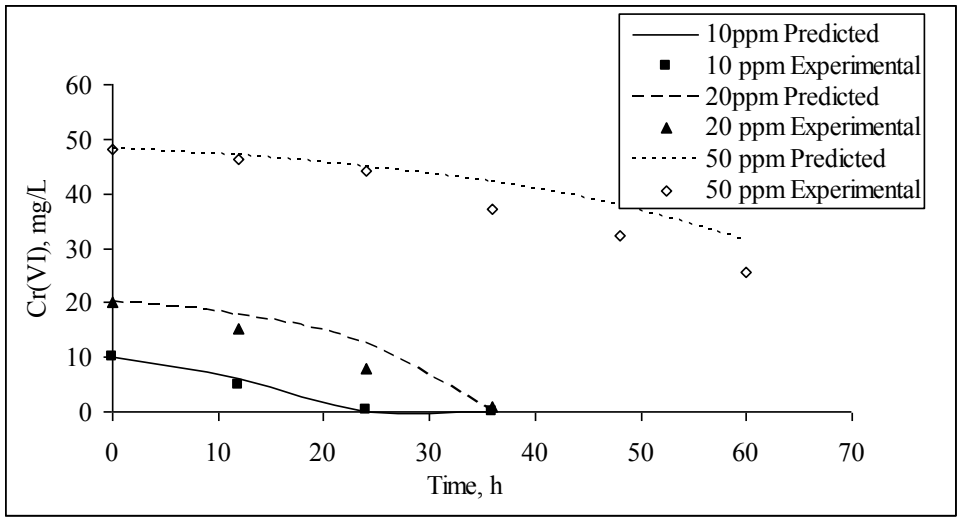

Fig. 7.5 (a): Experimental and model predicted Cr (VI) reduction by CRB, SRB and IRB under anaerobic conditions for different initial Cr (VI) concentrations (Initial sulphate concentration = 1000 mg/L, Initial Fe (III) concentration = 800 mg/L)

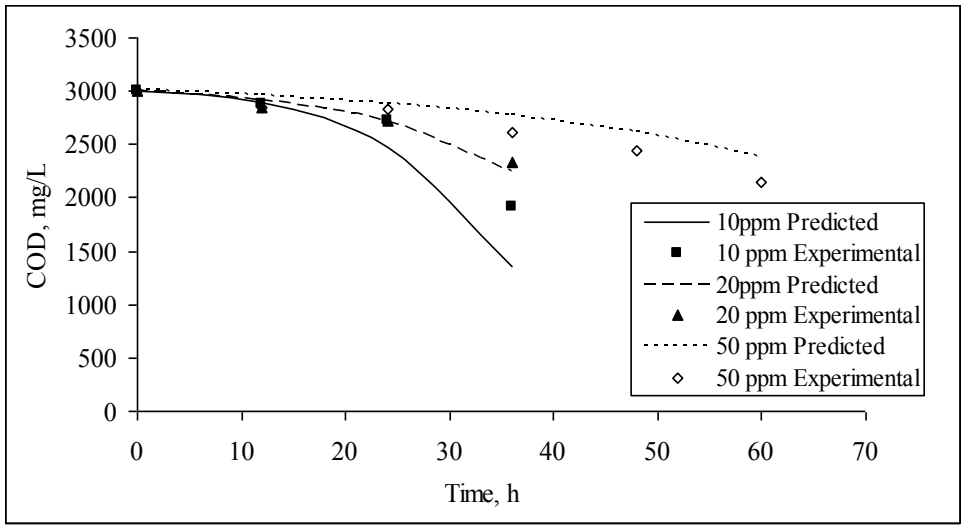

Fig. 7.5 (b): Experimental and model predicted COD consumption by CRB, SRB and IRB under anaerobic conditions for different initial Cr (VI) concentrations (Initial sulphate concentration = 1000 mg/L, Initial Fe (III) concentration = 800 mg/L)

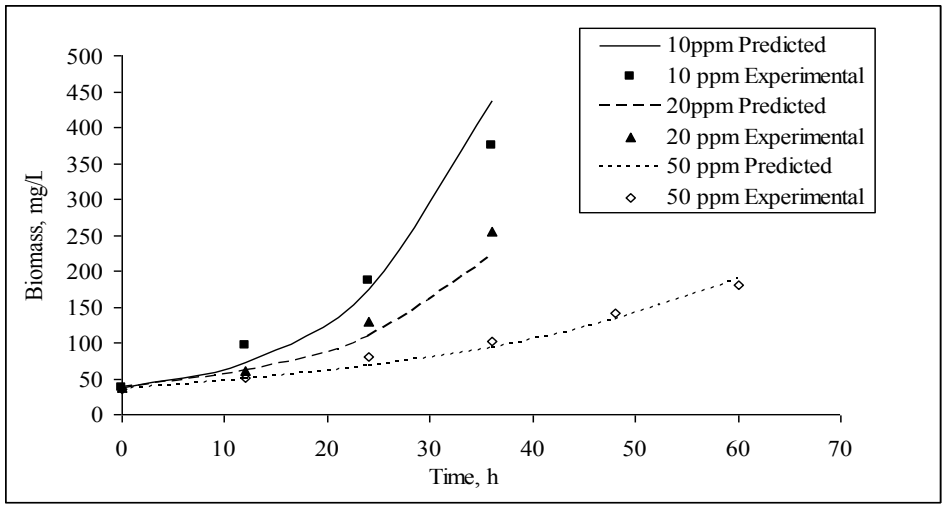

Fig. 7.5 (c): Experimental and model predicted growth of CRB, SRB and IRB under anaerobic conditions for different initial Cr (VI) concentrations (Initial sulphate concentration = 1000 mg/L, Initial Fe (III) concentration = 800 mg/L)

7.1.3 Conclusion

A mathematical model was proposed for simulating the chromium reduction, COD utilization and biomass growth, for individual cultures as well as for a combination of two or three different cultures, for different initial Cr (VI), SO_4^{2-} and Fe (III) concentrations. The major assumptions in the mathematical model were that SO_4^{2-} and Fe (III) concentrations were unlimiting and that they did not have any inhibition effect on microbial growth. Biokinetic parameters evaluated from one set of experiments for individual cultures were utilized in all the validation studies. Performance of the mathematical model in terms of the dimensionless modified coefficient of efficiency (E) indicated that the proposed model simulates the system behavior very well. E values varied from 0.4 to 1.0 in all the validation studies.

7.2 ONE-DIMENSIONAL MODEL FOR TRANSPORT WITH BIOTRANSFORMATION

In this study, a one-dimensional mathematical model was developed for simulation of transport and biotransformation of Cr (VI) through a homogeneous, isotropic confined aquifer. The bio-kinetic parameters and the adsorption isotherm constants, as obtained from the batch experiments were used in the application of this model. The lithium break through data, as obtained from the bench-scale column experiments was used to determine the dispersion coefficient. The efficiency factor, η i.e. ratio between amount of Cr (VI) bio-transformed to the amount of molasses consumed, as well as λ were determined by back-fitting the Cr (VI) breakthrough curve at port 20 cm using Genetic Algorithms. The mathematical model was then validated using the breakthrough curves for Cr (VI) and molasses at ports 40, 60, and 80 cm. Results for the model validation are presented in the following sections. Experimental data used in calibration and validation of this model has been described in Section 6.3.

7.2.1 Estimation of Bio-kinetic Parameters

μ_{max} and K_s were determined using the data from experiments (see sections 6.3.2 and 6.3.3) conducted without chromium, and with an initial molasses concentration of 5000 mg/L as COD. The bacterial growth in the exponential phase was fitted to the equation $M = M_0 e^{\mu_{max} t}$, where M_0 is the initial biomass concentration. Using this μ_{max} value as the initial estimate, the actual K_s and μ_{max} values were determined such that the simulated growth curve matched with the experimental growth curve (Fig. 7.6 (a)). K_i was then determined using the experiments for microbial growth rate in the presence of chromium, using Monod"s equation with inhibition. Figure 7.6 (b) shows the experimental and fitted variation of μ'_{max} ($\mu'_{max} = \mu_{max}$ obtained for different initial Cr (VI) concentrations, keeping all other conditions same) with different initial Cr (VI) concentrations. The bio-kinetic parameters obtained are: μ_{max} = 0.3 /h, K_s= 40.0 mg/L (as COD), K_i = 3.05 mg/L of Cr (VI), and Y = 0.263. The efficiency factor, η i.e. ratio between amount of Cr (VI) bio-transformed to the amount of molasses consumed, as well as λ were determined by back-fitting the Cr (VI) breakthrough curve at port 20 cm (transport studies, see section 6.3.5) using Genetic Algorithms. The same values were used in the mathematical simulations for breakthrough curves of Cr (VI), and molasses at all other ports located at 40, 60 and 80 cm. λ values were 0.1, 0.065, and 0.1 for Soils A,

B, and C, respectively, where as estimated value of η was 0.3, which is almost the same as reported in the literature (Guha, 2004).

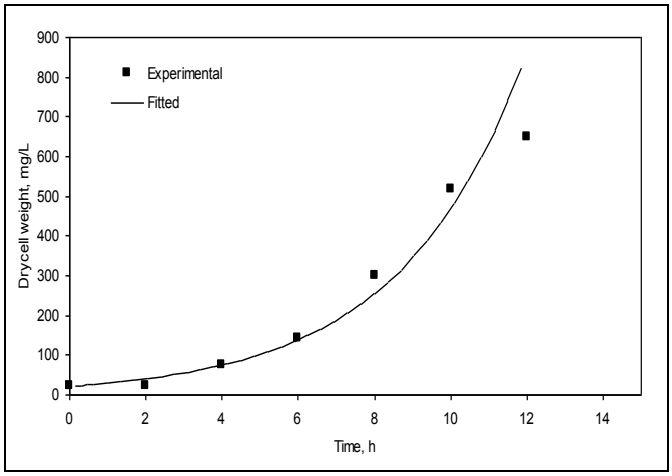

Fig. 7.6 (a): Experimental and fitted growth curve in absence of Cr (VI), Ks = 40 mg/L for microbial growth (Initial substrate concentration = 5000 mg/L as COD, pH = 7.0)

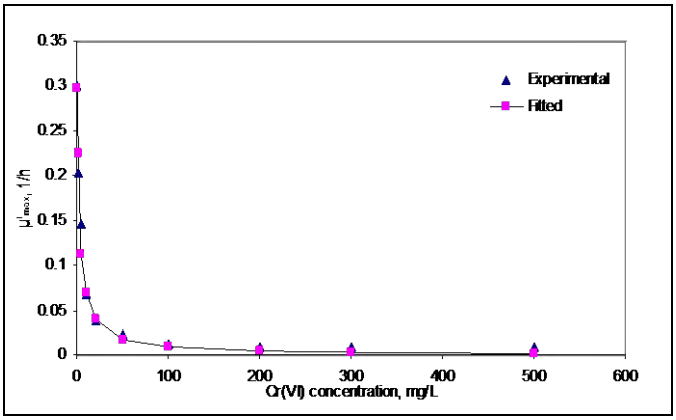

Fig. 7.6 (b): Experimental and fitted maximum specific growth rate at different initial Cr (VI) concentration (Initial substrate concentration = 5000 mg/L as COD, pH = 7.0)

7.2.2 Simulation of Transport without Biotransformation

It is essential to understand the transport of Cr (VI) without any biotransformation in order to study the role of biotransformation in the containment of Cr (VI) in aquifers, considering only the adsorption. Numerically simulated results along with the experimental data for the breakthrough of Cr (VI) at 20, 40, 60 and 80 cm ports, for three pore velocities in column with Soil C are presented in Figs. 7.7 (a) to 7.7 (d). The measured break through data at 20 cm port was used to back fit the dispersivity, α_L, and the same was used to simulate the break through curves at other ports. The dispersivity in these studies was equal to 4.46 cm, and the dispersion coefficient varied linearly with pore velocity. It is evident from Figs. 7.7 (a) to 7.7 (d). that the mathematical model simulates the experiments quite well. It is also obvious that adsorption alone was not able to contain Cr (VI) in the aquifer. The maximum Cr (VI) concentration at 80 cm port was almost equal to the inlet concentration irrespective of pore velocity.

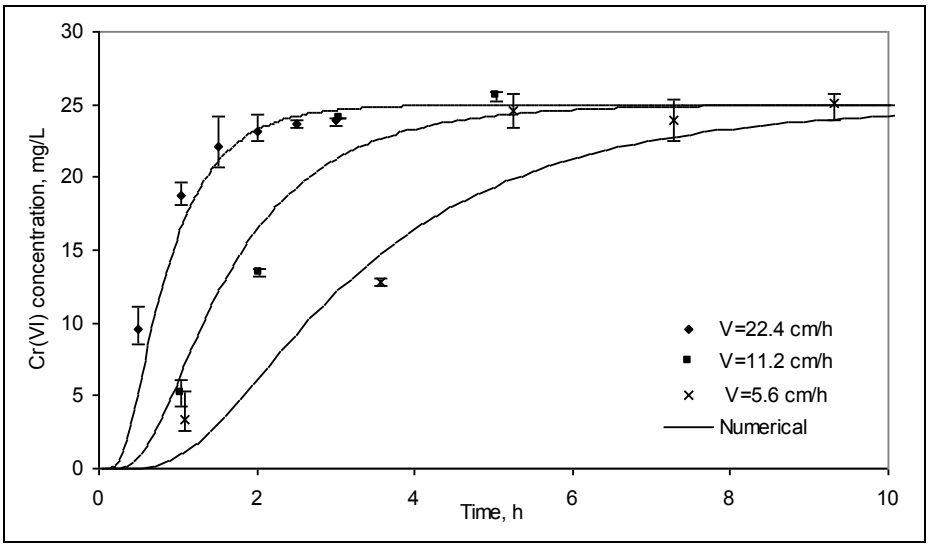

Fig. 7.7 (a): Experimental and numerical Cr (VI) breakthrough curve at 20cm port of soil C column for different pore velocities; No biotransformation (pH 6.7-7, inlet Cr (VI) concentration 25 mg/L)

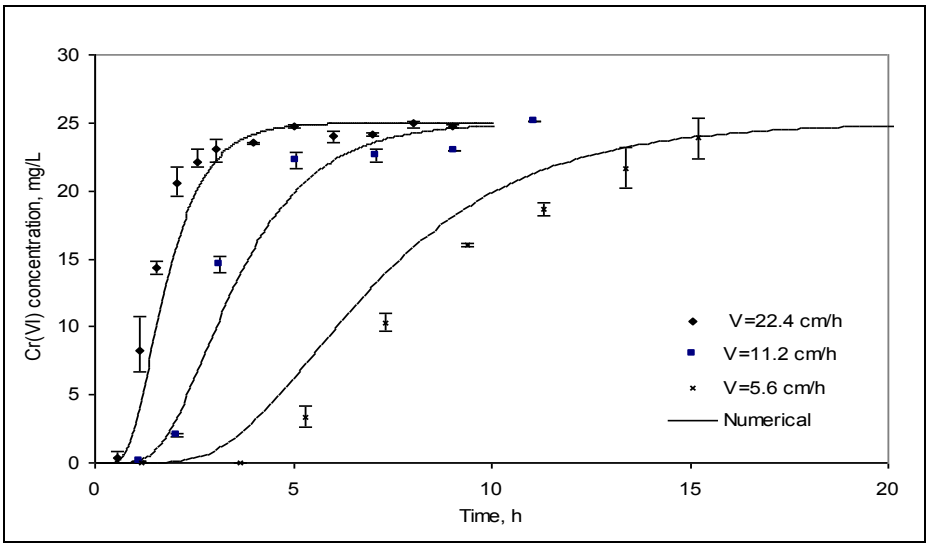

Fig. 7.7 (b): Experimental and numerical Cr (VI) breakthrough curve at 40cm port of soil C column for different pore velocities; No biotransformation (pH 6.7-7, inlet Cr (VI) concentration 25 mg/L)

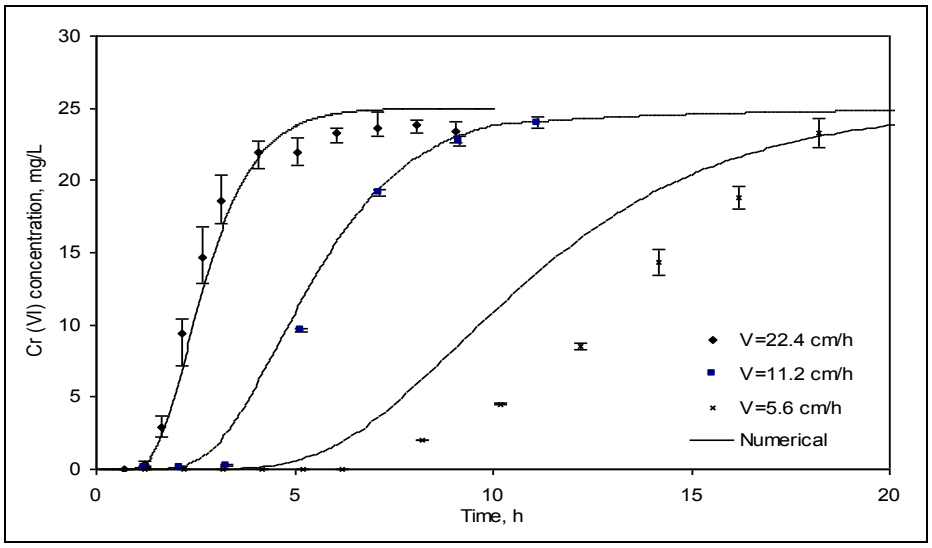

Fig. 7.7 (c): Experimental and numerical Cr(VI) breakthrough curve at 60cm port of soil C column for different pore velocities; No biotransformation (pH 6.7-7, inlet Cr (VI) concentration 25 mg/L)

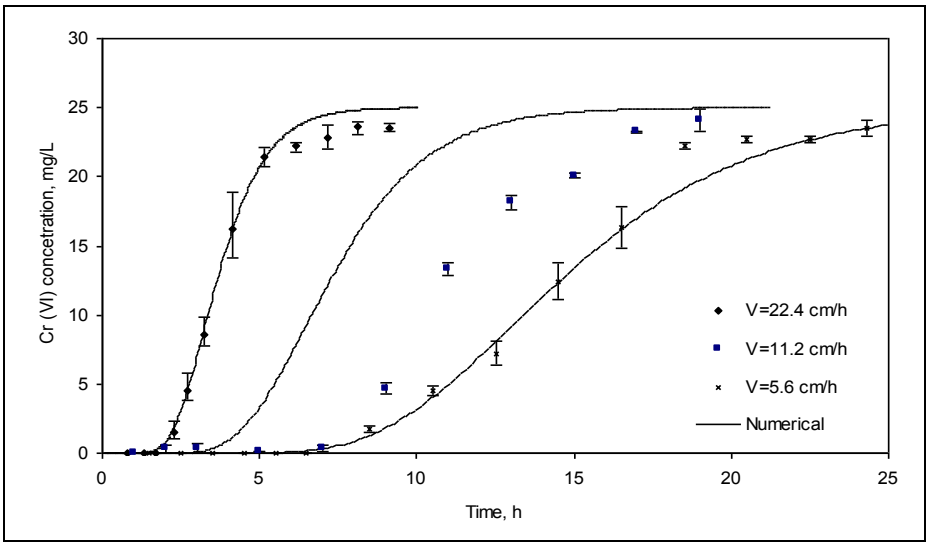

Fig. 7.7 (d): Experimental and numerical Cr(VI) breakthrough curve at 80cm port of soil C column for different pore velocities; No biotransformation (pH 6.7-7, inlet Cr(VI) concentration 25 mg/L)

7.2.3 Simulation of Transport with Biotransformation

Bench scale experiments were conducted for transport along with biotransformation in saturated, confined aquifer systems. As mentioned earlier, experiments were conducted for three different soils, A, B, and C. For soil B, experiments were conducted for two different pore velocities. Figs. 7.8 (a) to 7.8 (d) show the comparison between the numerically simulated and experimentally measured break through for Cr (VI) at x = 20 cm, x = 40 cm, x=60 and at x = 80 cm, for transport in column with soil A. Figs. 7.9 (a) to 7.9 (d) show the comparison between the numerically simulated and experimentally measured break through for substrate (molasses) at x = 20 cm, x = 40 cm, x=60 and at x = 80 cm, for the same experiment. Figs. 7.10 (a) to 7.10 (d) show the same for lithium tracer at x = 20 cm, x=40cm, x=60 cm and x = 80 cm. The dispersivity value was equal to 3.5 cm. This value was obtained by fitting the break through curves for lithium tracer at x = 20, 40, 60 and 80 cm. As mentioned earlier, a parameter λ has been introduced in the model to account for the differences in the microbial growth in a suspended batch system

and attached continuous system. It also implicitly accounts for metabolic retardation due to starving in the stabilization and acclimatization periods. The chromium break through curve at x = 20 cm was used to back fit the value of this parameter, and the same was used for simulating the chromium break through curve at the remaining ports. This value was equal to 0.1. It can be seen that numerically simulated break through curves for hexavalent chromium at x = 40, 60, and 80 cm match satisfactorily with the experimental data. Figs. 7.9 (a) to 7.9 (d) show that simulation of molasses transport was also satisfactory. It can be inferred from these results that the proposed model is able to explain the transport and biotransformation of hexavalent chromium in the confined aquifer. One calibrating parameter, λ was able to implicitly include most of the uncertainties associated with biotransformation in a confined silty aquifer.

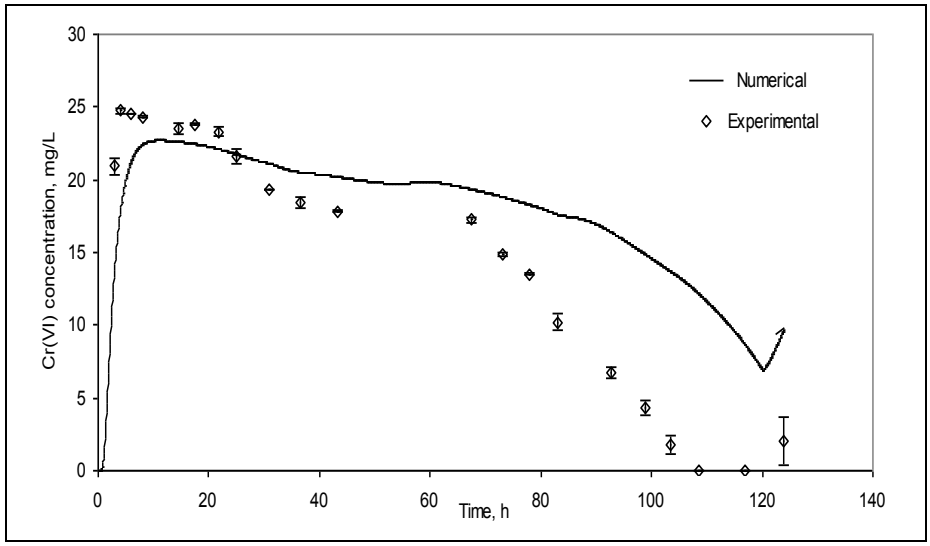

Fig. 7.8 (a): Experimental and numerical Cr(VI) breakthrough curve at 20cm port of soil A column; with biotransformation (pH 6.2-7.2, inlet Cr(VI) concentration 25 mg/L)

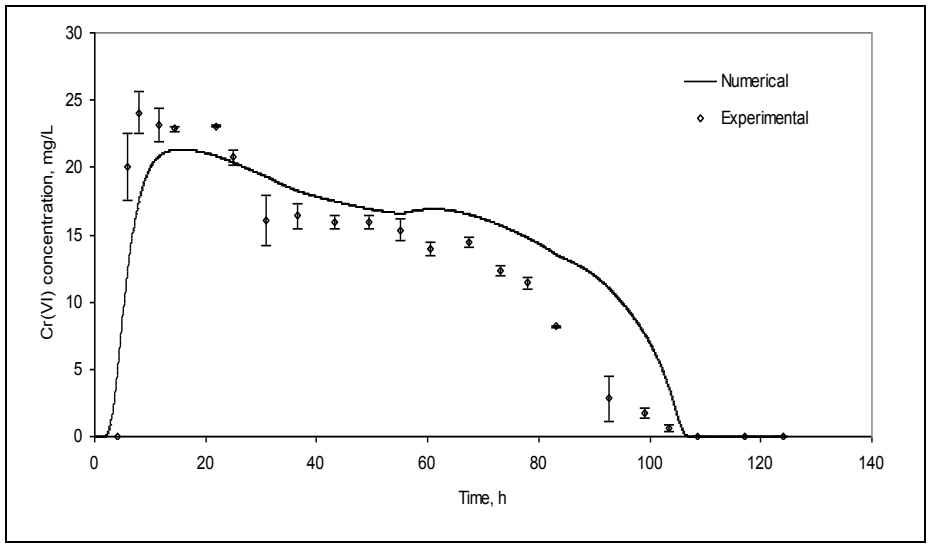

Fig. 7.8 (b): Experimental and numerical Cr(VI) breakthrough curve at 40cm port of soil A column; with biotransformation (pH 6.2-7.2, inlet Cr(VI) concentration 25 mg/L)

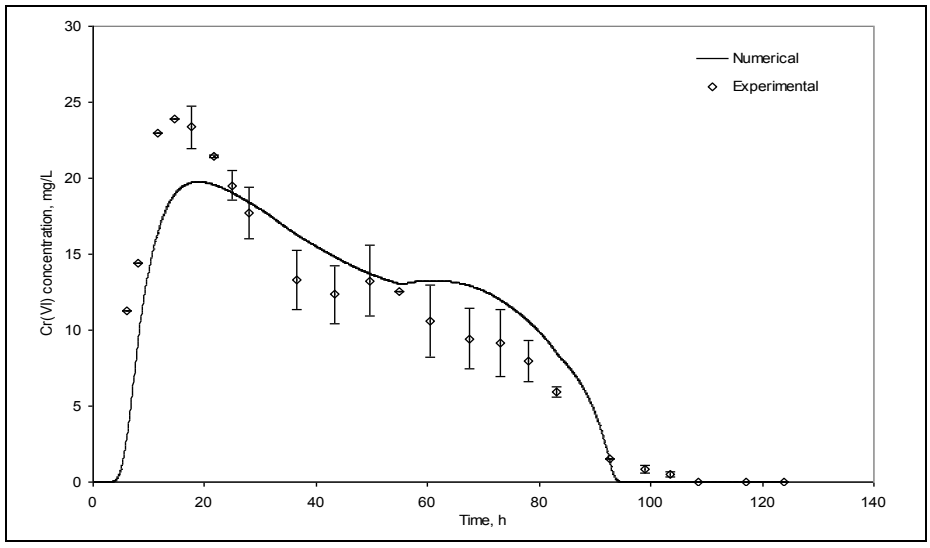

Fig. 7.8 (c): Experimental and numerical Cr(VI) breakthrough curve at 60cm port of soil A column; with biotransformation (pH 6.2-7.2, inlet Cr(VI) concentration 25 mg/L)

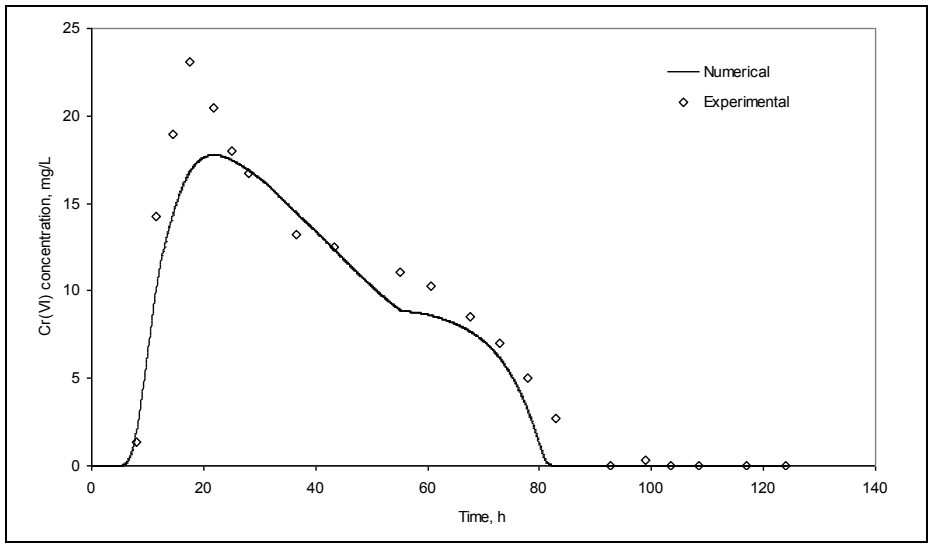

Fig. 7.8 (d): Experimental and numerical Cr(VI) breakthrough curve at 80cm port of soil A column; with biotransformation (pH 6.2-7.2, inlet Cr(VI) concentration 25 mg/L)

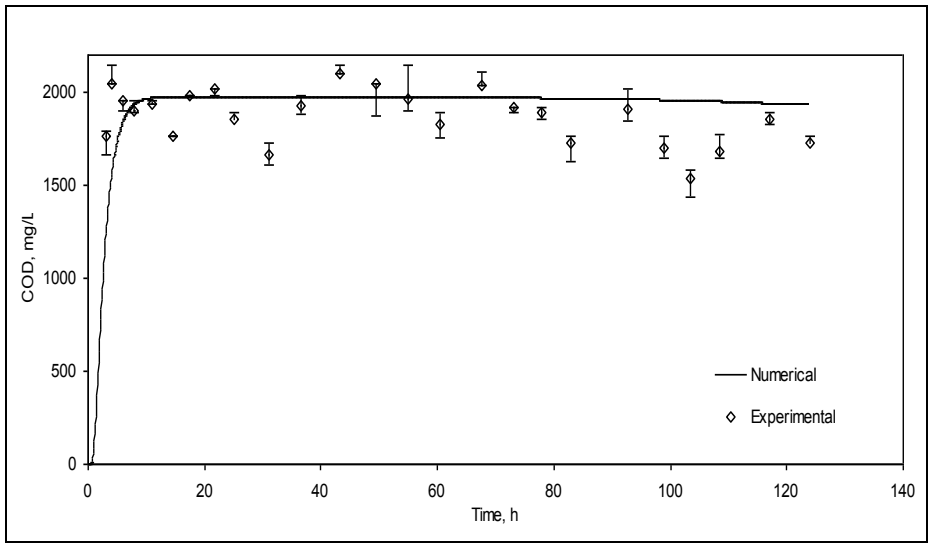

Fig. 7.9 (a): Experimental and numerical substrate breakthrough curve at 20 cm port of soil A column; with biotransformation (pH 6.2-7.2, inlet COD concentration 2000 mg/L)

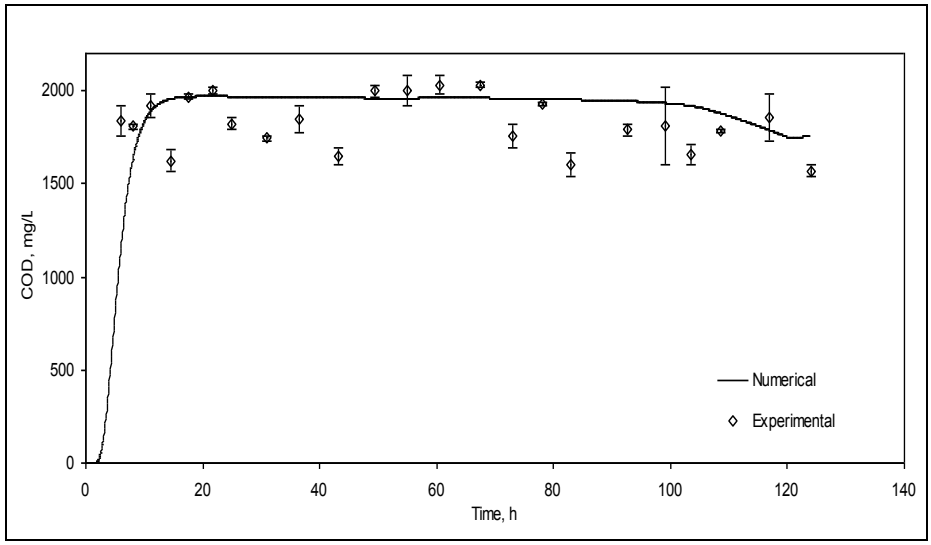

Fig. 7.9 (b): Experimental and numerical substrate breakthrough curve at 40 cm port of soil A column; with biotransformation (pH 6.2-7.2, inlet COD concentration 2000 mg/L)

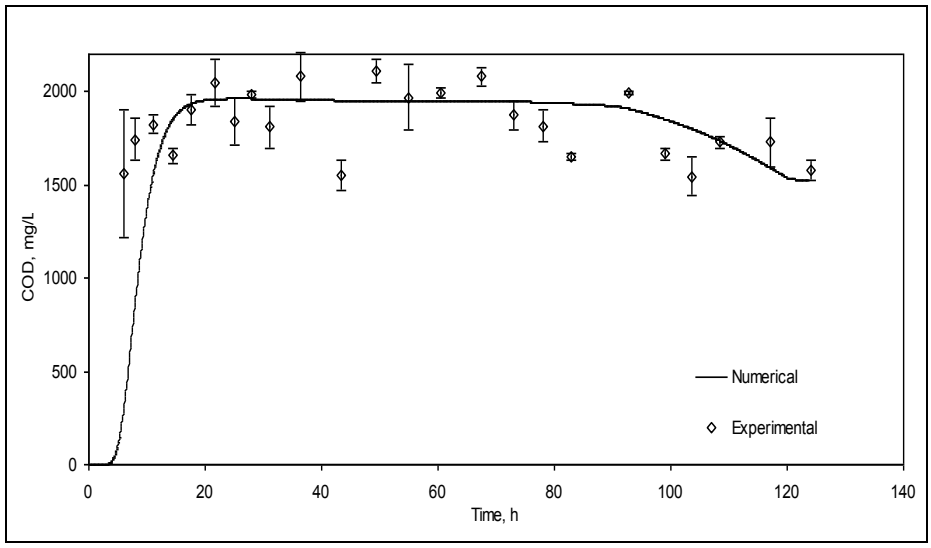

Fig. 7.9 (c): Experimental and numerical substrate breakthrough curve at 60cm port of soil A column; with biotransformation (pH 6.2-7.2, inlet COD concentration 2000 mg/L)

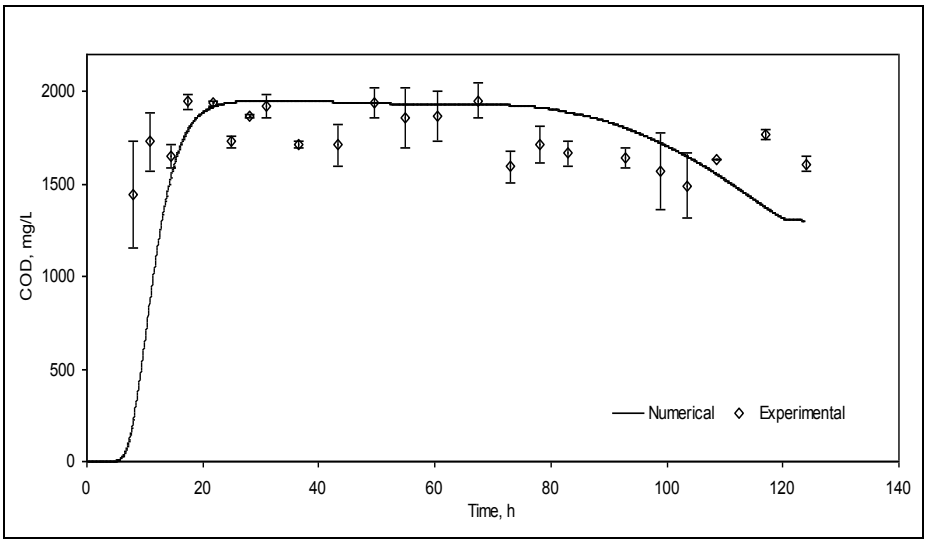

Fig. 7.9 (d): Experimental and numerical substrate breakthrough curve at 80cm port of soil A column; with biotransformation (pH 6.2-7.2, inlet COD concentration 2000 mg/L)

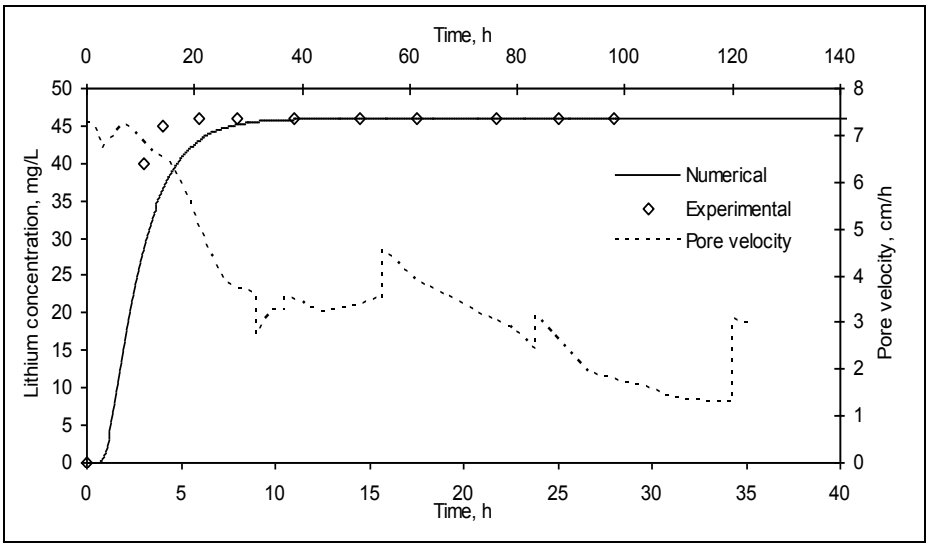

Fig. 7.10 (a): Experimental and numerical Lithium breakthrough curve at 20cm port of soil A column; with biotransformation (pH 6.2-7.2, inlet COD concentration 2000 mg/L)

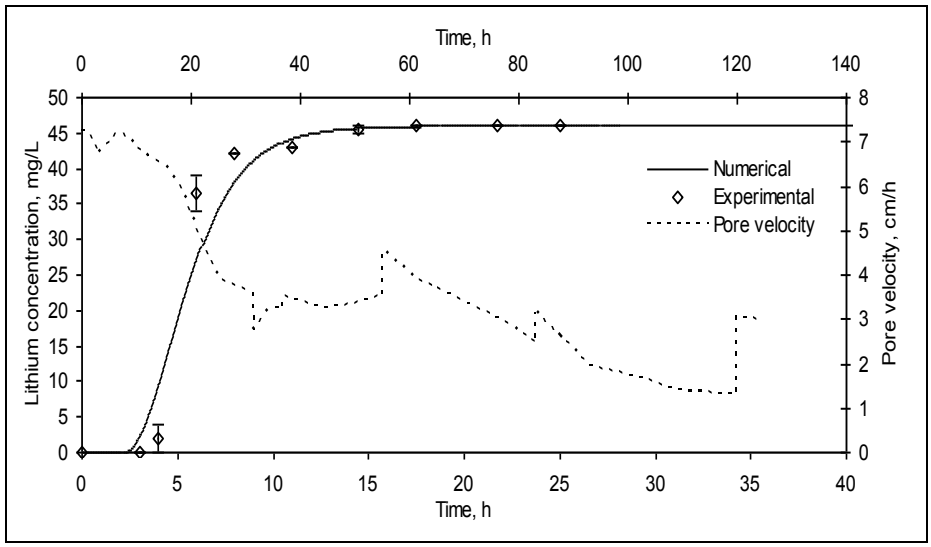

Fig. 7.10 (b): Experimental and numerical Lithium breakthrough curve at 40cm port of soil A column; with biotransformation (pH 6.2-7.2, inlet COD concentration 2000 mg/L)

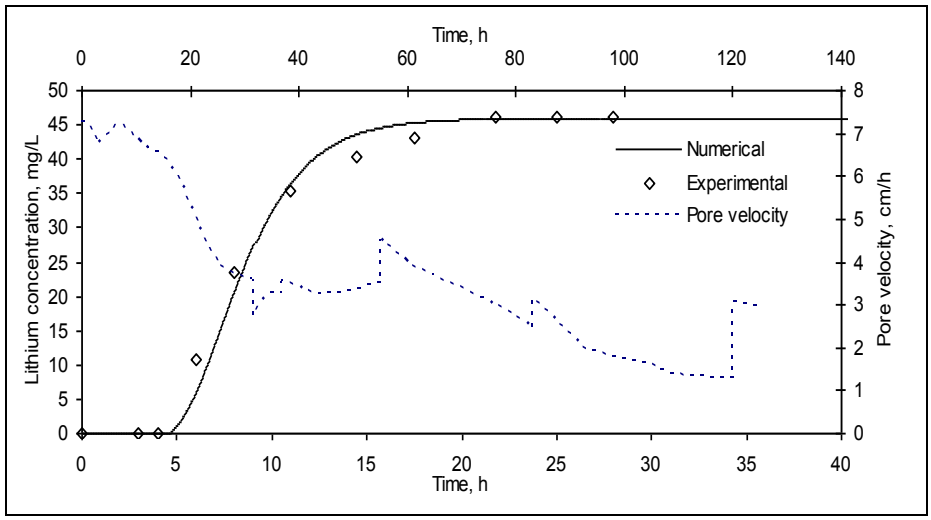

Fig. 7.10 (c): Experimental and numerical Lithium breakthrough curve at 60cm port of soil A column; with biotransformation (pH 6.2-7.2, inlet Li concentration 46 mg/L)

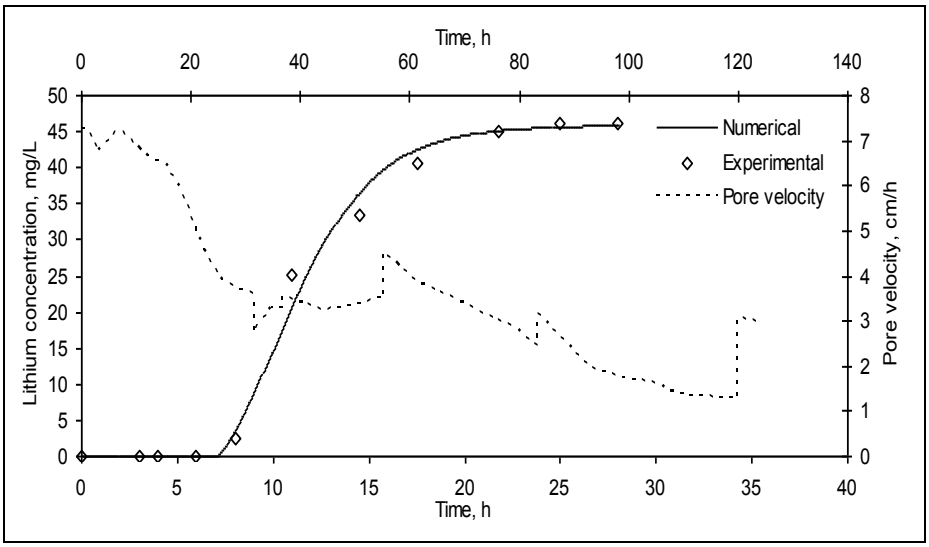

Fig. 7.10 (d): Experimental and numerical Lithium breakthrough curve at 80cm port of soil A column; with biotransformation (pH 6.2-7.2, inlet Li concentration 46 mg/L)

Figs. 7.11, 7.12 and 7.13 show the numerically simulated and experimental break through curves for hexavalent chromium, molasses and lithium, respectively, for soil C with 6.19% clay content. Dispersivity in this experiment was equal to 4.46 cm. This value was taken from the transport experiments without biotransformation in column with soil C. Estimation of the dispersivity value using the lithium breakthrough data proved to be unsuccessful. The same value of λ as obtained for soil A was used in this case also. It is clear from these figures that as the clay content increases, it becomes difficult to simulate even the lithium transport. The gas released due to microbial metabolic activity might have been trapped unevenly in the column and introduced non-homogeneities. It may be noted here that, for the same soil without biotransformation, transport of Cr (VI) was simulated well by the proposed model. Thus, it may be concluded that for modeling the transport and biotransformation of Cr (VI) in aquifers with high clay content, non-homogeneities introduced by biotransformation process should be considered for a better simulation.

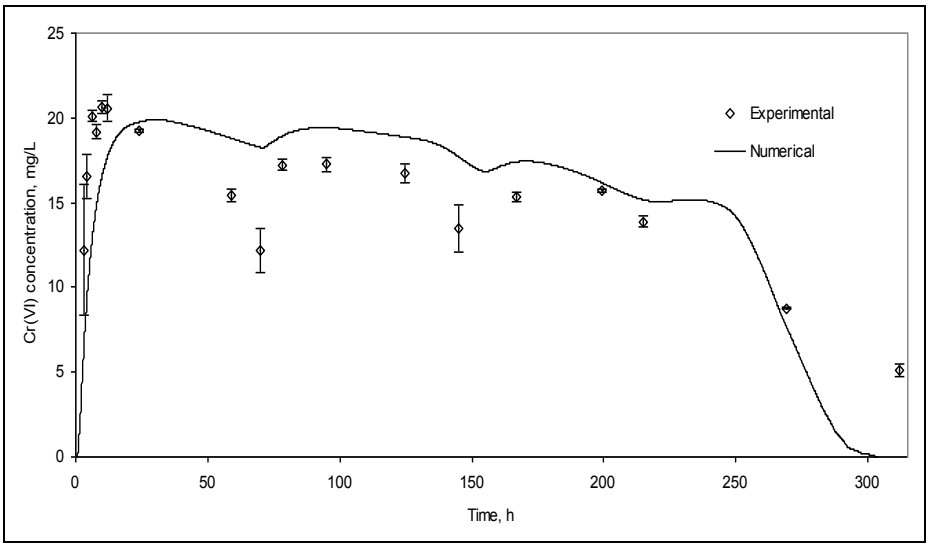

Fig. 7.11 (a): Experimental and numerical Cr (VI) breakthrough curve at 20cm port of soil C column; with biotransformation (pH 6.2-7.2, inlet Cr (VI) concentration 25 mg/L)

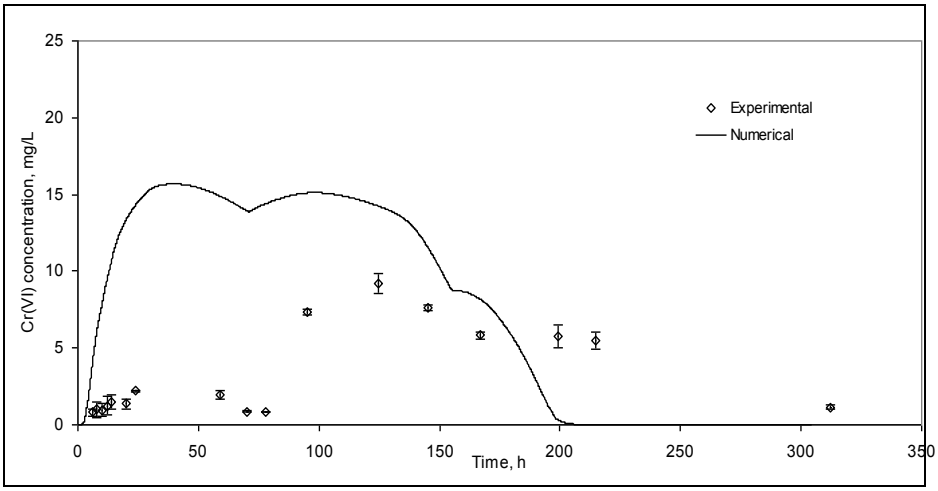

Fig. 7.11(b): Experimental and numerical Cr(VI) breakthrough curve at 40cm port of soil C column; with biotransformation (pH 6.2-7.2, inlet Cr(VI) concentration 25 mg/L)

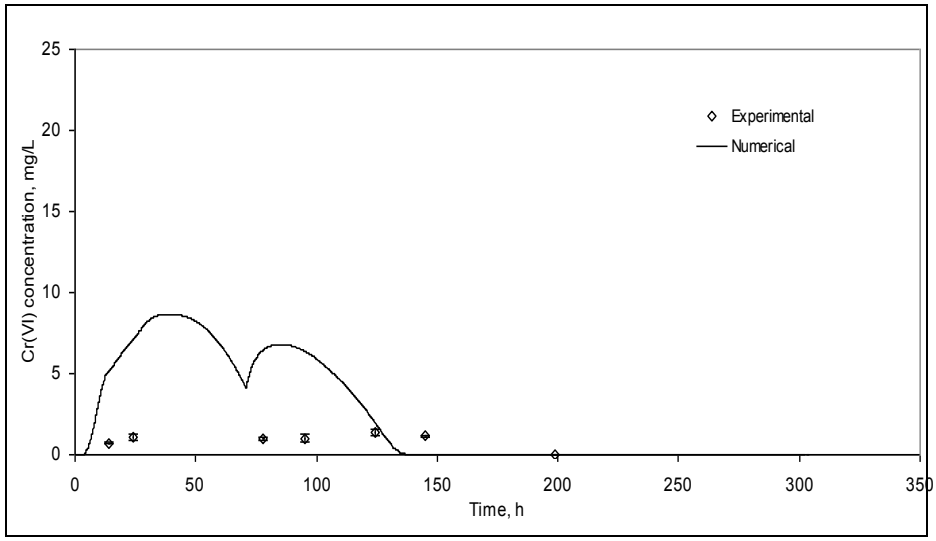

Fig. 7.11 (c): Experimental and numerical Cr (VI) breakthrough curve at 60cm port of soil C column; with biotransformation (pH 6.2-7.2, inlet Cr (VI) concentration 25 mg/L)

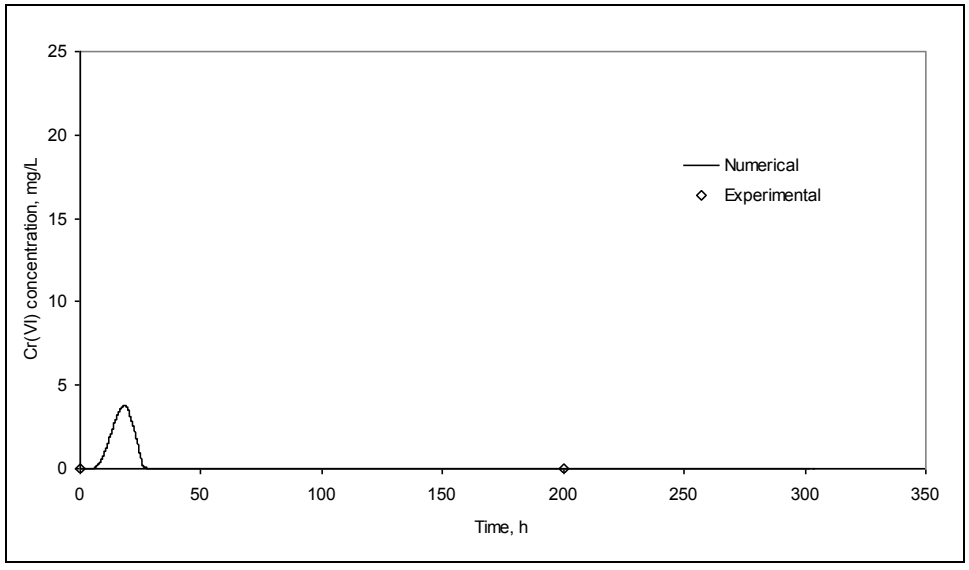

Fig. 7.11 (d): Experimental and numerical Cr (VI) breakthrough curve at 80cm port of soil C column; with biotransformation (pH 6.2-7.2, inlet Cr (VI) concentration 25 mg/L)

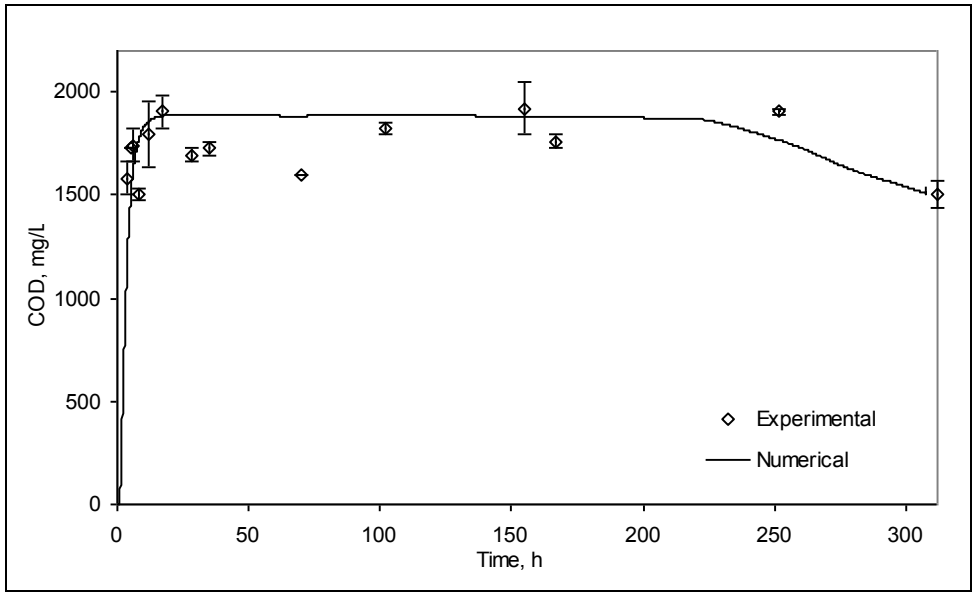

Fig. 7.12 (a): Experimental and numerical substrate breakthrough curve at 20cm port of soil C column; with biotransformation (pH 6.2-7.2, inlet COD concentration 2000 mg/L)

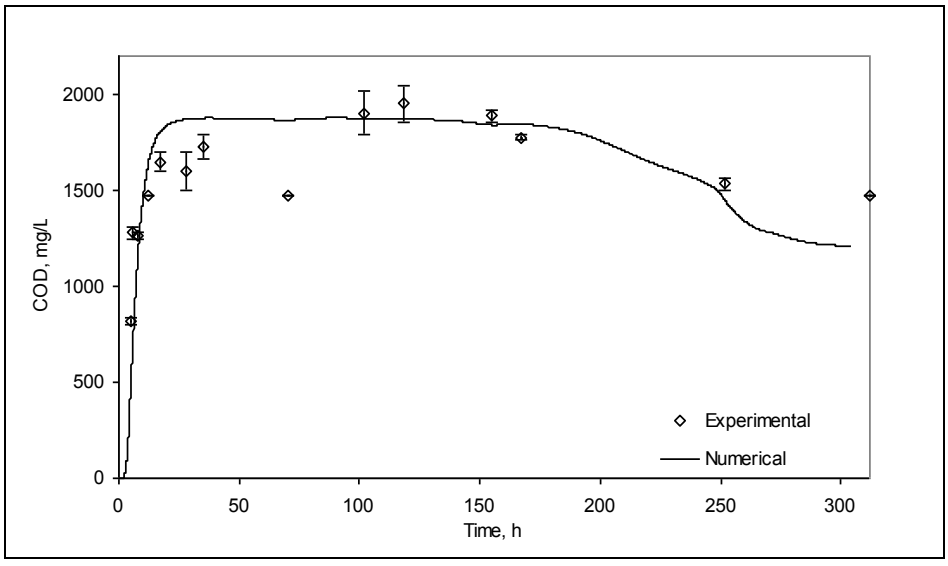

Fig. 7.12 (b): Experimental and numerical substrate breakthrough curve at 40cm port of soil C column; with biotransformation (pH 6.2-7.2, inlet COD concentration 2000 mg/L)

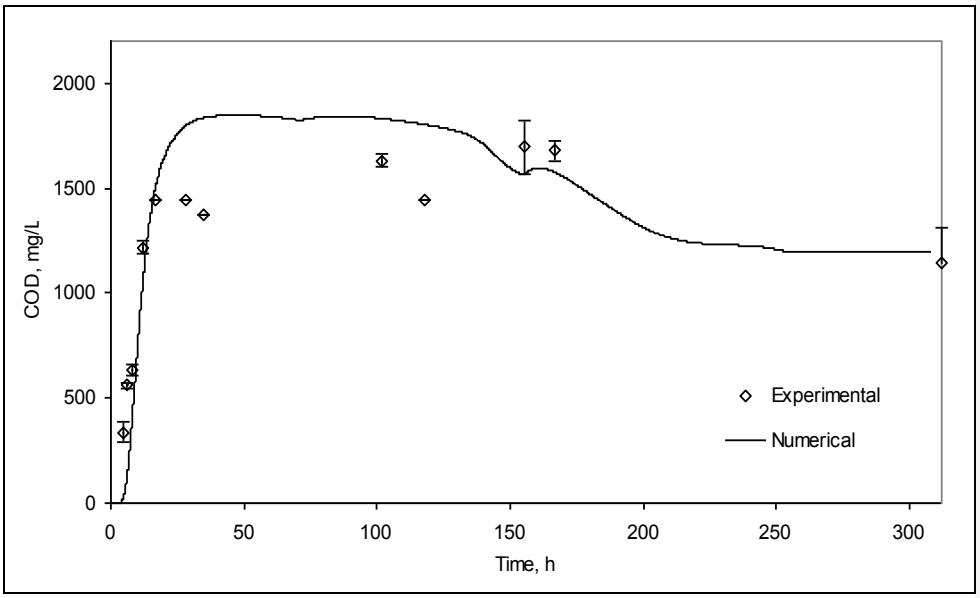

Fig. 7.12 (c): Experimental and numerical substrate breakthrough curve at 60cm port of soil C column; with biotransformation (pH 6.2-7.2, inlet COD concentration 2000 mg/L)

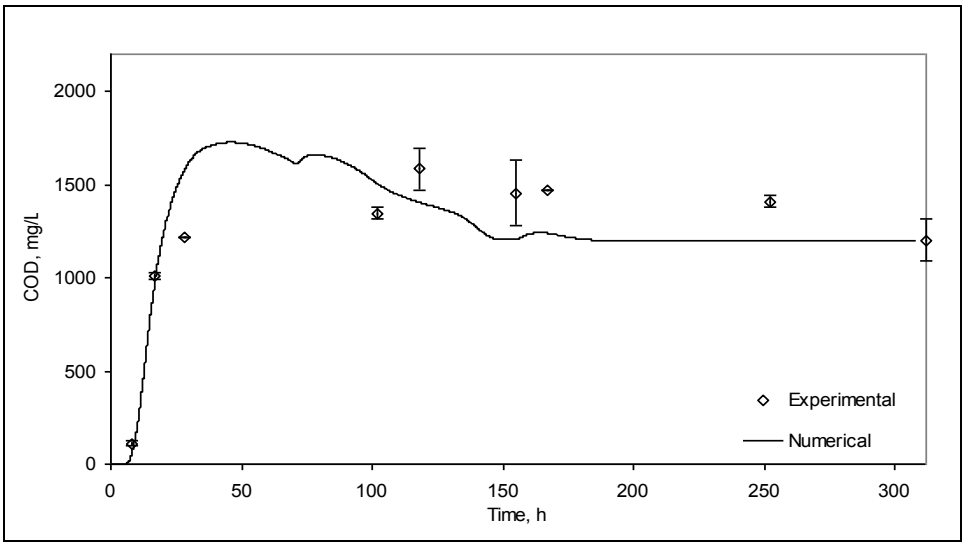

Fig. 7.12 (d): Experimental and numerical substrate breakthrough curve at 80cm port of soil C column; with biotransformation (pH 6.2-7.2, inlet COD concentration 2000 mg/L)

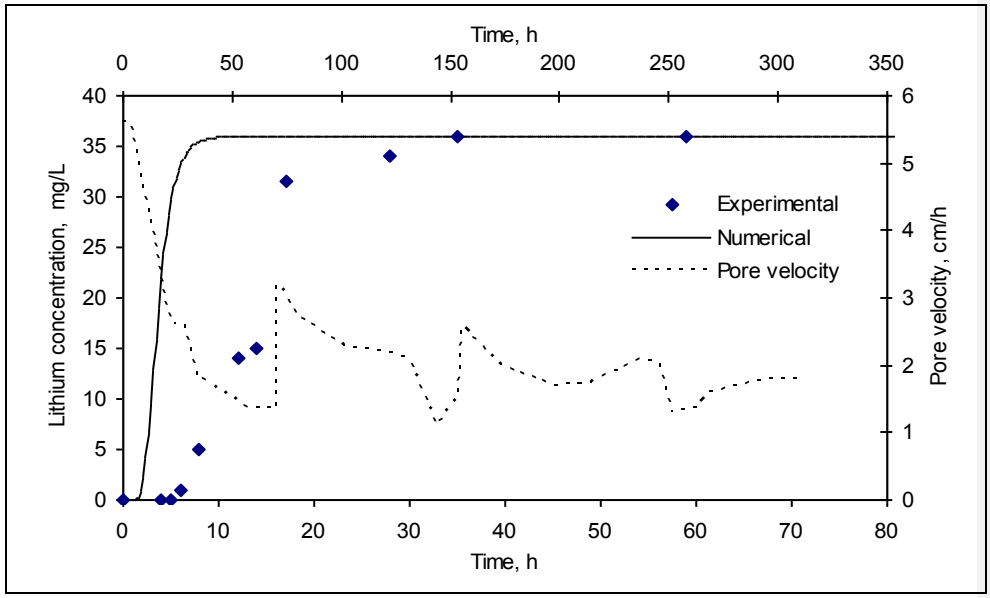

Fig. 7.13 (a): Experimental and numerical Lithium breakthrough curve at 20cm port of soil C column; with biotransformation (pH 6.2-7.2, inlet Li concentration 36 mg/L)

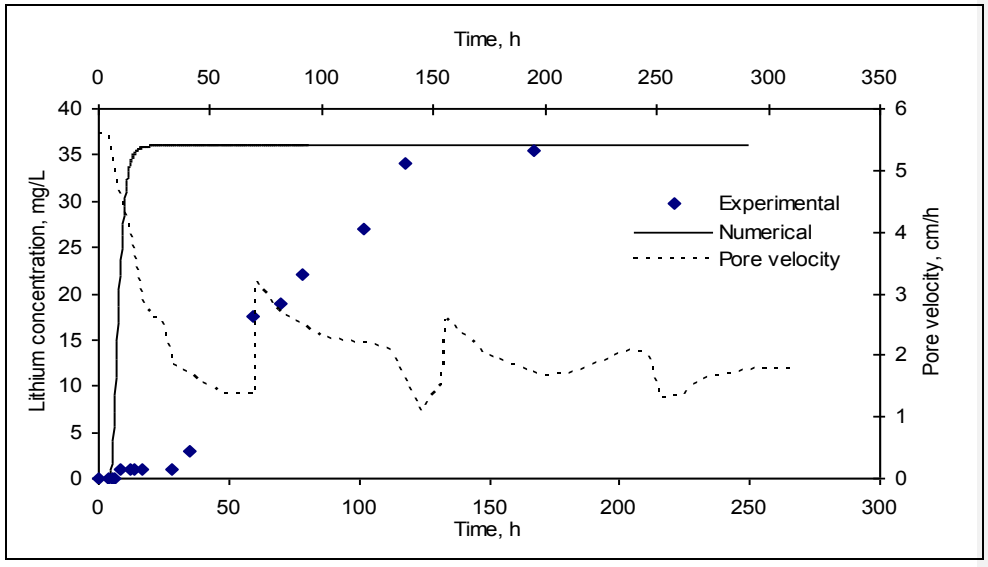

Fig. 7.13 (b): Experimental and numerical Lithium breakthrough curve at 40cm port of soil C column; with biotransformation (pH 6.2-7.2, inlet Li concentration 36 mg/L)

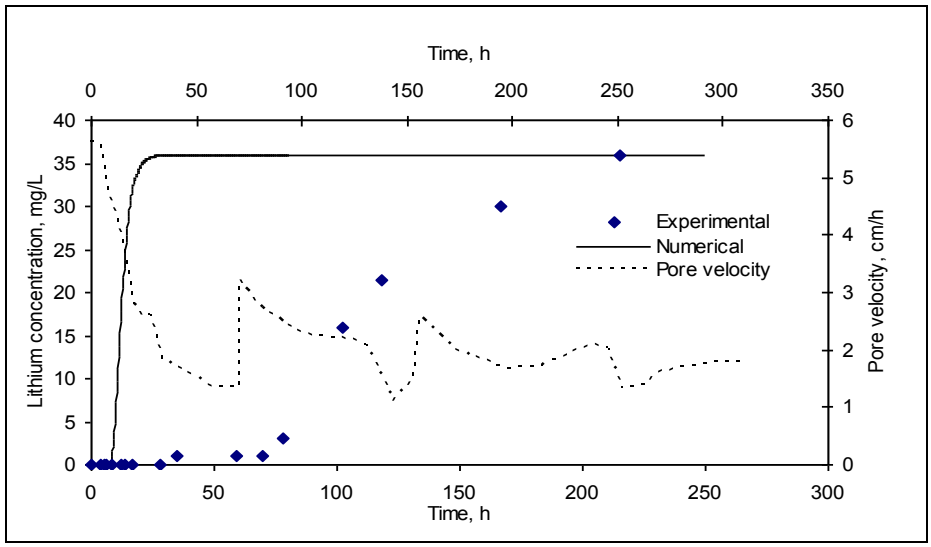

Fig. 7.13 (c): Experimental and numerical Lithium breakthrough curve at 60cm port of soil C column; with biotransformation (pH 6.2-7.2, inlet Li concentration 36 mg/L)

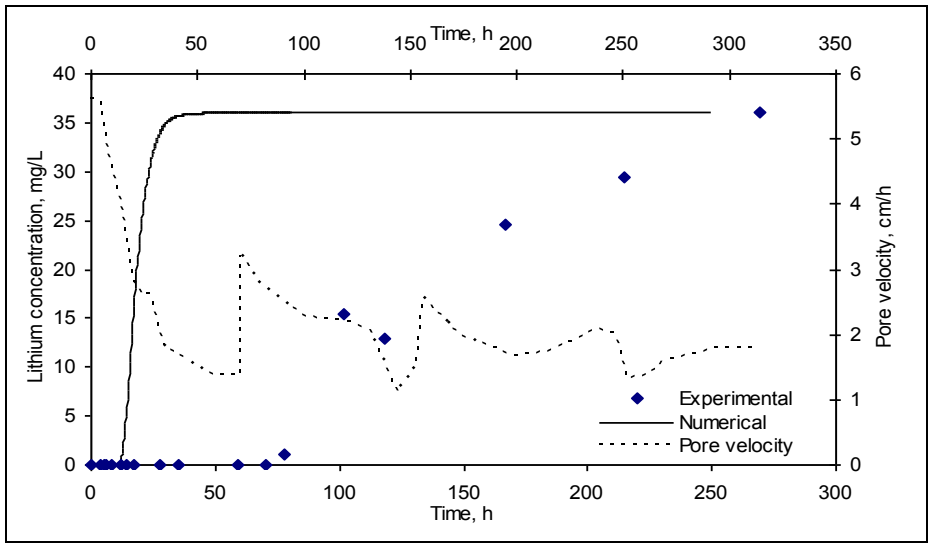

Fig. 7.13 (d): Experimental and numerical Lithium breakthrough curve at 80cm port of soil C column; with biotransformation (pH 6.2-7.2, inlet Li concentration 36 mg/L)

Figs. 7.14 (a) to 7.14 (d) and 7.15 (a) to 7.15 (d) present the break through for Cr (VI) at 20, 40, 60 and 80 cm ports for the case of transport and biotransformation experiments in soil B, for two different velocities of 6.67 cm/h and 1.16 cm/h, respectively. Dispersivities in these experiments (as obtained using the lithium tracer data) were 0.1cm and 0.3 cm, respectively. The λ value (as obtained from the Cr (VI) breakthrough data at x = 20 cm) was 0.065. It is very clear that the effect of biotransformation on Cr (VI) containment is very significant in the case of low pore velocity. In case of high pore velocity, breakthrough of Cr (VI) occurred much earlier and also the maximum concentration was almost equal to the inlet concentration even after150 hrs. These effects are well simulated by the mathematical model, as evident from the figures. Pore velocity had a significant effect on bacterial retention on the soil matrix. High pore velocity resulted in significant bacterial cell wash out from 0.021 to 0.005 mg/g, while the bacterial concentration reduced from 0.04 to 0.027 mg/g in the case of column with low pore velocity. It can be seen from Figs. 7.14 (a) to 7.15 (d) that the rate of Cr (VI) containment increased with respect to time because of corresponding increase in biomass concentration in the system.

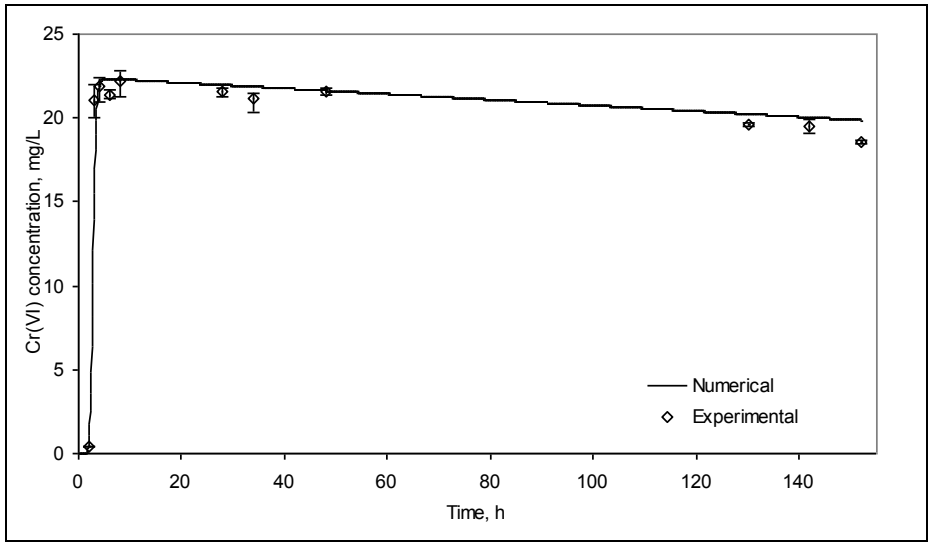

Fig. 7.14 (a): Experimental and numerical Cr (VI) breakthrough curve at 20cm port of soil B column; with biotransformation (pH 6.2-7.2, inlet Cr (VI) concentration 25 mg/L, pore velocity 6.67 cm/h)

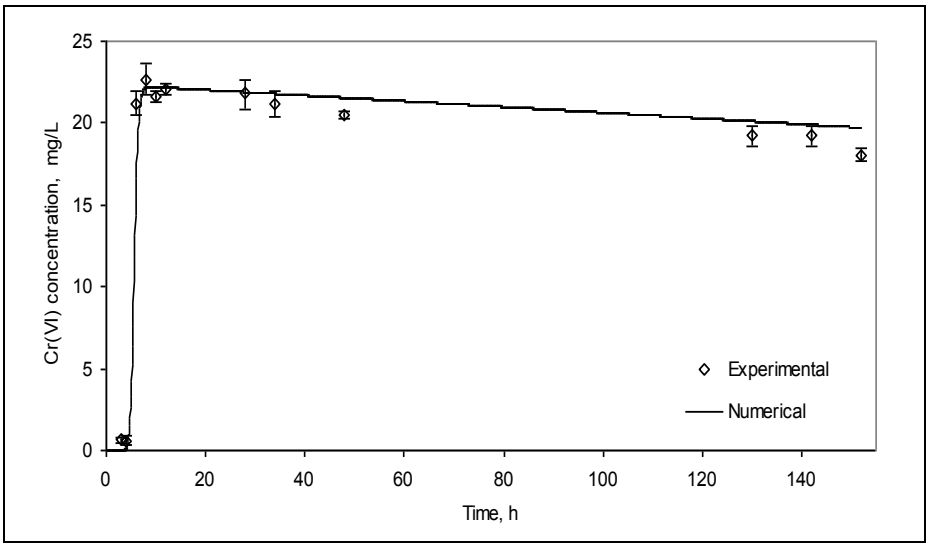

Fig. 7.14 (b): Experimental and numerical Cr (VI) breakthrough curve at 40cm port of soil B column; with biotransformation (pH 6.2-7.2, inlet Cr (VI) concentration 25 mg/L, pore velocity 6.67 cm/h)

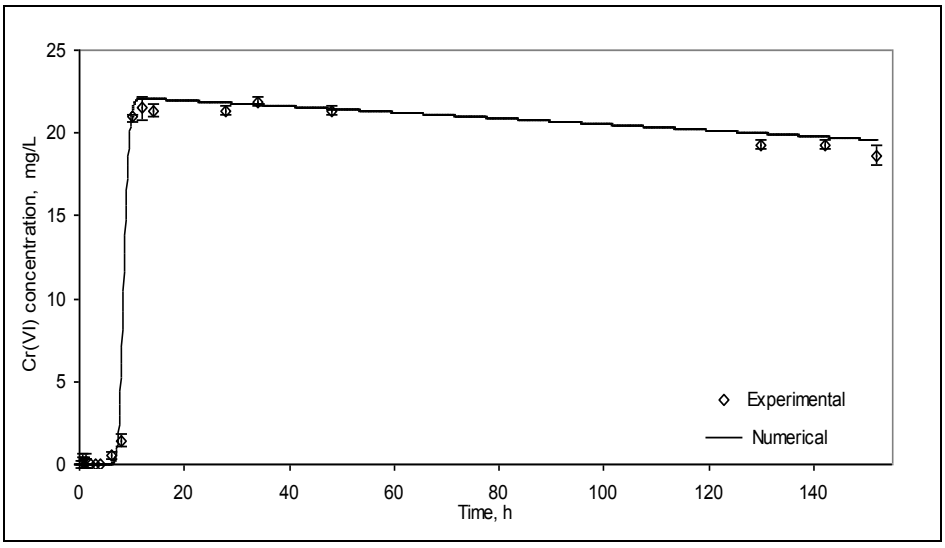

Fig. 7.14 (c): Experimental and numerical Cr (VI) breakthrough curve at 60cm port of soil B column; with biotransformation (pH 6.2-7.2, inlet Cr (VI) concentration 25 mg/L, pore velocity 6.67 cm/h)

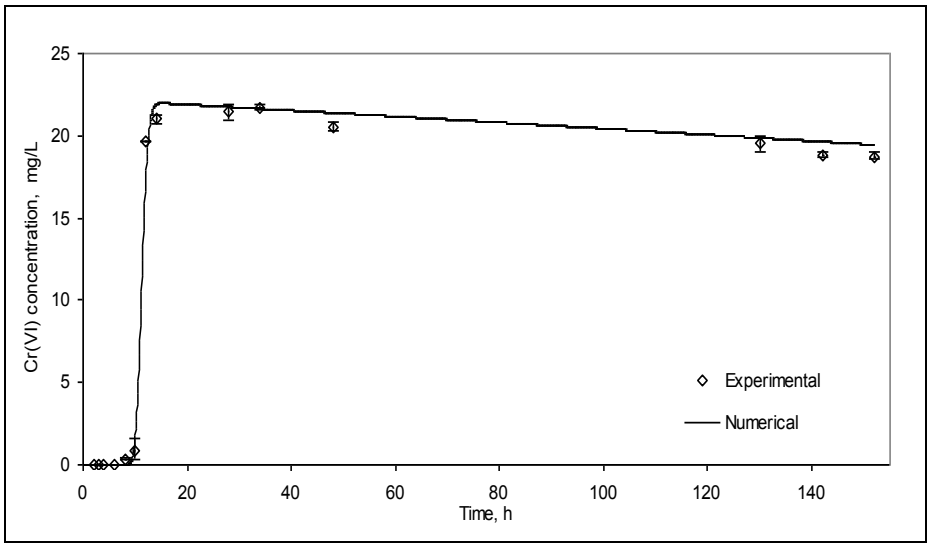

Fig. 7.14 (d): Experimental and numerical Cr (VI) breakthrough curve at 80cm port of soil B column; with biotransformation (pH 6.2-7.2, inlet Cr (VI) concentration 25 mg/L, pore velocity 6.67 cm/h)

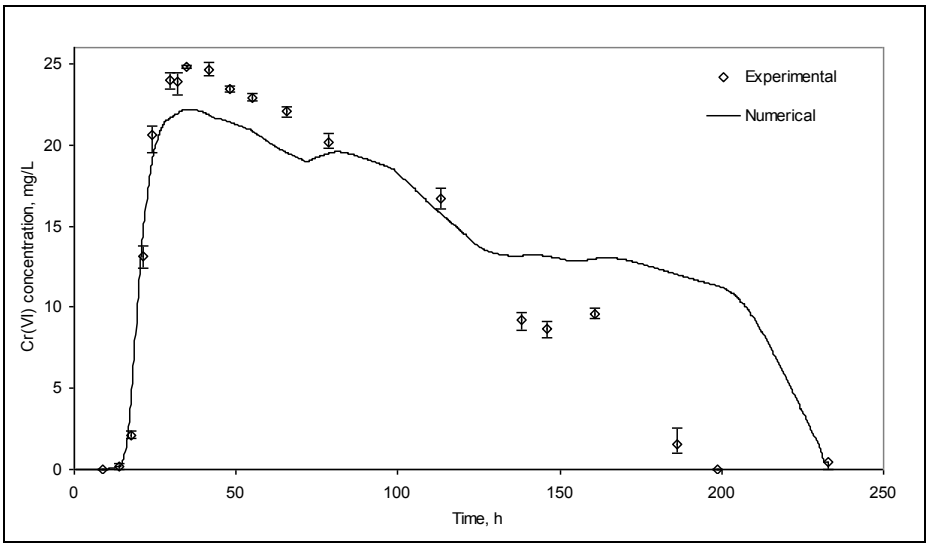

Fig. 7.15 (a): Experimental and numerical Cr(VI) breakthrough curve at 20cm port of soil B column; with biotransformation (pH 6.2-7.2, inlet Cr(VI) concentration 25 mg/L, pore velocity 1.16 cm/h)

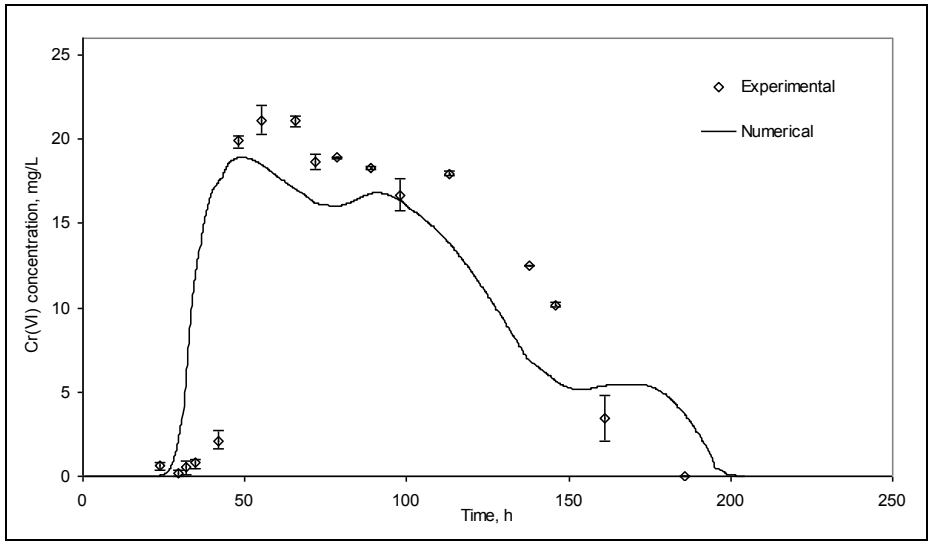

Fig. 7.15 (b): Experimental and numerical Cr (VI) breakthrough curve at 40cm port of soil B column; with biotransformation (pH 6.2-7.2, inlet Cr (VI) concentration 25 mg/L, pore velocity 1.16 cm/h)

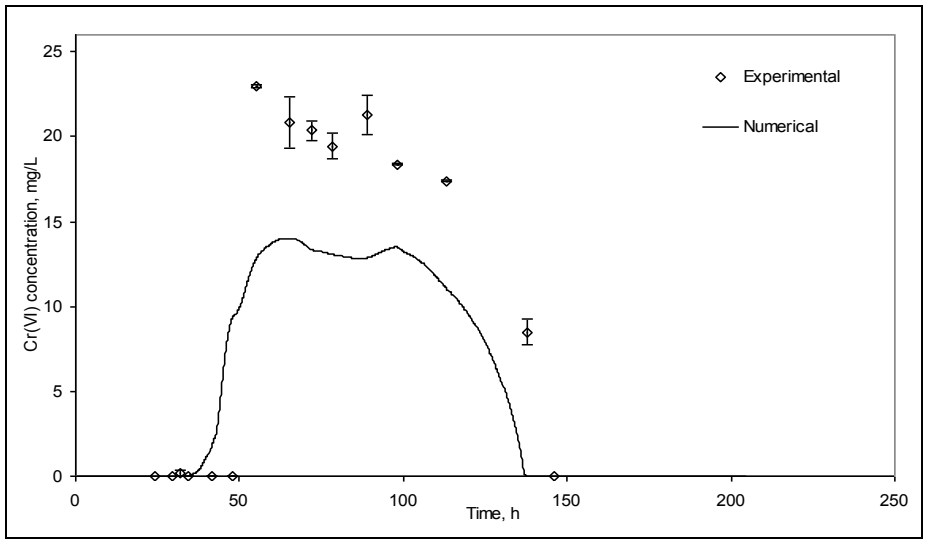

Fig. 7.15 (c): Experimental and numerical Cr (VI) breakthrough curve at 60cm port of soil B column; with biotransformation (pH 6.2-7.2, inlet Cr (VI) concentration 25 mg/L, pore velocity 1.16 cm/h)

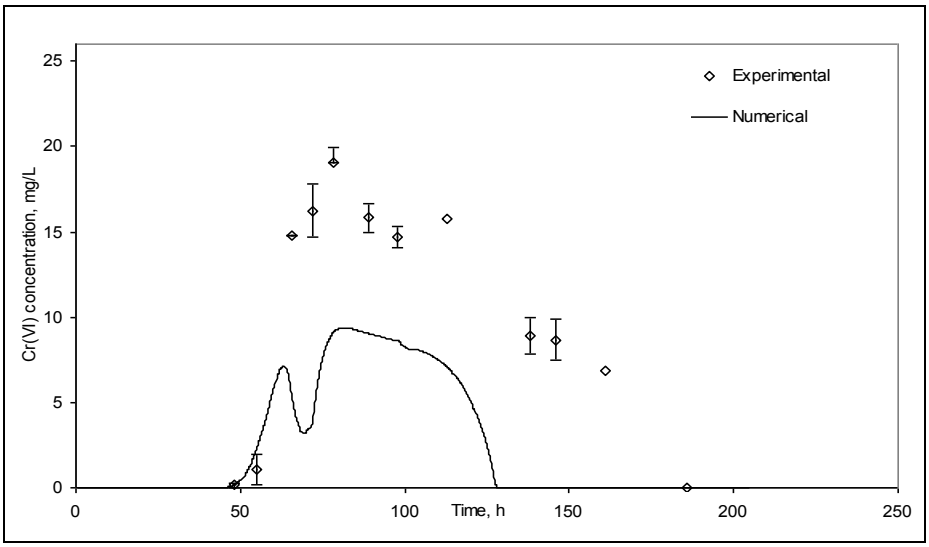

Fig. 7.15 (d): Experimental and numerical Cr (VI) breakthrough curve at 80cm port of soil B column; with biotransformation (pH 6.2-7.2, inlet Cr (VI) concentration 25 mg/L, pore velocity 1.16 cm/h)

Comparison of the mathematical model and experimental data for Soils A, B, and C shows that in case of Soil B (sand), the prediction of breakthrough curves was more accurate. This may be due to more homogeneity in the case of sand, compared to that of Soils A and C, which contained various levels of clay and silt. Non-even accumulation of gas generated due to biotransformation might have also introduced considerable non-homogeneity in case of clayey soils. This effect was not considered in the simple mathematical model.

7.2.4 Simulation of Transport and Biotransformation in Bio-barriers

Table 7.3 shows the input values for various parameters used in the mathematical simulations for the bio-barrier experiments. In these experiments, measurement of bacterial concentration in the outlet reservoir showed that there was considerable bacterial wash out during the stabilization period. Assuming that wash out had occurred uniformly from the bio-barrier and there was no retention of washed out biomass in the downstream column, the initial biomass concentration for biotransformation of Cr (VI) in

the bio-barrier was estimated as 0.0205 mg/g in BB1 and 0.1805 mg/g in BB2. The column experiments also indicated some biotransformation on the upstream side of the bio-barrier. This was due to the presence of small amount of biomass in the sand portion, which might have entered and accumulated through the feed. In the mathematical simulations, this concentration was assumed as 10 mg/L, which was almost negligible compared to the concentration of biomass in the barrier. As earlier, the dispersivity values for sand and barrier (Soil C) portions were estimated using the lithium breakthrough curves. These values matched closely with the values estimated earlier for sand and Soil C. Values of λ for sand and Soil C as determined from the earlier transport with biotransformation experiments were used here also.

Table 7.3: Input values for Model Simulations of Bio-barrier Experiments

S.NO.	PARAMETER	VALUE
1	μ_{max} (1/h)	0.3
2	Y	0.263
3	η	0.3
4	λ for Soil B	0.065
5	λ for Soil C	0.1
6	K_s (mg/L)	40.0
7	K_i (mg/L)	3.049
8	K_d (1/h)	0.0

Figs. 7.16 (a) to 7.16 (e) and 7.17 (a) to 7.17 (e) and 7.18 (a) to 7.18 (e) show the comparison between numerically simulated and experimental breakthrough curves for Cr (VI), molasses and lithium for BB1. It can be seen from these figures that the numerical model could simulate the experimental results satisfactorily.

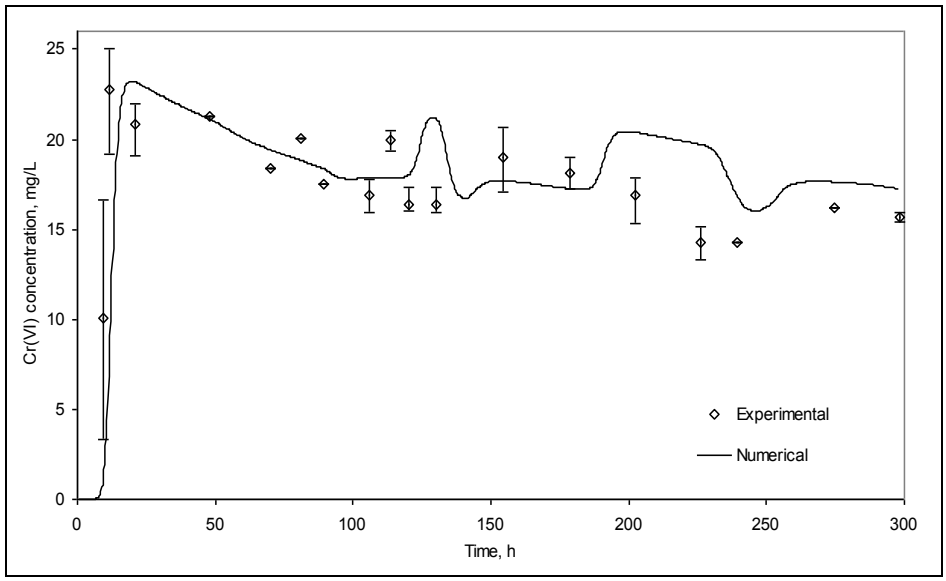

Fig. 7.16 (a): Experimental and numerical Cr (VI) breakthrough curve at 20 cm port of BB1; (pH 6.2-7.2, inlet Cr (VI) concentration 25 mg/L, pore velocity 1.6 cm/h)

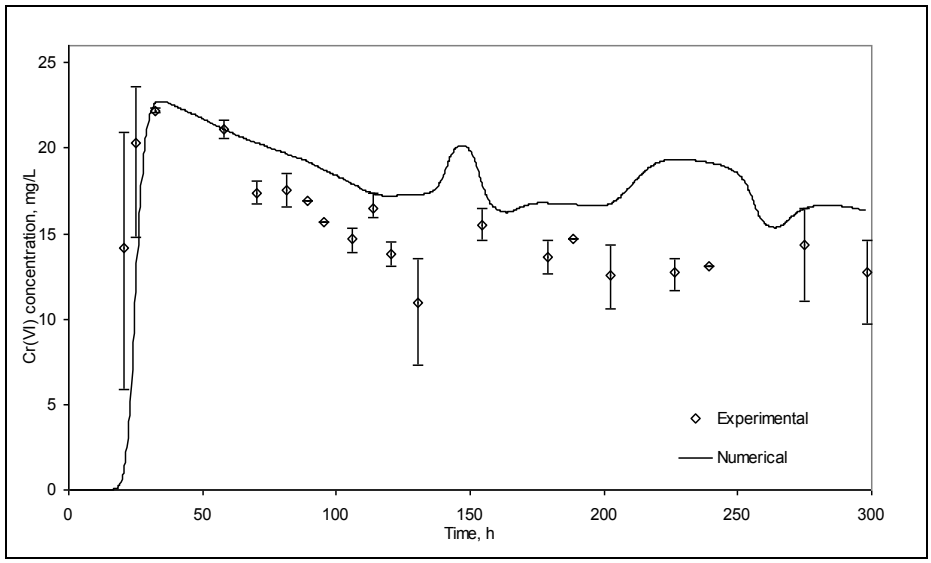

Fig. 7.16 (b): Experimental and numerical Cr (VI) breakthrough curve at 40cm port of BB1; (pH 6.2-7.2, inlet Cr (VI) concentration 25 mg/L, pore velocity 1.6 cm/h)

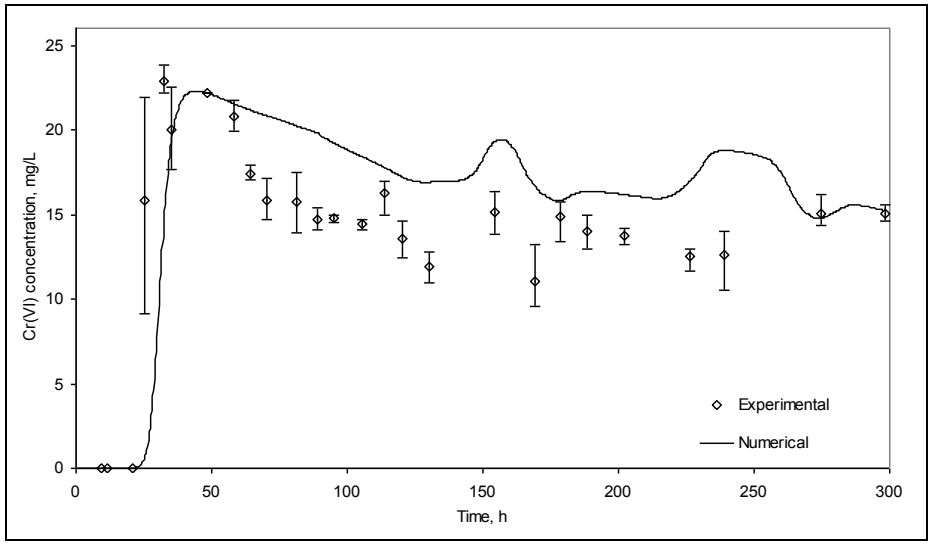

Fig. 7.16 (c): Experimental and numerical Cr (VI) breakthrough curve at 49cm port of BB1; (pH 6.2-7.2, inlet Cr (VI) concentration 25 mg/L, pore velocity 1.6 cm/h)

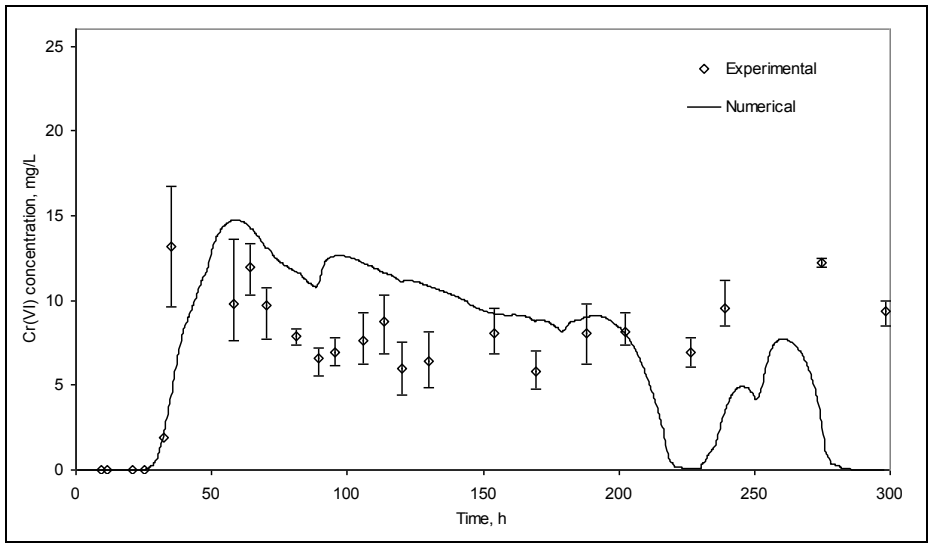

Fig. 7.16 (d): Experimental and numerical Cr (VI) breakthrough curve at 60cm port of BB1; (pH 6.2-7.2, inlet Cr (VI) concentration 25 mg/L, pore velocity 1.6 cm/h)

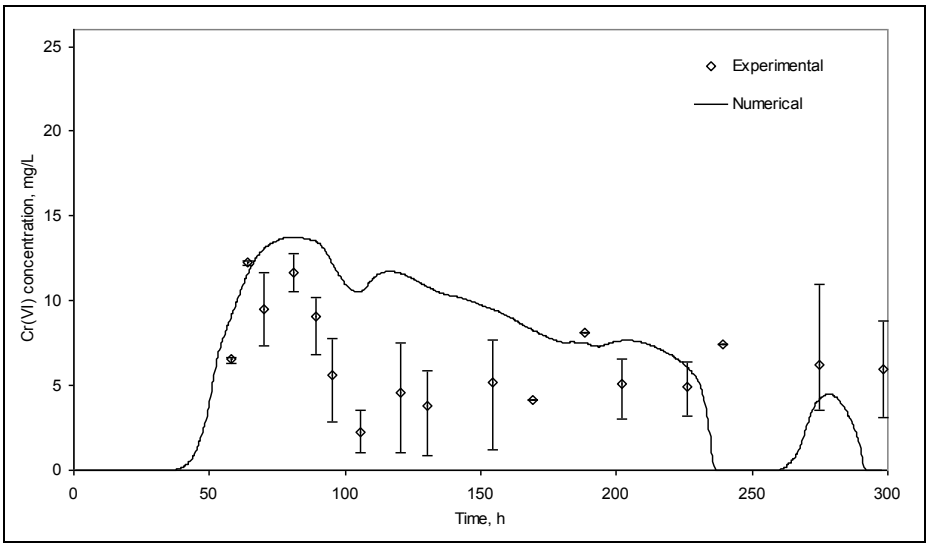

Fig. 7.16 (e): Experimental and numerical Cr(VI) breakthrough curve at 80cm port of BB1; (pH 6.2-7.2, inlet Cr(VI) concentration 25 mg/L, pore velocity 1.6 cm/h)

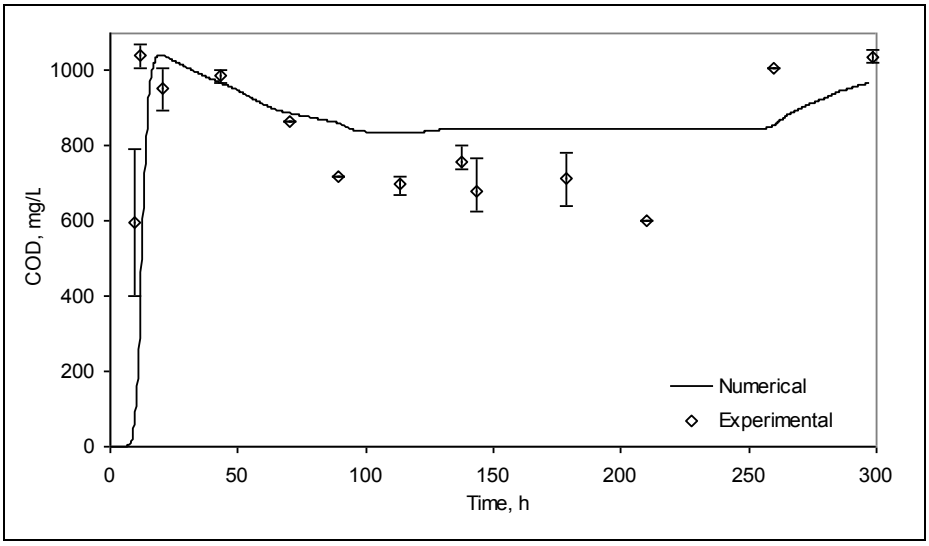

Fig. 7.17 (a): Experimental and numerical substrate breakthrough curve at 20cm port of BB1; (pH 6.2-7.2, inlet COD concentration 1000 mg/L, pore velocity 1.6 cm/h)

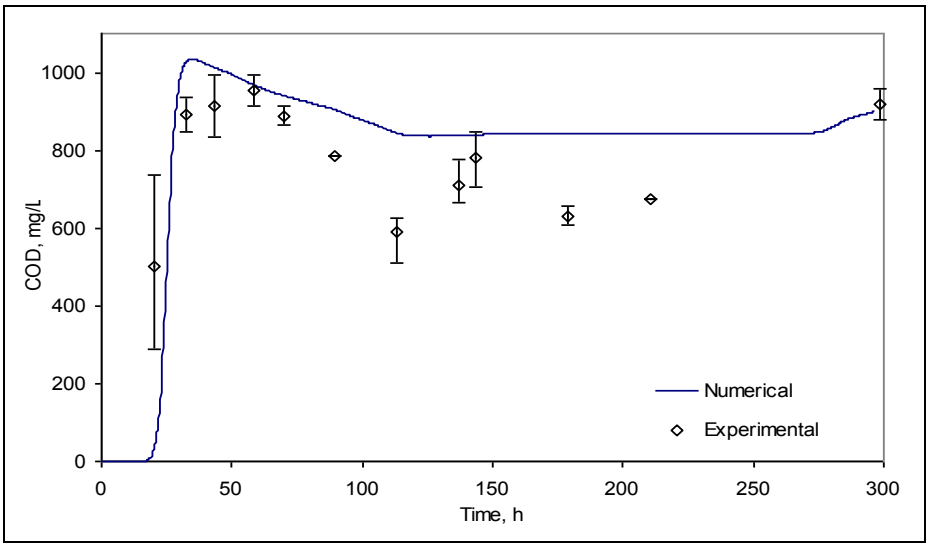

Fig. 7.17 (b): Experimental and numerical substrate breakthrough curve at 40cm port of BB1; (pH 6.2-7.2, inlet COD concentration 1000 mg/L, pore velocity 1.6 cm/h)

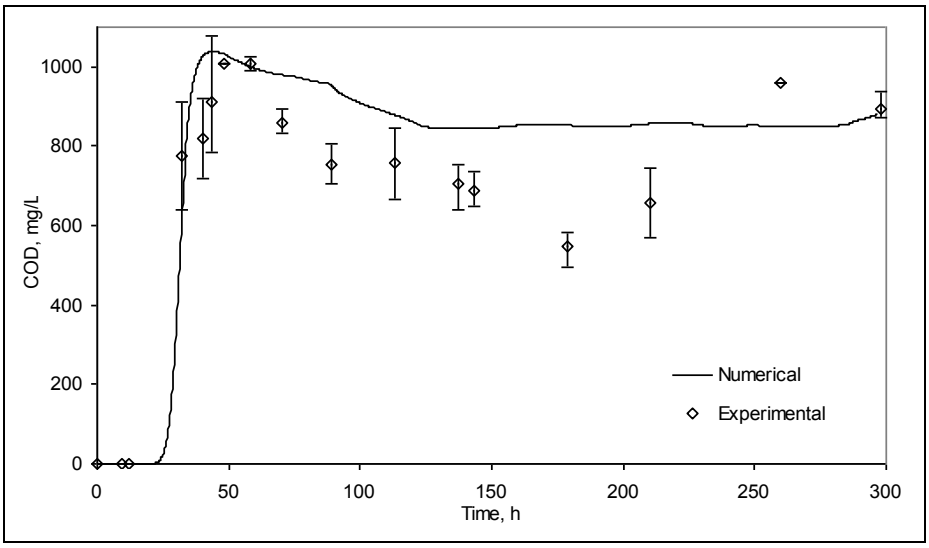

Fig. 7.17 (c): Experimental and numerical substrate breakthrough curve at 49 cm port of BB1; (pH 6.2-7.2, inlet COD concentration 1000 mg/L, pore velocity 1.6 cm/h)

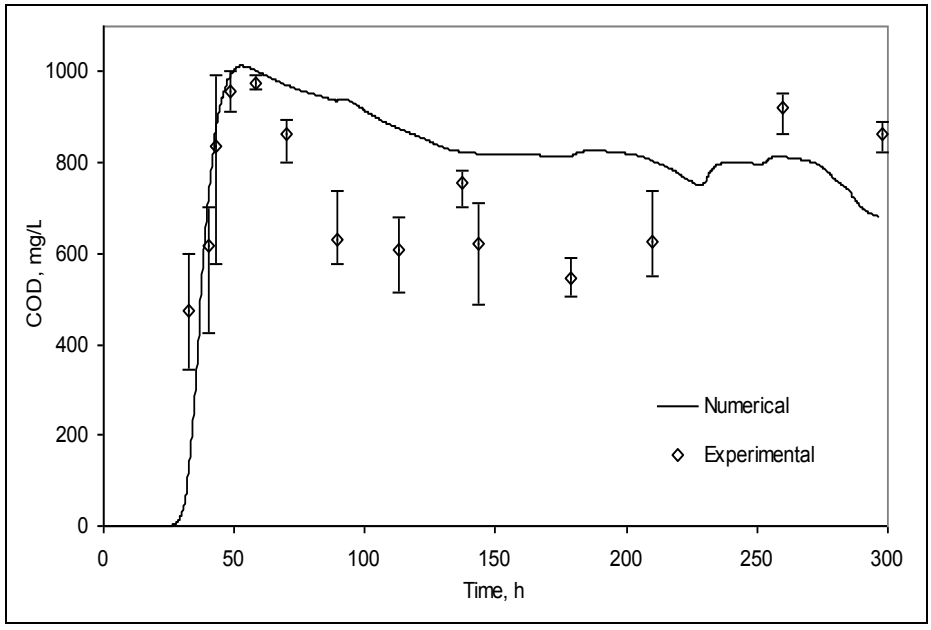

Fig. 7.17 (d): Experimental and numerical substrate breakthrough curve at 60cm port of BB1; (pH 6.2-7.2, inlet COD concentration 1000 mg/L, pore velocity 1.6 cm/h)

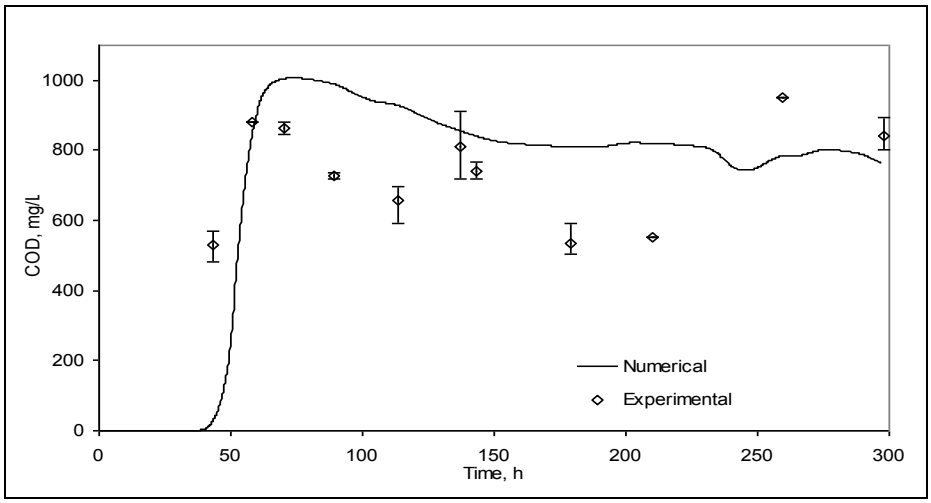

Fig. 7.17 (e): Experimental and numerical substrate breakthrough curve at 80cm port of BB1; (pH 6.2-7.2, inlet COD concentration 1000 mg/L, pore velocity 1.6 cm/h)

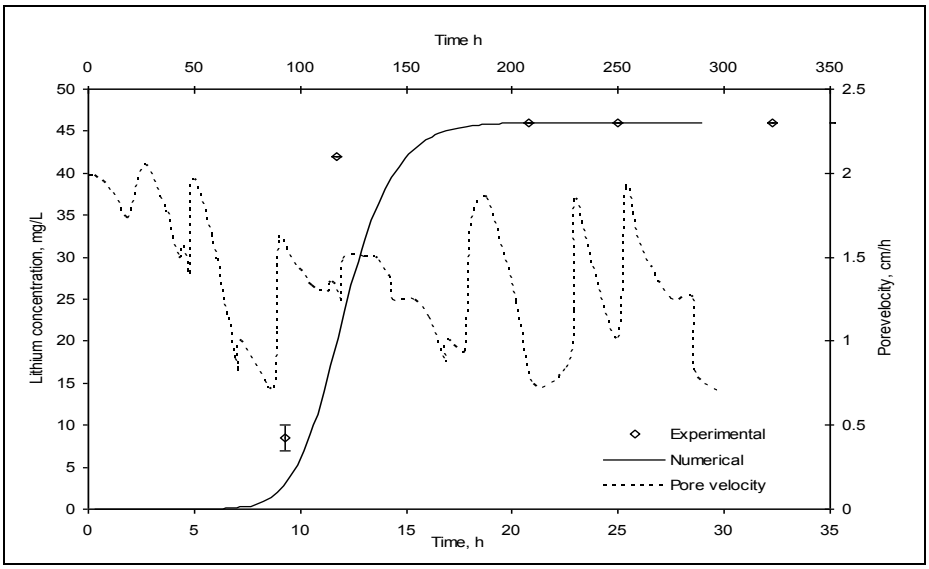

Fig. 7.18 (a): Experimental and numerical lithium breakthrough curve at 20cm port of BB1; (pH 6.2-7.2, inlet lithium concentration 46 mg/L, pore velocity 1.6 cm/h)

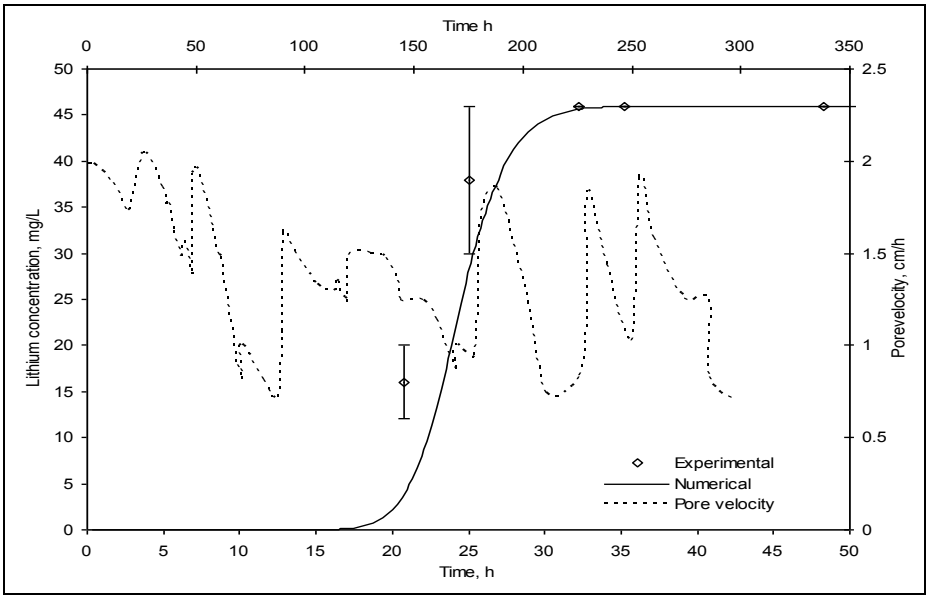

Fig. 7.18 (b): Experimental and numerical lithium breakthrough curve at 40cm port of BB1; (pH 6.2-7.2, inlet lithium concentration 46 mg/L, pore velocity 1.6 cm/h)

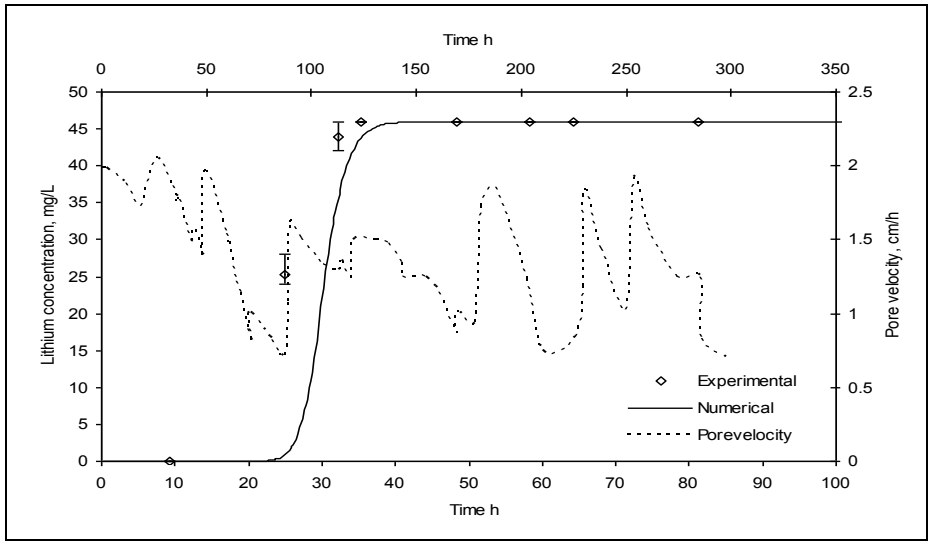

Fig. 7.18 (c): Experimental and numerical lithium breakthrough curve at 49cm port of BB1; (pH 6.2-7.2, inlet lithium concentration 46 mg/L, pore velocity 1.6 cm/h)

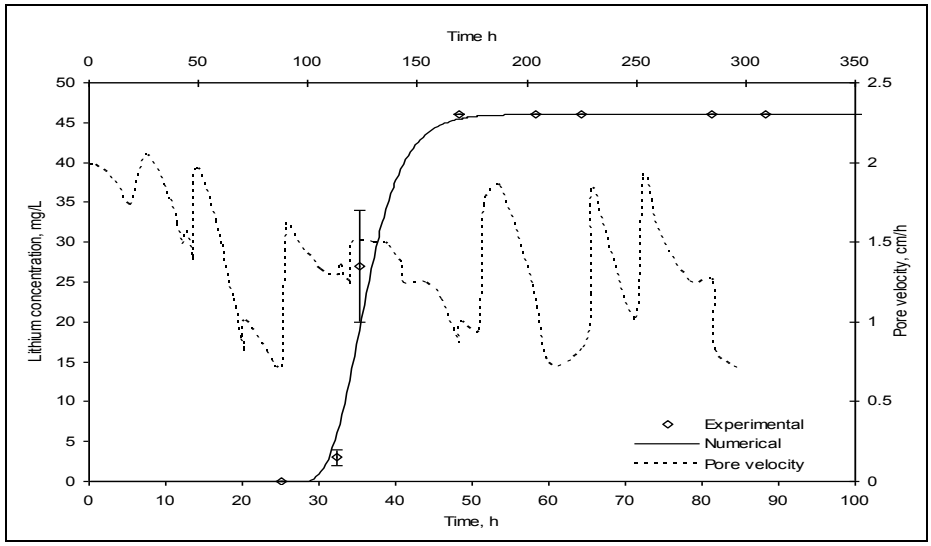

Fig. 7.18 (d): Experimental and numerical lithium breakthrough curve at 60cm port of BB1; (pH 6.2-7.2, inlet lithium concentration 46 mg/L, pore velocity 1.6 cm/h)

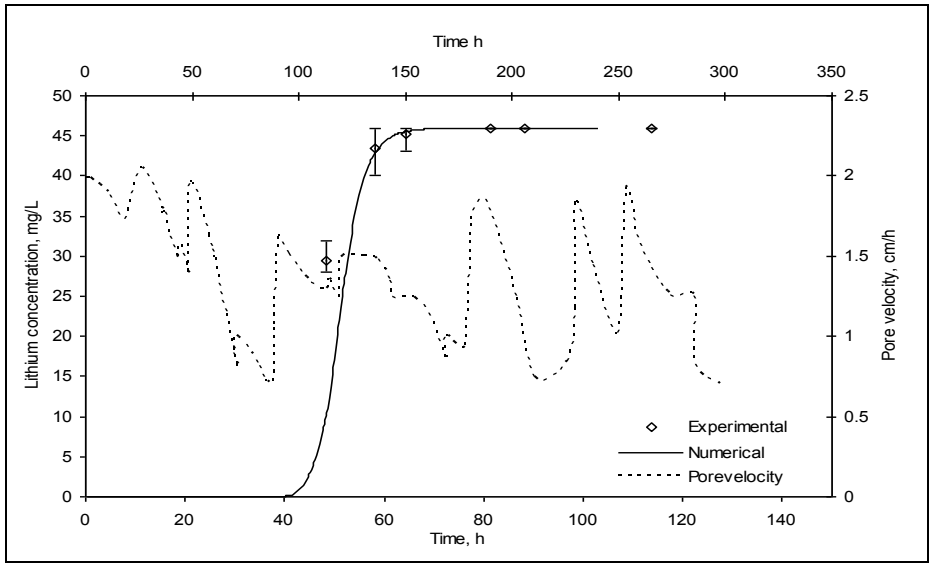

Fig. 7.18 (e): Experimental and numerical lithium breakthrough curve at 80cm port of BB1; (pH 6.2-7.2, inlet lithium concentration 46 mg/L, pore velocity 1.6 cm/h)

Comparison between the numerical model and experimental results for BB2 are presented in Figs. 7.19 (a) to 7.19 (e) and Figs. 7.20 (a) to 7.20 (e). It is evident from these figures that the matching between the numerical model and experimental results was not as good, especially at the 60 cm port (downstream of barrier). These results are in conformity with the earlier results that biotransformation affects the hydrogeology of the aquifer and increases the non-homogeneity. This affect was more significant in cases where the biomass concentration is high, as expected.

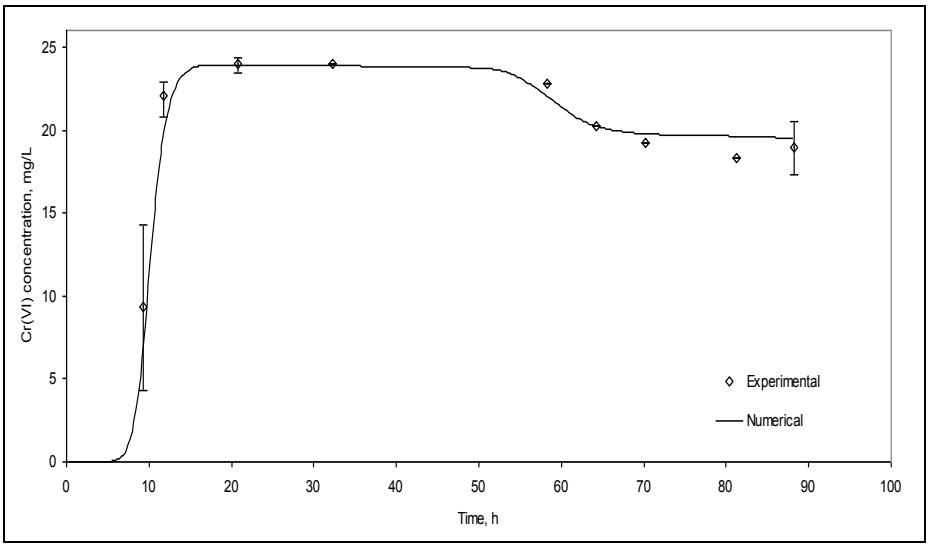

Fig. 7.19 (a): Experimental and numerical Cr (VI) breakthrough curve at 20cm port of BB2; (pH 6.2-7.2, inlet Cr (VI) concentration 25 mg/L, pore velocity 1.6 cm/h)

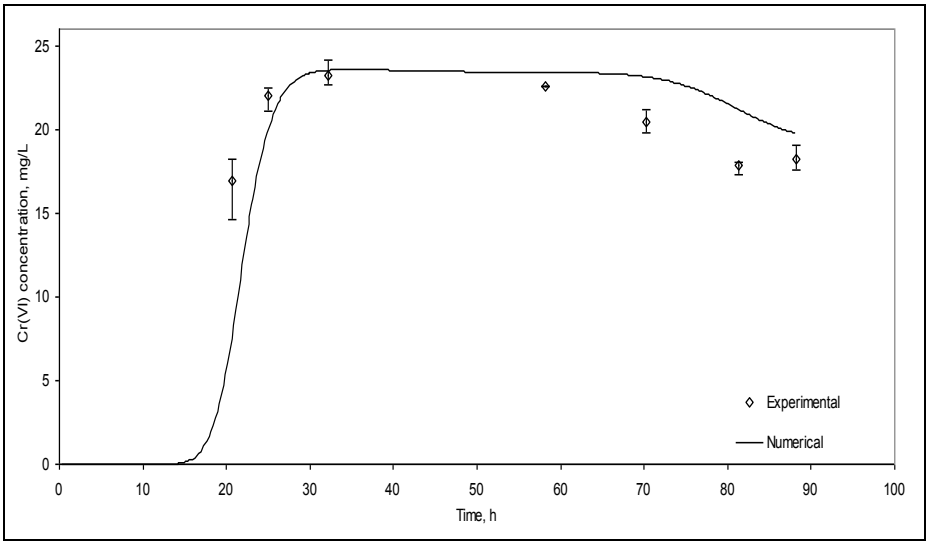

Fig. 7.19 (b): Experimental and numerical Cr (VI) breakthrough curve at 40cm port of BB2; (pH 6.2-7.2, inlet Cr (VI) concentration 25 mg/L, pore velocity 1.6 cm/h

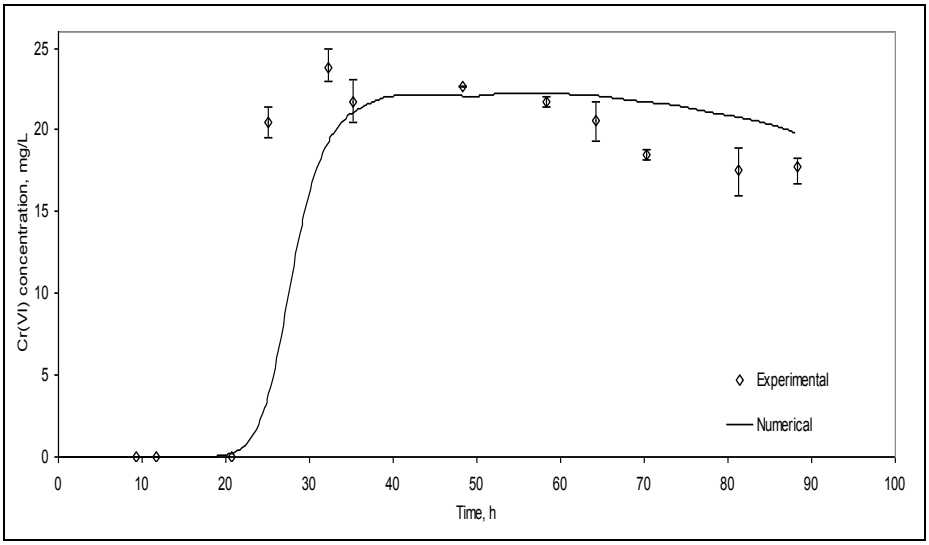

Fig. 7.19 (c): Experimental and numerical Cr (VI) breakthrough curve at 49 cm port of BB2; (pH 6.2-7.2, inlet Cr (VI) concentration 25 mg/L, pore velocity 1.6 cm/h)

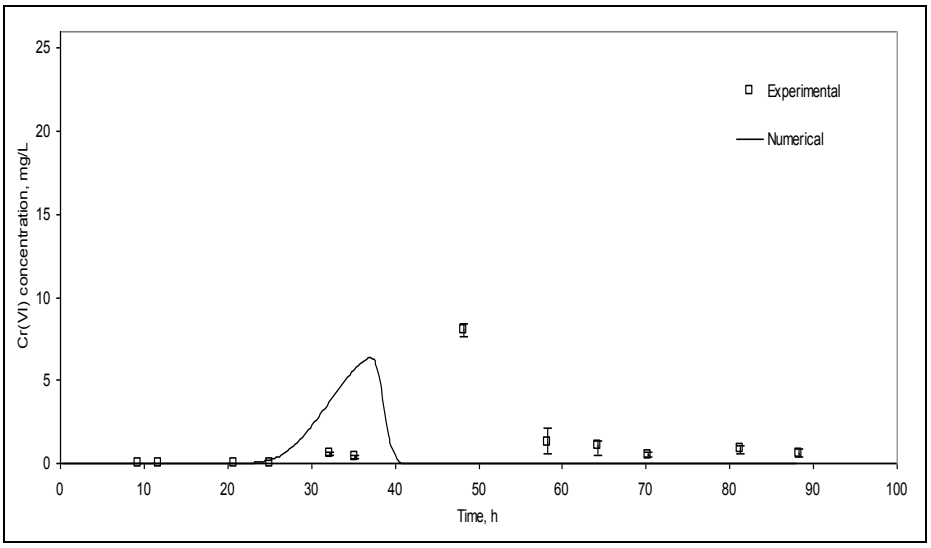

Fig. 7.19 (d): Experimental and numerical Cr (VI) breakthrough curve at 60cm port of BB2; (pH 6.2-7.2, inlet Cr (VI) concentration 25 mg/L, pore velocity 1.6 cm/h)

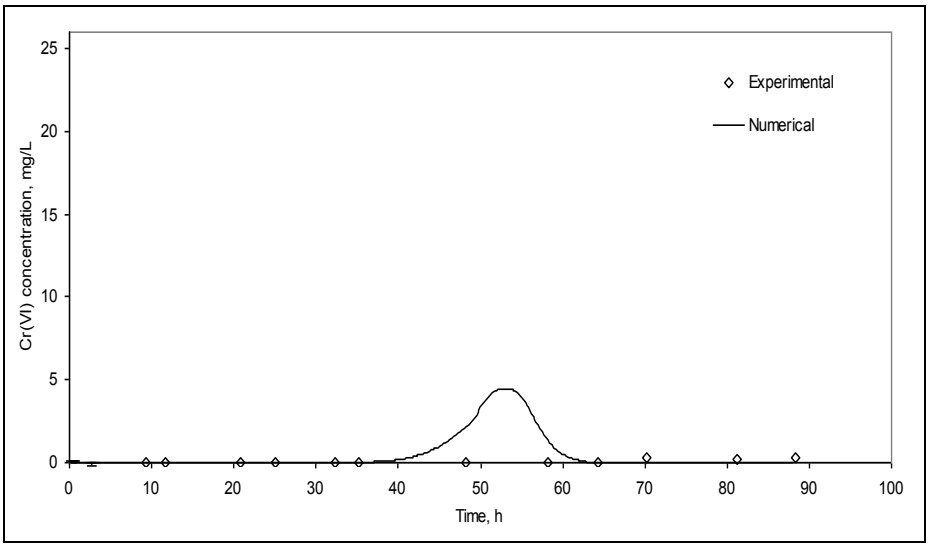

Fig. 7.19 (e): Experimental and numerical Cr(VI) breakthrough curve at 80cm port of BB2; (pH 6.2-7.2, inlet Cr(VI) concentration 25 mg/L, pore velocity 1.6 cm/h)

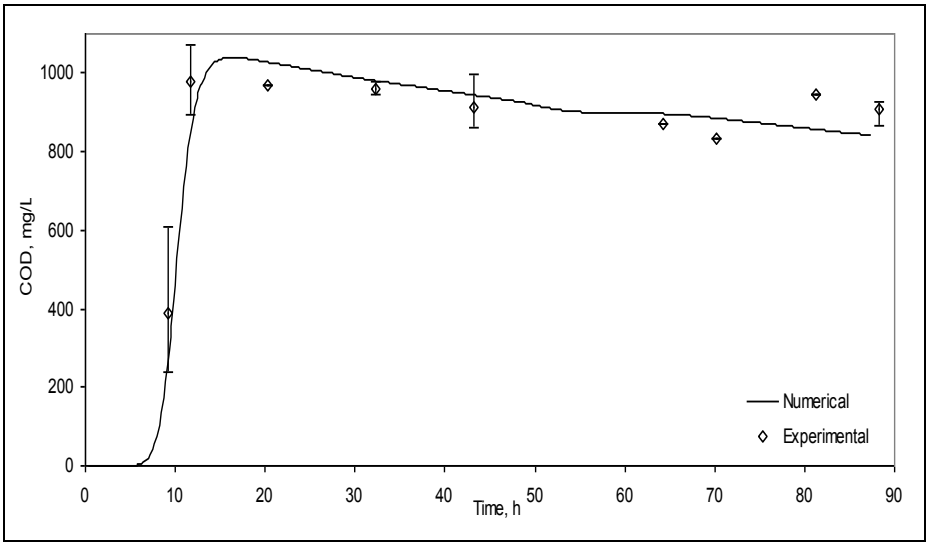

Fig. 7.20 (a): Experimental and numerical substrate breakthrough curve at 20cm port of BB2; (pH 6.2-7.2, inlet COD concentration 1000 mg/L, pore velocity 1.6 cm/h)

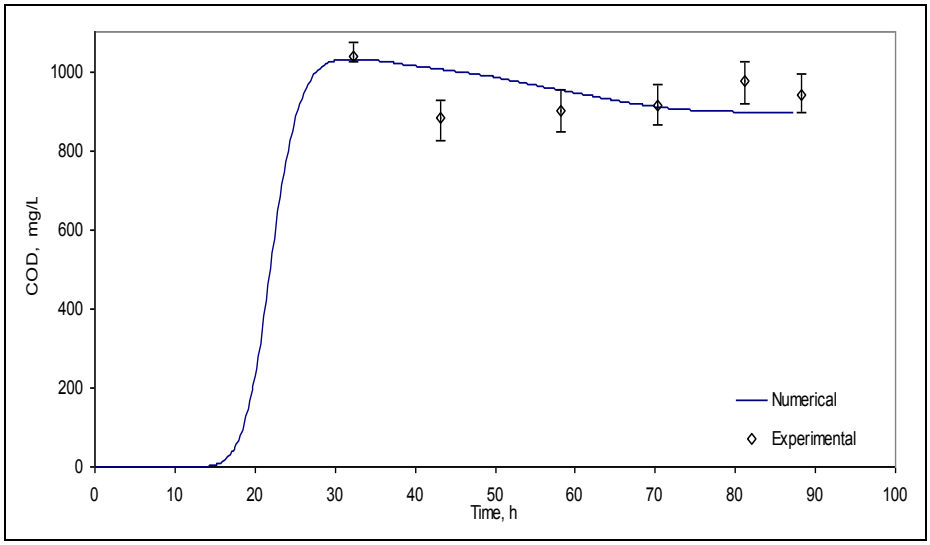

Fig. 7.20 (b): Experimental and numerical substrate breakthrough curve at 40cm port of BB2; (pH 6.2-7.2, inlet COD concentration 1000 mg/L, pore velocity 1.6 cm/h)

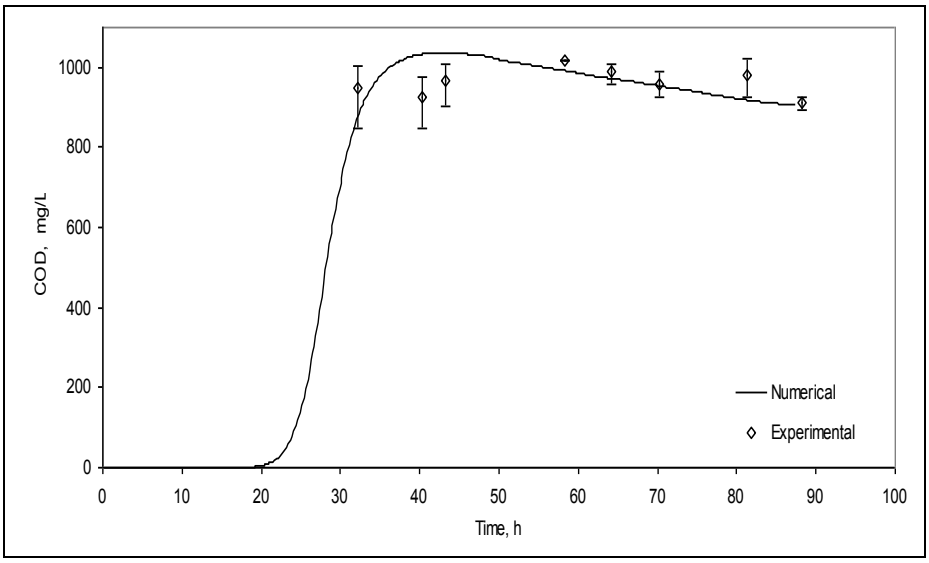

Fig. 7.20 (c): Experimental and numerical substrate breakthrough curve at 49cm port of BB2; (pH 6.2-7.2, inlet COD concentration 1000 mg/L, pore velocity 1.6 cm/h)

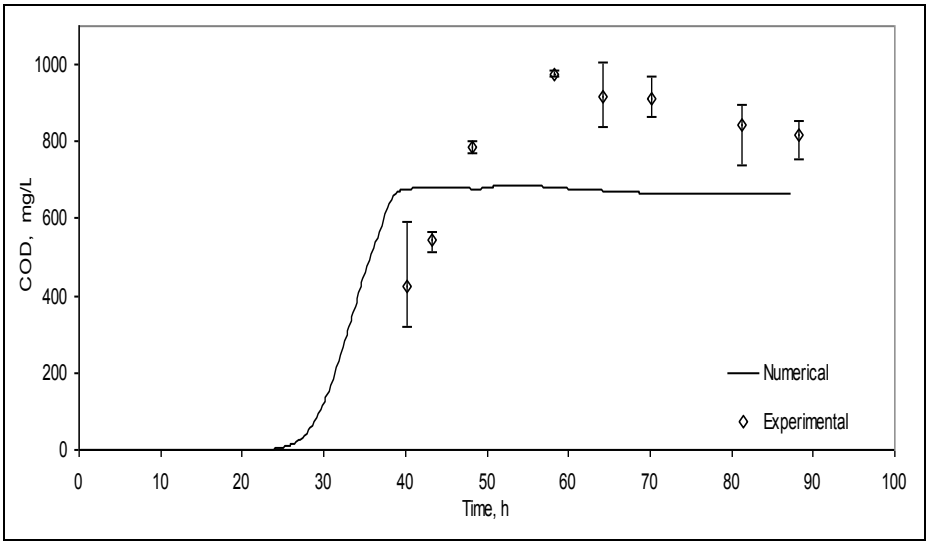

Fig. 7.20 (d): Experimental and numerical substrate breakthrough curve at 60cm port of BB2; (pH 6.2-7.2, inlet COD concentration 1000 mg/L, pore velocity 1.6 cm/h)

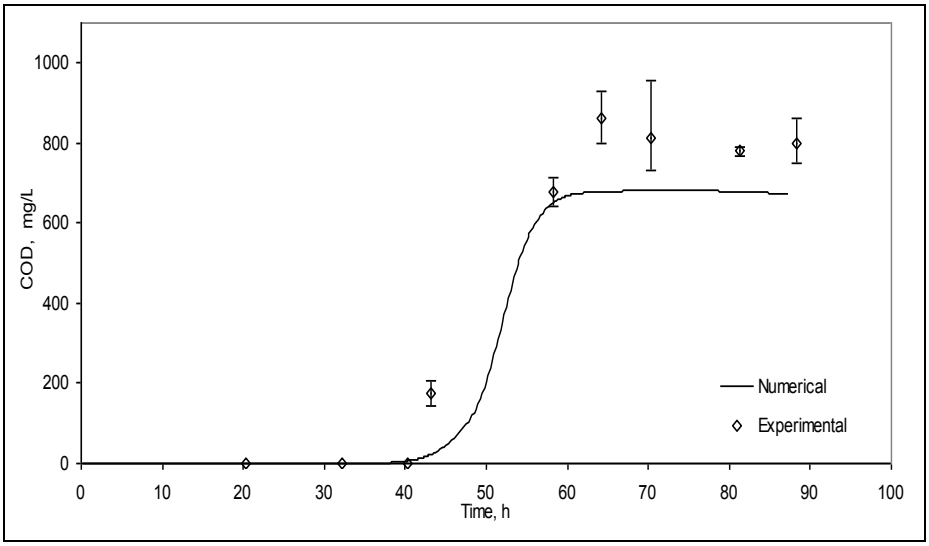

Fig. 7.20 (e): Experimental and numerical substrate breakthrough curve at 80cm port of BB2; (pH 6.2-7.2, inlet COD concentration 1000 mg/L, pore velocity 1.6 cm/h)

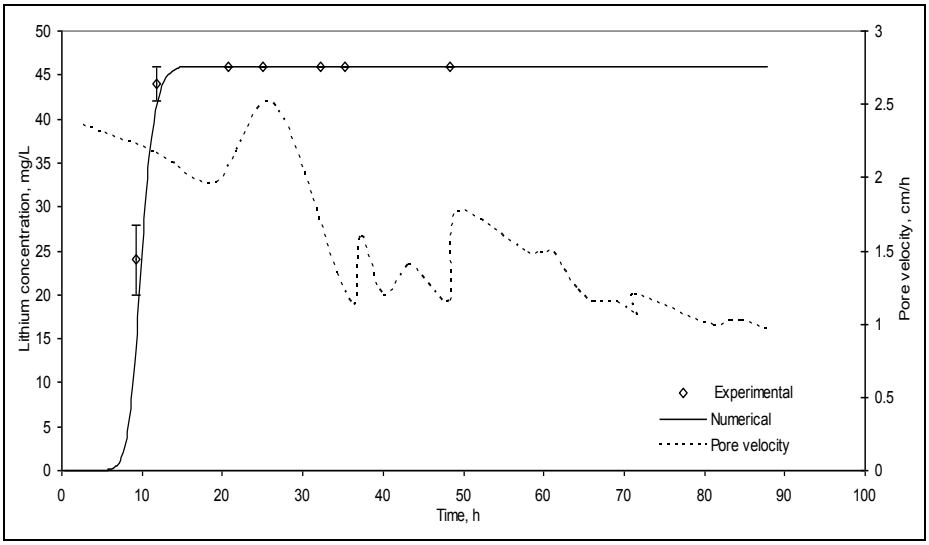

Fig. 7.21 (a): Experimental and numerical lithium breakthrough curve at 20cm port of BB2; (pH 6.2-7.2, inlet lithium concentration 46 mg/L, pore velocity 1.6 cm/h)

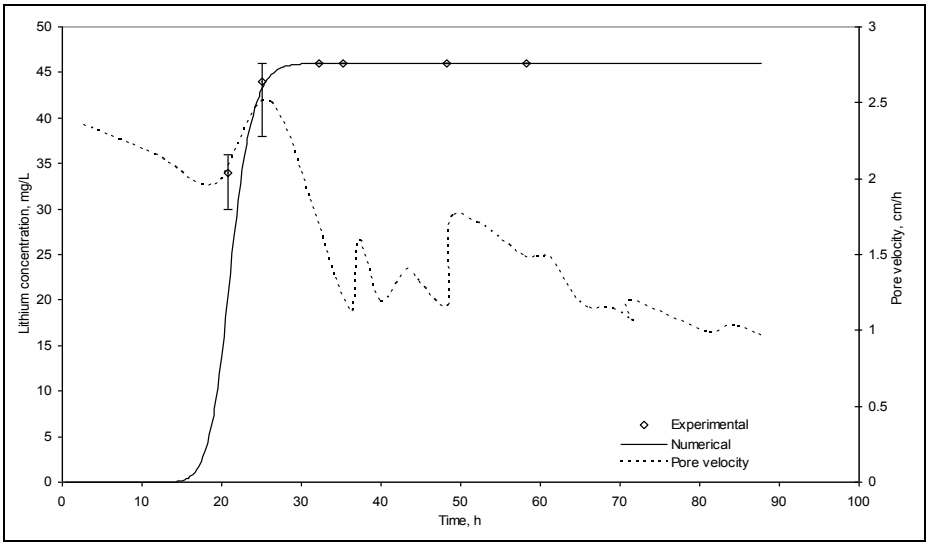

Fig. 7.21 (b): Experimental and numerical lithium breakthrough curve at 40cm port of BB2; (pH 6.2-7.2, inlet lithium concentration 46 mg/L, pore velocity 1.6 cm/h)

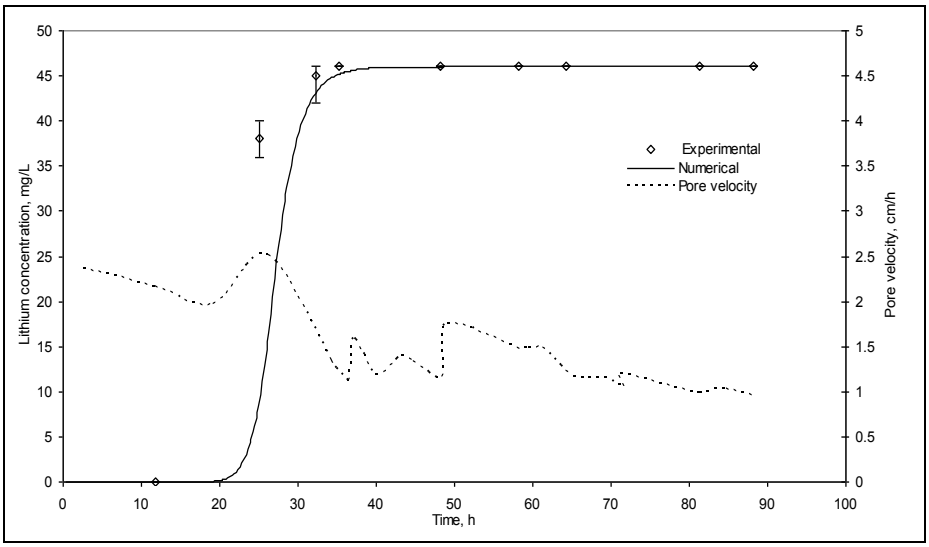

Fig. 7.21 (c): Experimental and numerical lithium breakthrough curve at 49 cm port of BB2; (pH 6.2-7.2, inlet lithium concentration 46 mg/L, pore velocity 1.6 cm/h)

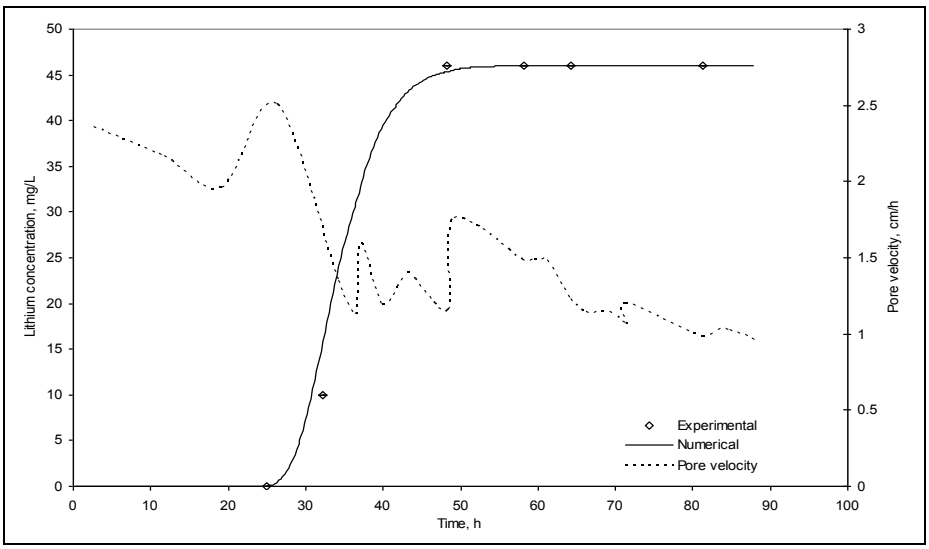

Fig. 7.21 (d): Experimental and numerical lithium breakthrough curve at 60cm port of BB2; (pH 6.2-7.2, inlet lithium concentration 46 mg/L, pore velocity 1.6 cm/h)

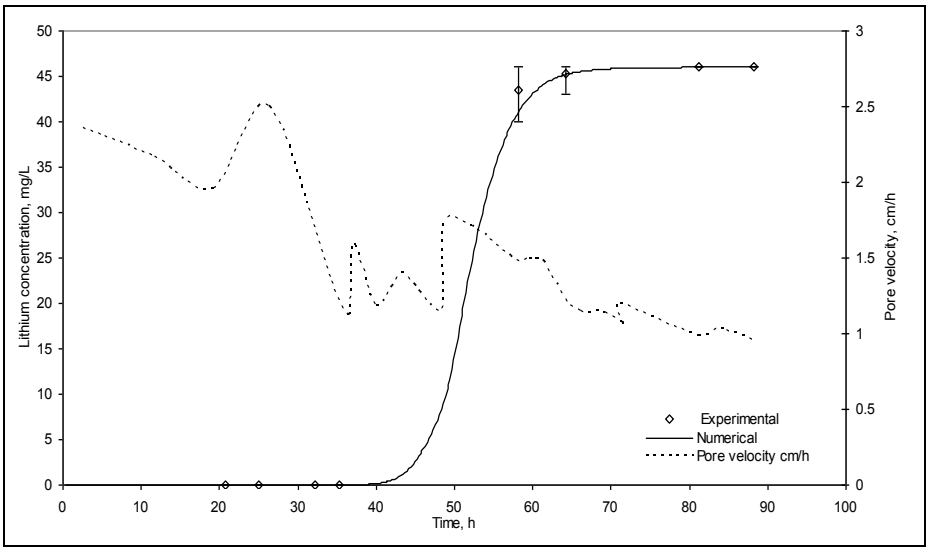

Fig. 7.21(e): Experimental and numerical lithium breakthrough curve at 80cm port of BB2; (pH 6.2-7.2, inlet lithium concentration 46 mg/L, pore velocity 1.6 cm/h)

7.3 TWO-DIMENSIONAL MODEL FOR TRANSPORT WITH BIOTRANSFORMATION

Based on the governing equations of the proposed two-dimensional model for transport with biotransformation, a computer code has been developed to solve the groundwater flow equations as well as the equations for transport and bioremediation of Cr^{6+} with the help of the numerical techniques discussed in previous chapters. This two-dimensional model is validated in this section using the results available in the literature and the experimental data obtained on pilot scale reactors. It is also demonstrated how the proposed model can be used to study the efficacy of reaction zone technique for containing the hexavalaent chromium in groundwater.

7.3.1 Validation of Groundwater Flow Code

The computer code for simulating the groundwater flow was tested for two illustrative cases. In the first case, a rectangular unconfined aquifer of length 1000 m was

considered. Initial conditions for this aquifer corresponded to a one-dimensional steady state, with constant heads on either side of flow direction (i.e. h_i = 4m and h_l = 3.5m) and no flow boundary conditions on the lateral boundaries. At time t = 0, piezometric head on one side, h_i was instantaneously increased from 4m to 4.5m. In response to this change in the head, the aquifer attained the steady state corresponding to h_i = 4.5m and h_l =3.5m as the boundary condition, after infinite time.

The computational time step Δt was 1000 seconds and the grid size was: Δx =20 m and Δy =20 m. Figure 7.22 shows the comparison between the analytical and simulated results corresponding to this new steady state. The maximum error occurred is at the center of the aquifer and its value is 0.15%, which is well within the tolerance limits.

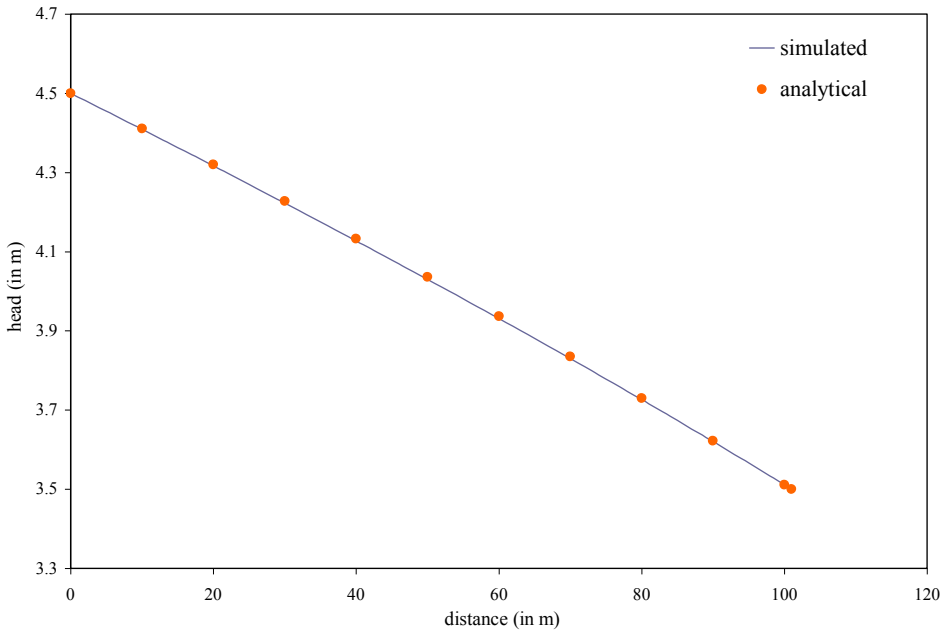

Fig. 7.22 Validation of groundwater flow code, Test 1

In the second case, an unconfined aquifer (1000m × 1000m) was recharged at a constant rate of 0.1 lit/s at the center of the aquifer. In response to this, the aquifer attained a steady state after a long time. At this stage, the head follows a logarithmic relationship. In

the numerical simulations for this case, the computational time step Δt was 1000 seconds and the grid size was: Δx=10 m and Δy=10 m. Figure 7.23 shows the comparison between simulated and analytical results for this test case. In both the test cases, the results obtained from the groundwater flow code are satisfactory. The first test case here validates the one-dimensional part of the code and the second test case validates the two-dimensional part of the code.

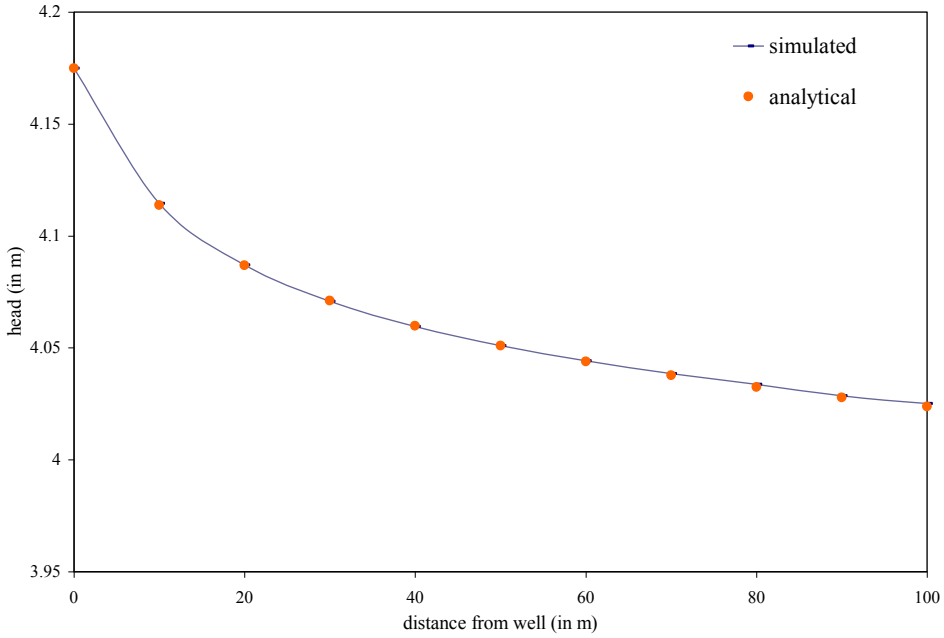

Fig. 7.23 Validation of groundwater flow code, Test 2

7.3.2 Validation of Transport Code with Analytical and Bench Scale Experimental Results

7.3.2.1 Transport Code for Conservative Contaminant

Two-dimensional transport code for a conservative contaminant is tested for three cases. The first case considered unsteady 2D solute transport in a domain as shown in Fig. 7.24. A finite-length strip solute source, whose concentration was a given function of time, was located asymmetrically along the z-axis at x=0 in a unidirectional seepage velocity field, as shown in Fig. 7.24. The rectangular domain is 75 m × 50 m. B_1= 5 m, B_2=10 m, B_3=

35 m. The uniform pore velocity was 0.1m/day. The longitudinal, transverse and cross dispersivities D_{xx}, D_{zz}, D_{xz} were 1.0, 0.1 and 0.0 m^2/day, respectively. The retardation factor was 1.0. The initial concentration was given by C(x, z, 0) =0. The boundary condition at x=0, t > 0, is given by

$$C(0, z, t) = 0 \qquad 0 < z < B_1$$

$$C(0, z, t) = 1 \quad B_1 < z < B_1 + B_2$$

$$C(0, z, t) = 0 \quad B_1 + B_2 < z < z_m$$

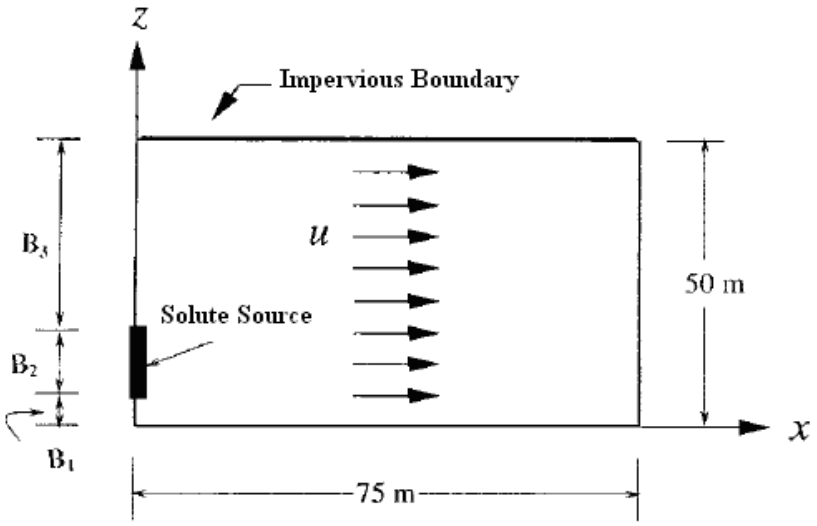

Fig. 7.24 Schematic diagram for validating transport code, Test 1

In the numerical simulations, the computational time step Δt was 1 day. The courant number, C_n =0.08, and the longitudinal grid Peclet number is P_Δ = 0.125. Total time t = 100 days. Figs. 7.25a and 7.25b show the comparison between the analytical and the simulated results as a function of distance x, at z = 10m and 16.25m, respectively, at time t = 100 days.

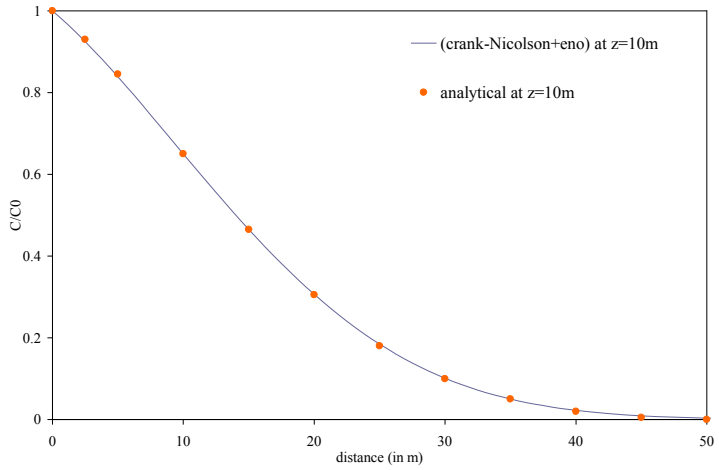

Fig. 7.25a Validation of transport code, Test 1, results at z = 10 m

The second test case for validating the transport code also considered a domain as shown in Fig. 7.24. However, the flow field is inclined throughout the domain, and the size of the domain is 7 m × 6 m. All the other conditions are similar to those for Test-1, with $B_1 = 0.5$ m, $B_2 = 1.0$ m, $B_3 = 4.5$ m. $D_{xx} = D_{zz} = 0.01\, m^2$/day.

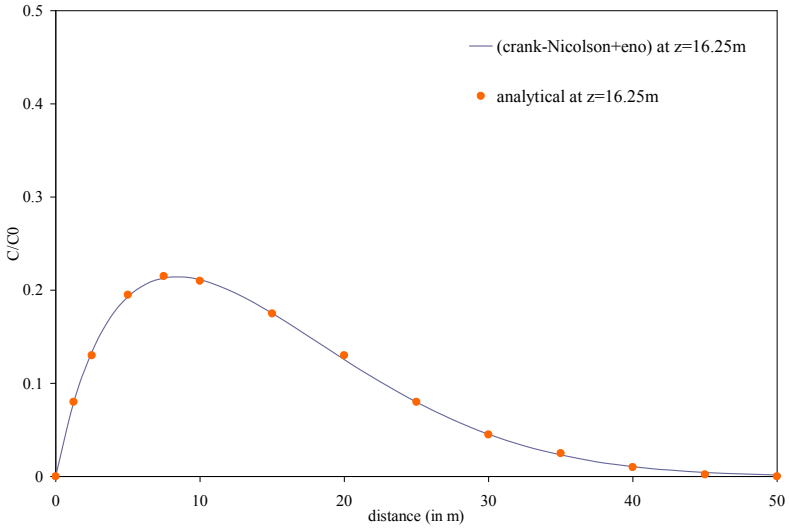

Fig. 7.25b Validation of transport code, Test 1, results at z = 16.25m.

In the numerical simulations, the computational time step Δt was 0.2 day. Uniform grid spacing $\Delta x = \Delta y$ =0.05 m. The courant number C_n = 0.4, and the Peclet number, P_Δ = 0.5. Total time t = 30 days. Figure 7.26 shows the comparison between the analytical and simulated results. This figure shows the concentration contour for C = 0.1 at the end of 30 days.

In the first two cases, the Peclet number was very small (i.e., P_Δ <1). So the numerical results did not exhibit any numerical oscillations. In order to see whether the simulations are free from numerical oscillations, the proposed model was tested for a third case. The third case considers a domain of length 120 m. The upstream boundary concentration is 1.0; the pore velocity, u = 0.5 m/day; Dispersion coefficient, D = 0.0025 m^2/day. The retardation factor was 1.0. This case pertains to an advection dominated transport.

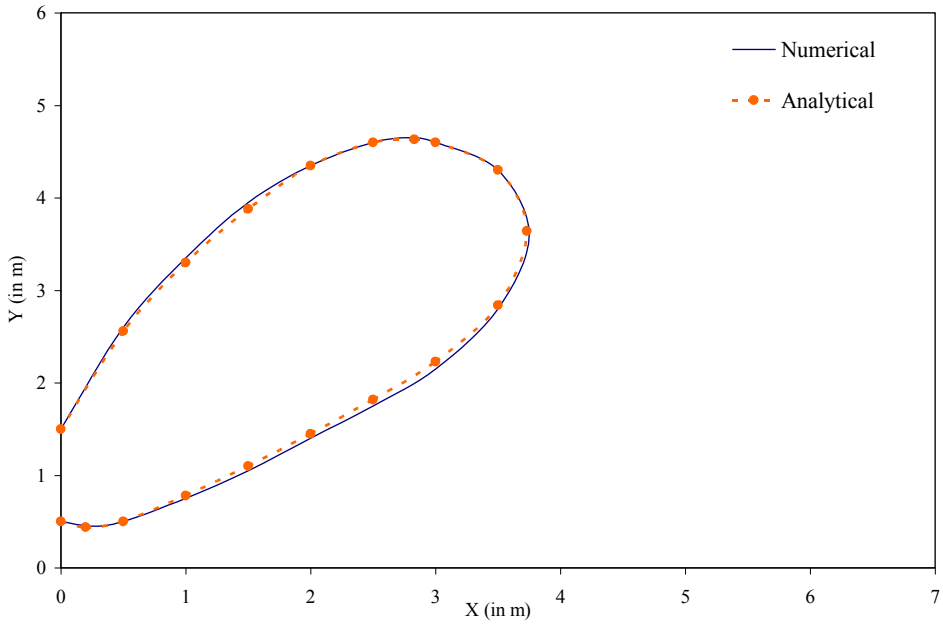

Fig. 7.26 Validation of transport code, Test 2

In the numerical simulations, the computational time step Δt was 2 days. Grid size Δx is 1 m. The courant number C_n =1, and Peclet number, P_Δ = 200. Total time t =150days.

Figure 7.27 shows the comparison between the analytical and simulated results as a function of distance x, at time t =150days.

From the three test cases, it can be seen that the results obtained using the proposed model for transport of conservative pollutant are numerically accurate and are free from numerical oscillations.

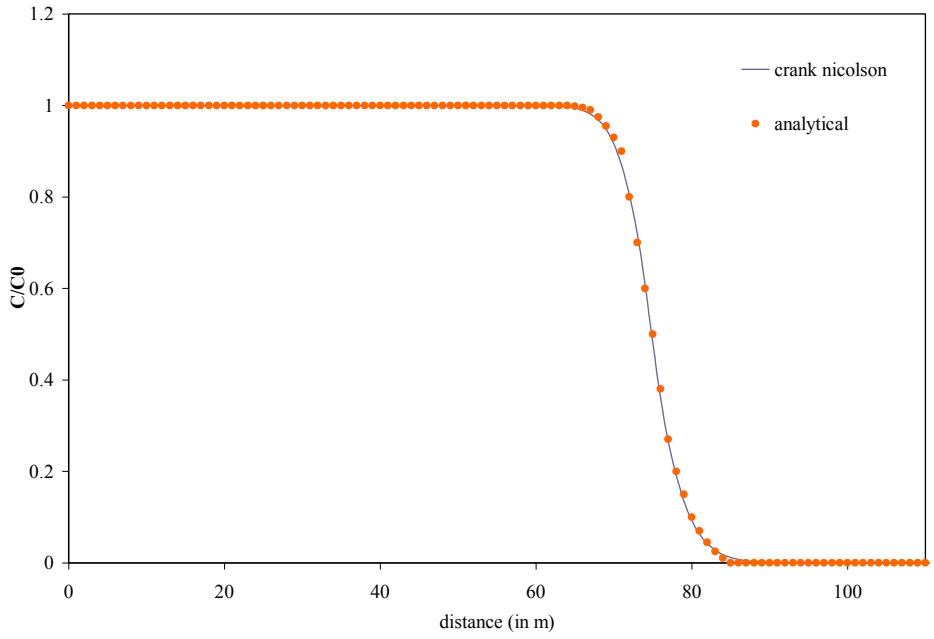

Fig. 7.27 Validation of transport code, Test 3 (advection dominated)

7.3.2.2. Transport Code for Non-Conservative Contaminant

Reactive Transport code was validated with the experimental results obtained from the literature (Shashidhar et al., 2007). In this test case, the transport and biotransformation of chromium was carried out in a model aquifer of length 100cms. Initial pore velocity was 7.32 cm/hr. The dispersivity value was equal to 3.5 cm. Initial concentrations of the chromium and the substrate in the soil were both zero. The upstream boundary concentrations of the chromium and substrate were 25 mg/l and 2000 mg/l respectively. The bacteria in the aquifer were assumed to be immobile and the initial concentration of

bacteria in the soil was 100.22 mg/L. Other input given to the model such as soil parameters, Freundlich isotherm constants and bio kinetic parameters are presented in Table 7.4, Table 7.5, and Table 7.6, respectively.

Table-7.4: Soil characteristics

soil characteristics	
porosity	0.375
bulk density	1.62

Table-7.5: Isotherm constants

Freundlich isotherm constants	K_f	n
for chromium	0.036694	1.2917
for substrate	0.044545	1.2721

Table 7.6: Biokinetic parameters

Biokinetic Parameters	
μ_{max} (1/h)	0.3
γ	0.263
η	0.3
λ	0.1
K_s (mg/l)	40
K_{im} (mg/l)	3.049

The above data was given as the input to the Reactive Transport Code. The computational time step Δt was 0.1 hr. The grid size used was $\Delta x = 2$ cm. The pore velocity, which was varying with respect to time, was taken as input. Figures 7.28 a, b, c and d show the comparison between numerically simulated and experimental data of

Cr^{6+} breakthrough at x = 20, x = 40, x = 60 and x = 80 cm respectively with time. The plot of pore velocity versus time is also shown in Fig. 7.28a.

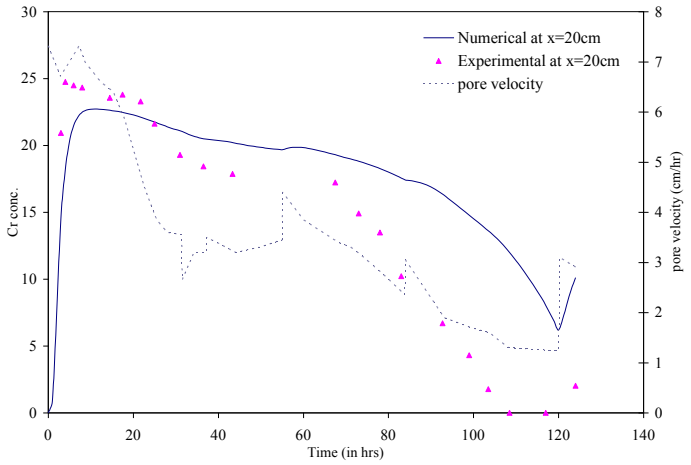

Fig. 7.28a Validation of Reactive Transport Code, numerical and experimental breakthrough curve at x = 20cm.

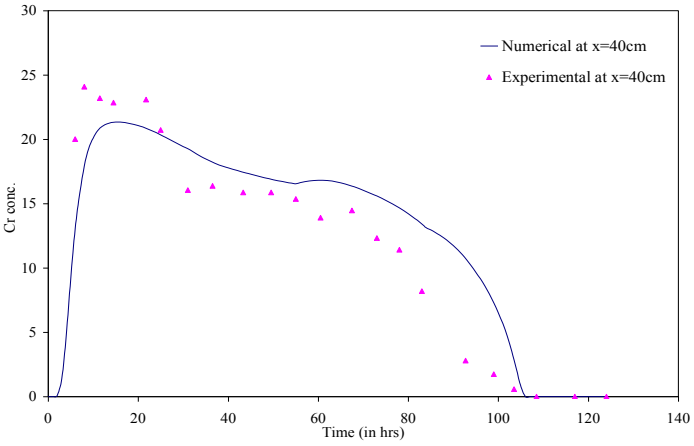

Fig. 7.28b Validation of Reactive Transport Code, numerical and experimental breakthrough curve at x = 40cm.

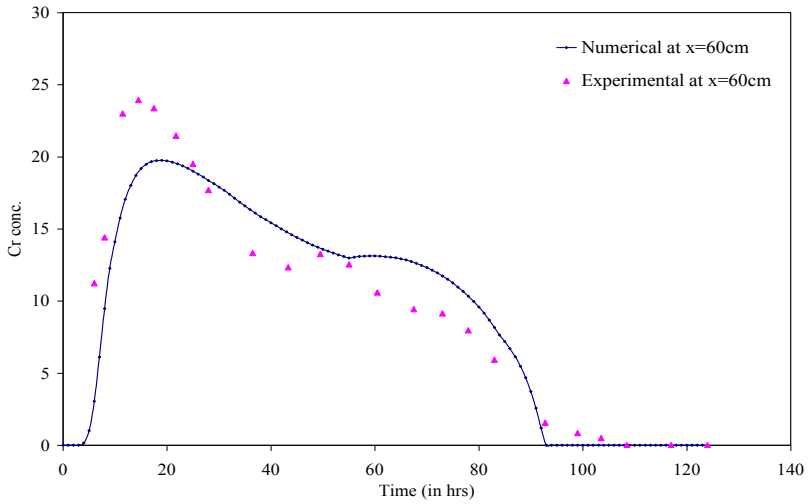

Fig. 7.28c Validation of Reactive Transport Code, numerical and experimental breakthrough curve at x = 60cm.

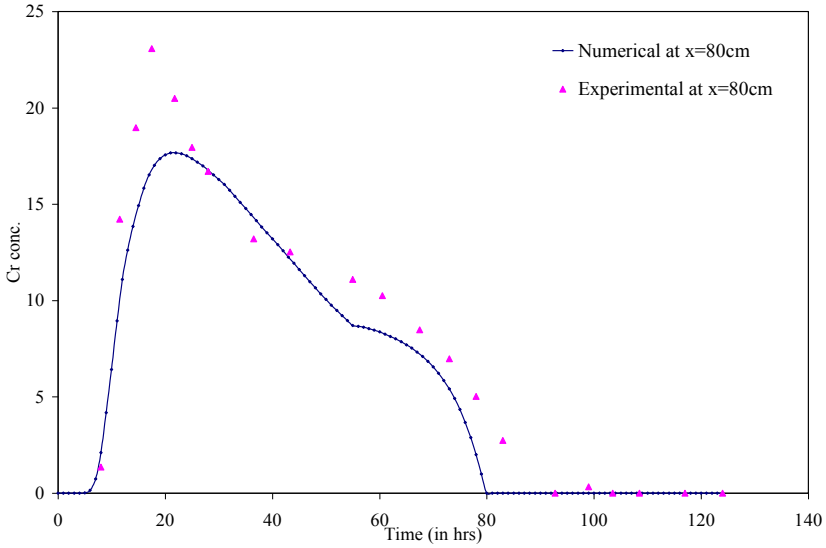

Fig. 7.28d Validation of Reactive Transport Code, numerical and experimental breakthrough curve at x = 80cm.

From Figs. 7.28 a, b, c and d, it can be seen that the numerically simulated breakthrough curves for hexavalent chromium match satisfactorily with the experimental data. It can be inferred from these results that when the pore velocity is less the biotransformation rate of hexavalent chromium is more and vice versa. It can be inferred from these results that the proposed mathematical model is able to explain the transport and biotransformation of hexavalent chromium.

7.3.3 Validation of Transport Code with Pilot Scale Experimental Results

In the previous section, two-dimensional models for groundwater flow and transport of hexavalent chromium were validated using simple bench mark problems for which analytical solutions are present, and with experimental data obtained using a bench scale column. This model is validated in this section using data obtained from pilot scale experimental reactors. The validation was carried out using data from both biobarrier and reactive-zone systems for chromium containment in an unconfined aquifer. An unconfined aquifer with either a biobarrier or injection wells (as described earlier for pilot scale reactor studies in Chapters 5 and 6) was considered for this purpose. Validation was carried out for conditions corresponding to the pilot scale studies with biobarrier (R1), control reactor (R2), two injection well system (R3), and four injection well system (R4). It may be noted that the transport module in these validation studies corresponded to the simplified model presented in Section 5.4.3. This simplified model was used here because the experimental results from pilot scale reactor studies showed that the employed bacteria could reduce Cr(VI) with a very less consumption of molasses and minimal growth. The reduction occurred by the resting cells.

7.3.3.1 Biobarrier

In the simulations for biobarrier, it was assumed that the bacteria, which was initially mixed with the sand in the biobarrier, were immobile. Therefore, the process of bacterial dispersion on to the upstream side, as observed in the experiments, was not simulated. In the simulations, K_f = 0.0367 and 0.0445 L/mg for chromium and substrate, respectively, and Freundlich exponent n = 1.292 and 1.272 for chromium and substrate, respectively,

as obtained from batch adsorption studies. Porosities of soil and sand portions were equal to 0.33 and 0.42, respectively. Hydraulic parameters (K_x, K_y, α_L, and α_T) were obtained from the measured data for concentrations of Cr(VI) in wells 1, 2 and 3 through calibration. Values of K_x and K_y were found to be 0.49 cm/h in soil and 1.6 cm/h in sand. These values are within the range for soils given in Freeze and Cherry (1979). Dispersivity α_L was equal to 0.75 cm for soil and 0.46 cm for sand. Transverse dispersivity α_T was 0.1 times the longitudinal dispersivity. The dispersivity values for sand are in the same range as those obtained by Moazed et al. (2009) in their experimental studies with medium and coarse sand. The model fitted values of Cr(VI) variation in wells 1, 2, 3 and 4 in reactor R1 are compared with the observed values in Fig. 7.29a. It may be noted that simulated Cr(VI) variation in all the wells 1, 2, 3 and 4 was exactly same because the simulations were made for homogeneous conditions, and there was no lateral variation in Cr(VI) concentration at the inlet.

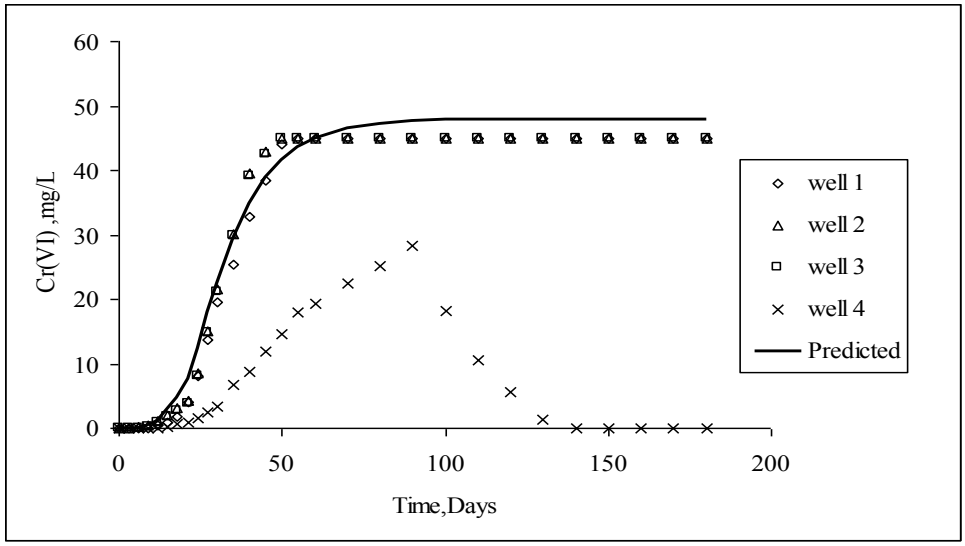

Fig. 7.29a Experimental and modeling results showing temporal variation of Cr(VI) concentration at wells 1, 2, 3, and 4 (at a distance of 50 cm from inlet) in reactor R1 (biobarrier).

It can be observed from Fig. 7.29a that the model fitted values compare well with the observed values in wells 1, 2 and 3. However, the model fitted values do not compare with the observed values in well 4. As mentioned earlier, bioremediation observed in well 4, due to upstream dispersion of microorganisms, was not considered in the model. This is the reason for the mismatch between the experimental and simulated results. The model predicted results for Cr(VI) variation in wells 1,2,3 and 4 in the reactor R2 are compared with the experimental results in Fig. 7.29b. It may be noted that same hydrogeologic parameters as obtained from reactor R1 were used in the predictions for reactor R2. It can be observed that the model predicted results match well with the observed data for wells 1, 2, 3 and 4.

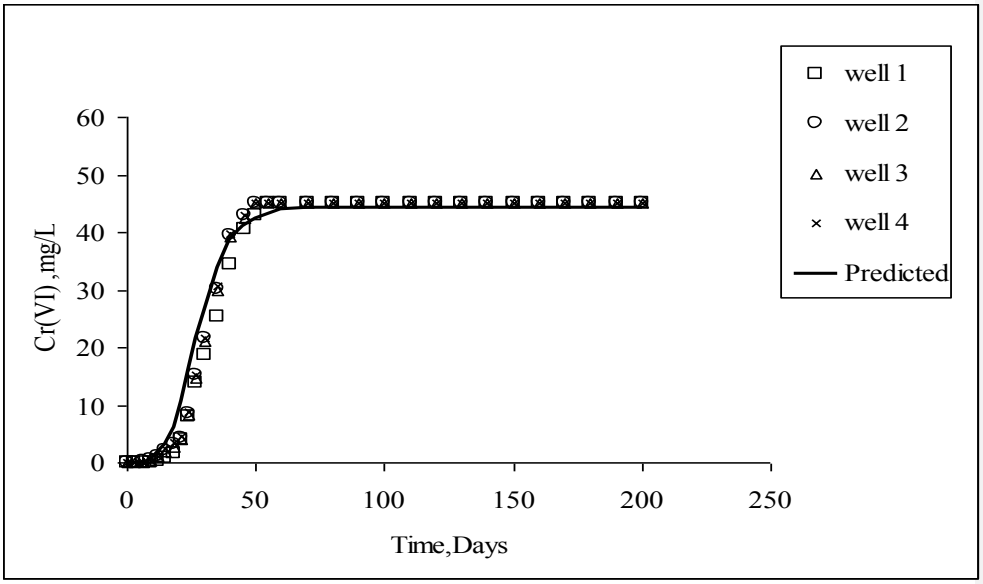

Fig. 7.29b Experimental and modeling results showing temporal variation of Cr(VI) concentration at wells 1, 2, 3, and 4 (at a distance of 50 cm from inlet) in reactor R2 (Blank Reactor).

The model which was calibrated for hydrogeologic parameters was then used for simulating the plume movement in R1 and R2 beyond the line of observation wells 1-4.

In these simulations the biokinetic parameters $\lambda = 0.01$, $K_i = 7.049$ mg/L and $\eta = 0.002$. Value of $\eta = 0.002$ was chosen such that the residual concentration of molasses at the outlet is approximately equal to 50 to 100 mg/L, as observed in the experiments. Values of λ and K_i were chosen such that complete biotransformation occurs when Cr(VI) concentrations are low, while only partial transformation occurs when Cr(VI) concentrations are high. Same biokinetic parameters are used in model simulations for all the pilot sacle experiments corresponding to reactors R1, R3 and R4.

Simulated results for chromium concentrations in wells 5-10 in R1 and R2 are compared with the experimental data in Figs. 7.30a and 7.30b, respectively. It can be observed from these figures that the simulated and observed data match satisfactorily in the case of wells in the reactor R2 (Fig. 7.30b). In the case of reactor R1, the arrival of plume at the line of wells 5-10 was predicted well. However, subsequent reduction in Cr(VI) concentration due to biotransformation was not predicted correctly. This is due to the limitation of the mathematical model, which did not consider the dispersion of bacteria on to the up stream side of the biobarrier. Figures 7.31 and 7.32 show the comparison between experimental and simulated variations in Cr(VI) concentration in wells 11-16 and in wells 17-20, respectively. It can be observed from Figs. 7.31a and 7.32a that the proposed mathematical model was successful in simulating the complete Cr(VI) reduction in the biobarrier. Non-containment of Cr(VI) plume in the control reactor R2 was also simulated satisfactorily (Figs. 7.31b and 7.32b). The deterioration in the performance of the model as the plume moved (Fig. 7.32b) could be due to uncertainty in the dispersivity and permeability values, arising from non-homogeneity of the porous medium, which was not considered in the simulations. It may be noted that constant values of dispersivity and permeability were used in all the simulations.

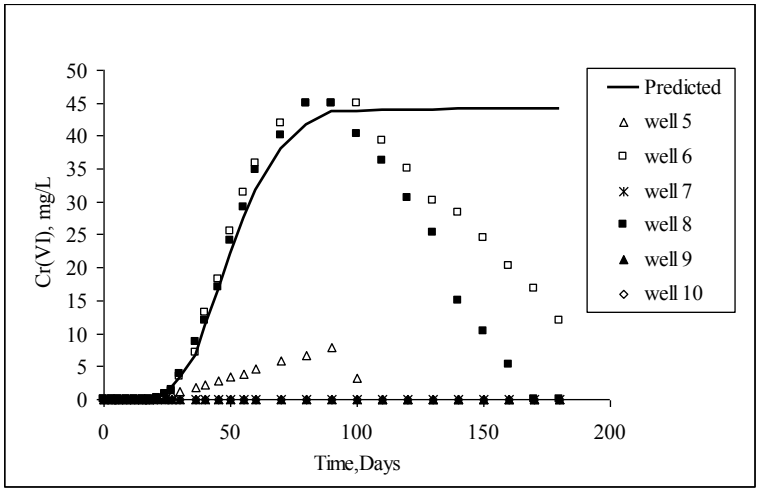

Fig. 7.30a.Experimental and modeling results for temporal variation of Cr(VI) concentration in wells 5 -10 (at a distance of 80 cm from inlet) in reactor R1

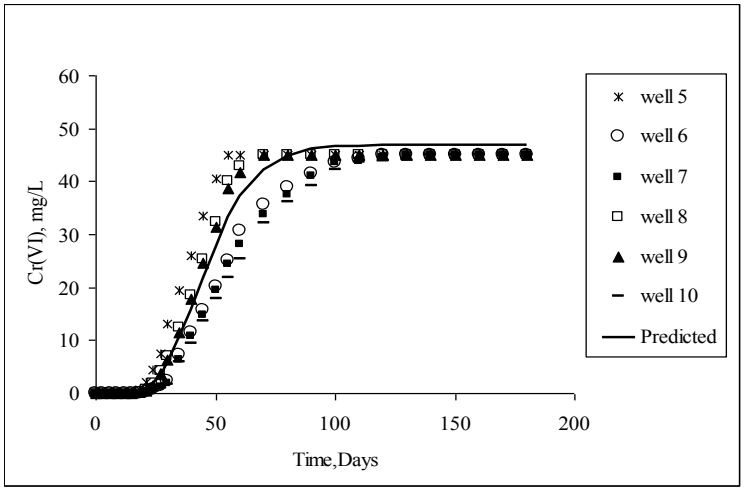

Fig. 7.30b.Experimental and modeling results for temporal variation of Cr(VI) concentration in wells 5 – 10 (at a distance of 80 cm from inlet) in reactor R2

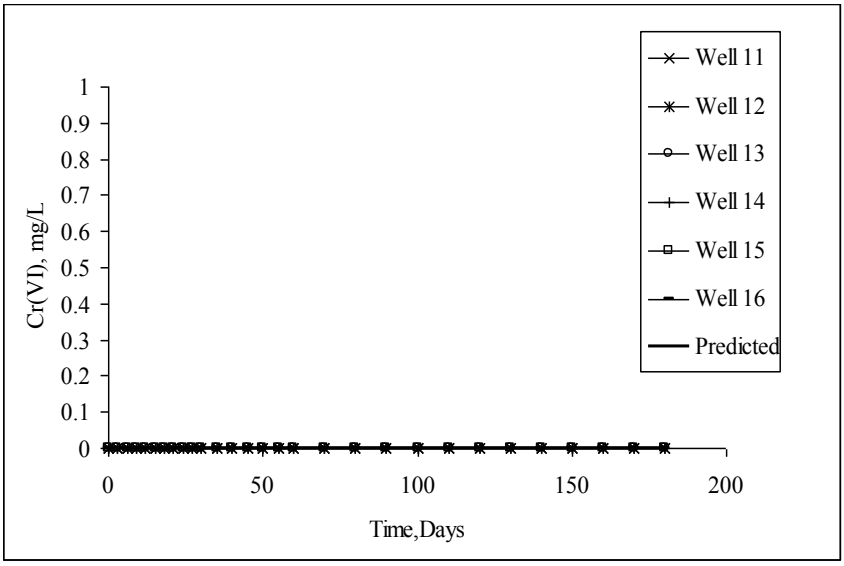

Fig. 7.31a Experimental and modeling results for temporal variation of Cr(VI) concentration in wells 11-16 (at a distance of 110 cm from inlet) in reactor R1

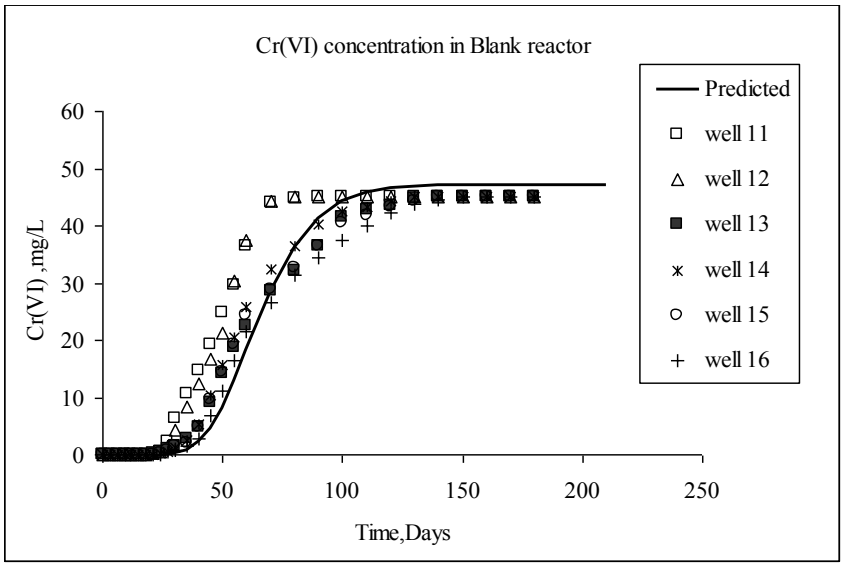

Fig. 7.31b Experimental and modeling results for temporal variation of Cr(VI) concentration in wells 11-16 (at a distance of 110 cm from inlet) in reactor R2

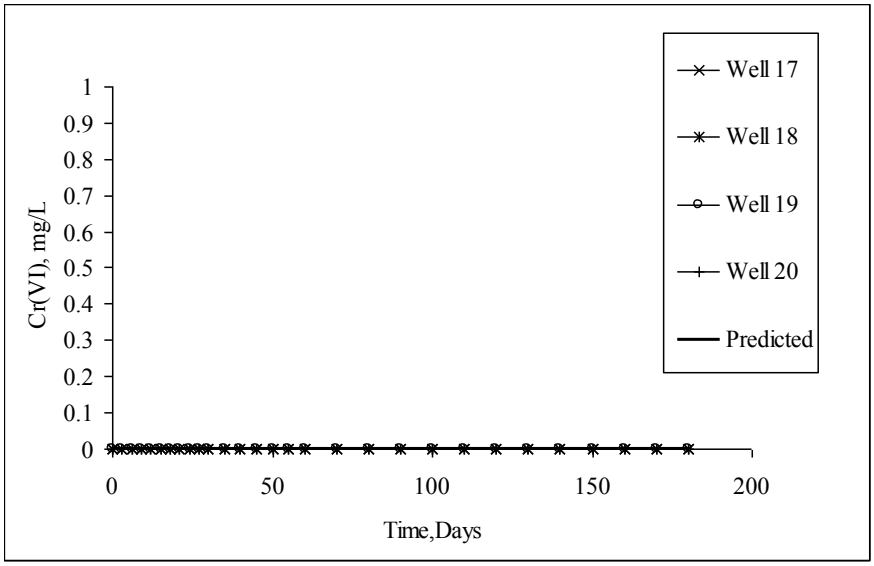

Fig. 7.32a Experimental and modeling results for temporal variation of Cr(VI) concentration in wells 17-20 (at a distance of 150 cm from inlet) in reactor R1

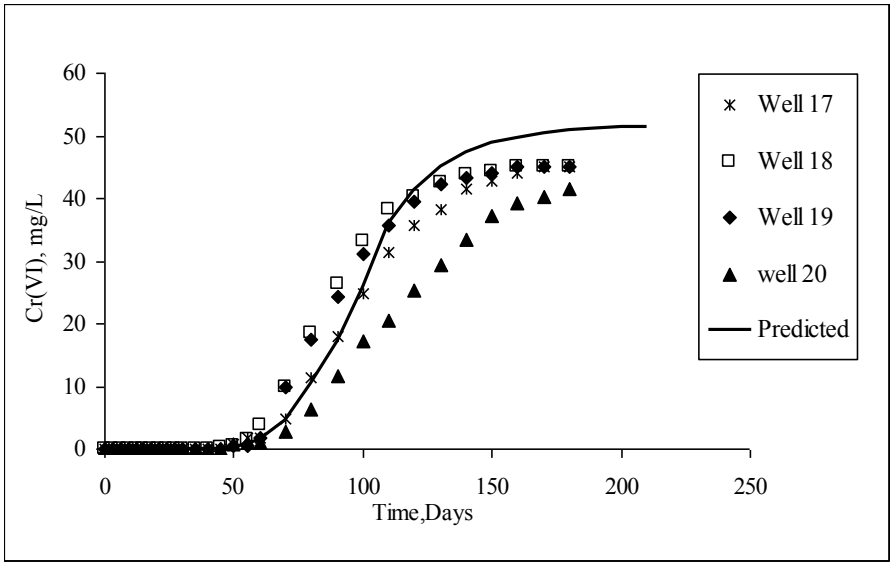

Fig. 7.32b Experimental and modeling results for temporal variation of Cr(VI) concentration in wells 17-20 (at a distance of 150 cm from inlet) in reactor R2

7.3.3.2 Recation Zone with Two Wells

In the simulations for biotransformation in the reaction zones with injection wells, it was assumed that the bacteria which was injected initially through injection wells spreads around the wells during the injection process, but eventually gets fixed onto the soil mass in a short period of time (approximately 2 hours). Therefore, initially, the advection-dispersion equation for bacterial transport was used for a period of 5 minutes (corresponding to period of injection) in order to simulate the injection of bacteria through injection wells. These mobile bacteria became immobile in due course of time after the start of transport of chromium and substrate. The partition coefficient for immobile to moble bacteria was 0.75. Same data for adsorption as employed in the simulations for biobarrier were used in the studies for reaction zone technology. Hydraulic parameters (K_x and K_y) were obtained from the measured data for concentrations of Cr(VI) in wells 1 and 2 through calibration. Porosity of the medium was equal to 0.33. These values are $K_x = K_y = 4.8$ cm/h. Dispersivities α_L and α_T are equal to 5 cm and 1 cm respectively. The model fitted variations in Cr(VI) concentrations in wells 1 and 2 are compared with observed values in Fig. 7.33a.

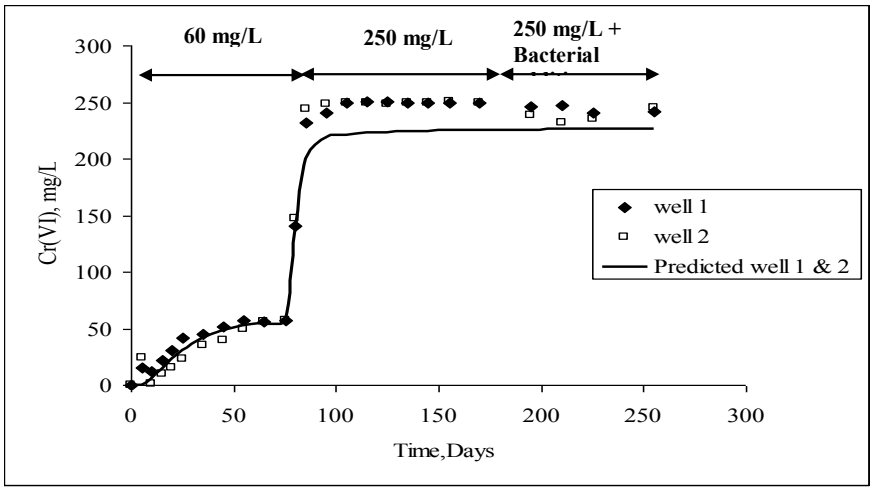

Fig. 7.33a Experimental and modeling results for temporal variation of Cr(VI) concentration at well no 1 and 2 (at a distance of 40 cm from inlet) in reactor R3

The calibrated model was then used for simulating the movement of Cr(VI) plume beyond the line of observation wells 1 and 2. λ and η values in these simulations were same as those used in simulations for reactor R1. The simulated results for Cr(VI) variation in wells 3-5 (in line with injection wells), in wells 8-12 (downstream of injection wells) and in wells 18-20 are compared with experimental data in Figs. 7.33b 7.33c and 7.33d, respectively. It is observed from Figs. 7.33b to 7.33d that the proposed mathematical model was able to simulate the biotransformation process in the reaction zones satisfactorily. Simulated results correspond with the observation that complete biotransformation occurred as long as the inlet Cr(VI) concentration was 60 mg/L. Appearnce of Cr(VI) plume beyond the line of injection wells when the inlet Cr(VI) concentration was increased to 250 mg/L was also simulated satisfactorily by the mathematical model. Subsequent slight reduction in Cr(VI) concentrations on the downstream side of injection wells after 170 h (as more bacteria got injected) was indicated in the numerical results also.

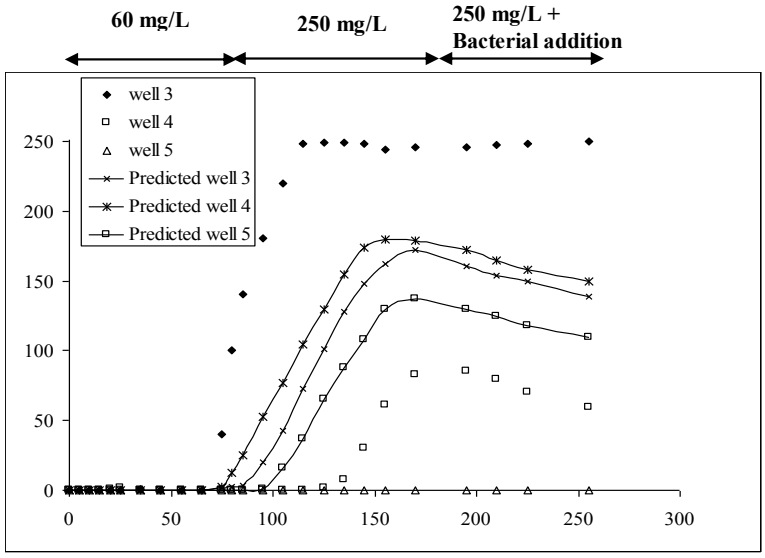

Fig. 7.33b Experimental and simulation results for temporal variation of Cr(VI) concentration at wells 3, 4 and 5 located (at a distance of 50 cm from inlet) in reactor R3

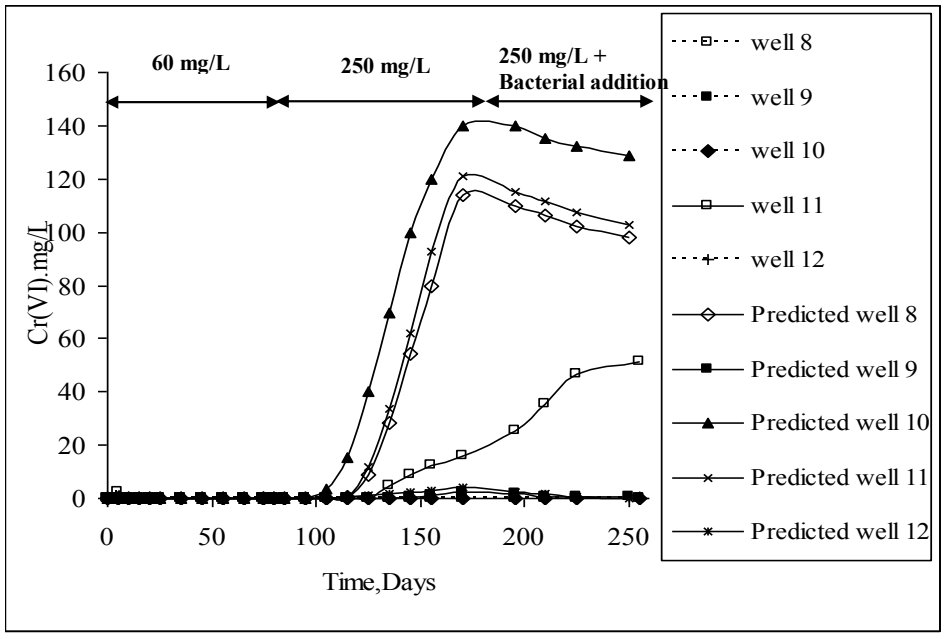

Fig. 7.33c Experimental and numerical results showing temporal variation of Cr(VI) concentration in wells 8-12 in reactor R3

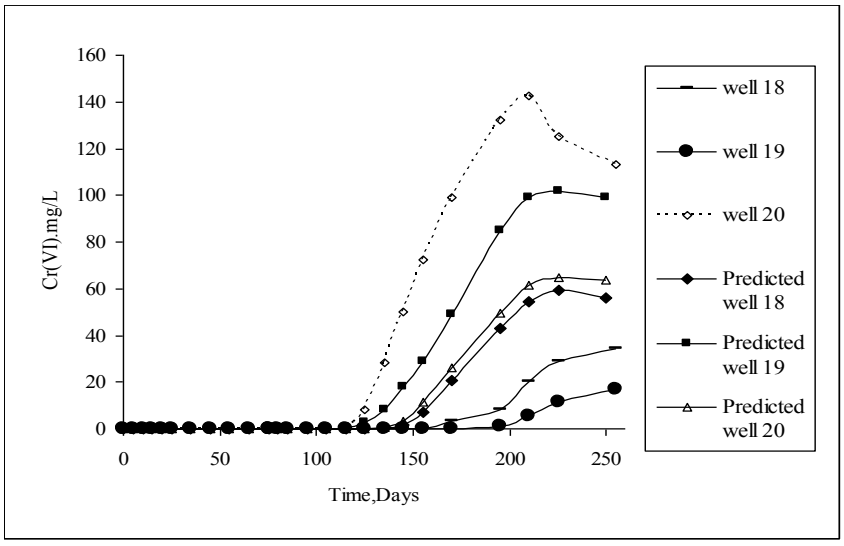

Fig. 7.33d Experimental and numerical results showing temporal variation of Cr(VI) concentration in wells 18-20 in reactor R3

7.3.3.3 Recation Zone with Four Wells

In this case also, it was assumed that the bacteria which was injected initially through injection wells spreads around the wells during the injection process, but eventually gets fixed onto the soil mass after the start of transport of Cr(VI). Therefore, same modelling procedure was used for injecting the bacteria during the initial period of 5 minutes (corresponding to period of injection) through four injection wells. As mentioned in the case of reactor with two injection wells, the injected bacteria were made immobile within a short period of time after the start of transport of chromium and substrate. Same data for adsorption as employed in the simulations for biobarrier were used in the studies for reaction zone technology. Hydraulic parameters (K_x and K_y) were obtained from the measured data for concentrations of Cr(VI) in wells 2 and 3 through calibration. Porosity of the medium was equal to 0.33. These values are $K_x = K_y = 10$ cm/h. Dispersivities α_L and α_T are equal to 5 cm and 1 cm respectively. The model fitted variations in Cr(VI) concentrations in wells 2 and 3 are compared with observed values in Fig. 7.34b.

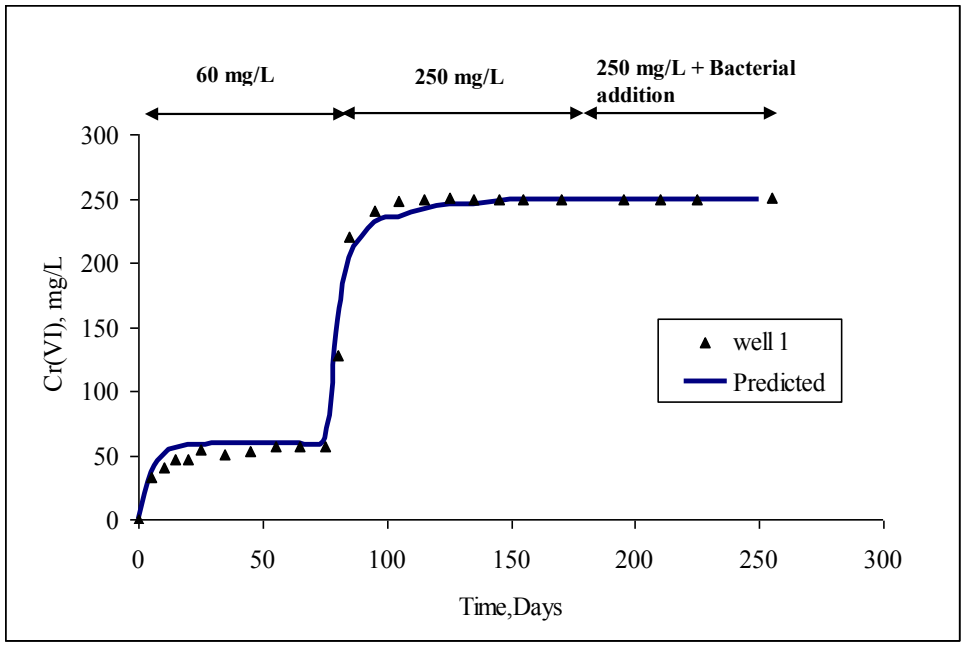

Fig. 7.34a Experimental and modeling results for temporal variation of Cr(VI) concentration at well no 1 (at a distance of 15 cm from inlet) in reactor R4

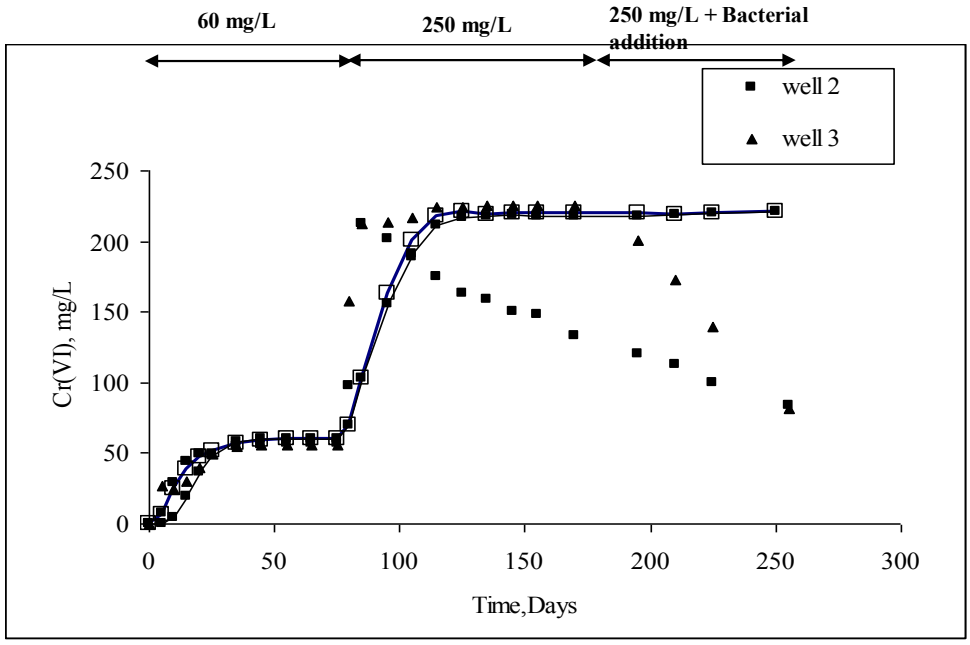

Fig. 7.34b Experimental and modeling results for temporal variation of Cr(VI) concentration in wells 2 and 3 (at a distance of 40 cm from inlet) in reactor R4

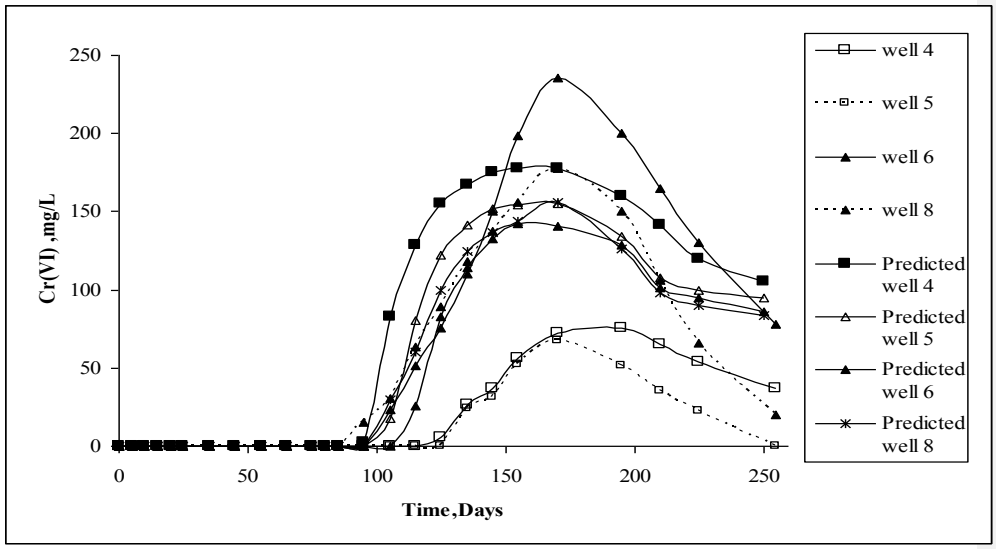

Fig. 7.34c Experimental and modeling results for temporal variation of Cr(VI) concentration in wells 4,5,6 and 8 (just downstream of injection wells) in reactor R4

The simulated values of Cr(VI) concentration in well 1 are compared with the observed values in Fig. 7.34a. It can be observed from this figure that the calibration of the model is satisfactory. The calibrated model was then used for simulating the movement of Cr(VI) plume beyond the line of injection wells. λ and η values in these simulations were same as those used in simulations for reactor R1. The simulated results for Cr(VI) variation in wells 4, 5, and 6 compared with experimental data in Fig. 7.34c. It can be seen that complete reduction of Cr(VI) in the reaction zones (up to 100 days) when inlet Cr(VI) concentration was 60 mg/L was simulated accurately. Also, deteroration in the performance of reaction zones for higher inlet Cr(VI) concentration of 250 mg/L due to inhibition effect could be simulated satisfactorily. However, transverse variation of Cr(VI) concentration across the reaction zone could not be simulated. This transverse variation was due to non-homogeneity in the soil characteristics as well as nonuniform spreading of bacteria in the actual experiment, which were ignored in the model.

7.3.4 Simulation Studies for Bio-attenuation

The validated computer code for transport and biotransformation of Cr(VI) was used for demonstrating the effectiveness of reactive-zone systems for chromium containment in an unconfined aquifer. A rectangular confined aquifer of domain, 100 cm x 100 cm, is initially maintained at a steady state with constant pore velocity of 3 cm/hr. The initial concentrations of Cr(VI), substrate and bacteria were 0, 0 and 100.22 mg/L, respectively. Here, the bacteria were assumed as immobile. The upstream boundary concentration of Cr(VI) was 20 mg/L. Injection wells were located at 70 cm from the upstream end to inject the molasses through these wells as shown in Fig. 7.35. The molasses was injected through the injection wells such that the system was under substrate unlimiting conditions. The Biokinetic parameters in these runs were the same oas thos taken in 7.3.2.2.

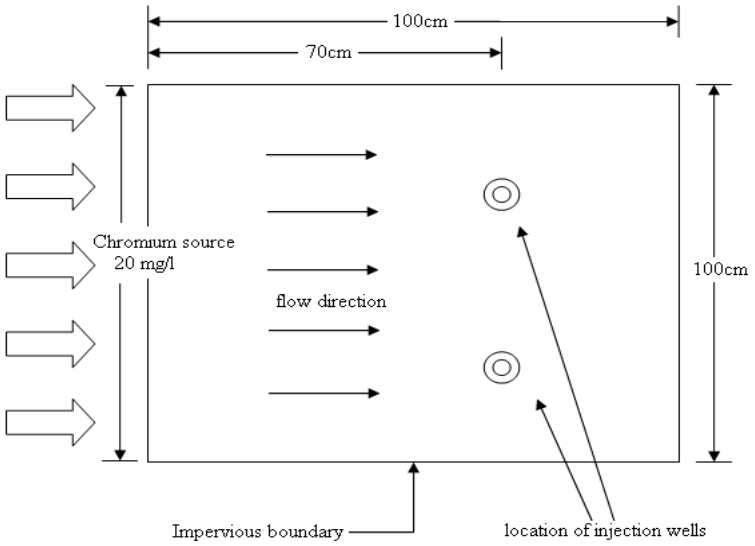

Fig. 7.35 Schematic diagram for simulation of reactive-zone mechanism

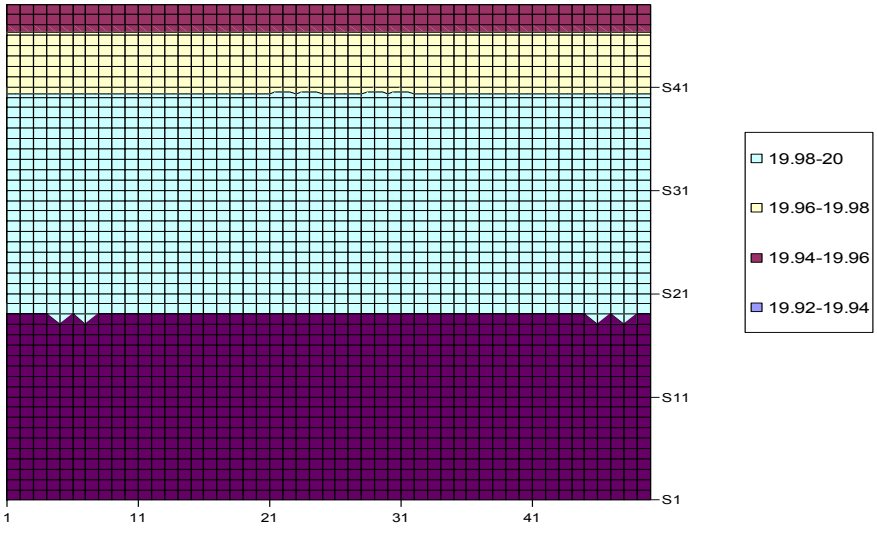

Fig. 7.36a Concentration contour for chromium after time = 80 hrs with no injection well in the aquifer.

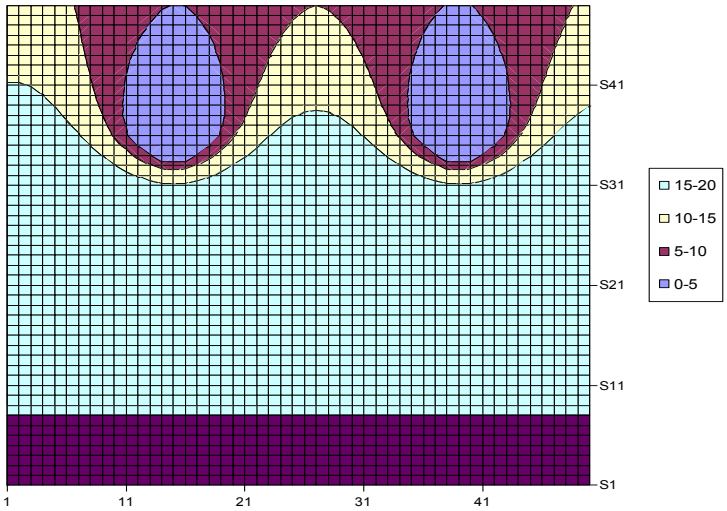

Fig. 7.36b Concentration contour for chromium after time = 80 h with two injection wells in the aquifer at x = 70cm

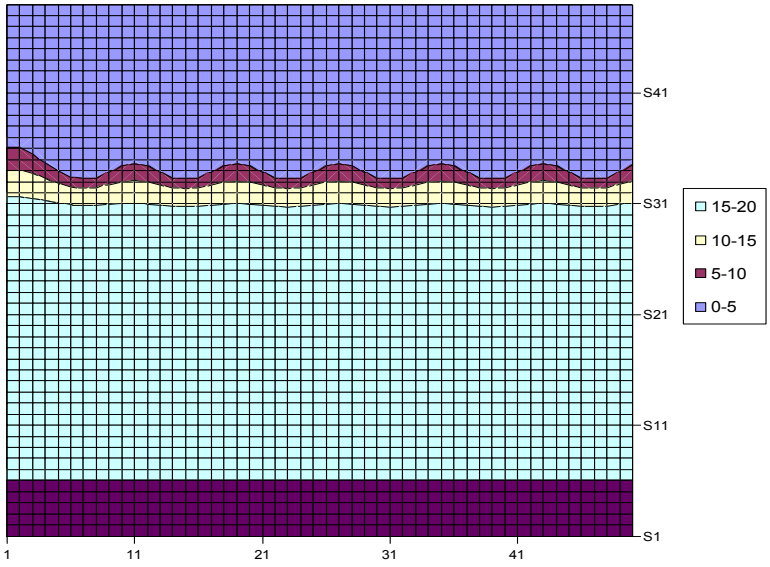

Fig. 7.36c Concentration contour for chromium after time = 80 h with seven injection wells in the aquifer at x = 70 cm.

Figures 7.36a, b and c shows the concentration contours for Cr(VI) at the end of 80 hours with no, two and six injection wells respectively. As the number of injection wells increases, the biotransformation of hexavalent chromium beyond 70 cm increases and when six injection wells are kept, the water beyond 70 cm is free from Cr(VI). In Fig. 7.36b, we can see the reactive-zone formed by each injection well, in blue colour. In this region, the water will be free from Cr(VI). These simulations demonstrate the applicability of developed model for studying the effectiveness of reactive zone systems for chromium containment. This model can be used for optimal design of bio-barriers as well as reaction-zone systems for remediation of aquifers contaminated with hexavalent chromium.

7.4 DATA NEEDS FOR A FIELD STUDY

In this section, data needs for actual field study in an area already showing contamination of Cr(VI) in drinking water tube wells are presented.

Mapping of the Plume:

The first task that needs to be carried out for field implementation is the mapping of the Cr(VI) contaminant plume. This can be accomplished by installing several observation wells in the suspected area of contamination, collecting samples from these wells, and analyzing them for Cr(VI). This data can be used for (i) obtaining the plume front (the areal extent of contamination) and (ii) Cr(VI) contour plots of concentration. This information is useful in (i) specifying the initial conditions while solving the transport equation, (ii) deciding the locations for injection wells in reaction zone methodology, and (iii) deciding the location for biobarrier. Typically, injection wells and biobarrier should be located all along the plume front. In addition, injection wells (in case of reaction zone technology) should also be located within the plume area. Water samples collected from the observation wells should be also analyzed for other constituents (other heavy metals, TDS, pH, other toxic compounds) which may interfere with the bioremediation process.

Source Characterization:

Field surveys need to be carried out to locate the source of the Cr(VI) contamination. This is important from the perspective of determining locations where the inflow boundary condition should be specified. It is also important to estimate the rate of Cr(VI) influx into the aquifer at the source location. However, it may be difficult to obtain the above information. In such cases, it is required to determine the present concentration of Cr(VI) in the aquifer at the source location, and an estimate (based on proposed activities) of Cr(VI) concentration in future. This data is essential for specifying the upstream boundary condition while solving the transport equation. For example, zero influx of Cr(VI) will be specified as upstream boundary condition if it is planned to completely prevent the entry of Cr(VI) into the aquifer by removing the source (as part of aquifer remediation).

Hydrogeologic Parameters:

Characterization of hydrogeologic parameters is one of the most important tasks which need to be carried out before the implementation of the technique in the field. Following data needs to be collected from the field:

1. Geophysical investigations (vertical electrical resistivity soundings and magnetic profiles) should be carried out to decipher the subsurface geology and delineate the structural features. For example, dykes and other geological features which act as natural barriers to groundwater flow should be identified. Also, lithological maps should be prepared. These investigations will help in planning the field tests for determination of spatial variation (including the variation with depth) in hydrogeologic parameters such as hydraulic conductivity, porosity, specific yield, specific storage coefficient etc., and in interpreting the test data.
2. An estimate for the spatial variation of porosity should be obtained.
3. Estimates for the spatial variation of hydraulic conductivity, specific storage coefficient (in case of confined aquifers), and specific yield (in case of unconfined aquifers) should be obtained. Hydraulic conductivities in both the principal directions i.e. K_x and K_y should be estimated. All this

data can be obtained by conducting pump tests at several locations in the contaminated area.

4. Spatial variation aquifer thickness in case of confined aquifers should be determined. This will help in estimating the spatial variation of transmissivity. Similarly, depth to the bottom of the aquifer (below ground level), in case of unconfined aquifer, should be obtained. These data can be obtained from geophysical investigations and bore well log data.
5. Historical data for spatial and temporal distribution of piezometric head in the aquifer and pumping rates (from existing wells) in the area should be obtained. Piezometric head may be obtained by measuring the levels in observation wells.
6. Information on piezometric heads / flow conditions at the boundaries of study area need to be collected for specification of boundary conditions for solving the groundwater flow equations. For example, water levels in the river can be specified as boundary condition if a river forms part of the boundary for the study area and the aquifer is unconfined. Similarly, a head boundary condition can be specified if the piezometric head values are known along the boundary. A no flow boundary condition can be specified as boundary condition if a dyke exists along the boundary.
7. The groundwater flow module of the mathematical model should be calibrated and validated using the values of measured piezometric heads. For known spatial and temporal variations in pumping rates and boundary conditions, and assumed spatial variation of hydrogeologic parameters (hydraulic conductivity, specific yield, and specific storage coefficient) groundwater flow model should be used to simulate the spatial and temporal variation of piezometric heads within the study area. These values should be compared with the measured values of piezometric head. Values of hydrogeologic parameters (and some times pumping and recharge rates, if significant uncertainty exists in their estimation) should be adjusted such that the difference between measured and estimated piezometric heads from the field is a minimum.

8. Tracer tests should be conducted to obtain data for the estimation of longitudinal and transverse dispersivities.

Soil Characteristics:

Representative soil samples (from different locations and at different depths) should be collected from the contaminated area and should be analyzed for various characteristics such as clay content, silt content, sand content, specific gravity, bulk density, and porosity. Geochemical characteristics of the soil should also be determined. Kinetic and equilibrium studies should be conducted to obtain parameters for adsorption of Cr(VI), and molasses onto the soil.

Biokinetic Parameters:

Batch experiments should be conducted to determine the biokinetic parameters for the particular strains of CRB, IRB, and SRB that will be employed in the filed. Also, a few column studies, containing the field soil, should be conducted to obtain the parameter λ, which accounts for difference in the microbial growth in a suspended batch system and attached continuous system.

Once all the data as outlined above is obtained, the transport and transformation model, along with the embedded groundwater flow model for the study area, can be used to evaluate the effectiveness of bioremediation strategy for the given situation. Numerical experimentation, corresponding to different scenarios (different biobarrier widths, different initial microbial concentrations, different locations for injection wells, number of injection wells, frequency and injection rate for injecting molasses into the aquifer etc.), can be made to design an efficient and effective strategy.

At this stage, attempt could not been made to see if the mathematical model can be used to simulate the field scale experiments because of non-availability of complete data, as described above. This will be taken up in future studies.

CHAPTER 8

RESULTS AND DISCUSSION – MANAGEMENT MODEL

As mentioned earlier, in any bio-augmentation problem, the design variables are length of the bio-barrier (L), initial microbial concentration (M_0) and the substrate to be provided for the microbial growth (S_0). The cost of construction of bio-barriers and time taken for bio-transformation vary depending upon these decision variables. Hence it is necessary to determine the optimal solutions of the decisions to be made for the proper functioning and management of a bio-barrier system, subjected to a specific site condition. The optimal decisions to be taken for the proper functioning of the trench type bio-barrier are determined by solving the optimization problem as discussed in Chapter 5. Results obtained in this study are presented in the following sections.

8.1 ONE-DIMENSIONAL MANAGEMENT PROBLEM

In this work, the one dimensional simulation-optimization model was run for different pore velocities, varying from 1 cm/h to 6 cm/h. The system parameters used in these optimization runs are presented in Table 8.1. In all these runs, values of Δx and Courant number were 1 cm, and 0.65, respectively. The bio-barrier was 10 Km wide normal to the contaminant plume and 10 m deep. Other input values required for the application of the optimization model are presented in Table 8.2 for different runs. In these runs, the number of generations was equal to 100, and the population size was equal to 10. The optimal decision so obtained was cross checked with the simulator in order to determine whether the constraints were satisfied. Design charts were prepared based on these optimal solutions.

Table 8.1 System characteristics

S.No.	Parameter	Value
1	**μ_{max} (1/h)**	**0.3**
2	***Y***	**0.263**
3	**H**	**0.3**
5	**λ**	**0.1**

6	**K_s (mg/L)**	**40.0**
7	**K_i (mg/L)**	**3.049**
8	**K_d (1/h)**	**0.0**
9	**Dispersivity (α_L) (cm)**	**1**
10	**Darcy velocity (m/day)**	**0.1**
11	**Porosity (ϕ)**	**0.35**
12	**Time for remediation (days)**	**14.5**
13	**Maximum length (cm)**	**100**
14	**Bulk density (g/cc)**	**1.8**
15	**Freundlich constants for Cr(VI)**	**K_f=0.012 n=1.9**
16	**Freundlich constants for Molasses**	**K_f=0.055 n=0.764**
17	**U/s Cr(VI) concentration (mg/L)**	**25**
18	**Maximum microbial concentration (mg/L)**	**530**

Table 8.2 Input values for the one-dimensional optimization model

Sl. No.	Variable	Set-A	Set-B	Set-C
1	L_{min} (cm)	10	10	10
2	L_{max} (cm)	100	100	100
3	M_{0min} (mg/L)	0	0	0
4	M_{0max} (mg/L)	300	300	300
5	S_{0min} (mg/L)	50	1000	50
6	S_{0max} (mg/L)	1000	2000	1000
9	C_1 (Rupees)	200	200	200
10	C_2 (Rupees)	1000	1000	500
11	C_3 (Rupees)	14	14	14
12	T (days)	14.5	14.5	14.5

Optimal solutions obtained for Set A, for different groundwater velocities are presented in Table 8.3, and in Figs. 8.1 to 8.4. In this set of runs, the Darcy velocity varied from 0.417 cm/h to 2.0 cm/h, which corresponded to a variation of 0.0525 to 0.252 in the π_1 value. It is observed that, as π_1 increases, length of the bio-barrier decreases, and consequently, the cost of the bio-barrier decreases. A high value of π_1 implies that microbial activity and dispersion effects are more significant compared to the advection effect. Therefore, the residence time of the pollutant inside the barrier is higher. Moreover, because of high dispersion, the concentration of the pollutant coming in contact with the microbes at the plume front is lower compared to that in case of high advection. This reduces the inhibition effect.

Table 8.3 Optimal solution for different groundwater velocities for Set-A

Darcy velocity (cm/h)	Pore velocity (cm/h)	π_1	L (cm)	M_0 (mg/L)	S_0 (mg/L)	Cost (Rs.)
2.0	5.71	0.0525	69.5	150.5	420.3	2.17e007
1.8	5.14	0.0584	48.5	208.5	500.8	1.76e007
1.4	4.0	0.075	39.5	215.2	450.5	1.39e007
1.0	2.86	0.1049	30.4	190.3	492.5	1.05e007
0.8	2.29	0.131	25.7	220.3	378.0	0.86e007
0.65	1.86	0.162	24.5	163.3	384.1	0.75e007
0.55	1.57	0.191	23.2	128.9	507.4	0.71e007
0.417	1.19	0.252	21.5	93.2	671.6	0.64e007

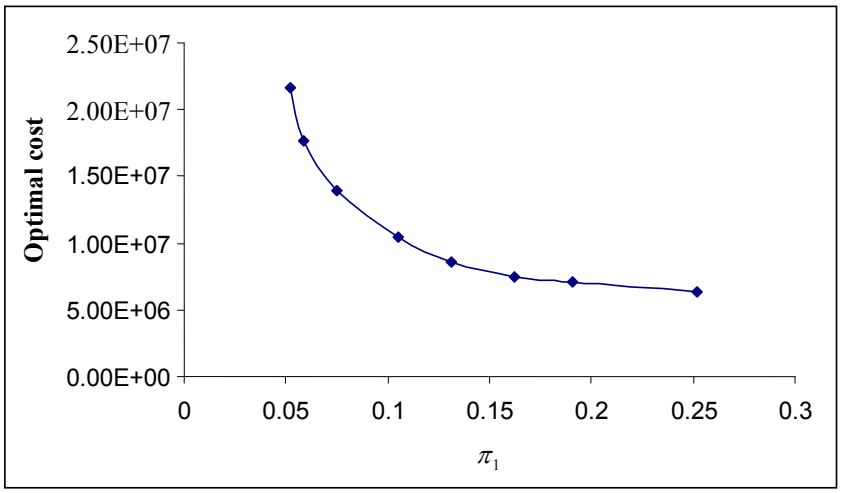

Fig. 8.1 Variation of optimal cost with π_1, Set- A

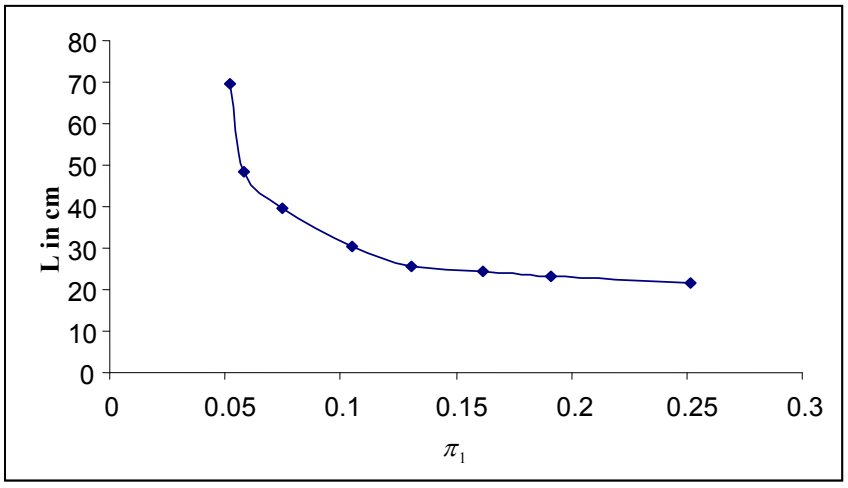

Fig. 8.2 Variation of optimal length with π_1, Set- A

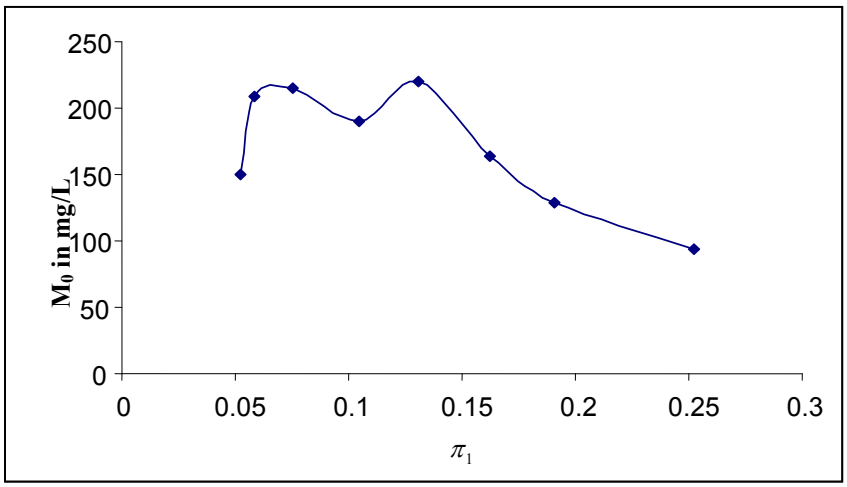

Fig. 8.3 Variation of optimal initial microbial concentration with π_1, Set- A

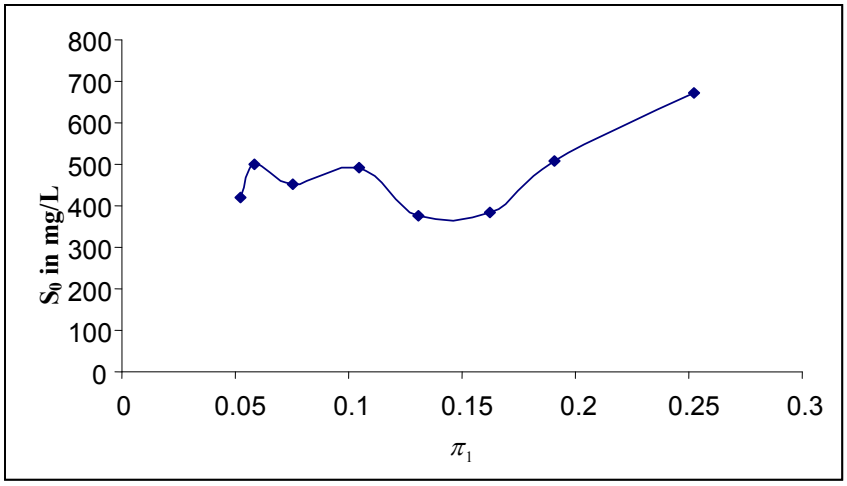

Fig. 8.4 Variation of optimal substrate concentration with π_1, Set-A

As the π_1 value increases, the initial bio-mass concentration required also decreases in general. This is compensated by a general increase in the inlet substrate concentration. Microbial concentration at any instant depends on both the initial microbial concentration and the specific growth rate. The specific growth rate can be increased by taking a higher substrate concentration. For lower values of π_1, there is a trade of between the M_0 and S_0 values, and the actual values chosen depend upon the cost function.

Optimal solutions obtained for Set B, for different groundwater velocities are presented in Table 8.4 and in Figs 8.5 to 8.8. The difference between Sets A and B was only in terms of range for the S_0 value. In set B, higher substrate concentrations were considered. Results for the optimal cost and the optimal bio-barrier length follow similar trend as before. However, the optimal substrate concentration, S_0 was mostly taken near the lower end of the range. This might be due to the fact that the specific growth rate cannot be greater than μ_{max} value whatever be the substrate concentration, S_0.

Table 8.4: Optimal solution for different groundwater velocities for Set-B

Darcy Velocity (cm/h)	Pore velocity (cm/h)	π_1	L (cm)	M_0 (mg/L)	S_0 (mg/L)	Cost (Rs.)
2.0	5.714	0.0525	53.8	147.9	1033.7	2.36e007
1.8	5.1429	0.0583	45.7	165.4	1010.7	2.06e007
1.4	4.0	0.075	40.3	142.4	1020.4	1.70e007
1.0	2.857	0.105	30.6	133.0	1030.3	1.26e007
0.8	2.286	0.131	29.9	108.3	1010.7	1.11e007
0.65	1.857	0.162	22.9	121.5	1050.2	0.89e007
0.55	1.5714	0.191	22.9	98.8	1244.8	0.87e007
0.417	1.1914	0.252	22.9	75.2	1253.3	0.77e007

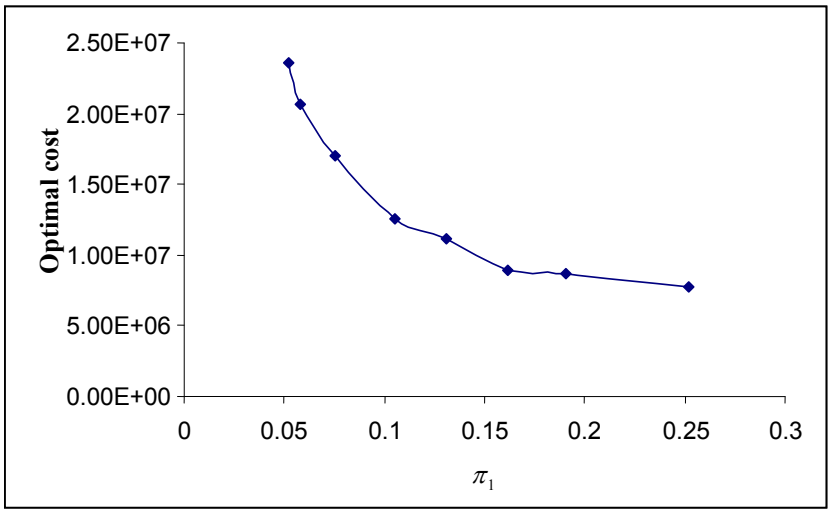

Fig. 8.5 Variation of optimal cost with π_1, Set-B

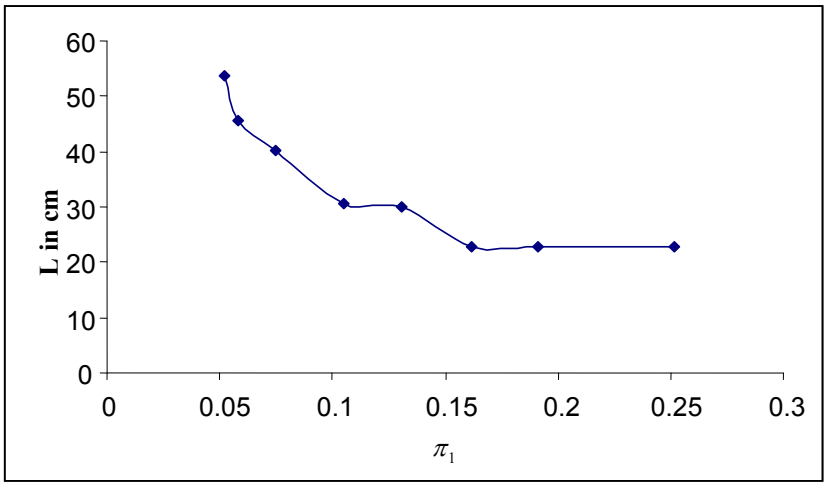

Fig. 8.6 Variation of optimal length with π_1, Set-B

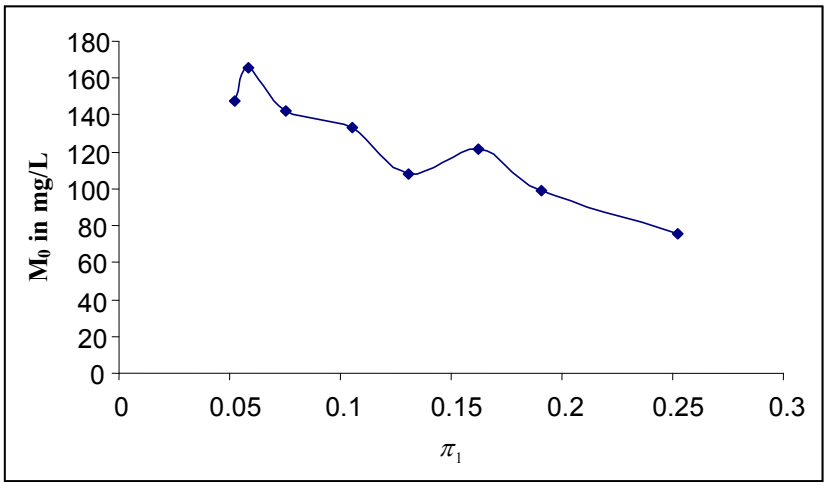

Fig. 8.7 Variation of optimal initial microbial concentration with π_1, Set-B

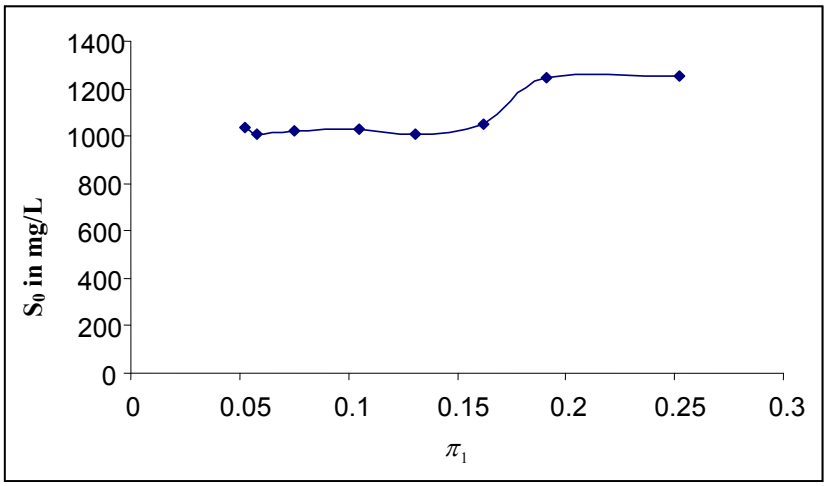

Fig. 8.8 Variation of optimal substrate concentration with π_1, Set-B

Optimal solutions obtained for Set C, for different groundwater velocities are presented in Table 8.5 and in Figs 8.9 to 8.12. The difference between Sets A and C was only in terms of the unit cost of the microbes. Unit cost for the microbes was half of that in the case of Set-A. These runs were made to demonstrate how the optimal solution depends on the relative costs of trenching, microbes, and the substrate. Results for the optimal cost and the optimal bio-barrier length follow similar trend as before. However, there is a trade of between the initial microbial concentration, M_0, and the inlet substrate concentration, S_0. If there is an increase in the M_0 value with π_1, there is a corresponding decrease in the S_0 value, and vice versa. There is no definitive trend in the variations of M_0 and S_0 with π_1. Optimal solution depends on system characteristics, bounds on the decision variables, and unit costs. Non-linearities are involved in the objective function as well as the constraints in the optimization problem. This underscores the need for a formal technique for determining the optimal solutions.

Table 8.5: Optimal solution for different groundwater velocities for Set-C

Darcy Velocity (cm/h)	**Pore velocity (cm/h)**	π_1	**L (cm)**	**M_0 (mg/L)**	**S_0 (mg/L)**	**Cost (Rs.)**
2.0	5.71	0.0525	67.7	151.6	440.6	1.96e007
1.8	5.14	0.0584	55.5	132.9	796.4	1.94e007
1.4	4.0	0.075	44.8	175.8	415.3	1.32e007
1.0	2.86	0.1049	33.6	196.9	349.5	0.96e007
0.8	2.29	0.131	30.6	131.2	508.2	0.88e007
0.65	1.86	0.162	21.9	193.9	413.7	0.64e007
0.55	1.57	0.191	20.3	205.4	360.3	0.58e007
0.417	1.19	0.252	20.1	130.8	414.1	0.53e007

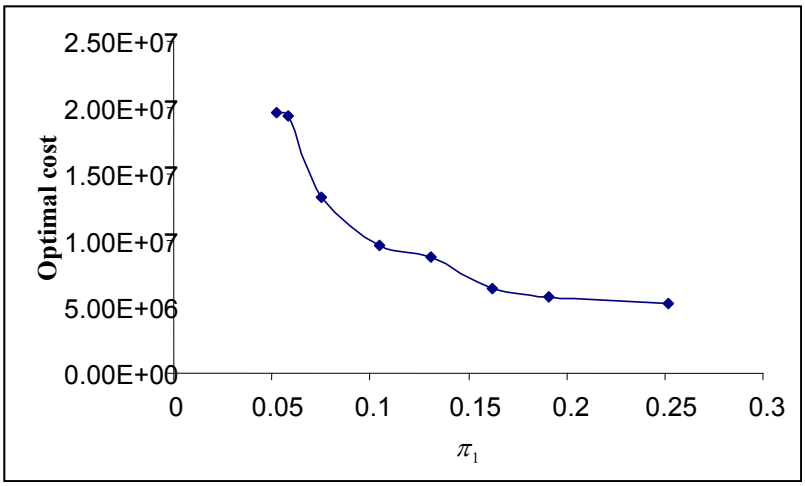

Fig. 8.9 Variation of optimal cost with π_1, Set C

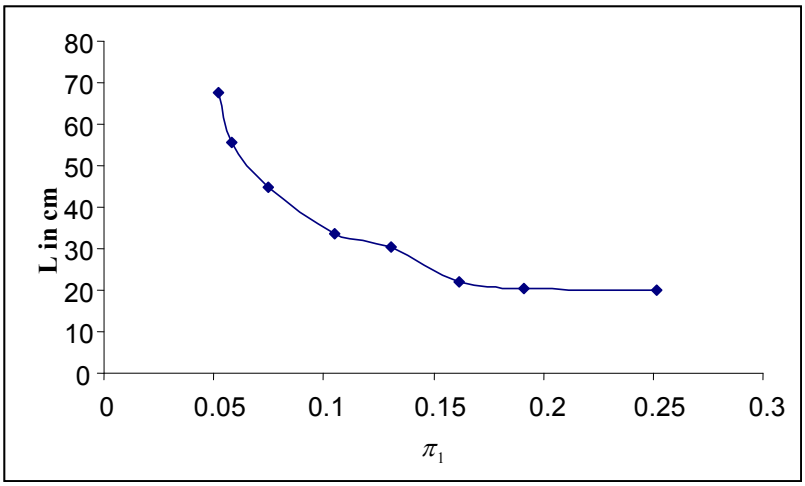

Fig. 8.10 Variation of optimal length with π_1, Set C

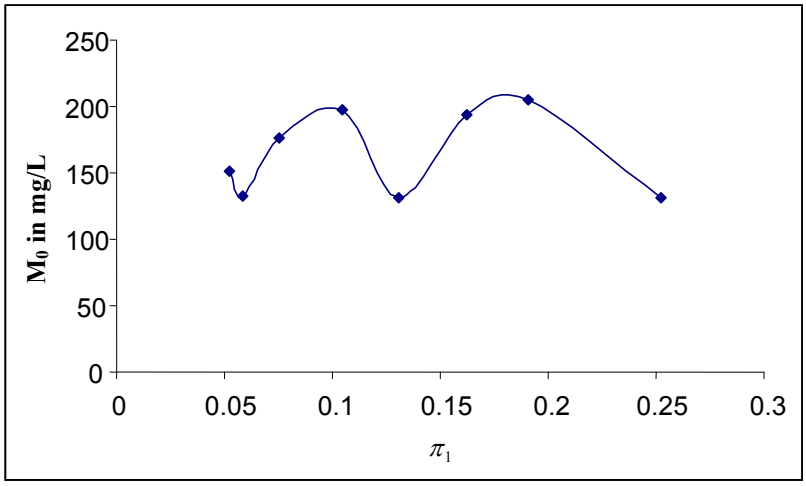

Fig. 8.11 Variation of optimal initial microbial concentration with π_1, Set C

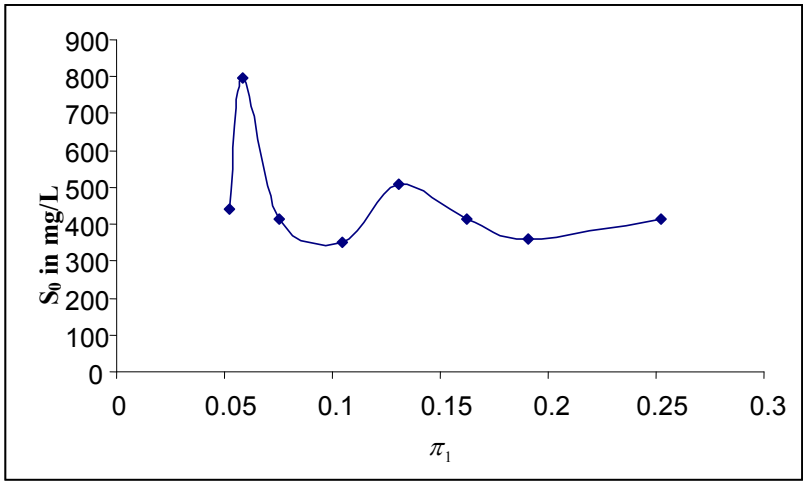

Fig. 8.12 Variation of optimal substrate concentration with π_1, Set C

Chapter 9

SUMMARY AND CONCLUSIONS

First part of the batch studies focused on the ability of a mixed population of microbial culture isolated from hexavalent chromium contaminated site to biotransform Cr(VI). Batch and continuous experiments were carried out to study the biotransformation pattern of Cr(VI) with molasses as the electron donor. Among the bacterial strains isolated from seven different locations of the contaminated site, the bacterial strain (H1) which was isolated from a clay mat near the effluent treatment plant (ETP) showed high Cr (VI) reduction potential. Optimum concentration of bacteria and molasses for the reduction of Cr (VI) to Cr (III) was observed as 15 mg/g of soil and 34 mg/g of soil respectively. 97 $\pm$ 1.2% reduction of Cr (VI) was achieved within 20 days under optimum concentration of molasses and bacteria under anaerobic conditions. The results of the present study suggest that indigenous microorganisms are capable of anaerobic reduction of high concentration of Cr (VI) in contaminated soil. Reduction of Cr(VI) to Cr(III) is a microbialy mediated process, and provision of a suitable electron donor to contaminated aquifer shall greatly speed up this reaction.

Different bacterial cultures, CRB, SRB and IRB, were enriched and isolated from contaminated soils. These cultures were used for Cr(VI) reduction studies, individually and in combination. Studies were conducted with different initial Cr(VI), SO_4^{2-} and Fe(III) concentrations. Biokinetic parameters such as μ_{max}, K_s, Y_T and K_i for individual cultures were evaluated. A mathematical model was proposed for simulating the chromium reduction, COD utilization and biomass growth, for individual cultures as well as for a combination of two or three different cultures, for different initial Cr(VI), SO_4^{2-} and Fe(III) concentrations. Biokinetic parameters evaluated from one set of experiments for individual cultures were utilized in all the validation studies. Performance of the mathematical model in terms of the dimensionless modified coefficient of efficiency (E) indicated that the proposed model simulated the system behavior very well, especially for higher Cr(VI) concentrations. However, the model performance for lower concentrations

was not as good. Monod‟s inhibition model used in this study might not have represented the inhibition correctly for lower Cr(VI) concentrations.

Different types of microorganisms are generally present in contaminated aquifers. It is important to understand the interaction between various microorganisms under different environmental conditions with respect to chromium reduction. Based on the kinetic studies for single culture, it was possible to develop a model for simultaneous action of three different cultures (CRB, SRB and IRB), having distinct characteristics, with respect to chromium reduction. This basic mathematical model was used as a reaction module in any mathematical model, based on the solution of advection-dispersion-reaction equations, for in-situ bioremediation of contaminated aquifers.

In this study, containment of hexavalent chromium in contaminated aquifers was investigated. Role of adsorption and biotransformation in Cr(VI) containment were investigated using batch experiments, bench-scale column studies, and mathematical modelling. Adsorption characteristics of different soils for lithium, Cr(VI), Cr(III), and molasses were evaluated. Transport and biotransformation of Cr(VI) in different soils, under different operating conditions, were evaluated using bench-scale column experiments. Bio-barrier studies for hexavalent chromium containment were also carried out. For simulating the transport and biotransformation of Cr(VI) in confined aquifers, a mathematical model was developed, and validated using experimental data obtained from this study. Bio-barriers of relatively small thickness with bio-augmentation can effectively contain the Cr(VI) in confined aquifers. Containment is more effective in aquifers with silty soil compared with sandy soils.

The pilot scale studies revealed that even after 180 days, Cr(VI) concentration was zero in wells located downstream of the biobarrier and at the outlet, whereas in the blank reactor Cr(VI) concentration in the outlet has reached the maximum of 43 mg/L. Experiments also revealed that even after 75 days, Cr(VI) concentration was zero in almost all wells located downstream of the injection wells and at the outlet in both the reactors with two and four injection wells, for an inlet Cr(VI) concentration of 60 mg/L.

However, Cr(VI) reduction potential decreased when the Cr(VI) concentration was increased to 250 mg/L after 75^{th} day because of the inhibitory effect of high concentrations of Cr(VI). The experimental results clearly showed that both the bio barrier and reaction zone technologies can be successfully employed for remediating the Cr(VI) contaminated aquifer. As expected, reaction zone experiments with four wells showed better performance compared to that by reaction zone technology with two injection wells. Results from the modeling study indicated that the proposed mathematical model could simulate the working of reaction zone technique for bio-remediation.

Optimal solution for trench type biobarrier depends on system characteristics, bounds on the decision variables, and unit costs. The variation of optimal cost with system characteristics, bounds on the decision variables and unit cost have been studied in the present study. It should be noted that the results presented in this study indicate only a general trend in the optimal design parameters. Non-linearities are involved in the objective function as well as the constraints in the optimization problem. This underscores why the design parameters should be determined using formal optimization techniques. It should also be noted that the optimal design is limited by the limitations of the simulator. The present simulation-optimization models should be used only for screening level designs. The screening level design can be the starting point for optimal design where more sophisticated simulators are used. It may be noted that non-homogeneities introduce local scale dispersion, which is equivalent to having a higher value of α_L in the present simple model. This increases the π_1 value. As a result, thinner bio-barriers would be able to contain the contaminant plume.

REFERENCES

1. **Ackerley, D.F., C.F. Gonzalez, M. Keyhan, R. Blake, and A. Matin (2004),** Mechanism of chromate reduction by the Escherichia coli protein, NfsA, and the role of different chromate reductases in minimizing oxidative stress during chromate reduction. *Environ. Microbiol.,* 6, 851-860.

2. **Aiyar, J., H.J. Berkovits, R.A. Floyd, and K.E. Wetterhahn (1991),** Reaction of chromium(VI) with glutathione or with hydrogen peroxide: identification of reactive intermediates and their role in chromium(VI)-induced DNA damage. *Environ. Health Perspect.,* 92, 53-62.

3. **Alam, M.M., A. Hossain, D.R. Yonge, B. M. Peyton** and **J. N. Petersen (2006),** Bioreduction of hexavalent chromium in flow-through quartz sand columns. *J. Environ. Engg.*, *ASCE*, 132, 358-366.

4. **Alesii, B.A.**, **W.H. Fuller** and **M.V. Boyle (1980),** Effect of leachated flow rate in metal migration through sols. *J. Environ. Qual.*, 9, 119-126.

5. **Amacher, M.C., H.M. Selim**, and **I.K. Iskandar (1988),** Kinetics of chromium (VI) and cadmium retention in soils: A nonlinear multireaction model. *Soil Science Society of American Journal*, 52, 398-408.

6. **Amacher, M.C., J. Kotuby-Amacher**, **H.M. Selim** and **I.K. Iskandar (1986)**, Retention and release of metals by soils-evaluation of several models. *Geoderma*, 38, 131-154.

7. **APHA (1998),** (American Public Health association), American waterworks Association(AWWA), Water Environment Federation(WEF), Standard methods for Examination of Water and Wastewater, 20th Edition, Washington DC.

8. **Bader J.L., Gonzalez G., Goodell P.C., Ali A.S., and S.D. Pillai (1999b).** "Chromium resistant bacterial populations from a site heavily contaminated with hexavalent chromium". Water, Air and Soil pollution, 109, 263-274.

9. **Barlett, R.J.** and **B. James (1979),** Behavior of chromium in soils III. Oxidation. *J. Environ. Qual.*, 8, 31-35

10. **Barnhart, J. (1997),** Occurrences, uses, and properties of chromium. *Regulatory toxicology and pharmacology*, 26, 3-7.

11. **Barry, D., C. Miller** and **P. Culligan-Hensley (1996),** Temporal discretization errors in noniterative split-operator approaches to solving chemical reaction/ groundwater transport models. *J. Conta. Hydrol.* , 22,1-17.

12. **Baveye, P.** and **A.J. Valocchi (1989),** An evaluation of mathematical models of the transport of reacting solutes in saturated soils and aquifers. *Water Resour. Res.,* 25**,** 1413-1421.

13. **Baveye, P., and Valocchi, A.J. (1989)**. An evaluation of mathematical models of the transport of reacting solutes in saturated soils and aquifers. Water Resour. Res. 25, 1413-1421.

14. **Bell, L.S.J.** and **P.J. Binning (2004),** A split operator approach to reactive transport with the forward particle tracking Eulerian Lagrangian localized adjoint method. *Adv. Water Resour.*, 27, 323-334.

15. **Bilkent (2000), "**http://www.ie.bilkent.edu.tr/~lors/ie572/burhaneddin.pdf

16. **Birke.V, Burmeier, H., and Rosenau, D. (2003),** Design, Construction, and Operation of Tailored Permeable Reactive Barriers. Practice Periodical of Hazardous, Toxic, and Radioactive, Waste Management, 7(4), 264-280.

17. **BIS (1989),** *Compendium of Indian Standards on Soil Engineering. Part 1, 1989*. Bureau of Indian Standards, India.

18. **Bopp L.H., and Echrlich (1998),** "Chromate resistance and reduction in *pseudomonas fluorescents strain LB300*, Arch Microbiol., 150, 426-431.

19. **Bopp, L.H. (1980),** Chromate resistance and chromate reduction in bacteria. Ph.D Theses Rensselaer Polytechnic Institute, Troy, New York.

20. **Borden, R.C., Goin, R.T., Kao, C.M. (1997),** Control of BTEX migration using a biologically enhanced permeable barrier. Ground Water Monitoring and Remediation, 17(1), 70-80.

21. **Boupha, K., J.M. Jacobs and K. Hatifield (2004),** MDL Groundwater software: Laplace transforms and the De Hoog algorithm to solve contaminant transport equations. *Computers & Geosciences*, 30*,* 445-453.

22. **Brady, D.**, **B. Letebele, J.R. Duncan** and **P.D. Rose (1994),** Bioaccumulation of metals by *Scenedesmus, Selenastrum* and *Chlorella algae. Water* SA 20, 213-218.

23. **Brun, A.** and **P. Engesgaard (2002a),** Modelling transport and biogeochemical processes in pollution plumes: literature review and model development. *J. Hydrol.,* 256, 211-227.

24. **Brun, A., P. Engesgaard** and **D. Rosbjerg (2002b),** Modelling transport and biogeochemical processes in pollution plumes: Vejen land fill, Denmark. *J. Hydrol.,* 256, 228-247.

25. **Buczko, U., L. Hopp, W. Berger, W.Durner, S. Peiffer,** and **M.Scheithauer (2004),** Simulation of chromium transport in the unsaturated zone for predicting contaminant entries into the groundwater. *Journal of Plant Nutrition Soil Science,* 167, 284-292.

26. **Budavari, S. (1996),** *The Merck Index: Encyclopedia of Chemicals, Drugs, and Biologicals*, Whitehouse Station NJ., 12, 374.

27. **Campos J, M. Martinez-Pacheco, C. Cervantes, (1995),** Hexavalent-chromium reduction by a chromate resistant Bacillus sp. strain, Anton. Leeuwenhoek 68, 203–208.

28. **Cappuccino, J.G.** and **N. Sherman (1996),** *Microbiology. A Laboratory Manual.* The Benjamin/Cummings Publishing Co., Inc. Menlo Park, California.

29. **Carrayrou, J., R. Mose** and **P. Behra (2004),** Operator-splitting procedures for reactive transport and comparison of mass balance errors, *J. Conta. Hydrol.*, 68, 239-68.

30. **Cercona Inc. (1995),** Status Report-Test Results Using Cercona Iron Based Foams for Dehalogenation Chlorinated Solvents& Adsorption of Heavy Metals, Contaminated Groundwater.

31. **Cervantes, C., J. Campos-Garcia, S. Devars, F. Gutierrez-Corona, H. Loza-Tavera, J.C. Torres-Guzman, and R. Moreno-Sanchez (2001),** Interactions of chromium with microorganisms and plants. *FEMS Microbiol. Rev.,* 25, 335-347.

32. **Chapelle, F.H. (1995),** Factors affecting the efficiency of intrinsic bio-remediation under anaerobic conditions. *Platform abstracts, in situ and on-site bioreclamation, 3rd Int'l Symp.,* April, San Diego, Calif.

33. **Chen J.M. and O.J. Hao, (1998),** Microbial chromium (VI) reduction, Crit. Rev. Environ. Sci. Technol. 28 (3) 219–251.

34. **Chen, J.M.** and **O..J. Hao (1997)**, Biological removal of aqueous hexavalent chromium. *J. Chem Technol. Biotechnol*., 69, 70.

35. **Chen, J.M. and O.J. Hao (1996),** Environmental factors and modeling in microbial chromium (VI) reduction. *Water Environ. Res.,* 68 , 1156.

36. **Chen, Y.M., L. M. Abriola, P. J.J. Alvarez, P. J. Anid,** and **T. M.Vogel (1992),** Modeling Transport and Biodegradation of Benzene and Toluene in sandy aquifer material: Comparisons with experimental measurements. *Water Resour. Res.,* **28**, 1833-1847.

37. **Chiang, C.Y., C.N. Dawson** and **M.F. Wheeler (1991)**, Modeling of in-situ biorestoration of organic compounds in groundwater. *Transport Por Med,* 6, 667-702.

38. **Chilakapati, A., S. Yabusaki, J. Szecsody,** and **W. Macevoy (2000),** Groundwater flow, multicomponent transport and biogeochemistry: Development and application of a coupled process model. *J. Conta. Hydrol*., 43, 303-325.

39. **Cirpka, O.A, E.O. Frind** and **R. Helmig (1999),** Numerical methods for reactive transport on rectangular and streamline-oriented grids. *Adv. Water Resour.*, 22,711-728.

40. **Clement, T.P, B.M. Peyton, R.S. Skeen, D.A. Jennings** and **J.N. Petersen (1997),** Microbial growth and transport in porous media under denitrification conditions: Experiment and simulations. *J. Conta. Hydrol.,* 24, 269-285.

41. **CPCB** (1996) *Groundwater Quality in Kanpur, Status, Sources and Control Measures: GWQS/8/1996* CPCB Publications, India. http://www.envfor.nic.in /cpcb/ cpcbpub.html

42. **Das, S. and A.L. Chandra (1990),** Chromate reduction in Streptomyces. *Experientis*, 46, 731.

43. **Dayan, A.D. and A.J. Paine (2001),** Mechanisms of chromium toxicity, carcinogenicity and allergenicity: review of the literature from 1985 to 2000. *Human Exp. Toxicol.,* 20, 439-451.

44. **De Camp, Shannon (2006),** *OSHA's New Hexavalent Chromium Standard: What it means to you and your employees.* Practical Welding Today.

45. **Dowdy, R.H.** and **V.V. Volk (1983),** Movement of heavy metals in soils. Chapeter15 in Chemical Mobility and Reactivity in Soil Systems (D.W.Nelson, Ed.). Soil Science Society of America (SSSA) Special Publication 11. Madison, Wisconsin: American Society of Agronomy. 229-240.

46. **Eary, L.E.** and **D. Rai (1987),** Kinetics of chromium (III) oxidation to chromium(VI) by reaction with manganese dioxide. *Environ. Sci. Technol*., 21, 1187-1193.

47. **Ellis, B.G., B.D. Knezek** and **L.W. Jacobs (1983),** The movement of micronutrients in soils. Chapter 8 in Chemical Mobility and Reactivity in Soil Systems (D.W.Nelson, Ed.). Soil Science Society of America (SSSA) Special Publication 11. Madison, Wisconsin: American Society of Agronomy. 109-122.

48. **Engesgaard, P.** and **K.L. Kipp (1992),** A geochemical model for redox-controlled movement of mineral fronts in ground-water flow systems: a case of nitrate removal by oxidation of pyrite. *Water Resour. Res.,* 28, 2829-2843.

49. **Farthing, M.W.** and **C. T. Miller (2001),** A comparison of high-resolution, finitevolume, adaptive-stencil schemes for simulating advective-dispersive transport. *Adv. Water Resour.,* 24, 29-48.

50. **Federal Remediation Technologies Roundtable (2008),** "www.frtr.gov"

51. **Fetter**, **C.W. (1993),** Contaminant Hydrogeology, Prentice Hall, Canada.

52. **Freeze and Cherry (1979)**.*Groundwater*, Prentice-Hall.

53. **Friedly, J. C., J. A. Davis** and **D.B. Kent (1995),** Modeling hexavalent chromium reduction in groundwater in field-scale transport and laboratory batch experiments. *Water Resour. Res.*, 31, 2783-2794.

54. **Fujie, K., T. Tsuchida, K. Urano and H. Ohtake (1994),** Development of a bioreactor system for the treatment of chromate wastewater using *Enterobacter cloacae* HOI. *Wat. Sci. Technol.,* 30, 235.

55. **Fuller, W.H. (1977),** Movement of selected metals, asbestos, and cyanide in soil; applications to waste disposal problems. EPA-600/2-77-020. Cincinnati, Ohio:USEPA.

56. **Ganguli, A.** and **A.K. Tripathi (2002),** Bioremediation of toxic chromium from electroplating effluent by chromate-reducing *Pseudomonas aeruginosa* A2Chr in two bioreactors. *Appl. Microbiol. Biotechnol.,* 58**,** 416-420.

57. **Gerritsee, R.G., R.Vriesema, J.W. Dalenberg** and **H.P.D. Roos (1982),** Effect of sewage sludge on trace element mobility in soils. *J. Environ. Qual*., 11, 359-364.

58. **Goldberg, D.E. (1989),** GeneticAlgorithm in Search, Optimization and Machine Learning. Addison-Wesley, Reading, MA.

59. **Gopalan R, H. Veeramani, (1994),** Studies on microbial chromate reduction by Pseudomonas sp. in aerobic continuous suspended growth cultures, Biotechnol. Bioeng. 42, 471-576.

60. **Grevatt, P.C. (1998),** *Toxicological Review of Hexavalent Chromium*. US Environmental Protection Agency.

61. **Guha H, (2004),** Biogeochemical influence on transport of chromium in manganese sediments: experimental and modeling approaches Journal of Contaminant Hydrology, 70 (1-2) pp.1-36.

62. **Guha, H., J.E. Saiers, S.Brooks, P.M. Jardine** and **K. Jayachandran (2001),** Chromium transport, oxidation, and adsorption in manganese-coated sand. *J. Conta. Hydrol.,* 49, 311-334.

63. **Guha, H., K. Jayachandran, and F. Maurrasse (2003),** Microbiological reduction of chromium (VI) in presence of pyrolusite-coated sand by *Shewanella alga* Simidu ATCC 55627 in laboratory column experiments. *Chemosphere*, **52**, 175-183.

64. **Gvozdyak, P.L., N.F. Mogilavich, A.F. Rylskii, and N.I. Grishchenko (1986),** Reduction of hexavalent chromium by collection strains of bacteria. *Microbiologiya,* 55, 962.

65. **Gwo, J.P., E.F. D'Azevedo, H. Frenzel, M. Mayes, G. Yeh, P. M. Jardine, K.M. Salvage and F.M. Hoffman, (2001),** HBGC123D: a high-performance computer model of coupled hydrogeological and biogeochemical processes. *Computers & Geosciences*, 27, 1231-1242.

66. **Haran, B.S.**, **B. N. Popov, G. Zheng** and **R.E. White (1997),** Mathematical modeling of hexavalent chromium decontamination from low surface charged soils. *J. Hazard. Mater.*, **55**, 93-107.

67. **Haran, B.S., B.N. Popov, G. Zheng** and **R.E. White (1996),** Development of a new electrokinetic technique for decontamination of hexavalent chromium from low surface charged soils. *Environ. Prog.,* 15, 166-172.

68. **Herbert, D., P.J. Phipps, and J.E. Strange, (1971),** Chemical analysis of microbial cells, in: J.R. Norris, D.W. Ribbons (Eds.), *Methods in Microbiology*, Academic Press, New York.

69. **Herzer, J**. and **W. Kinzelbach (1989),** Coupling of transport and chemical processes in numerical transport models. *Geoderma,* 44, 115–127.

70. **Herzer, J., and Kinzelbach, W. (1989).** Coupling of transport and chemical processes in numerical transport models. Geoderma, 44, 115–127.

71. **Horitsu, H., S. Tuto, Y. Miyazawa, S. Ogal and K. Kawai (1987),** Enzymatic reduction of hexavalent chromium tolerant Pseudomonas ambigua G-1, *Agri. Biol.Chem.*, 51*,* 2417.

72. **Hossain, M.A., M. Alam** and **D.R. Yonge (2005a),** Estimating the dual-enzyme kinetic parameters for Cr (VI) reduction by Shewanella oneidensis MR-1 from soil column experiments, *Wat. Res.,* 39, 3342–3348.

73. **Hossain, M.A., M. Alam** and **D.R. Yonge (2005b),** Finite element modeling of Cr(VI) reduction by Shewanella oneidensis MR-1 employing the dual-enzyme kinetic model. *Computers & Geosciences,* 31*,* 1286-1292.

74. **Hu, Z., Chan, C.W., and Huang, G.H. (2006),** Model predictive control for in situ bioremediation system, Advances in Engineering Software. 37(8), 514-521.

75. **Ishibashi, Y., C.Cervantes and S. Silver (1990),** Chromium reduction in Pseudomonas putida. *Appl. Environ. Microbiology,* 56, 2268.

76. **James, B.R. (1996),** The Challenge of remediating chromium-contaminated soil. *Environ Sci. Technol.*, 30, A248-A251.

77. **Jardine PM, SF Fendorf, MA Mayes, L. Larsen, SC Brooks, B Bailey, (1999),** Fate and transport of chromium in undisturbed heterogeneous soil. Environmental Science and Technology,. 33, 2939-2944.

78. **Jardine, P.M.** and **D.L. Taylor (1995),** Kinetics and mechanisms of Co (II) EDTA oxidation by pyrolusite. *Geochim. Cosmochim. Acta.,* 59**,** 4193-4203.

79. **Jardine, P.M.**, **S.F. Fendorf**, **M.A. Mayes, L. Larsen, S.C. Brooks** and **B. Bailey (1999),** Fate and transport of chromium in undisturbed heterogeneous soil. *Environ. Sci. Technol.,* 33, 2939-2944.

80. **Johnson, C.A.** and **A.G. Xyla (1991),** The oxidation of chromium (III) to chromium (VI) on the surface of magnetite (γ-MnOOH). *Geochim. Cosmochim*, 55**,** 2861-2866.

81. **Kabata-Pendias, A.** and **H. Pendias, (1984),** Trace Elements in Soils and Plants, CRC Press, Boca Raton, Florida

82. **Kalin, R.M. (2004),** Engineered passive bioreactive barriers:risk-managing the legacy of industrial soil and groundwater pollution. Current Opinion in Microbiology, 7(3), 227-238.

83. **Kanney, J. F., C. T. Miller** and **C. T. Kelley (2003),** Convergence of iterative split operator approaches for approximating nonlinear reactive transport problems, *Adv. Water Resour.*, 26, 247-261.

84. **Kao, C.M., Chen, S.C., Liu, J.K. (2001),** Development of a biobarrier for the remediation of PCE-contaminated aquifer. Chemosphere, 43, 1071-1078.

85. **Kent, D.B., J.A. Davis, L.C.D. Anderson** and **B.A. Rea (1994),** Transport of chromium and selenium in the suboxic zone of a shallow aquifer: influence of redox and adsorption reactions. *Water Resour. Res.,* 30, 1099-1114.

86. **Kent, D.B., J.A. Davis, L.C.D. Anderson** and **B.A. Rea (1995),** Transport of chromium and selenium in a pristine sand and gravel aquifer: role of adsorption processes. *Water Resour. Res.,* 31**,** 1041-1050.

87. **Khan, H.M., A. Mahmood (2007),** Radiation induced decontamination of Cr(VI), Cu(II) and phenol in some tannery effluents. *Nuclear Science and Techniques*, 4, 212-217.

88. **Kindred, S. J. and M.A. Celia** and **(1989),** Contaminant Transport and Biodegradation: 2. Conceptual Model and Test Simulations, *Water Resour. Res.,* 25, 1149-1159.

89. **Kinzelbach, W., W. Schafer** and **J. Herzer (1991),** Numerical modeling of natural and enhanced denitrification processes in aquifers. *Water Resour. Res*. 27, 1123–1135.

90. **Kohne, J. M., S. Kohne, and J. Simunek (2006),** Multi-process herbicide transport in structured soil columns: experiments and model analysis, *J. Contam. Hydrol. 85*, 1-32.

91. **Komori, K., P. Wong and H. Ohtake (1989),** Factors affecting chromate reduction in *Enterobacter cloacae strain* HOI. *App. Microbiol. Biotechnol,* 31, 567.

92. **Kvasnikov E.I, Stepanyuk V.V, Kiyushnikova T.M, Serpokrylov N.S, Simonova G.A, Ksathina T.P and Panchenko L.P (1985),** "A new chromium reducing gram-variable bacterium with mixed type of Flagellation, Mikrobiologiya, 54, 83-88.

93. **Kvasnikov, E.I., T.M. Klyushnikova, T.P. Kasatkina, V.V. Stepanyuk, and S.L. Kuberskaya (1988),** Chromium reducing bacteria in nature and industrial sewage. *Microbiologiya*, 57, 680.

94. **Langard, S**. **(1980)**, Chromium. In: Waldron HA (eds.) Metals in the environment. Academy Press Inc, New York,

95. **Lebedeva, E.V. and N.N. Lyalikova (1979),** Reduction of crococite by *Pseudomonas chromatpphila.*. *Mickrobiologiya,* 48, 517.

96. **Liu, C. and J. M. Zachara, (2001).** Uncertainties of Monod Kinetic Parameters Nonlinearly Estimated from Batch Experiments, *Environ. Sci. Technol. 35,* 133-141.

97. **Liu.Y., and Minsker, B.S. (2004),** Full multiscale approach for optimal control of in situ bioremediation, Journal of Water Resources Planning and Management, 130(1), 26–32.

98. **Llovera S., R.Bonet, M.D. Simon-Pulol and F.Congregado (1993),** Chromate reduction by rsting cells of Agrobacterium radiobacter EPS-916. *Appl. Environmental Microbiology*, 59, 3516.

99. **Lofroth, G., B.N. Ames (1978),** Mutagenicity of inorganic compounds in Salmonella typhimurium: arsenic, chromium and selenium. *Mutat. Res.,* 53, 65–66**.**

100. **Luo, H., Y. Lu, X. Shi, Y. Mao and N.S. Delal (1996)**, Chromium (IV)-mediated Fenton-like reaction causes DNA damage: implication to genotoxicity of chromate. *Ann Clin. Lab. Sci.,* 26, 185–191.

101. **Manceau, A.** and **L. Charlet (1992),** X-ray absorption spectroscopic study of the sorption of Cr(III) at the oxide/water interface: I. Molecular mechanism of Cr(III) oxidation on manganese oxides. *J. Colloid Interface Sci.* 148**,** 425-442.

102. **Manivasakam, N. (1987),** *Industrial effluents (origin, characteristics, effects analysis and treatment)*. Sakthi Publications Kovaipur, Coimbatore.

103. **Maskey, S., Jonoski, A., and Solomatine, D. (2002),** Groundwater remediation strategy using global optimization algorithms. Journal of Water Resources Planning and Management, 128(6), 431-440.

104. **Mayer, K. U., D.W. Blowes and E. O. Frind (2001),** Reactive transport modelling of an insitu reactive barrier for the treatment of hexavalent chromium and trichloroethylene in groundwater. *Water Resour. Res.*, 37, 3091-3103.

105. **Mayer, K. U., E. O. Frind and D.W. Blowes (2002)**, Multicomponent reactive transport modeling in variably saturated porous media using a generalized formulation for kinetically controlled reactions. *Water Resour. Res.,* 38, 13.

106. **Meegoda, J.N., K. Partymiller, M. K. Richards, W. Kamolpornwijit, W. Librizzi, T. Tate, B. A. Noval, R. T. Mueller** and **S. Santora (2000),** Remediation of Chromium-Contaminated Soils- Pilot-Scale Investigation. *Pract. Periodical of Haz., Toxic, and Radioactive Waste Mgmt*., *ASCE,* 4, 1, 7-15.

107. **Meegoda, J.N., W. Kamolpornwijit, D.A. Vaccari, A. S. Ezeldin, B. A. Noval, R. T. Mueller and S. Santora (1999),** Remediation of Chromium-Contaminated Soils: Bench-Scale Investigation. *Pract. Periodical of Haz., Toxic, and Radioactive Waste Mgmt*., *ASCE,* 3, 124-131.

108. **Miller, R.R. (1996),** Phytoremediation. "Ground-Water Remediation Technologies Analysis Center Technology Overview Report."

109. **Minsker, B.S.** and **C.A. Shoemaker (1998),** Dynamic Optimal Control of In-Situ Bioremediation of Ground Water. *Journal of Water Resources Planning and Management, ASCE,* 124, 149-161.

110. **Moazed, H.**, E. Maroufpour, H.A. Kashkouli, and J.M.V. Samani (2009), Laboratory scale effect of aquifer thickness on dispersivity of porous media. *J. of Applied Sciences, Asian Network for Scientific Information,* 9(3), 542-548.

111. **Mohamed, M.A.M., K. Hatfield** and **A.E. Hassan (2005),** Monte Carlo evaluation of microbial-mediated contaminant reactions in heterogeneous aquifes, *Adv. Water Resour.*, *In Pres, Corrected Proof. Available online*

112. **Mohan, D., and C.U. Pittman Jr. (2006),** Activated carbons and low cost adsorbents for remediation of tri- and hexavalent chromium from water. *J. Hazard. Mater.* B 137, 762- 811.

113. **Murphy, E.M., T.R. Ginn, A. Chilakapati, C.T. Resch, J.L. Phillips, T.W. Wietsma** and **C.M. Spadoni (1997),** The influence of physical heterogeneity on microbial degradation and distribution in porous media. *Water Resour. Res.*, **33**, 1087–1103.

114. **Myers, C., J.M. Myers (**1998**),** Iron stimulates the rate of reduction of hexavalent chromium by human mi**cr**osomes**.** *Carcinogenesis,* 19, 1029-39.

115. **Nakamuro, K., K. Yoshikawa, Y. Sayato, and H. Kurata (1978),** Comparative studies of chromosomal aberration and mutagenicity of trivalent and hexavalent chromium. *Mutat. Res.*, 58: 175-181.

116. **Nishioka, H. (1975),** Mutagenic activities of metal compounds in bacteria. *Mutat. Res.,* 31, 185-189.

117. **O'Brien, T. J., J. L. Fornsaglio, S. Ceryak and S.R. Patierno (2002),** Effects of hexavalent chromium on the survival and cell cycle distribution of DNA repair-deficient S. cerevisiae. *DNA Repair,* 1**,** 617-627.

118. **O'Brien, T., J. Xu, and S.R. Patierno (2001)**, Effects of glutathione on chromium-induced DNA crosslinking and DNA polymerase arrest. *Mol. Cel.l Biochem.,* 222, 173-182.

119. **O'Hannesin, S. (1999)**, An Overview of Installation Methods for PRBs, USEPA Conference on Abiotic In Situ Technologies for Groundwater Remediation, Dallas, Texas.

120. **Ohtake, H., E. Fujii** and **K. Toda (1990),** Bacterial reduction of hexavalent chromium: Kinetic aspects of chromate reduction by *E.Cloacae* HO1. *Biocatalysis,* 4, 227-235.

121. **Palmer, C.D.** and **P.R. Wittbrodt (1991)**, Processes Affecting the Remediation of Chromium-Contaminated sites, *Environmental Health Perspectives,* 92, 25-40.

122. **Park, K.** and **A.Y. Kuo (1996),** A multi-step computation scheme: decoupling kinetic processes from physical transport in water quality models. *Wat. Res.*, 30, 2255-2264.

123. **Patterson, J.W. (1985),** Hexavalent chromium. In: Industrial waste water treatment technology, Butterworth Publishers, Stoneham.

124. **Pelczar Jr. M.J., E.C.S. Chan** and **N.R. Krieg, (1993),** *Microbiology*, Tata McGraw Hill Edition, New Delhi,

125. **Philip L, L. Iyenkar and C. Venkobacher (1998),** Cr (VI) reduction by Bacillus coagulans isolated from contaminated soil, J of Env Engg. ASCE.,124 (12), 1165-1170.

126. **Philip L., L. Iyengar and C. Venkobachar (1999),** Immobilized Microbial Reactor for the Biotransformation of Hexavalent Chromium. *Int. J. Environment and Pollution*. 11, 202-210.

127. **Press, W.H., S.A. Teukolsky, W.T. Vetterling,** and **B.P. Flannery** *Numerical Recipes in C++: The Art of Scientific Computing,* Cambridge University Press, 2002.

128. **Puls RW, JP Cynthia, RM Powell, (1999),** The application of in situ permeable reactive (zero-valent iron) barrier technology for the remediation of chromate-contaminated groundwater, Applied Geochemistry 14 989-1000.

129. **Putti, M., W.W.G. Yeh,** and **W.A. Mulder (1990),** A triangular finite volume approach with high resolution upwind terms for the solution of groundwater transport equation. *Water Resour. Res.*, 26, 2865-2880.

130. **Rai D, L. E. Eary,** and **J. M. Zachara (1989)**, Environmental chemistry of chromium. *Sci. Total Environ*. 86, 15-23.

131. **Rai, D., B.M. Sass** and **D.A. Moore (1987),** Chromium(III) hydrolysis constants and solubility of chromium(III) hydroxide. *Inorg. Chem*. 26, 345-349.

132. **Rai, D., J.M. Zachara, L.E. Eary, D.C. Girvin, D.A. Moore, C.T. Resch, B.M. Sass** and **R.L. Schmidt (1986)**, Geochemical behaviour of chromium species. Interim Report EPRI EA-3356, E.P.R.I Palo Alto, Calif.

133. **Reddy, K.** and **S. Chinthamreddy (1999),** Electrokinetic remediation of heavy metal-contaminated soils under reducing environments. *Waste Manage*, 19, 269-282

134. **Reddy, K.** and **U.S. Parupudi (1997),** Effects of soil composition on the removal of chromium by electrokinetics. *J. Hazard. Mater.,* 55, 135-158.

135. **Remoundaki, E., A. Hatzikioseyian and M. Tsezos (2007),** A systematic study of chromium solubility in the presence of organic matter: consequences for the treatment of chromium-containing wastewater. *Journal of Chemical Technology and Biotechnology*. **82**(9), 802-808.

136. **Reynolds, M., E. Peterson, G. Quievryn, and A. Zhitkovich** (2004) Human nucleotide excision repair efficiently removes chromium- DNA phosphate adducts and protects cells against chromate toxicity. *J. Biol. Chem.,* **279**, 30419-30424.

137. **Ribesa, J., K. Keesmanb** and **H. Spanjers** (2004) Modelling anaerobic biomass growth kinetics with a substrate threshold concentration, *Wat. Res.,* **38**, 4502-4510.

138. **Richard, FC** and **ACM Bourg (1991),** Aqueous geochemistry of chromium: *A* review. *Wat. Res.,* 25, 807-816.

139. **Riley, R.G., J.M. Zachara, and F.J. Wobber (1992)**, Chemical contaminants on DOE lands and selection of contaminant mixtures for subsurface science research. Washington, DC: US Department of Energy. Pii-77.

140. **Robinson, B. A., H. S. Viswanathan** and **A. J. Valocchi** (**2000**), Efficient numerical techniques for modeling multicomponent ground-water transport based upon simultaneous solution of strongly coupled subsets of chemical components, *Adv. Water Resour.*, 23, 307-324.

141. **Romanenko, V.I.and V.N. Korenkov (1977),** A pure culture of bacteria utilizing chromate and dichromate as hydrogen acceptors in growth under anaerobic conditions. *Mikrobiologiya,* 46**,** 414-417.

142. **Saaltink, M.W., J. Carrera and C. Ayora (2000),** A comparison of two approaches for reactive transport modelling. *Journal of Geochemical Exploration,* 69*,* 97-101.

143. **Saaltink, M.W., J. Carrera** and **C. Ayora (2001),** On the behavior of approaches to simulate reactive transport. *J. Conta. Hydrol.*, 48, 213-235.

144. **Sah, J.G**. and **J.Y. Chen (1998)**, Study of the electrokinetic process on Cd and Pb-spiked soils. *J. Hazard. Mater.* 58, 301-315.

145. **Selim, H.M., M. C. Amacher, I. K. Iskandar**, **(1990),** Modeling the transport of heavy metals in soils. USA Cold Regions Research and Engineering Laboratory, CRREL Monograph, Hanover, NH,

146. **Shen and Wang Y.T (1995),** "Hexavalent chromium removal in two stage bioreactor system", J. of Env. Engg., 11, 798-804.

147. **Shieh, H.J., and Peralta, R. (2005),** Optimal in situ bioremediation design by hybrid genetic algorithm-simulated annealing. *Journal of Water Resources Planning and Management*, 131(1), 67-78.

148. **Sidle, R.C., L.T. Kardos** and **M.Th. van Genuchten (1977),** Heavy metals transport in a sludge treated soil. *J. Envi. Qual.*, 6, 438-445.

149. **Skeffington, R.A., P.R. Shewry and P.J. Petersen (1976)**, Chromium uptake and transport in barley seedlings Hordeum vulgare. *Planta*, 132**,** 209-214.

150. **Srivastava, R.** and **T.C. J. Yeh (1992)**, A three dimensional numerical model for water flow and transport of chemically reactive solute through porous media under variably saturated conditions. *Adv. Water Resour.*, 15, 275-287.

151. **Steefel, C. I.** and **K.T.B. MacQuarrie** (1996) Approaches to modeling of reactive transport in porous media, *in* Lichtner, P. C., Steefel, C. I., and Oelkers, E. H., editors, Reactive transport in porous media: Mineralogical Society of America, *Reviews in Mineralogy*, 34, 83-129.

152. **Steefel, C. I.** and **K.T.B. MacQuarrie (1996),** Approaches to modeling of reactive transport in porous media, *in* Lichtner, P. C., Steefel, C. I., and Oelkers, E. H., editors, Reactive transport in porous media: Mineralogical Society of America, *Reviews in Mineralogy*, 34, 83-129.

153. **Steefel, C.I., D.J. DePaolo** and **P.C. Lichtner, (2005**), Reactive transport modeling: An essential tool and a new research approach for the earth sciences. *Earth and Planetary Science Letters*, 240, 539-558.

154. **Stefanovic, D.**L. and **H.G. Stefan (2001),** Accurate two-dimensional simulation of advective-diffusive-reactive transport. *J. Hydraulic Eng.* 127, 728-37

155. **Suthersan, S. (1997),** Remediation Engineering: Design Concepts. Lewis Publishers, Boca Raton,

156. **Tebes-Stevens, C., A. J. Valocchi, J. M. VanBriesen** and **B. E. Rittmann (1998),** Multicomponent transport with coupled geochemical and microbiological reactions: model description and example simulations, *J. Hyrol.,* 209, 8-26.

157. **Tokunaga, T.K. , J. Wan, M.K. Firestone, T. C. Hazen, E. Schwartz, S.R. Sutton** and **M. Newville (2001),** Chromium Diffusion and Reduction in Soil Aggregates. *Environ. Sci. Technol.*, 35, 3169-3174.

158. **U.S. Environmental Protection Agency, (1996),** 3060A Alkaline digestion for hexavalent chromium SW-846., http://www.epa.gov/ sw-846/pdfs/3060a.pdf

159. **U.S. Environmental Protection Agency, (1997),** Technology Alternatives for the Remediation of Soils Contaminated with As, Cd, Cr, Hg, and Pb. Engineering Bulletin. EPA/540/S-97/50.

160. **U.S. Environmental Protection Agency, (1997a),** Ppermeable reactive subsurface barriers for the interception and remediation of chlorinated hydrocarbon and chromium (VI) plumes in ground water. U.S. EPA Remedial Technology Fact Sheet. EPA/600/F-97/008.

161. **U.S. Environmental Protection Agency, (2000),** In situ treatment of soil and groundwater contaminated with chromium EPA/625/R-00/005, 2000.

162. **Van Leer, B. (1977a)**, Towards the ultimate conservative difference scheme:III. Up-stream centered finite difference schemes for ideal compressible flow. *J. Computational. Physics*, **23**, 263-275.

163. **Van Leer, B. (1977b),** Towards the ultimate conservative difference scheme:IV. A New Approach to Numerical convection. *J. Computational. Physics,* **23,** 276-299.

164. **Venitt, S., L. S. Levy (1974),** Mutagenicity of chromates in bacteria and its relevance to chromate carcinogenesis. *Nature* 250, 493-495.

165. **Virkutyte, J., M. Sillanpaa, P. Latostenmaab, (2002),** Electrokinetic soil remediation - critical overview. *The Science of the Total Environment,* 289, 97-121.

166. **Vogan, J.L., Focht, R.M., Clark, D.K., and Graham, S.L. (1999),** Performance evaluation of a permeable reactive barrier for remediation of dissolved chlorinated solvents in groundwater. Journal of Hazardous Materials, 68, 97-108.

167. **Waddill, D.W.** and **Widdowson, M.A. (1998)**, Three-dimensional model for subsurface transport and biodegradation. *J. Environ. Engg.*, *ASCE,* 124**,** 336-344.

168. **Wang L.K. and L. Li (2006),** *Chemical Reduction/Oxidation, in: Advanced Physicochemical Treatment Processes*, Humana Press. *Inc*., USA.

169. **Wang P, Mori, T.K., Kamori, M., Sesatu, K. and H. Ohtake, (1989),** Isolation and characterization of an *Enterobacter cloacae* strain that reduces hexavalent chromium under anaerobic condition. Appl. Environ. Microbiol., 55, 1665-1669

170. **Wang, C.H., Huang, C.P., and P.F. Sanders, (2002),** "Transport of Cr(VI) in soils contaminated with chromite ore processing residue(COPR)." *Practice Periodical of Hazardous,Toxic, and radioactive waste management*.,6,6-13.

171. **Wang, Y.T** and **C. Xiao (1995),** Factors affecting hexavalent chromium reduction in pure cultures of bacteria. *Wat. Res.,* 29, 2467.

172. **Warith, M., Fernandes, L., Gaudet, N. (1999),** Design of in-situ microbial filter for the remediation of naphthalene. Waste Management, 19, 9-25.

173. **Weng, C.H., C.P. Huang** and **P.F. Sanders (2002),** Transport of Cr (VI) in soils contaminated with Chromite Ore Processing Residue (COPR), *Practice periodicals of Hazardous, toxic and radioactive waste management*. 6, 6-13.

174. **Wilkin, R.T., Su, C.M., Ford, R.G., Paul, C.J. (2005),** Chromium-removal processes during groundwater remediation by a zerovalent iron permeable reactive barrier. Environ. Sci. Technol. 39(12), 4599-4605.

175. **Yang, Z.Y. and Z.S. Fan (1990),** Treatment of leather and fur wastewater by a rotating biological contactor. *Water Sci. Technol.,* 22, 119-126.

176. **Yeh, G. T., M. D. Siegel** and **M. H. Li (2001),** Numerical Modeling of Coupled Fluid Flows and Reactive Transport Including Fast and Slow Chemical Reactions. *J. Conta. Hydrol*., 47, 379-390.

177. **Yeh, G.T. and Tripathi, V.S. (1991),** A model for simulating transport of reactive multi-species components: Model development and demonstration. Water Resour. Res. 27, 3075-3094.

178. **Yoon, J.H., and Shoemaker, C.A. (1999),** Comparison of optimization methods forground-water bioremediation, Journal of Water Resources Planning and Management, Vol. 125, No. 1, 57-63.

179. **Zachara, J.M., D.C. Girvin, R.L. Schmidt** and **C.T. Resch (1987),** Chromate adsorption on amorphous iron oxyhydroxide in the presence of major groundwater ions. *Environ. Sci. Technol*., 21, 589-594.

180. **Zheng, C., and Wang , P. (1999),** An integrated global and local optimization approach for remediation system design. Water Resour. Res., 35(1), 137-148.

181. **Zysset, A., F. Stauffer** and **T. Dracos (1994),** Modeling of reactive groundwater transport governed by biodegradation. *Water Resour. Res.,* 30**,** 2423-2434.

PROJECT OUTPUTS

1. Publications Based on the Work:

1. T. Shashidhar, L. Philip, and S. Murty Bhallamudi, "Bench scale column experiments to study the containment of Cr(VI) in confined aquifers by biotransformation", Journal of Hazardous materials, **Elsevier**, B 131, 200-209, 2006.

2. T. Shashidhar, S. Murty Bhallamudi, Ligy Philip, Development and validation of a model of bio-barriers for remediation of Cr(VI) contaminated aquifers using laboratory column experiment, Jl. of Hazardous Materials, **Elsevier**, Vol. 145, No. 3, 437-452, 2007.

3. T. Shashidhar, Nisha Nandanan, Ligy Philip, S. Murty Bhallamudi, "Design of a passive bio-barrier system for chromium containment in confined aquifers", Practice Periodical of Hazardous, Toxic, and Radioactive Waste Management, **ASCE,** Vol. 11, No. 4, 216 – 224, 2007.

4. V. Somasundaram, Ligy Philip, S. Murty Bhallamudi, "Experimental and mathematical modeling studies on Cr(VI) reduction by CRB, SRB, and IRB, individually and in combination", Jl. of Hazardous Materials, **Elsevier**, Vol. 172, No. 2-3, pp. 606-617, 2009.

5. J. Jeya Singh, Ligy Philip, S. Murty Bhallamudi, "Experimental and Modeling Studies for the Bioremediation of Cr(VI) Contaminated Aquifers", accepted for publication in the ASCE-EWRI International Conference to be held in Chennai in January 2010.

6. J. Jeya Singh, Ligy Philip, S. Murty Bhallamudi, "Pilot scale studies for the bioremediation of Cr(VI) contaminated aquifers using biobarrier and reactive zones", paper under preparation for submission to Jl. of Hazardous Materials.

2. Theses Submitted / to be Submitted:

1. **T. Shashidhar,** "Experimental and modeling studies on transport and bio-transformation of chromium in contaminated aquifers", Ph.D.

2. **Nisha Nandanan,** "Optimal design of bio-barriers for Cr(VI) containment in confined aquifers", M. Tech.

3. **G. Siva Prakash,** "Two-dimensional mathematical modeling of fate and transport of Cr(VI) in groundwater", B. Tech.

4. **V. Somasundaram,** "Biotic and abiotic remediation of chromium contaminated aquifers", M.S. (to be submitted in 2010)

5. **J. Jeya Singh,** "Remediation of Cr(VI) contaminated sites using biological systems", Ph.D. (to be submitted in 2010)

3. New Projects Formulated:

1. **Clean-up of Cr(VI) Contaminated aquifers in Ranipet, Tamilnadu, Sponsoring Agency: Central Pollution Control Board, Amount: Rs. 1.0 Lakhs.**

   Dr. Ligy Philip and Dr. B.S. Murty were advisers on this pilot project which was jointly investigated by Central Pollution Control Board (CPCB), Tamilnadu Pollution Controil Board (TNPCB), and National Geophysical Research Institute (NGRI). Based on the above pilot study as well as studies carried out by Dr. Ligy Philip and Dr. B.S. Murty as part of the MoWR project, CPCB decided to try the option of bioremediation

2. **Demonstration project for bioremediation of chromium contaminated soil and aquifer in Ranipet area, Sponsoring Agency: Central Pollution Control Board, Value of Project: Rs. 14,41,200/-**

   Based on the results obtained as part of the current study sponsored by the MoWR, a new project has been formulated. This new project is being sponsored by the Central Pollution Control Board. This new project involves field demonstration for bioremediation of chromium contaminated soils and aquifer in Ranipet area. A plot of 5 m X 5 m has been chosen and 4 recharge wells have been sunk at one end of the plot. Chromium Reducing Bacteria (CRB) and molasses will be injected through these wells to create reactive zones around the wells. Monitoring wells have been sunk around these wells. Water samples will be collected from these monitoring wells and analyzed for Cr(VI) to assess the biotransformation of Cr(VI) to less toxic Cr(III) under field conditions. The project duration is 18 months. The data obtained from this new project along with the mathematical models developed as part of the current project can be

utilized for designing the field level remediation of Cr(VI) contaminated aquifers using reaction zone technology.

4. Major Facilities Built / Equipment Procured:

1. Two pilot scale reactors of size 3 m X 1 m X 0.5 m where elaborate experiments can be conducted for studying transport of any contaminant through aquifers.
2. Peristaltic pumps -5 nos.
3. Deep Freezer- 1000 L capacity
4. Ion meter (pH and ORP measurements)